



Universidade do Minho
Escola de Engenharia

Lelis Gonzaga Fraga Wood pellets combustion in a fixed bed combustor

Lelis Gonzaga Fraga

Wood pellets combustion in a fixed bed
combustor

UMinho | 2019

November, 2019



Universidade do Minho
Escola de Engenharia

Lelis Gonzaga Fraga

Wood pellets combustion in a fixed bed
combustor

Doctoral Thesis for PhD Degree in
Mechanical Engineering

Work Performed Under the Supervision of
Professor José Carlos Fernandes Teixeira
Professor Manuel Eduardo Cardoso Ferreira

DIREITOS DE AUTOR E CONDIÇÕES DE UTILIZAÇÃO DO TRABALHO POR TERCEIROS

Este é um trabalho académico que pode ser utilizado por terceiros desde que respeitadas as regras e boas práticas internacionalmente aceites, no que concerne aos direitos de autor e direitos conexos. Assim, o presente trabalho pode ser utilizado nos termos previstos na licença abaixo indicada. Caso o utilizador necessite de permissão para poder fazer um uso do trabalho em condições não previstas no licenciamento indicado, deverá contactar o autor, através do RepositóriUM da Universidade do Minho.

Licença concedida aos utilizadores deste trabalho



Atribuição

CC BY

<https://creativecommons.org/licenses/by/4.0/>

ACKNOWLEDGMENTS

This thesis was concluded with the support and contribution from many parts. Hereby, I would like to acknowledge the government of Timor Leste through Universidade Nacional Timor Lorosa'e for scholarship that supported my study. I would like to express my deepest gratitude to Professor Aurelio Guterres, the former rector of UNTL, for providing this opportunity. I also wish to thank my supervisors Professor José Carlos Fernandes Teixeira and Professor Manuel Eduardo Cardoso Ferreira who provided orientation and guidance during my studies from the beginning of the research planning, through the experimental activities, to the thesis writing.

I also wish to thank Professor Delfim Soares who provided the equipment to conduct the TGA analysis, and I would like to thank Mr. Miguel Abreu and Mrs. Leonor Carneiro who gave technical support in conducting the TGA experiments. I would like to thank Mr. Carlos Costa and Mrs. Irene Morais at CVR (*Centro para a Valorização de Resíduos*), for support on the preparation of the wood particles, and chemical analysis test on wood pellets. I also wish to thank the CVR director, Professor Cândida Vilarinho, for providing the facilities for conducting the experimental tests. I also wish to thank Professor Hélder Puga and others colleagues in Laboratory of Foundry, the Department of Mechanical Engineering University of Minho, Mr. José Pereira and Mr. Víctor Lopes who were available during my experiment. A special message of gratitude to Mr. Pedro Ribeiro for the support and enlighten discussions during the experiments on the pellet boiler. I would like to thank Dr. Ricardo Falcão for the support and contribution discussions and numerical analysis. I also wish to thank Mr. Carlos Costa for the support and contribution on the experimental tests. I would like to thank Professor Senhorinha F. Teixeira and my colleague Mr. João Silva for the contribution on the discussion of the scientific issues and papers. My gratitude also extends to Professor Celina Pinto Leão and Professor Sérgio Sousa for the contributions on the ANOVA analysis.

Last but not least, I would like to express my special gratitude to my wife Honoria Freitas, my daughters Mareza Luisa Freitas Fraga and Févia Januario Freitas Fraga for their love, patience and support during my absence in Portugal. I also wish to thank my mother Luisa Gonzaga Bento, my brothers Plenio Gonzaga Fraga, Deonísio Gonzaga Meles Fraga and Ondínio Gonzaga Fraga for their support and contribution during my study.

Finally thanks to everyone, colleagues, and friends who have already contributed to my successfulness.

Guimarães, November, 2019.

STATEMENT OF INTEGRITY

I hereby declare, that I having conducted my thesis with integrity. I confirm that I have not used plagiarism or any form of falsification of results in the process of the thesis elaboration.

I further declare that I have fully acknowledged the Code of Ethical Conduct of the University of Minho.

University of Minho, November, 2019

ABSTRACT

The development of biomass as a future sustainable energy resource, requires the continuous development of technologies that improve its efficiency of conversion and the reduction of harmful emissions to the environment. Biomass can be burned directly from the environmental state or processed through densification in the form of wood pellets. The combustion behavior of pine wood pellets was investigated in this study.

The decomposition of wood particles under different heating and air flow rates were analyzed using the TGA device. The wood pellets burning in a small scale reactor were investigated under different temperatures and time. The wood pellets combustion in a fixed bed combustor with the boiler capacity of 20 kW were tested with several parameters including Power, excess air (EA), the split ratio (SR) and grate area (GA). In this work, the Taguchi method was applied to conduct the experiments. From these experiments, several parameters were evaluated including the mass loss and elemental analysis of wood pellets, kinetic parameters, gas emissions (CO), fuel bed temperature, efficiency, the ashes agglomeration, and the combustion instability.

The results obtained from TGA showed that the heating rate affects the heat flow, ignition temperatures, burnout temperatures, and mass loss rate value and different kinetic parameters. But there was no significant influence of the air flow rates on the thermal decomposition of wood particles. The results of the experiment in a small scale reactor revealed that the mass losses increase for any specific temperature and the higher the temperature, the faster the pellets volatilize, and the mass loss occurs at a very slow rate for very low temperature.

The reaction rate increased with the temperature and the higher the combustion temperature applied the higher the mass loss of all substances observed. The remaining mass as fixed carbon and ashes or unburned substances was about 3%. The residence time and temperature influenced the species concentration of wood pellets. The wood pellets combustion in a fixed combustor showed that the highest temperature in fuel bed was observed at 15 mm followed by 25 mm, 5 and 60 mm. The lower CO emission or higher efficiency was obtained at a medium thermal load.

The results obtained from the ANOVA analysis showed that the SR and the Power are the most important parameters contributing to CO reduction and also the fuel bed temperature. In addition, the parameters that may change the temperature mean value in the core of fuel bed is Power, followed by GA. The combustion instability resulted from the accumulation of unburned wood pellets on the grate, which caused low combustion rate and generated the vortex and oscillation in the air flow rate, thus creating noise and disturbances, and increasing the CO emission.

Keywords: wood pellets, combustion, gas emission, Taguchi method, Thermogravimetric analysis, heating rate, devolatilization.

RESUMO

O desenvolvimento da biomassa como fonte energética sustentável para o futuro requer o desenvolvimento de tecnologias que melhorem a sua eficiência de conversão e a redução de emissões. A biomassa pode ser queimada diretamente no seu formato original, com apenas algumas operações de recolha e processamento, ou através de um conjunto de processos de densificação no formato de pellets de madeira.

Neste projeto investigou-se o comportamento da combustão de pellets de madeira de pinho. Utilizou-se um equipamento TGA para analisar a decomposição de partículas de madeira sobre diferentes condições de taxas de aquecimento e de caudais de ar. Investigou-se também a combustão de pellets de madeira num reator de pequena escala, variando a temperatura e o tempo de reação.

Utilizou-se uma caldeira de 20 kW com grelha fixa para investigar a combustão de pellets, nomeadamente a influência de vários parâmetros, incluindo: potência de queima, excesso de ar, relação de ar primário/secundário e área da grelha. Utilizou-se o método de Taguchi para o planeamento das experiências. Foram avaliados diversos parâmetros como: perda de massa e análise elementar dos pellets, cinética de reação, emissões gasosas (CO), temperatura no leito, eficiência, aglomeração de cinzas e instabilidades no processo de combustão.

Os resultados dos ensaios TGA demonstraram que as taxas de aquecimento afetam o escoamento de calor, temperatura de ignição e extinção, taxa de perda de massa e vários parâmetros da cinética de reação. No entanto, verificou-se que não há qualquer influência dos caudais de ar na decomposição térmica das partículas de madeira.

Os resultados das experiências no reator de pequena escala revelaram que as perdas de massa aumentam para qualquer valor de temperatura e que quanto maior a temperatura, maior a taxa de volatilização dos pellets, e que para temperaturas baixas a perda de massa ocorre a uma taxa reduzida. As taxas de reação aumentam com a temperatura, assim como se observou que para todas as substâncias, a perda de massa aumentava com o aumento da temperatura. A massa final na forma de carbono fixo, cinzas e inqueimados foi de cerca de 3%.

Na combustão de pellets em grelha fixa verificou-se que a temperatura mais elevada se situava a 15 mm, seguida por 25, 5 e finalmente a 60 mm de altura. Na potência média obtiveram-se os níveis de emissões mais baixos de CO e os valores mais elevados de eficiência de combustão.

Os resultados de aplicação da análise ANOVA permitiram concluir que os parâmetros que mais contribuem para a redução de emissão de CO e para o valor da temperatura, foram a potência e a relação ar primário/secundário. Para além disso, os parâmetros que mais influenciam o valor médio da temperatura no leito são a potência, seguida da área de grelha.

Conclui-se que as instabilidades resultam da acumulação de pellets não queimados na grelha, que provocam uma redução na taxa de combustão, geram vórtices e oscilações no escoamento de ar, provocando assim ruído, aumentando a emissão de CO.

Palavras-chave: pellets de madeira, combustão, emissão de gases, método de Taguchi, análise Termogravimétrica, taxa de aquecimento, desvolatilização.

LIST OF CONTENTS

ACKNOWLEDGMENTS	iii
ABSTRACT	v
RESUMO	vi
LIST OF CONTENTS	vii
LIST OF FIGURES	xii
LIST OF TABLES	xvii
LIST OF SYMBOLS.....	xx
1. INTRODUCTION	1
1.1 Motivation	1
1.1.1 Background	1
1.1.2 Research opportunities.....	8
1.2 Objectives	9
1.3 Research methodology	9
1.4 Structure of the thesis	10
1.5 Contributions of this work	11
2. LITERATURE REVIEW.....	12
2.1 Major literature sources on wood pellets combustion.....	12
2.2 Biomass.....	15
2.2.1 Biomass conversion technologies	17
2.2.2 Contribution of biomass in the renewable sector	18
2.2.3 Pellets	18
2.2.3.1 Characterization of raw materials and pellets	19
2.2.3.2 Advantages of pellets.....	23
2.2.3.3 Applications of pellets.....	24
2.2.3.4 Raw material for pellets	24
2.3 Combustion.....	26
2.3.1 Reactant and product mixture	27
2.3.2 Biomass combustion.....	29
2.3.2.1 Wood combustion theory.....	30
2.3.2.2 Biomass combustion systems	33
2.3.3 Parameters influencing biomass combustion	33

2.3.3.1 Grate size	33
2.3.3.2 Excess air ratio.....	34
2.3.3.3 Residence time	35
2.3.3.4 Primary and secondary air ratio.....	35
2.3.4 Combustion temperature.....	36
2.3.5 NO _x	37
2.3.6 Ashes	39
2.4 Fuel devolatilization	40
2.4.1 Thermogravimetric analysis (TGA)	41
2.4.2 Mechanism of devolatilization	42
2.4.3 The influence of variables on devolatilization	42
2.4.3.1 Influence of temperature	42
2.4.3.2 Influence of particle size	42
2.4.3.3 Influence of heating rate.....	43
3. MATERIALS AND METHODS	44
3.1 Combustion facility	44
3.2 Measurement techniques	47
3.2.1 Flow rate and velocity measurement.....	47
3.2.2 The split ratio of primary and secondary air	49
3.2.3 Fuel mass flow measurement.....	50
3.2.4 Temperature measurement.....	51
3.2.5 Data collection	53
3.3 Flue gas analyzer.....	54
3.4. Data acquisition and control system.....	57
3.4.1 Data acquisition mechanism	57
3.4.2 LabVIEW	59
3.5 Uncertainty analysis.....	60
3.6 Operation system	62
3.6.1 Feeding procedure	62
3.6.2 Measurement condition.....	63
3.6.3 Operating conditions for wood pellets combustion.....	63
3.7 TGA device	64

3.7.1 Experimental procedure	65
3.7.2 Sample preparation.....	66
3.7.3 Operating conditions for TGA experiment	67
3.8 Mass loss experiments	68
3.8.1 Experimental procedure	68
3.8.2 Elemental analysis of pellets.....	69
3.8.3 Temperature profile of the pellets	70
3.8.4 Moisture content of pellets	70
3.8.5 Sample preparation.....	70
4. TGA ANALYSIS OF PINE WOOD PARTICLES	72
4.1 Test conditions	72
4.2 Thermal decomposition of pine wood particles	72
4.2.1 Influence of the heating rate	73
4.2.2 Influence of air flow rate	80
4.2.3 Influence of particle size	84
4.3 Kinetic analysis of pine wood particles	88
4.3.1 Influence of the heating rate	90
4.3.2 Influence of the air flow rate	91
4.3.3 Influence of particle size	92
5. MASS LOSS AND ELEMENTAL ANALYSIS OF PINE WOOD PELLETS IN A SMALL SCALE REACTOR	94
5.1 Test conditions	94
5.2 Results and discussion	94
5.2.1 Mass loss of wood pellets.....	94
5.2.2 Elemental analysis of wood pellets.....	96
6. EMISSIONS AND TEMPERATURE MEASUREMENT IN A FIXED BED COMBUSTOR.....	107
6.1 Test conditions	107
6.1.1 Excess air	107
6.1.2 Thermal load calculation	108
6.1.3 Split ratio	109
6.1.4 Grate size	109
6.2 Experimental plan.....	110

6.2.1 Levels	111
6.2.2 Plan of tests.....	112
6.3 Combustion of wood pellets	115
6.3.1 Ignition conditions.....	115
6.3.2 Emission characteristics.....	116
6.3.3 The thermal efficiency	117
6.3.4 Combustion instability	120
6.3.5 Ashes formation and agglomeration.....	125
6.4 CO emissions	126
6.4.1 Overview of CO emissions	126
6.4.2 ANOVA analysis of CO emissions.....	127
6.5 Temperature in fuel bed	132
6.5.1 Temperature profile in fuel bed.....	132
6.5.2 Temperature profile after the shut off of the boiler	133
6.5.3 ANOVA analysis on temperature	134
7. CLOSURE	152
7.1 Conclusions	152
7.2 Future work.....	154
REFERENCES.....	155
ANNEXES	168
A. Biomass characteristics and experimental auxiliary.....	168
B. Experimental procedure.....	172
B.1 Verification of the boiler	172
B.2 Calibration of gas analyzer	172
B.3 Experimental phase.....	173
B.4 Turn off procedure.....	173
B.5 Safety issues	174
C. TGA data.....	175
C.1 Data for different heating rate	175
C.2 Data for different air flow rate	179
C.3 Kinetic analysis data for different heating rate	183
C.4 Kinetic analysis data for different air flow rate	184

D. Preliminary set up for mass loss of wood pellets	186
D.1 Mass loss.....	186
D.2 Elemental analysis	187
D.3 Transient behavior of pellets	188
E. Experimental data.....	192

LIST OF FIGURES

Figure 1.1. The estimated number of the energy crops of biomass in different regions.....	2
Figure 1.2. Evolution of pellet production in the World by regions.....	3
Figure 1.3. The utilization of biomass energy for power in Portugal.....	4
Figure 1.4. Removal of biomass sources from forests in Portugal.	4
Figure 1.5. Evolution of pellet consumption in the world by regions.....	7
Figure 1.6. Flow chart for research activities.	10
Figure 2.1. Thermochemical conversion technologies	18
Figure 2.2. Four different qualities of wood pellets.....	26
Figure 2.3. Five sequential combustion stages.	27
Figure 2.4. The combustion process of a small biomass particle	30
Figure 2.5. Combustion characteristics of wood.....	32
Figure 2.6. Thermal decomposition of wood as a function of temperature with its cellulose, hemicellulose and lignin components.	33
Figure 2.7. CO remaining as a function of residence time, combustion temperature and oxygen concentration in an ideal stirring reactor.....	35
Figure 2.8. The relationship between the adiabatic combustion temperature and the excess air ratio.....	37
Figure 2.9. Ash formation mechanisms in biomass combustion.....	40
Figure 2.10. Mass loss and DTG curves for pine sawdust.	41
Figure 3.1. Experimental diagram.	45
Figure 3.2. Heat exchanger pipes, bottom view.	46
Figure 3.3. Boiler unit.....	46
Figure 3.4. Grate unit.	47
Figure 3.5. Flow through a constriction in a pipe.	48
Figure 3.6. Pressure transducer.....	48
Figure 3.7. Primary and secondary air tube.....	49
Figure 3.8. Digital mass scale.....	50
Figure 3.9. Time interval for pellet feeding (5 s ON and 3 s OFF).	51
Figure 3.10. Thermocouple location on the boiler.....	52
Figure 3.11. Temperature characteristics for some standard thermocouple materials	53
Figure 3.12. Type K thermocouple installed in the fuel bed.....	53

Figure 3.13. Thermocouple unit.....	53
Figure 3.14. Flue gas analyzer scheme.....	55
Figure 3.15. (a) Multi-gas analyzer 9000, and (b) NO _x gas analyzer.....	55
Figure 3.16. Gas emissions collection unit.....	56
Figure 3.17. Schematic diagram of data acquisition system.....	58
Figure 3.18. The LabVIEW 8.6 and the user interface.....	60
Figure 3.19. Comparison of the random and systematic errors, using the example of target practicing.....	61
Figure 3.20. DSC-TGA device unit.....	65
Figure 3.21. TGA experiments procedure.....	65
Figure 3.22. Knife mill device.....	66
Figure 3.23. Calibrated sieving machine and vibration unit.....	66
Figure 3.24. Pellets and pine wood particles.....	67
Figure 3.25. (a) The small scale reactor, (b) Cup, and (c) Scale.....	68
Figure 3.26. Experimental diagram of mass loss and elemental analysis.....	70
Figure 4.1. (a) Weight loss and heat flow, and (b) Rate of mass loss (particles smaller than 0.063 mm).....	74
Figure 4.2. (a) Weight loss and heat flow, and (b) Rate of mass loss (particles between 0.125 - 0.25 mm).....	75
Figure 4.3. (a) Weight loss and heat flow, and (b) Rate of mass loss (particles larger than 1 mm).....	76
Figure 4.4. The combustion behavior test at different heating rates for particles between 0.125 – 0.25 mm: (a) Max. comb. rate and temperature at various conditions, (b) Max. heat release and burning time, (c) Remaining mass, and (d) Heat release.....	78
Figure 4.5. The remaining mass of the three tests in the same condition with middle particles size.....	78
Figure 4.6. Combustion parameters of the pine wood particles at different heating rates: (a) Ignition index, and (b) Combustion index.....	80
Figure 4.7. (a) Weight loss and heat flow, and (b) Rate of mass loss (particles smaller than 0.063 mm).....	81
Figure 4.8. (a) Weight loss and heat flow, and (b) Rate of mass loss (particles between 0.125 and 0.25 mm).....	81
Figure 4.9. (a) Weight loss and heat flow, and (b) Rate of mass loss (particles larger than 1 mm).....	82

Figure 4.10. The combustion behavior test at different air flow rates for particles between 0.125 – 0.25 mm: (a) Max. comb. rate and temperature at various conditions, (b) Max. heat release and burning time, (c) Remaining mass, and (d) Heat release.83

Figure 4.11. Combustion parameters of the pine wood particles at different air flow rates.84

Figure 4.12. (a) Weight loss and heat flow, and (b) Rate of mass loss (for heating: 5 °C/min).85

Figure 4.13. (a) Weight loss and heat flow, and (b) Rate of mass loss (for heating: 10 °C/min).86

Figure 4.14. (a) Weight loss and heat flow, and (b) Rate of mass loss (for heating: 20 °C/min).86

Figure 4.15. (a) Weight loss and heat flow, and (b) Rate of mass loss (for heating: 51 °C/min).86

Figure 4.16. The combustion behavior test at different particle sizes for the heating rate 10 °C/min and air flow rate 100 mL/min: (a) Max. comb. rate and temperature at various conditions, (b) Max. heat release and burning time, (c) Remaining mass, and (d) Heat release.88

Figure 4.17. Kinetic parameter for three different stages at particle size is 0.063 mm, HR is 5 °C/min, and the air flow rate is 100 mL/min.89

Figure 4.18. Activation energy vs heating rates for particles: (a) < 0.063 mm, (b) 0.125 - 0.25 mm, and (c) > 1 mm.91

Figure 4.19. Activation energy vs air flow rates for particles: (a) < 0.063 mm (size 1), (b) 0.125 - 0.25 mm (size 2), and (c) > 1 mm (size 3).92

Figure 4.20. Activation energy vs heating rates for three particles size: (a) < 2nd stage, (b) 3rd stage, and (c) Total combustion.93

Figure 5.1. Mass loss of wood pellets vs time at temperature 264 – 734 °C.95

Figure 5.2. Mass loss of dry and wet pellets.96

Figure 5.3. Elemental analysis of wood pellets at T = 650 °C: (a) in percentage, and (b) in gram.98

Figure 5.4. Elemental analysis of wood pellets at T = 264 °C: (a) in percentage, and (b) in gram. 100

Figure 5.5. Elemental analysis of wood pellets at T = 351 °C: (a) in percentage, and (b) in gram. 100

Figure 5.6. Elemental analysis of wood pellets at T = 444 °C: (a) in percentage, and (b) in gram. 101

Figure 5.7. Elemental analysis of wood pellets at T = 541 °C: (a) in percentage, and (b) in gram. 102

Figure 5.8. Elemental analysis of wood pellets at T = 650 °C: (a) in percentage, and (b) in gram. 102

Figure 5.9. Elemental analysis of wood pellets at T = 734 °C: (a) in percentage, and (b) in gram. 103

Figure 5.10. Fixed Carbon profile at different temperature during the combustion. 105

Figure 5.11. Carbon ratio for different temperature. 105

Figure 5.12. O ₂ and H ₂ concentration of dry pellets for the temperature of 264 °C at 30 s and 4 min ((a) in percentage, and (b) in gram).....	106
Figure 6.1. Specific ignition rate and fuel supply for three different GA as function of the PA mass flow.....	115
Figure 6.2. Gas emissions profiles for TN15.....	116
Figure 6.3. The efficiency obtained for each test.....	118
Figure 6.4. Relationship between efficiency and GA with different EA and SR: (a) At 10 kW, (b) At 13 kW, and (c) At 16 kW.....	120
Figure 6.5. Temperature and emissions profiles for (a) TN9, and (b) TN20.....	123
Figure 6.6. Temperature and emissions profiles for (a) TN11, and (b) TN8.....	123
Figure 6.7. Temperature profiles for (a) TN25, and (b) TN14.....	124
Figure 6.8. Combustion characteristics on the instability.....	124
Figure 6.9. Combustion characteristics on the ashes.....	126
Figure 6.10. Individual influence of factors on the response (CO).....	129
Figure 6.11. Indices of interaction between factors on CO.....	130
Figure 6.12. Temperature profiles for TN15.....	132
Figure 6.13. Temperature profiles for TN17.....	133
Figure 6.14. Temperature profiles for TN10.....	134
Figure 6.15. Temperature profiles for (a) TN10, and (b) TN12.....	134
Figure 6.16. Individual influence of factors on the temperature at 5 mm.....	139
Figure 6.17. Indices of interaction between factors (T at 5 mm).....	140
Figure 6.18. Individual influence of factors on the temperature at 15 mm.....	142
Figure 6.19. Indices of interaction between factors (T at 15 mm).....	143
Figure 6.20. Individual influence of factors on the temperature at 25 mm.....	144
Figure 6.21. Indices of interaction between factors (T at 25 mm).....	145
Figure 6.22. Individual influence of factors on the temperature at 60 mm.....	147
Figure 6.23. Indices of interaction between factors (T at 60 mm).....	148
Figure 6.24. Temperature and emissions profiles for A2–B1–C1–D1.....	151
Figure A.1. Grate design.....	171
Figure D.1. Mass loss of wood pellets for experimental and modelling at temperature: 144, 191 and 225 °C.....	187
Figure D.2. Temperature profile for CS and HSS cup.....	189

Figure D.3. Temperature profile on the center ($r = 0$) and surface ($r = 3$ mm) of wood pellets (experiment)	190
Figure D.4. Temperature profile at in the center of the pellet ($r = 0$).....	191
Figure E.1. Experimental results.....	195
Figure E.2. The ashes agglomeration data.....	201

LIST OF TABLES

Table 2.1. Concentrations of C, H, O and volatiles matter in different biomass materials.	21
Table 2.2. Application of pellet standards ISO 17225-2.	25
Table 2.3. Typical excess air ratio (λ) and the resulting of air content in the flue gas.	35
Table 2.4. Typical NO _x emission in small scale boiler, normalized by the thermal output.	38
Table 2.5. Emissions limits defined by ÖNORM EN 303-5.	38
Table 2.6. Ash melting temperature for a range of fuels.	39
Table 3.1. Study parameters.	50
Table 3.2. Properties of pine wood pellets.	54
Table 3.3. Parameters reading in data acquisition.	59
Table 3.4. Thermal load.	64
Table 6.1. O ₂ content and excess air coefficient.	108
Table 6.2. Chemical composition of pine wood pellets.	108
Table 6.3. Grate area.	110
Table 6.4. Factor and Level of the experimental plan, using the Taguchi method.	111
Table 6.5. Matrix L ₂₇ , with indication parameter (1, 2, 5, 10), interaction (3, 4, 6, 7, 8, 11), and independent (9, 12, 13).	112
Table 6.6. The experiments plan and value of responses, according to the Taguchi method.	114
Table 6.7. The input parameter for TN15.	117
Table 6.8. The experimental data for TN15.	117
Table 6.9. Highest thermal efficiency experiments.	118
Table 6.10. Stability and instability combustion condition of the experiment identified.	121
Table 6.12. Analysis of the relative contribution of the parameters based on the mean concentration of CO.	128
Table 6.11. Mean values of S/N index and maximum differences between levels on CO.	128
Table 6.13. ANOVA worksheet for CO.	131
Table 6.14. ANOVA F critic calculation for CO.	132
Table 6.15. Mean values of S/N index and maximum differences between levels on T at 5 mm.	136
Table 6.16. Mean values of S/N index and maximum differences between levels on T at 15 mm.	136
Table 6.17. Mean values of S/N index and maximum differences between levels on T at 25 mm.	136
Table 6.18. Mean values of S/N index and maximum differences between levels on T at 60 mm.	137

Table 6.19. (a) Analysis of the relative contribution of the parameters on the mean temperature at 5 mm.	137
Table 6.19. (b) Analysis of the relative contribution of the parameters on the mean temperature at 15 mm.	137
Table 6.19. (c) Analysis of the relative contribution of the parameters on the mean temperature at 25 mm.	138
Table 6.19. (d) Analysis of the relative contribution of the parameters on the mean temperature at 60 mm.	138
Table 6.20. ANOVA worksheet for the temperature at 5 mm.	141
Table 6.21. ANOVA F critic calculation for the temperature at 5 mm.	141
Table 6.22. ANOVA worksheet for the temperature at 15 mm.	143
Table 6.23. ANOVA F critic calculation for the temperature at 15 mm.	144
Table 6.24. ANOVA worksheet for the temperature at 25 mm.	146
Table 6.25. ANOVA F critic calculation for the temperature at 25 mm.	146
Table 6.26. ANOVA worksheet for the temperature at 60 mm.	148
Table 6.27. ANOVA F critic calculation for the temperature at 60 mm.	149
Table 6.28. The overall influences of the parameters on fuel bed temperature.	150
Table 6.29. Mean value and variance of the best combination parameters (A2-B1-C1-D1).	151
Table A.1. Threshold values of the most important pellet parameters based on ISO 17225-2.	168
Table A.2. Standard thermocouple types.	169
Table A.3. Physical and chemical properties of wood pellets.	170
Table C.1. Ignition, peak and burnout temperatures and maximum combustion rates at different heating rates for the particles < 0.063 mm.	175
Table C.2. Ignition, peak and burnout temperatures and maximum combustion rates at different heating rates for the particles 0.125-0.25 mm.	175
Table C.3. Ignition, peak and burnout temperatures and maximum combustion rates at different heating rates for the particles >1 mm.	176
Table C.4. Mass loss per stage of conversion at different heating rates and particle sizes.	177
Table C.5. Effect of heating rates on combustion parameters of the pine wood particles.	178
Table C.6. Ignition, peak and burnout temperatures and maximum combustion rates at different air flow rates for the particles < 0.063 mm.	179

Table C.7. Ignition, peak and burnout temperatures and maximum combustion rates at different air flow rates for the particles 0.125 – 0.25 mm.....	179
Table C.8. Ignition, peak and burnout temperatures and maximum combustion rates at different air flow rates for the particles > 1 mm.....	180
Table C.9. Mass loss per stage of conversion at different air flow rates and particle sizes.....	181
Table C.10. Effect of air flow rates on combustion parameters of the pine wood particles.....	182
Table C.11. Estimated kinetic parameters for the combustion of pine wood particles at different heating rates (particles smaller than 0.063 mm).	183
Table C.12. Estimated kinetic parameters for the combustion of pine wood particles at different heating rates (particles between 0.125 and 0.25 mm).....	183
Table C.13. Estimated kinetic parameters for the combustion of pine wood particles at different heating rates (particles larger than 1 mm).	184
Table C.14. Estimated kinetic parameters for the combustion of pine wood particles at different air flow rates (particles smaller than 0.063 mm).....	184
Table C.15. Estimated kinetic parameters for the combustion of pine wood particles at different air flow rates (particles between 0.125 and 0.25 mm).....	185
Table C.16. Estimated kinetic parameters for the combustion of pine wood particles at different air flow rates (particles larger than 1 mm).	185
Table D.1. Time and temperature for the preliminary test.	186
Table D.2. Mass loss difference between experimental and modelling.....	187
Table D.3. Mass loss at T = 225 °C.	187
Table D.4. Elemental analysis at T = 225 °C.	188
Table E.1. The experimental data.....	193

LIST OF SYMBOLS

Symbol	Meaning	SI Unit
A	Area, pre-exponential factor	(m ²), (min ⁻¹)
A_1	Constants and as function of the Bi	(-)
B	Expansion factor	(-)
Bi	Biot number	(-)
C	Specific heat	(kJ/kg.K)
C_x	Proportion of mole carbon	(kmol)
d	Diameter	(mm)
D	Ignition index	(s ⁻³)
e	Error, excess air	(-), (%)
E	Activation energy	(kJ/mol)
g	Gravitational acceleration	(m/s ²)
h	Heat transfer coefficient, height	(W/m ² .K), (mm)
HHV	Higher heating value	(kJ/kg)
H_y	Number of hydrogen mole	(kmol)
k	Rate constant	(s ⁻¹)
LHV	Lower heating value	(kJ/kg)
m	Mass	(kg)
\dot{m}	Mass flow rate	(kg/s)
M	Molecular weight, moisture	(kg/kmol), (g)
n	Measurement number	(-)
N_{mix}	Sum of the number of moles	(kmol)
p	Pressure	(Pa)
P	Power	(kW)
$\%O_{2,dry}$	Oxygen concentration in the exhaust/gases flow	(%)
$\%m$	Percentage of mass	(%)
$\%O_2$	Percentage of oxygen	(%)
\dot{Q}	Volumetric flow rate	(m ³ /s)
r	Radius	(mm)

R	Radius, universal gas constant, true value, coefficient of determination	(mm), (kJ/kmol.K), (-), (-)
R_a	Average mass loss rate	(s ⁻¹)
Re	Reynolds number	(-)
R_{max}	Maximum combustion rate	(s ⁻¹)
S	Combustion index	(s ⁻² . K ⁻³)
S_x	The sample standard deviation	(-)
S_x^-	Standard deviation of the sample mean	(-)
t	Time	(s)
T	Temperature	(K)
U	Uncertainty	(-)
V	Volume, voltage	(m ³), (volt)
x	Mass fraction, coefficient, measurement	(-), (-), (-)
\bar{x}	Measurement mean	(-)
x_i	Individual measurement	(-)
X_i	Corrected concentration of a given species	(ppm)
y	Mass fraction, coefficient	(-), (-)

Greek symbols

α	Extent of reaction, level of significance	(-), (-)
β	Nominal heating rate, diameter ratio	(°C/min), (-)
δ	Total measurement error	(-)
ΔT	Temperature difference	(K)
Δt	Time interval	(s)
ϕ	Equivalence ratio	(-)
η	Efficiency	(%)
J_0	Zeroth-order Bessel function of the first kind	(-)
λ	Excess air ratio	(-)
λ_1	Constants and as function of Bi	(-)
μ	True population mean	(-)
v	Velocity	(m/s)

List of symbols

$\theta(r, t)$	Dimensionless temperature	(-)
ρ	Density	(kg/m ³)
σ	Population standard deviations	(-)
σ_w	Variance	(-)
τ	Dimensionless time	(-)

Superscripts

$^{\circ}$	Standard state
$-$	Mean value

Subscripts

a	Air
av	Average
b	Boiler, bulk, burnout
c	Cold
$chamb$	Chamber
cyl	Cylinder
e	Energy
ex	Exhaust
f	Fluid, final, fuel
fd	Feeding
fb	Fuel bed
h	Hot
i	Ignition, initial, in, inlet, input
id	Initial decomposition
ins	Instability
l	Loss
max	Maximum
mr	Maximum combustion rate
n	Nominal
o	Initial condition
s	Surface

<i>stoic</i>	Stoichiometry
<i>t</i>	Time
<i>th</i>	Thermal
<i>w</i>	Water, weight
∞	Ambient

Abbreviations

AFR	Air fuel ratio
BC	British Columbia
CCA	Chromium-cadmiumarsenic
CEN	European Committee for Standardization
CFD	Computational fluid dynamics
CHP	Combined heat and power
CS	Carbon steel
CTI	Comitato Termotecnico Italiano
DAEM	Distributed Activation Energy Model
d.b.	Dry basis
dB	Decible
df	Degree of freedom
DIN	Deutsches Institut für Normung (German Institute for Standardization)
DSC	Differential scanning calorimetry
DT	Deformation Temperature
e	Error
EA	Excess air
EU	European Union
EN	European Norms
FB	Fuel Bed
FC	Fixed Carbon
FSU	Former Soviet Union (Eastern Europe and Central Asia)
FT	Flow Temperature
GA	Grate area
HCl	Hydrochloric acid

HE	Heat Exchanger
HR	Heating Rate
HSS	High Stainless Steel
HT	Hemisphere Temperature
HTAC	High Temperature Air Combustion
Mha	Million hectares
NF	<i>Norme Française</i>
NM VOC	Non-methane volatile organic compounds
NO _x	Nitrogen oxides
NO ₃	Nitrate
NPV	Negative net present value
odt	Oven dry tonnes
OECD	Organization for Economic Co-operation and Development
OGC	Organic Gaseous Carbon
Odt	Oven dry ton
PA	Primary Air
PAH	Polycyclic Aromatic Hydrocarbon
PAH _{tot}	Total Polycyclic Aromatic Hydrocarbons
PCDD	Polychlorinated Dibenzo-p Dioxin
PCDD/F	Polychlorinated Dibenzodioxins and Furans
PIC	Products from Incomplete Combustion
PM	Particulate Matter
PM _{tot}	Total emissions of Particulate Matter
PROMETHEE	Preference ranking organization method for enrichment and evaluation
SA	Secondary Air
SDT	Simultaneous Differential Techniques
Si (OH) ₄	Silicic acid
SR	Split ratio
SRC	Short Rotation Coppice
SO ₄	Sulphate
SO _x	Sulphur Oxides
SST	Shrinkage Starting Temperature

S/N	Signal to Noise ratio
TA	Thermogravimetric
TaHE	Temperature after Heat Exchanger
TGA	Thermogravimetric Analysis
TM	Taguchi method
TN	Test Number
TSP	Totals Suspended Particulate matter
UHC	Unburned Hydrocarbons
US	United States
sq	Sum of square
var	Variance
VC	Volatile Carbon
VOC	Volatile Organic Compound
w.b	Wet basis
Wt%	Weight fraction

1. INTRODUCTION

1.1 Motivation

If properly developed biomass energy sources are abundant and can add value to the economy and ensure sustainability for future energy supply. Availability of biomass energy can be managed and developed in accordance with the requirements of existing technologies to produce useful energy. Among the various biomass fuels, wood pellets (made of wood materials) have been developed over the last few years by both industries and R&D institutions in order to maximize the combustion efficiency and provide simple and reliable utilization.

Wood pellets are a solid fuel that can be used to generate heat from the combustion process, which can subsequently be used for heating, in both domestic and industrial facilities. The overall performance of wood pellets combustion depends upon the specific design and characteristics of the grate and of the combustion chamber. Good combustion occurs when all the fuel and air are well mixed, resulting in high combustion efficiency. Incomplete combustion will result in undesirable emissions such as CO, unburned carbon, NO_x, etc. which have a negative impact on health and the environment.

1.1.1 Background

Biomass is one of the renewable energy sources that are abundant in nature (Ghodke and Mandapati, 2019), widely available and with enormous potential for future sustainable energy supply. It could be said that most of the countries have substantial potential for biomass energy. Biomass also has advantages for providing employment opportunities in rural areas (González *et al.*, 2011). In addition, its use is increasing because it is considered carbon neutral (Euh *et al.*, 2016) and contributes to reducing greenhouse gas emissions (Alakoski *et al.*, 2016). Data presented from Hoogwijk and Graus (2008) estimated that the energy potential for a number of energy crops of biomass in different regions is 271 EJ/yr (see Figure 1.1).

The existence of biomass on earth covers wide regions including forests and oceans. Most of the biomass potential is available on the ground, at a total of about 1,800 billion tonnes while the potential in the ocean is 4 only billion tonnes, with a comparable amount of biomass existing in the soil (ABA Japan, 2002). In addition, the total biomass on the ground is 33,000 EJ on an energy basis, which corresponds to over 80 times the total annual energy consumption of the world. Biomass has a high potential for future energy resources and is an enormous renewable resource comprising of approximately 4,500 EJ (220 odt), of annual primary production. The data regarding annual bioenergy

potential is approximately 2,900 EJ including 1,700 EJ from forests, 850 EJ from grasslands and 350 EJ from agricultural areas (Hall and Rao, 1999, cited by Rosillo-Calle, 2007). In addition, energy farming is also contributing in existing agricultural land alone, which indicate over 800 EJ without affecting the world's food supply (Faaij *et al.*, 2002, cited by Rosillo-Calle, 2007).

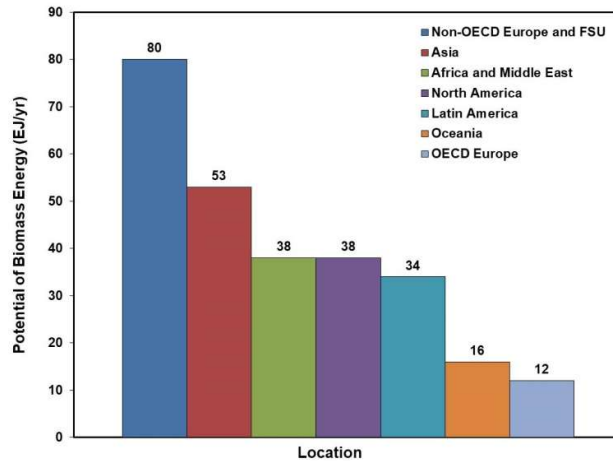


Figure 1.1. The estimated number of the energy crops of biomass in different regions. (Hoogwijk and Graus, 2008).

The main sources of biomass outside the EU (Bjerg *et al.*, 2011) are Canada, the US, and Russia. Russia, Southern US, and South America, and Africa, are the fastest growing regions as shown by the worldwide pellet production between 2012 and 2017, depicted in Figure 1.2. The pellet production has grown significantly in developing markets, including South America (primarily Brazil and Chile), Asia and Oceania, and Europe outside of the EU28. In Asia and Oceania, the pellet production volume increased by more than 40% in 2017, mostly in Vietnam and Malaysia. In addition, Canada has boreal forests which contain an abundance of dead trees or wood from dead and diseased forests (Bjerg *et al.*, 2011; Barrette *et al.*, 2017).

Depending on the source, different estimatives of biomass resources have been presented which suggests that the stock of biomass depends on the world consumption itself, giving some uncertainty to the actual figures. Thrän *et al.* (2010) calculated the energy crop potentials for 133 individual countries, which indicates that the food demand takes priority. Moreover, Wang and Dunn (2015) stated that the biofuel feedstocks must come from land that was neither forested before nor necessary for food crops (set aside land) as adopted by the U.S. Renewable Fuel Standard.

About half of the Portuguese land area is covered by forests and other wooded land to a total of approximately 4.91 Mha (Bioenergy Europe, 2018). Meanwhile, more than one-third (3.2 Mha) of the

territory is forests (Ferreira *et al.*, 2017), out of which 2.1 Mha forests are available for wood supply (Bioenergy Europe, 2018). Such figures show great potential for reducing its dependence on fossil fuels (Ferreira, 2016). The large biomass resources in Portugal includes wood residues, animal waste and municipal solid waste (Ferreira *et al.*, 2017). The biomass resources in Portugal from the forest residues and energy crops are 11,611 and 8,378 GWh/year, respectively. Moreover, biomass is considered as the third renewable source in Portugal after hydro and wind.

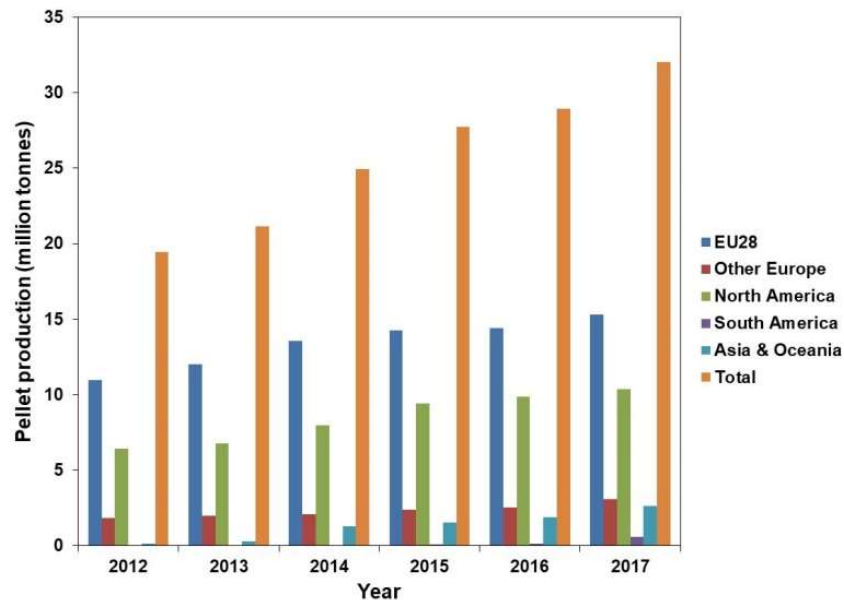


Figure 1.2. Evolution of pellet production in the World by regions.
(adapted from Bioenergy Europe, 2018).

The utilization of biomass energy in Portugal is growing significantly with a sharp increase in 2010, which is related to the Portuguese strategy in developing the biomass source for the energy production as described in Figure 1.3 (Ferreira *et al.*, 2017). In fact, Portugal is one of the EU28 countries, which uses the majority of Roundwood for industrial purposes, as shown in Figure 1.4 (Bioenergy Europe, 2018). This dynamism occurs despite the forest fires that devastated the country in 2017 that have destroyed around 520 thousand hectares of forest including several wood processing mills and 2 pellet plants.

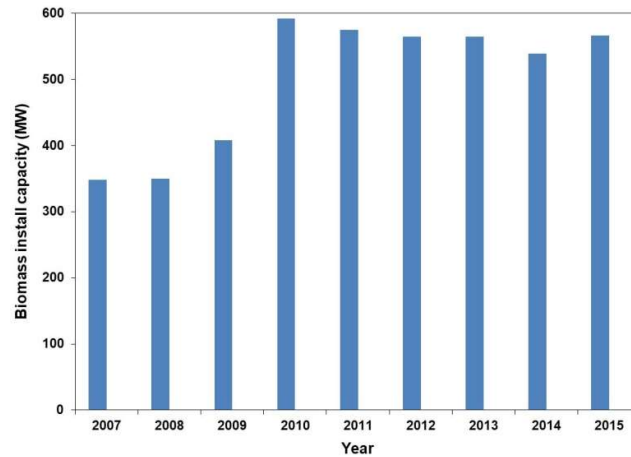


Figure 1.3. The utilization of biomass energy for power in Portugal (Ferreira *et al.*, 2017).

Biomass energy can be utilized in multiple domestic and industrial applications, such as cooking, heating, electricity generation and transportation (Hoogwijk and Graus, 2008; Paulauskas *et al.*, 2015). It can also replace all fossil fuels used for the production of synthetic materials (i.e. chemicals, polymers) and for generating low and medium temperature steam. The operating costs depend on the technology used for the actual biomass conversion. For example, cost-effective opportunities exist for steam production from biomass residues and for the substitution of high-value petrochemicals. Together this would require by 2030 more than 20 EJ of biomass worldwide, in addition to baseline. The potential could double by 2050 and reach 38–45 EJ (25% of the total industrial energy use), with most demand in Asia, and other developing countries and economies in transition (Saygin *et al.*, 2014).

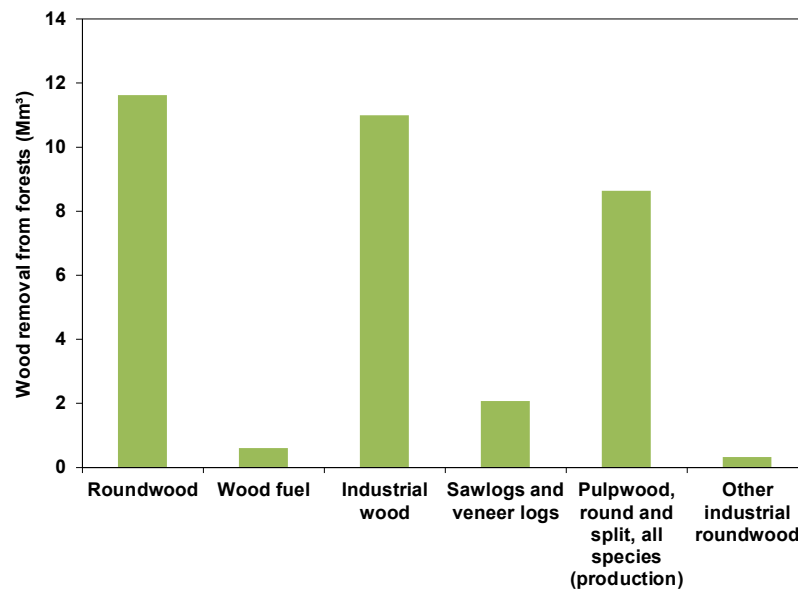


Figure 1.4. Removal of biomass sources from forests in Portugal (Bioenergy Europe, 2018).

Energy conversion from low quality biomass or by using inadequate technology (such as inefficient combustion) can cause harm to human health and contribute to the increase in air pollution. Inefficient combustion can produce high levels of particulate emissions, which have been a subject of interest regarding their formation, characteristics and implications to human health (Boman, 2005). In order to reduce the gas emissions from incomplete combustion, one needs to apply an efficient combustion process. McKendry (2002) evaluated the utilization of biomass as a traditional energy source mostly in the third world. This condition can play a pivotal role in helping the developed world reduce the environmental impact of burning fossil fuels to produce energy but only if significant areas for energy crops are made available.

Biomass energy resources are abundant, especially in developing countries. If it is not properly developed, then the condition can be regarded as a lost opportunity, due to the waste or disposal of useful energy. Biomass wastes occur in various forms, such as wood, paper, and other materials which are available in vast quantities (Olsson, 2006a). In this context, a plant for wood pellets production is supported by both an economic and energetic analysis and this activity can produce valuable environmental and agricultural benefits in terms of improvement of tourist potentiality (e.g. the quality of the environment is at a high level), reduction of greenhouse emissions and recovery of soil fertility (Di Giacomo and Taglieri, 2009). Developing the biomass energy requires all sectors and fields to establish the policies on energy, material, agriculture (food, feed), resource use and international collaboration across the industry, energy and transportation sectors. Besides, the industrial sector plays an important role in defining the policies. These need continuous improvement of bio-based alternatives by using the efficient and effective cost with new technologies through biomass to produce low CO₂ emissions to the environment (Saygin *et al.*, 2014).

Feedstock or biomass fuels can be produced in various forms and different materials before they are converted into useful energy such as pulp, waste paper, wood residue, cork pellet, wood pellet (hardwood pellet and softwood pellet). Wood residues for biomass fuel result from various activities or treatments such as manufacturing, discarded wood products diverted from landfills, and non-hazardous wood debris from construction and demolition activities (Ciferno and Marano, 2002). Development of biomass energy such as wood pellets will encourage wood pellet production to increase rapidly. This condition could be seen in several countries such as in the United States, as manufacturing and trade of wood pellets has seen an exponential growth in the last few years. This has been triggered by its potential utilization in applications typically dominated by fossil fuels, such as heat, power, and combined cycle generation (Pirraglia *et al.*, 2013).

The methods for converting biomass to useful energy include pyrolysis, gasification, direct combustion, and liquefaction. The use of feedstocks can be adapted to the process applied. Cork pellets have several characteristics similar to those of forest waste, opening new horizons for its use outside of the cork industry for energy recovery or raw materials production. This can be completed either in traditional form (direct combustion) or using alternative technologies (gasification), or even in co-firing with coal (Nunes *et al.*, 2013). As stated by Milne *et al.* (2002) biomass conversion technologies can be divided into two categories: direct production routes and conversion of storable intermediates.

Residential biomass combustion appliances can produce various emission characteristics (such as VOC and PAH) according to different fuel and operational conditions. VOC emissions include methane, ethane, acetylene, and benzene with Non-methane volatile organic compounds (NMVOC) emissions in the range of 20-2,500 mg/MJ for wood stoves and 1-20 mg/MJ for pellet stoves. On the other hand, PAH_{tot} emissions have been observed in the range of 1,300-220,000 µg/MJ for wood stoves and 2-300 µg/MJ for pellet stoves. Phenanthrene, fluoranthene, and pyrene are usually present in all cases as major PAH's (Boman, 2005). In general, the emissions productions of PIC's as well as PM_{tot} were shown to be considerably higher from wood stoves when compared to those from pellet stoves. Different combustion appliances will produce different combustion characteristics and the use of high-quality pellets under continuous and controlled conditions gives advantageous combustion conditions compared to the traditional batch firing of wood logs. The emission levels are directly correlated with the combustion quality. The total emissions of particulate matter (PM_{tot}) varied in the range of 35-350 mg/MJ_{fuel} for wood log stoves and 15-45 mg/MJ_{fuel} for the pellet stoves, (Boman, 2005). The emission concentration from different biomass fuels (for example from the combustion of both softwood pellets and hardwood pellets) has been investigated by Fachinger *et al.* (2017). Olsson (2006a) mentioned that the emissions from softwood pellets in residential appliances were generally low and are environmentally well suited to replace traditional firewood and oil boilers.

Wood pellets as biomass fuel are very practical to use and provide an alternative for a more controlled and optimized combustion process with low emissions of products from incomplete combustion (PIC's) (Boman, 2005). Wood pellets have been one of the most attractive forms of biomass conversion as a standardized fuel and play an important role in various countries. In 2017, the world pellet consumption has increased by more than 13% or about 31.39 million tonnes compared to its level of 2016 as shown in Figure 1.5 (Bioenergy Europe, 2018). The available data shows that the pellet consumption in industrial and residential/commercial sectors increased 2.1 and 1.49 million tonnes respectively. Figure 1.5 shows that the pellet consumption in South America is only available in 2014 and 2015 with

the capacity of 58 and 90 thousand tonnes respectively. As a biomass fuel, the wood pellet is considered of low emissions, environmentally friendly and suitable to use in domestic applications and industry (Olsson, 2006a; Olsson, 2006b). Because of its low emission and affordability, the demand for wood pellets has increased in many countries as a residential heating energy source (Olsson, 2006b). Pa *et al.* (2013) stated that by replacing firewood with wood pellets such as in British Columbia (BC) residential heating will significantly lowering the impacts on human health, ecosystem quality, climate change, and primary energy consumption.

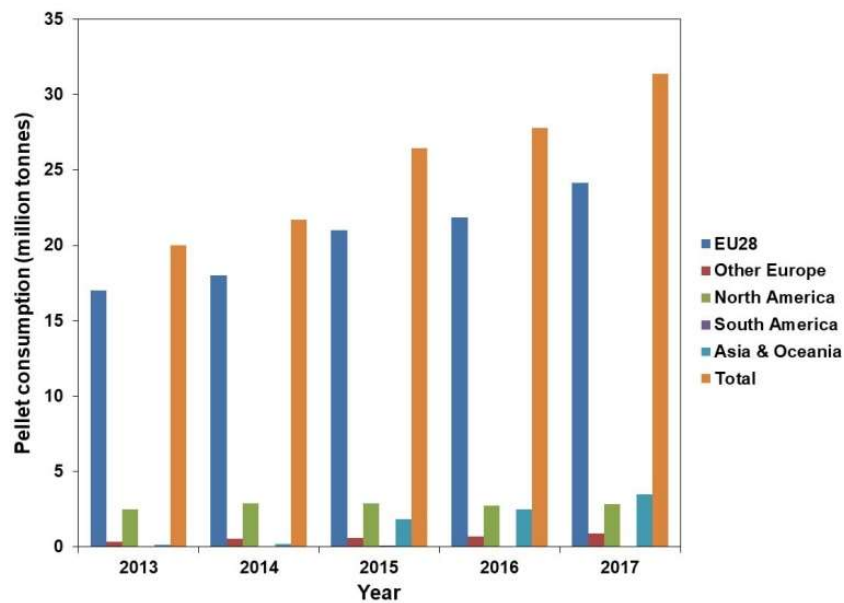


Figure 1.5. Evolution of pellet consumption in the world by regions (Bioenergy Europe, 2018).

Although the utilization or production of wood pellets requires adequate technology, the relative benefits from their storage and transportation (Jenkins, 2010) make them a very compelling fuel carrier. Once processed, the wood pellets are stable, denser and with lower moisture than comparable fuels such as wood chips. As wood pellets are easier to supply to the market, their production might be economical at a commercial and industrial scale (Ravichandran, 2013). However, the use of energy derived from wood pellets, needs to be considered regarding the availability and costs. In the economic and environmental scenarios, based on the Preference Ranking Organization Method for Enrichment and Evaluation (PROMETHEE) rankings shows that wood pellets are the best energy source among other biomass sources observed (Sultana and Kumar, 2012). Pellets supply, pricing and the requirement of equipment maintenance need to be considered in using wood pellet boiler systems especially suited to application in domestic consumption due to the range of end-user problems that can occur such as

unintentional system shut down, noise, excessive maintenance and difficulties in handling the pellets (Thomson and Liddell, 2015).

As previously mentioned regarding the energy utilization, there are several ways to harness the energy from biomass such as through the combustion process. Efficient combustion occurs when all the fuel is converted into useful energy. That depends on several conditions such as the mixture of fuel and air, and the specific design of the equipment used for the combustion process. One parameter that shows combustion quality is temperature. The importance of high temperature ($>850\text{ }^{\circ}\text{C}$) in the bed zone with intensive, air rich and well-mixed conditions with isothermal conditions for 0.5-1.0 s in the post-combustion zone were illustrated as requirements to obtain complete combustion conditions of wood pellets (Boman, 2005).

Fuel-air mixing could be improved by applying various methods. For example, swirling flow provides enhanced fuel mixing with air flow and completes the combustion of volatiles (Suzdalenko *et al.*, 2012). The combustion process in the wood boiler has been applied in the real world, and several studies are dealing with this condition. For example, the eco-labelled wood boiler studied by Olsson (2006a) showed a very high combustion efficiency. The impact of the emission on the health and environment produced from wood combustion in a boiler were low, therefore the boiler is recommended as an environmentally sound option for residential firewood combustion (Olsson, 2006a).

The qualities of biomass feedstocks concern the cost, distribution, mass, physical, and chemical characteristics in which both moisture and energy content are key parameters in the evaluation of biomass (Milne *et al.*, 2002). The composition of biomass feed will also influence the biomass feedstocks. As an example the increased durability up to 99% of canola meal pellets resulted of adding a binder (5 wt%) and the inherent protein (40 wt%) and lignin (12 wt%) content in the feed. The effects of moisture content, additives, applied load and temperature on the mechanical properties of canola meal pellets was found to significantly affect the pellet quality (Tilay *et al.*, 2015).

1.1.2 Research opportunities

Some problems can occur in converting the wood pellets into useful energy such as high gas emission produced from inappropriate combustion of wood pellets in the boiler, stove or furnace. Several gas emissions such as high CO and particle emissions are an indication of the incomplete combustion and fuel bed instability. These phenomena provided the opportunity to conduct the investigation for improving and optimize the apparatus and methods applied in the combustion process.

Wood pellets are often combusted in a furnace within the grate, as this grate becomes an essential part of the contribution on the quality of the combustions besides thermal load, split ratio, and excess air. These conditions can be considered and managed to create the good combustion of wood pellets in the boiler to produce low emissions, maintain good fuel bed stability and high efficiency.

1.2 Objectives

The combustion of wood pellets for applications such as heating is developed, in order to improve its efficiency and reduce its environmental impact. Taking into account the current knowledge, the main objective of the present work is to study the combustion of wood pellets in a 20 kW fixed bed combustor. Within this study several specific objectives are investigated:

- 1) The mass loss and kinetics parameter of pine wood particles using TGA device.
- 2) The mass loss and elemental analysis of pine wood pellets in a small scale reactor.
- 3) The influence of the thermal load, grate area, excess air, and the split ratio of primary to the secondary air on the fuel bed temperature, gas emission, efficiency and ashes on the grate.
- 4) The influence of the different parameters on the stability of the fuel bed and the onset of instabilities.

1.3 Research methodology

This research activity was initiated from the observation of the problems in the related fields. As the problem observation, was a motivation to conduct the literature review and identify the specific problem, then followed by developing the research hypothesis.

Through the hypothesis phase, the possible solution was developed, followed by the apparatus and experimental design and set up.

The research methodology to conduct this research activity is schematically shown in Figure 1.6. This research was conducted in the Laboratory of Energy and Fluids at the Mechanical Engineering Department of the University of Minho.

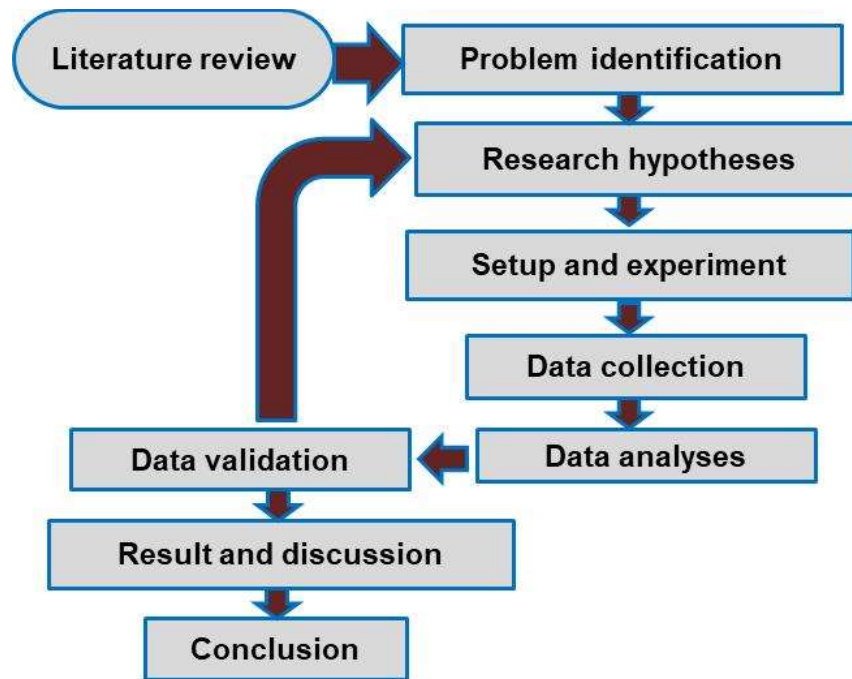


Figure 1.6. Flow chart for research activities.

1.4 Structure of the thesis

The structure of this thesis is organized in seven chapters, as follows: (1) Introductions; (2) Literature Review; (3) Materials and methods; (4) TGA analysis of pine wood particles; (5) Mass loss of pine wood pellets in a small scale reactor; (6) Emissions and temperatures measurement in a fixed bed combustor; and finally, (7) Closure.

Chapter 1 presents the motivation of this work, the objectives of this study, research methodology, the structure of the thesis and the contribution of this work.

Chapter 2 describes the literature review including the previous studies on wood pellets, biomass fuel, the combustion of biomass fuel, and fuel devolatilization.

Chapter 3 discusses the materials and methods including the facility, material, and the methods applied in this study. The material used was pine wood pellet, the equipment used includes TGA devices, small scale reactor, boiler, and gas analyzer devices.

Chapter 4 presents the experiment of TGA analysis of pine wood particles.

Chapter 5 presents the experiment of mass loss of pine wood pellets in a small scale reactor.

Chapter 6 presents the experiment of emissions and temperatures measurement in a fixed bed combustor, with the application of the Taguchi method.

Chapter 7 details the main conclusions and opportunities for future work.

1.5 Contributions of this work

From this study we can provide some contributions referred to the application of wood pellets combustion behavior, as follows:

- The application of a higher heating rate on wood particles in TGA analysis may provide important information on thermal decomposition and kinetic parameters.
- Different residence time and temperature applied to the thermal decomposition of wood pellets in a small scale reactor may provide knowledge about the devolatilization process in a commercial fuel (wood pellets).
- Develop the Taguchi method for experimental planning to assess the influence of Power, EA, GA, and SR on the emissions and fuel bed temperature, which can be used to control ashes sintering.
- A contribution to understanding the burning rate of wood pellets in a grate with a gravity feeding system.

2. LITERATURE REVIEW

In this chapter, a literature review on wood pellets combustion is presented and discussed.

2.1 Major literature sources on wood pellets combustion

Combustion of wood pellets and different combustion appliances has been the object of various studies. Four types of wood pellets such as a pruning fruit tree, two commercial pellets from pine wood and Pyrenean Oak were analyzed by Arranz *et al.* (2015). Several parameters such as heating value, durability, bulk density, ash characterization and ash melting temperature were determined and analyzed in a domestic pellet stove. This study shows that pine wood pellets have better characteristics for their domestic use in small-sized stoves due to the lower ash content and higher heating value.

Garcia-Maraver *et al.* (2014) conducted a study on the fuel quality and the gaseous and particulate matter (PM) emissions in a domestic boiler fired with five different types of pellets such as two commercial pellets from pine residues, cork residues, olive wood, and olive pruning. The authors measured various parameters including thermal loads, gaseous and PM emissions, ash composition in PM emissions, (characterized both morphologically and chemically), bulk density and durability indexes, and particle densities. This study reveals that gaseous and PM emissions are significantly affected by fuel type.

Pine pellets, industrial wood wastes, and peach stones were combusted in a domestic boiler to study and evaluate the combustion and emission characteristics of the boiler (Rabaçal *et al.*, 2013). This study shows that the type of pellets significantly affects the boiler operating conditions, the emissions characteristics, although the boiler thermal efficiency is not negatively affected.

A study on the pellet quality and compression characteristics of canola meal was reported by Tilay *et al.* (2015). Several fuel characteristics were analyzed such as protein, fiber, fat, lignin, feed moisture content, binder, lubricant, in addition to densification process parameters. This study shows that by pelletization of canola meal with moisture-resistant and reasonable fuel characteristics provides a promising alternative for the utilization as an alternative source of renewable energy.

The air-dried distilled spirit lees and its char in an oxygen-enriched laboratory scale, fluidized bed combustion, were performed by Zhu *et al.* (2015) to study the influence of water vapor in the combustion atmosphere on NO_x emissions. This work shows that in a combustion atmosphere with excessive water vapor, this will inhibit the release of fuel-N in the devolatilization stage, promote the

formation of some reducing gases and also shortened the reaction time for homogeneous and heterogeneous NO_x reduction.

The quality of pellets from raw material (leaves, pruning, and wood) and different olive tree pruning residues was investigated by Garcia-Maraver *et al.* (2015). In this study, the physical and mechanical parameters, moisture content, compression, and temperatures for the pelleting conditions was analyzed. This study shows that low moisture content (9%), short compression lengths (20–24 mm), and temperatures above 40 °C were the best pelleting parameters observed. Biomass fuel of beechwood was studied both experimentally and numerically under high radiative heat flux (Pozzobon *et al.*, 2014). Sample diameter, incident heat flux, initial moisture content, char, temperature, and reflectivity were assessed. This study shows the visible phenomena occurring inside the degrading sample, where the drying phase is followed by pyrolysis.

Combustion of four biomass materials (willow, miscanthus, pine, and segregated waste) with different fuel properties was experimentally investigated in a fixed bed under fuel-rich conditions by Ryu *et al.* (2006). The study assessed the influence of gas composition, bulk density, particle size and analyzed the combustion characteristics by interpreted with the ignition front speed, burning rate, mass loss, equivalence ratio, and temperature gradient. This study reveals that the ignition front speed and the burning rate increased with increasing air flow.

Qiu (2013) studied the combustion of biomass fuel in a domestic biomass boiler with a primary and secondary air supply to investigate the flue gas emissions, particularly pollutants CO, NO_x, and particle emissions. The authors tested three types of biomass fuels such as wood pellets, miscanthus pellets, and straw pellets and, also, the temperature and gas emissions. It shows that biomass flue gas cleaning is highly concerned, while the ceramic filter cleaning technology proved to be very effective to meet the environment targets.

The parameters of the grate furnaces were discussed by Loo and Koppejan (2008) and Burkhard and Russell (2010). Different grates are applied in the grate furnace technologies such as fixed grates, travelling grates, moving grates, rotating grates, and vibrating grates (Loo and Koppejan, 2008).

The study of combustion and emissions of biomass pellets in a prototype pellet furnace with 7–32 kW capacity using four biomass pellets such as one grass pellet and three wood pellets was investigated by Roy *et al.* (2013). The study reveals that the grass pellets can successfully be combusted with similar performance and emissions to those of other wood pellets if burned in appropriate combustion installations.

Krugger-Emden *et al.* (2013) showed that mixing of wood pellets is influenced by several parameters such as particle mass, the stroke length, particle shape, and the motion pattern, while the stroke velocity only has a minor effect on mixing and the amount of particles discharged from the grate.

The numerical and experimental studies of Klason and Bai (2007) in a small-scale wood pellet furnace were compared while applying secondary and tertiary air jets. The flame temperature and species concentrations, including CO and NO were analyzed. It reveals that the fuel-NO path is responsible for the rapid NO increase and the high NO peak near the fuel bed.

The behavior of dynamic combustion of a BioGrate boiler was investigated by Boriouchkine *et al.* (2014). This study shows that combustion dynamics is dependent not only on the air flow but also on the fuel. Using fuels with a lower devolatilization temperature allows for increased drying rate. Meanwhile, drying can be enhanced by increasing the air flow rate.

Combustion of wood pellets in a High Temperature Air Combustion (HTAC) furnace, with rich and diluted air and applied high temperature air combustion to examine the mass loss and emission concentration, was conducted by Dinu (2006). This study shows that the mass loss rate of pellets increases with the temperature. The mass loss, emission concentrations (CO₂, CO, and NO_x), the ignition time and flame behavior was measured at two oxidizer temperatures and oxygen concentration. Devolatilization behavior of fuel pellets of wood and wood/coal in a fluidized bed was studied by Miccio *et al.* (2013). During the devolatilization, two events were observed in this study such as the eruption of a hot bubble and the generation of flames at the bed surface. This study shows that the trend of the devolatilization time is consistent with the volatile content of the fuel, and two kinds of events can be distinguished during devolatilization including the eruption of a hot bubble produced by bursting a submerged fuel-rich bubble and the generation of flames at the bed surface. A study on the devolatilization behavior including ignition, flame temperature, flame life-time, devolatilization time of different fuels of coal from lignite to anthracite and wood was investigated by Bu *et al.* (2015). The study reveals that for all the fuels tested, the ignition-delay time is much longer, and the flame temperature is lower in the O₂/CO₂ atmosphere than in an O₂/N₂ atmosphere. The devolatilization, activation energy and the frequency factor (pre-exponential factor) for different heating rates were evaluated by Soria-Verdugo *et al.* (2014). With the TGA tests, this study concluded that the activation energy and the frequency factor should be carried out at high heating rates, in which a high heating rate contributes to the better application of the Distributed Activation Energy Model (DAEM).

Several parameters such as the flame stability limits, flame temperature, pressure drop, and pollutant emissions were measured from alumina pellets of different diameters as they were burned in a double-

layer fuel bed packed (Gao *et al.*, 2012). This study reveals that the unburned hydrocarbon emissions decreased with increased alumina pellet diameter.

Measurement of the oxidation behavior of particulate matter (PM) from the combustion zone of a domestic pellet-fired boiler was conducted by Fernandes *et al.* (2013). Oxidation tests indicate that the PM samples obtained from locations near the visible flame boundary were significantly less reactive towards O₂ than those sampled from locations along the burner axis.

Pine chips and pine pellets were burned in a 50 kW domestic biomass boiler to analyze the influence of the excess air and rate of secondary air on the combustion efficiency and emissions (Serrano *et al.*, 2013). The work shows that the excess air reduces the gaseous emissions but also the boiler efficiency while increasing the rate of secondary air had no effects on efficiency but reduced the CO emissions below the standardization limit (EN 14785).

The experimental study of the effect of pellet length on utility and combustion temperature was conducted by Sikanen and Vilppo (2012). Several parameters were measured in this study such as combustion temperature and stability and flue gas temperature. It shows that increasing the length of the pellets from 5.8 mm to 13.1 mm decreased the average burning temperature by 31% and flue gas temperature by 25%.

Han *et al.* (2008) studied the combustion and emission behavior of cedar pellets fuel in a fluidized bed combustor from the effect of the particle size of alumina sand. The authors analyzed the temperature profile, fluidization velocity, and bed material particle size on emission and combustion efficiency. This study shows that high temperature can improve combustion efficiency and decrease CO emission. A CFD modelling of thermal conversion and packed bed compaction in biomass combustion was conducted by Gómez *et al.* (2014). This study modeled the ignition rates, maximum temperatures, and the transient evolution of bed height. The model presents the comparison of the drying, devolatilization, and char thicknesses for different air mass fluxes shows reasonably good tendencies even though the values are excessively high.

2.2 Biomass

Biomass is a cellulose material which can be broadly classified into two categories: woody and nonwoody biomass. Woody biomass may be further split into softwoods and hardwoods. Wood fuel includes round wood or cordwood, limb wood, wood chips, bark, sawdust, forest residues, charcoal, pulp waste, and spent pulping liquor (Borman and Ragland, 1998).

Softwoods are evergreen trees with needles often called conifers because their seeds are formed in cones (Borman and Ragland, 1998). They include species such as Douglas fir, pine, spruce, beech and oak, miscanthus (Fachinger *et al.*, 2017). The hardwoods are generally denser compared to the softwoods and include species such as apple, ash, bangkirai, birch, beech, cherry, hickory, oak, olive, plum, sugar maple (Fachinger *et al.*, 2017). Hardwoods have shorter fibers and are more porous, making it more difficult to pulverize than coal (Borman and Ragland, 1998). Bark differs from hardwood and softwood in both structure and composition. Structurally, bark appears more spongelike than the organized fiber. It also contains more resin and more ash than wood (Borman and Ragland, 1998). Softwood and hardwood show different behavior in terms of emissions, such as the emission of organic carbon (OC) which is usually higher for softwood than for hardwood in residential devices. The same condition applies for higher PAH emissions in residential wood combustion (Vicente and Alves, 2018). In addition, the rate at which the hardwood and softwood release their energy can be different, as that for hardwood is usually much slower than for softwood (Jenkins, 2010).

Dry wood consists of cellulose, hemicelluloses, lignin, resin (extractives), and ash-forming minerals. Cellulose ($C_6H_{10}O_5$)_n is a condensed polymer of glucose ($C_6H_{12}O_6$) (Borman and Ragland, 1998). The fiber wall consists mainly of cellulose and represents 40 to 45% of the dry weight of wood. Hemicellulose ($C_5H_8O_4$)_n (Ferreira, 2016) consists of various sugars other than glucose that encase the cellulose fibers and represent 20 to 35% of the dry weight of wood (Borman and Ragland, 1998). Lignin ($C_{11}H_{12}O_4$)_n (Ferreira, 2016) is a nonsugar polymer that gives strength to the wood fiber, accounting for 15 to 30% of its dry weight (Borman and Ragland, 1998). Wood extractives include oils, resins, gums, fats, waxes, etc., that originally do not exceed a few percents. However, extractives in bark range from 20 to 40%. The constituents which make up the ash when wood burns amount to 0.2 to 1% by weight and are mainly calcium, potassium, magnesium, manganese, and sodium oxides and lesser amounts of other oxides such as iron and aluminum. The mineral matter is dispersed throughout the cells in molecular form. The ash from the bark is greater than from wood and typically is 1 to 3% (Borman and Ragland, 1998).

Biomass fuels are a source for the combustion besides fossil fuel, and combustion can be applied to biomass feedstock with water contents up to 60% (Nussbaumer, 2008). The pollutant and deposit formation, corrosion, and ash in carbon, hydrogen, and oxygen are undesired. There are most relevant constituents in native biomass such as nitrogen as a source of NO_x, and ash components, for example, K and Cl as a source of KCl that leads to particulate emissions (Nussbaumer, 2008). Native wood is domestic wood which grows naturally (Bishop, 2001; Hansen *et al.*, 2009; Nichols and Vanclay, 2012).

Native wood is the most favorable biofuel for combustion due to its low content of ash and nitrogen (Nussbaumer, 2008). While wood is well-suited for household heating and other energy production as well as for larger plants, herbaceous biomass is reserved for larger plants. The same condition is true for urban waste wood and demolition wood. Efficient combustion is important, in order to limit the contaminated biomass to combustion plants, and with efficient flue gas cleaning for the abatement of toxic pollutants such as heavy metals and chlorine compounds (Nussbaumer, 2008). The driving force and potential for biomass combustion for energy purposes is both the CO₂ neutrality of the sustainably cultivated biomass or the use of biomass residues and waste. As renewable resources, large potentials of both native biomass and biomass wastes are still untapped and allow a relevant increase of sustainable bioenergy use in the future. Combustion is the most important technology available today for biomass to continue to meet energy demand, though improvements in efficiency, emissions, and cost for further exploitation are required (Nussbaumer, 2008).

2.2.1 Biomass conversion technologies

Biomass is one of the renewable energy sources to use as useful energy mostly for direct heat (in a household and industry) and in power plants.

The methods of converting biomass into useful energy include several routes such as biological, chemical and thermochemical conversion (flash pyrolysis, gasification, carbonization, and combustion) (Loo and Koppejan, 2008). Thermochemical conversion technologies show different stages of development, where combustion is the most developed and most frequently used (Loo and Koppejan, 2008). Figure 2.1 depicts an overview of thermochemical conversion technologies, products, and potential end uses.

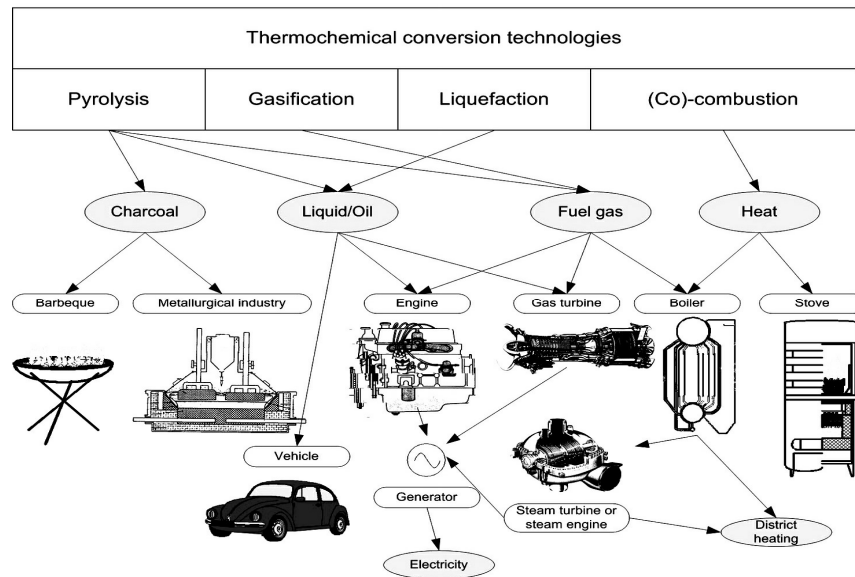


Figure 2.1. Thermochemical conversion technologies (adapted from Loo and Koppejan, 2008).

2.2.2 Contribution of biomass in the renewable sector

Biomass can contribute to reducing the consumption of fossil fuel, as fossil fuel is a limited resource and being rapidly depleted due to the population and economic growth, among other issues. Besides, biomass development can create more jobs and also reduce the impact on the environment (Nunes *et al.*, 2016). Approximately 60% of the need for process energy in pulp, paper, and forest products is obtained directly from biomass combustion (Chum and Overend, 2001). In addition, in the United States, among other renewable resources, biomass use as a primary energy source (approximately 43%) is just behind hydropower with 51%. Besides, biomass has the highest potential to contribute to the energy needs of modern society for both the industrialized and developing countries worldwide (Demirbas *et al.*, 2009), and also of its cost-effectiveness.

2.2.3 Pellets

Pellet is wood densified into a small cylindrical mass (Bjerg *et al.*, 2011; Obernberger and Thek, 2010). Wood pellets are a certified product ranging from 6-12 mm in diameter, and a typical length of 10-40 mm. The lower heating value of pellets varies between 10.8 and 18 MJ/kg (as received), and the bulk density is in the range of 600 kg/m³, may also be between 500 and 680 kg/m³. In addition, the water content is between 5-10% (Bjerg *et al.*, 2011). The respective parameter of wood pellet depends on the quality of the respective pellet product, with the higher values referring to premium pellets (Bjerg *et al.*,

2011). Pellets can be used for automatically charged stoves and boilers because of their good feeding and flowability, uniform properties. Consequently, pellet stoves and boilers for domestic use or applications are of easy operation (Loo and Koppejan, 2008).

With the oil crisis in the 1970s, pellets were introduced in Europe and North America as a fuel substitute for solid fuels and oil (Bjerg *et al.*, 2011). Since the 1990s wood pellets production has become commercially viable and has grown steadily throughout the last years. Wood pellets are used in various facilities such as in large-scale plants as well as in medium-sized plants and households. The quality of the wood pellets is varied as well, with different pellet qualities required for different applications. The material of the pellets and the characteristics of the respective plant will determine their usefulness in the industrial segment such as dedicated biomass plants as well as in co-firing installations (Bjerg *et al.*, 2011).

Regarding the standardization, throughout the years a wide range of wood pellet standards has been developed. The standards were developed independently in different regions, both in the EU and the US. The European Union has introduced the first EN standards (EN 14961 and EN 15234) in 2010. Besides other standards in place include DIN 51731/DINplus in Germany/Netherlands/Belgium, ÖNORM M 7315 in Austria and SS 187120 in Sweden, (Bjerg *et al.*, 2011). In 2010, AEBIOM has launched the new European certification system *ENplus*, managed by the European Pellets Council, which has reached an international expansion.

2.2.3.1 Characterization of raw materials and pellets

The characteristics and quality of biomass fuel are mostly dependent mainly on the raw materials and the pre-treatment technologies applied (Loo and Koppejan, 2008). For example, the moisture content of the fuel may vary from 25 to 60wt% (w.b.) for bark and sawmill side-products or drop below 10wt% (w.b.) for pellets and dry wood-processing residues. Monedero *et al.* (2015) revealed that the swelling of the pellet occurs when the pellet moisture content is higher than 10 wt.%. With suitable pre-treatment technologies, fuel quality can be influenced and improved, though with a cost penalty. On the other hand, various combustion technologies are available according to the fuel quality. In this context, it must be noted that less homogeneous and low-quality fuels require more sophisticated combustion systems. Because of this condition and economy of scale reasons, only medium and large scale systems are suitable to utilize low-grade biomass fuels. Thus, the smaller the combustion plant, the higher the demands concerning fuel quality and fuel homogeneity (Loo and Koppejan, 2008).

The main components of biomass fuels consist of C, H and O. Carbon and hydrogen are oxidized during combustion by exothermic reactions to form CO₂ and H₂O (Loo and Koppejan, 2008). The organically bound oxygen released through the thermal decomposition of biomass fuels covers part of the overall oxygen required for the combustion reactions taking place, and the rest is supplied by air injection. In comparison to coal, C in biomass fuels is present in partly oxidized forms, which explains the low HHV of biomass fuels. In addition, biomass fuels contain a larger variety of inorganic materials than coal (Saidur *et al.*, 2011). The C concentration in wood fuels (including bark) is higher than those of herbaceous biomass fuels, which justify the slightly higher HHV of wood fuels. On the other hand the carbon concentrations of olive residues are higher than those of wood fuels, which results in a higher HHV (Loo and Koppejan, 2008).

➤ **Carbon, hydrogen, oxygen and volatiles content of pellets**

Table 2.1 summarizes the expected range of C, H, O, and volatiles concentrations in different biomass fuels (Oberberger and Thek, 2010), although in the applicability of the materials for the pelletization is not influenced by these elements. However, the concentrations of these elements do have an effect on the calorific value, and the volatiles release influencing the combustion behavior. For different types of biomass, the high fixed carbon and volatile matter increase the heating value (Saidur *et al.*, 2011). Moreover, C and H tend to raise the heating value compared to oxygen. The concentration of carbon, hydrogen, and oxygen are the main components of biomass fuels (since cellulose, hemi-cellulose, and lignin consist of these elements), whereby carbon and hydrogen are the main elements responsible for the energy content due to the exothermic conversion to CO₂ and H₂O, during combustion (Oberberger and Thek, 2010).

The amount of volatile matter in biomass fuels is higher than in coal and varies between 70 and 86 wt% (d.b.) (Loo and Koppejan, 2008), although the specific value depends upon, the actual source of biomass. Such a high content of volatiles leads to fast devolatilization. The volatiles have a strong impact on the thermal degradation and combustion behavior of the biomass, because the gases formed and burned in homogenous gas phase reactions, and the remaining charcoal burns relatively slowly in heterogeneous combustion reactions (Oberberger and Thek, 2010). prEN 15104 sets the standards for C and H in biomass fuel. Approximated, the oxygen content can be determined as the difference between 100 minus the sum of carbon, hydrogen, sulphur, nitrogen, and ash in wt.% (dry basis). The content of volatile is determined according to EN 15148 (Oberberger and Thek, 2010).

Table 2.1. Concentrations of C, H, O and volatiles matter in different biomass materials.
(Loo and Koppejan, 2008 cited by Obernberger and Thek 2010).

Fuel type	C	H	O	Volatiles
	Wt.% (d.b.)	Wt.% (d.b.)	Wt.% (d.b.)	Wt.% (d.b.)
Wood chips (spruce, beech, poplar, willow)	47.1 – 51.6	6.1 – 6.3	38.0 – 45.2	76.0 – 86.0
Bark (coniferous trees)	48.8 – 52.5	4.6 – 6.1	38.7 – 42.4	69.6 – 77.2
Straw (rye, wheat, triticale)	43.2 – 48.1	5.0 – 6.0	36.0 – 48.2	70.0 – 81.0
Miscanthus	46.7 – 50.7	4.4 – 6.2	41.7 – 43.5	77.6 – 84.0

➤ Nitrogen, sulphur and chlorine content of pellets

The Standard prEN 14961-2 limits the acceptable levels of nitrogen, sulphur and chlorine in pellets. Compared to the herbaceous biomass, the limiting values of the standard are based on wood as the reference input material for pelletization, which indicates significantly lower concentrations of nitrogen, sulphur and chlorine. Although such elements do not have any influence on the palletization process, they should be taken into account when searching potential raw materials. By this condition, one should avoid the use of contaminated materials or materials that are not biological for the production of pellets. The presence of such elements can be the result of chemical contamination by, for example, insecticides, adhesives, glues, lacquers, dyestuff, wood preservatives or of admixing agricultural biomass (Obernberger and Thek, 2010).

Nitrogen is easily volatile and is almost completely released to the flue gas during combustion to form the N_2 and NO_x . The formation of NO_x is mostly dependent on the nitrogen content of the biomass fuel. Sulphur and chlorine are also very volatile gases and are mainly released into the gas phase during combustion. In gas phase reactions of aerosols, they are then formed together with potassium and sodium (sulphates, chlorides) as well as SO_x and HCl. There are limitations concerning these elements due to technical as well as environmental issues (Obernberger and Thek, 2010). In combustion, the concentrations of nitrogen, sulphur and chlorine have different impacts. High levels of nitrogen, sulphur, and chlorine boost or increase the emissions of NO_x , SO_x and HCl. Chlorine itself also augments the formation of polychlorinated dibenzodioxins and furans (PCDD/F). Moreover, the combustion products of chlorine and sulphur have corrosive effects and are of great relevance in fouling/deposit formation. Nunes *et al.* (2016) revealed that the presence of Cl makes as active oxidation, and as the main factor that is responsible for accelerated corrosion rates in the boiler tubes. There are several conditions that contribute to corrosion from biomass combustion such as: deposits of ash containing alkali metal; chlorides on the heating exchange surfaces; the sulfation of the deposits in contact with SO_2/SO_3 in the

gases that generate HCl through the metal surface (Nunes *et al.*, 2016) and large amounts of potassium chloride that vaporize in combustion which represent a high deposition and corrosion risk (Wang *et al.*, 2017).

➤ **The higher heating value, lower heating value and energy density of pellets**

The higher heating value is basically defined as the energy content on a dry basis (Saidur *et al.*, 2011). The HHV is a measured value of the specific energy of combustion for a mass unit of a fuel burned in oxygen (Obernberger and Thek, 2010). The HHV of raw material should be as high as possible as it determines the energy density of the pellets. The HHV is purely dependent on the material used, i.e. the chemical composition of the raw material and can therefore not be influenced (Obernberger and Thek, 2010). According to ÖNORM C 1138, HHV is the heat released during combustion per mass unit fuel under the constraints that the water formed during combustion is in a liquid phase and that the water and the flue gas have the same temperatures as the temperature of the fuel prior to combustion (Loo and Koppejan, 2008). The HHV of biomass fuels usually ranges between 18 and 22 MJ/kg (d.b.) (Loo and Koppejan, 2008), the value for woody biomass (including bark) lies around 20.0 MJ/kg (d.b.) and for herbaceous biomass is around 18.8 MJ/kg (d.b.) (Obernberger and Thek, 2010). The HHV can be calculated by using the following empirical formula (Eq. 2.1) (Loo and Koppejan, 2008).

$$\begin{aligned} \text{HHV} = & 0.3491 X_C + 1.1783 X_H + 0.1005 X_S - 0.0151 X_N \\ & - 0.1034 X_O - 0.0211 X_{\text{ash}} \end{aligned} \quad (2.1)$$

where, X is the mass concentration of carbon (C), hydrogen (H), sulphur (S), nitrogen (N), oxygen (O) and ash.

The lower heating value (LHV) is defined (according to ÖNORM C 1138) as the heat released during combustion per mass unit of fuel under the constraints that the water formed during combustion is in a gaseous phase and that the water and the flue gas have the same temperature as the fuel prior to combustion (Loo and Koppejan, 2008). The lower heating value depends mainly on the HHV, moisture content, and the content of hydrogen in the fuel. Other substances such as nitrogen, oxygen or ash content considered has a small influence (Obernberger and Thek, 2010). The calculation for LHV is by subtracting the energy needed to evaporate the moisture content of the fuel (Saidur *et al.*, 2011) or it can be calculated from the HHV (Obernberger and Thek, 2010). The lower heating value calculated based on the moisture content and the hydrogen content of the fuel as input parameters is described in Eq. (2.2) (Loo and Koppejan, 2008; Obernberger and Thek, 2010).

$$\text{LHV} = \text{HHV} \left(1 - \frac{M}{100}\right) - 2.447 \frac{M}{100} - \frac{X_H}{200} 18.02 \times 2.447 \left(1 - \frac{M}{100}\right) \quad (2.2)$$

where LHV is lower heating value (MJ/kg) (w.b.); HHV is higher heating value (MJ/kg) (d.b.); M is moisture content (wt.%) (w.b.) and X_H is hydrogen content (wt.%) (d.b.). For woody biomass, for example, pellets, the content of hydrogen is around 6.0 wt.% (d.b.), and the value for herbaceous biomass is around 5.5 wt.% (d.b.) (Obernberger and Thek, 2010). The LHV is also calculated according to EN 14961-1 standard, as formulated in Eq. (2.3). Comparing the results obtained for the two equations produce nearly the same results.

$$\text{LHV} = \left[\text{HHV} - 0.2122 X_H - 0.0008 (X_O + X_N) \right] \left(1 - \frac{M}{100}\right) - 2.443 \frac{M}{100} \quad (2.3)$$

where X_O is the oxygen content in wt.% (d.b.) and X_N is the nitrogen content wt.% (d.b.). It can be concluded that the energy density of biomass is lower compared with fossil fuels, and the low energy density is one of the disadvantages of biomass fuel (Saidur *et al.*, 2011). The energy density can be calculated according to Eq. (2.4).

$$\rho_e = \text{LHV} \cdot \rho_b \quad (2.4)$$

where ρ_e is energy density (MJ/m³) and ρ_b is bulk density (kg (w.b)/m³).

2.2.3.2 Advantages of pellets

As stated, wood pellets have several advantages such as (being) easy to transport, affordable price, high energy density, low emissions, and to be considered carbon neutral, while the pelletization delivers solid biomass feedstock of high physical and mechanical homogeneity (Bjerg *et al.*, 2011). In terms of emissions, moving from 100% coal to wood pellets can decrease CO₂ emissions by 75-85%, taking into account all CO₂ emissions over the whole life cycle (Bjerg *et al.*, 2011). Overall, the CO₂ emissions related to wood pellet production and provision depend mainly on transport distances (sourcing of biomass, local or global distribution). The combustion of biomass with other fuels (co-firing) can have some advantages regarding the cost, efficiency, and emissions (Nussbaumer, 2008). Rybak *et al.* (2017) have shown that the co-combustion of 40% unburned carbon with lignite showed no indication of deteriorating the behavior of the combustion including ignition behavior, flame stability, NO_x and SO₂ emissions.

2.2.3.3 Applications of pellets

Pellets as a biomass fuel are used to produce energy in terms of heat through combustion process. Pellets can be burned in several appliances such as boilers and stoves or furnaces. As an example, a residential wood stove and a pellet stove was used by Fachinger *et al.* (2017) and a domestic wood pellet-fired boiler, with a maximum thermal capacity of 22 kW, was reported by Rabaçal *et al.* (2013). The use of wood pellets for energy purposes with boiler depends on the energy requirement. Typically for example for domestic use, the boiler capacity is below 100 kW_{th}; for micro-grids and by small scale industrial users 100 - 1,000 kW_{th}; and for large scale heating system > 1,000 kW_{th} (Oberberger and Thek, 2010). The numbers of pellets consumption in the EU-28 in 2016 and 2017 revealed that mostly pellets are applied in the residential sector (66.64 and 64.62%) following by the commercial sector (21.52 and 22.36) and CHP/industry (11.84 and 13.03), respectively. The total pellets consumption in those years is 13.5 and 15.1 million tonnes, an increase of about 11.59% (Bioenergy Europe, 2018).

Wood pellets can be used as co-firing with different fuels such as coal (Guo and Zhong, 2018) and pellets with industrial waste (Ferreira *et al.*, 2014). In Europe, the use of co-fired pellets is considered an attractive fuel for producing cost-effective renewable electricity and mitigating CO₂ emissions (Ehrig and Behrendt, 2013; Kokko, 2012) and reducing NO_x and SO_x emissions (Adams, 2013).

Bjerg *et al.* (2011) reveal that the demand for co-firing for electricity generation estimated in 2020 shows that an estimated growth of 5%, corresponds to 110 million toe and for 10%, it will correspond to 220 million toe in almost all the regions. In addition, the bio-coal pellets (black pellets) production and consumption are estimated to increase from 0.6 Mt in 2015 to 7.5 Mt/a by 2020 (Kokko, 2012).

2.2.3.4 Raw material for pellets

The main components of wood pellets are cellulose, hemicellulose, and lignin. The extracts (e.g. fats, proteins, resin, and oils) act as binders. The quality of wood pellets is visually associated with color. Dark pellets can contain bark, which indicates a lower quality compared to bright wood pellets, because bark yields higher amount of inorganic matter and thus higher amount of ashes (Bjerg *et al.*, 2011). Oberberger and Thek (2010) define three different types of pellets based on color: white pellets, brown pellets, and black pellets. White pellets are made of sawdust or planer shavings without bark, and brown pellets are made from raw materials containing bark (not to be confused with bark pellets, which are produced solely from bark). Then, black pellets are produced from exploded wood pulp or torrefied wood.

The different types of pellet classification which are depending on fuel specification and standardization as mentioned in Obernberger and Thek (2010). The *ENplus* certification scheme for three pellet quality classes (A1, A2 and B) based on the classes of ISO 17225-2 with different composition is presented in Table 2.2, and other standardization can be seen in the annex (Table A.1) (European Pellet Council, 2015).

Pellets can be made from a wide variety of raw materials (such as herbaceous biomass, waste or peat); all forthcoming definitions are to be regarded and the term densified biomass fuels denote both pellets and briquettes made of solid biomass fuels (Obernberger and Thek, 2010). Figure 2.2 shows wood pellets of four different qualities and the wood pellets in the lower right corner are of good quality without dust, produced from clean and dry wood (Hansen *et al.*, 2009). Then the pellets in the lower left corner are a mix of pellets produced from two different types of raw materials. This mix of pellets has caused heavy, and a glass-like slag formation in a small boiler because of the lower melting point of the ash. For the dark pellets pictured in the top left corner porous cinders were formed which caused the ash screw conveyor in a small boiler system to block up. The pellets shown in the top right corner had a very high content of dust and fine particles when delivered to the consumer. As a result, these pellets formed a bridge in the feeding system yielding poor combustion (Hansen *et al.*, 2009).

Table 2.2. Application of pellet standards ISO 17225-2.

Property	Unit	<i>ENplus</i> A1	<i>ENplus</i> A2	<i>ENplus</i> B	Testing Standard ¹¹⁾
Diameter	mm	6 ± 1 or 8 ± 1			ISO 17829
Length	mm	3.15 < L ≤ 40 ⁴⁾			ISO 17829
Moisture (as received)	w-%	≤ 10			ISO 18134
Ash (dry basis)	w-%	≤ 0.7	≤ 1.2	≤ 2.0	ISO 18122
Net Calorific Value (as received)	kWh/kg	≥ 4.6 ⁹⁾			ISO 18125
-Nitrogen (dry basis)	w-%	≤ 0.3	≤ 0.5	≤ 1.0	ISO 16948
Sulfur (dry basis)	w-%	≤ 0.04	≤ 0.05		ISO 16994
Chlorine (dry basis)	w-%	≤ 0.02		≤ 0.03	ISO 16994

According to Obernberger and Thek (2010) pelletization is the production of uniform bodies from powdery, granulous or coarse material of partly dissimilar particle size and the output is called a pellet. The term compressed wood is a fuel made by densification of wood particles (Obernberger and Thek, 2010). Depending on the dimensions, it is classified as wood pellets or wood briquettes. On the other hand, compressed bark (either as pellets or briquettes) is a fuel made by densification of bark particles.



Figure 2.2. Four different qualities of wood pellets (Hansen *et al.*, 2009).

2.3 Combustion

Combustion is defined as the oxidation of fuel with the release of energy (Döring, 2013) as heat, or both light and heat or oxidation followed by a slow low-heat release and no flame (Turns, 2000). Carbon and hydrogen are oxidized in the presence of oxygen to produce carbon dioxide and water, respectively (Döring, 2013). Turns (2000) described that the combustion can occur in either a flame or non-flame mode, and flames are categorized as being either premix flames or non premix (diffusion) flames. The difference between combustion in a flame and non-flame modes can be illustrated by processes occurring in a knocking spark-ignition engine. This phenomenon shows a thin zone of intense chemical reaction propagating through the unburned fuel-air-mixture. The thin reaction zone is commonly referred to as a flame. The phenomena behind the flame are the hot products of combustion. When the flame moves across the combustion space, the temperature and pressure rise in the unburned gas. Under certain conditions, rapid oxidation reactions take place at many locations within the unburned fuel, leading to very rapid combustion throughout the volume (Turns, 2000). Olsson, (2006a) stated that in wood pellets combustion, there are five sequential combustion stages including initial smouldering, early flaming, late flaming, after-flame smouldering and final glowing (Figure 2.3).



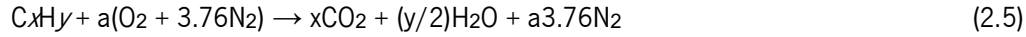
Figure 2.3. Five sequential combustion stages (Olsson, 2006a).

Figure 2.3 shows that during the short initial smouldering stage the concentrations of organic compounds ($\leq 7C$) were high and the main compounds emitted were methane, furan and ethene. In addition, the initial smouldering reflects pyrolysis of the original softwood, and high proportions of furan-related compounds, such as furan, 2-methylfuran and 2,5-dimethylfuran, were released. Meanwhile, the combustion during the early and late flaming stages was very efficient, with high concentrations of carbon dioxide, together with low concentrations of carbon monoxide and organic compounds ($\leq 7C$). The temperature between the pellets was 400-500 °C during early flaming and around 500 °C during late flaming. About 80% of the dry biomass was combusted during the flaming stages with the dominant organic compounds ($\leq 7C$) emitted were methane, ethene and ethyne. During the short after-flame smouldering stage the highest concentrations of organic compounds ($\leq 7C$), especially methane, ethane, ethene and benzene, were found. Regarding the emissions from the final glowing of softwood pellets were even lower than from flaming burning and very different in composition, with only methane, ethyne and benzene as prominent compounds. However, the CO emissions were higher for glowing than for flaming combustion. Besides, the formation of ethyne and benzene may be explained by the charcoal-like character of the glowing pellets, with a high carbon content (more than 80% compared to about 50% in dry wood) and a low hydrogen/carbon ratio. It is said that the combustion during the early and late flaming stages was very efficient and only low emissions of organic compounds ($\leq 7C$) were determined. The emissions from initial and after-flame smouldering were much higher and are likely to occur mainly as a result of improperly functioning pellet combustion appliances (Olsson, 2006a).

2.3.1 Reactant and product mixture

The stoichiometric quantity of oxidizer is defined as the right amount needed to completely burn a quantity of fuel. If supplied more than a stoichiometric quantity of oxidizer, the mixture is said to be a fuel lean mixture, while supplying less than the stoichiometric oxidizer results in a rich fuel mixture

(Turns, 2000). To determine the stoichiometric oxidizer- (or air-) fuel ratio (mass) one has to write simple atom balances, assuming that the fuel reacts to form an ideal set of products. For any hydrocarbon fuel, given by C_xH_y , the stoichiometric reaction can be defined as in Eq. (2.5).



where,

$$a = x + y / 4 \quad (2.6)$$

For simplification purposes the composition for air is 21% O_2 and 79% N_2 (by volume), i.e. that for each mole of O_2 in the air, there are 3.76 moles of N_2 . The stoichiometric air-fuel ratio can be found as in Eq. (2.7).

$$(A/F)_{stoic} = \left(\frac{m_a}{m_f} \right)_{stoic} = \frac{4.76 a M_a}{1 M_f} \quad (2.7)$$

where M_a is the molecular weights of the air and M_f is the molecular weight of the fuel. The equivalence ratio (Φ), is used to indicate quantitatively whether a fuel-oxidizer mixture is rich, lean or stoichiometric. The equivalence ratio is defined as in Eq. (2.8).

$$\Phi = \frac{(A/F)_{stoic}}{(A/F)} = \frac{(F/A)}{(F/A)_{stoic}} \quad (2.8)$$

From the definition above, it turns out that for fuel-rich mixture $\Phi > 1$, for fuel-lean mixture $\Phi < 1$, and for a stoichiometric mixture $\Phi = 1$.

In most combustion applications, the equivalence ratio is the single most important factor in determining a system's performance. Other parameters frequently used to define relative stoichiometry are percent stoichiometric air, which is related to the equivalence ratio as defined in Eq. (2.9a) and percent of excess air in Eq. (2.9b) (Turns, 2000).

$$\% \text{ stoic} = \frac{100\%}{\Phi} \quad (2.9a)$$

$$\% e = \frac{(1 - \Phi)}{\Phi} 100\% \quad (2.9b)$$

For efficient combustion to occur, most of the hydrocarbon combustion processes use an excess air. Therefore, it is common to relate the proportion of reagent mixing is not according to the fuel content, but due to the excess air for a more convenient and real perception. This relationship is called as the excess air ratio (λ) and corresponds to the inverse of the equivalence ratio as defined in Eq. (2.10) (Ribeiro, 2012).

$$\lambda = \frac{1}{\Phi} \quad (2.10)$$

and the percentage of excess air is defined as:

$$\% e = (\lambda - 1)100\% \quad (2.11)$$

2.3.2 Biomass combustion

Biomass combustion is defined as a complex process that consists of consecutive heterogeneous and homogeneous reactions. The main steps in biomass combustion are drying, devolatilization, gasification, char combustion, and gas phase oxidation. During the combustion process, time used is a variable of utmost relevance, and for each reaction, it depends on several parameters such as the fuel size, properties, temperature, and combustion conditions. Figure 2.4 shows the combustion process for a small biomass particle (Loo and Koppejan, 2008). Regarding the batch combustion of a small particle shows a distinct separation between a volatile and a char combustion phase with time. For the large particles, the phases overlap to a certain extent. Nonetheless, even for logwood furnaces, a certain separation of distinct combustion regimes with time can be found (Nussbaumer, 2008).

Automatic combustion systems are operated continuously, as the consecutive reactions take place simultaneously at different places in the furnace (for example in different sections on and above a grate). Through careful furnace design, the zones for different steps during combustion can be optimized. In addition, a distinct separation of different steps can be advantageous with respect to pollutant formation. Excess air ratio (λ) as the main combustion parameter describes the local ratio between the available and the stoichiometric amount of combustion air (Nussbaumer, 2008).

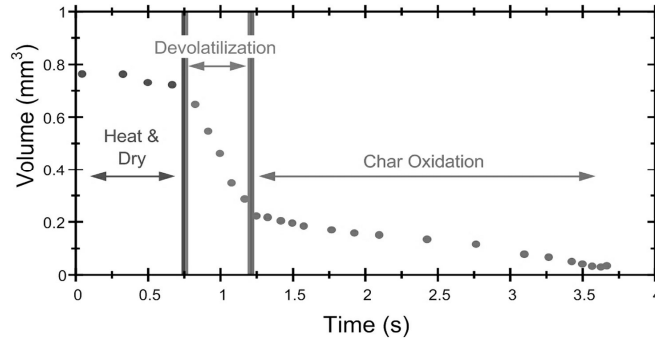
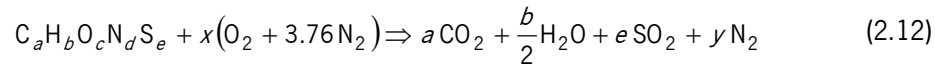


Figure 2.4. The combustion process of a small biomass particle (Loo and Koppejan, 2008).

2.3.2.1 Wood combustion theory

Because biomass has a wider spectrum of components when compared with hydrocarbons, the general reaction equation for combustion (Eq. 2.12) is modified to account for such differences (Eq. 2.13) (Ribeiro, 2012).



where a , b , c , d , and e relate to the moles' fraction of each constituent of the fuel knowable by elemental chemical analyzes. The x factor corresponds to the quantity of air involved in the reaction, also in moles, and can be calculated for the stoichiometry depending on the chemical composition of the fuel:

$$x = a + \frac{b}{4} - \frac{c}{2} + e \quad (2.13)$$

The factor y depends directly on x and relates to the amount of nitrogen which passes through the reaction without reacting (Ribeiro, 2012), see Eq. (2.14) (Flagan and Seinfeld, 1988):

$$y = 3.76x + d / 2 \quad (2.14)$$

The mass of air (m_a) can be calculated by multiplying the amount of molecular weights by x each species constituting the air, as follows:

$$m_a = x(M_{O_2} + 3.76M_{N_2}) \quad (2.15)$$

Complete combustion occurs when all oxidation becomes oxidizable components. The excess air ratio (λ) must then always be equal to or greater than 1 ($\lambda \geq 1$).

Some prerequisites for complete combustion are firstly a high combustion temperature, well-mixed combustion air and combustible gases, a small amount of excess air and a sufficiently long stay of the fuel molecules in the hot combustion zone. The combustion of wood is shown diagrammatically in Figure 2.5 and can be described as follows (Döring, 2013).

- 1) As the biomass enters into the combustion chamber, the fuel begins to be heated up due to reflected-radiation from the flame, fire bed, and combustion chamber walls.
- 2) From about 100 °C onwards, the fuel begins to dry out due to evaporation and removal of the water. In this process, the water is expelled both from the porous structure of the organic material and from the interior of the cells (at higher temperatures).
- 3) Whilst the biomass is still drying in its interior, the pyrolytic decomposition begins at a surface temperature of about 200 °C with the dissociation of the macromolecules (i.e. cellulose, hemicellulose, lignin), the volatile components (CO, CH₄, H₂O_{steam}, etc.), tars and organic vapors/aromatics being transported to the surface of the wood and released, leaving solid carbon (charcoal).
- 4) At about 500 °C, the solid carbon (about 15–20% of the biomass) begins to become gasified with carbon dioxide, water vapor, and oxygen to become carbon monoxide. At the same time, the volatile compounds (about 80–85%) become mixed with the oxygen supplied, starting a homogeneous combustion reaction of the gases.
- 5) The charcoal begins to oxidize at about 700 °C with a heterogeneous gas/solid reaction which is why this phase is much slower than the combustion of the gases in the combustion chamber. Depending on the fuel and heating system used, the temperatures in wood-burning systems rise up to 1,500 °C (2,000 °C max, but typically between 900 and 1,300 °C) in the main reaction zone during the 2-stage combustion and are about 600–700 °C at the end of the combustion chamber.
- 6) The high temperatures in the combustion chamber are due to the exothermal oxidation reaction of the products formed during the pyrolytic decomposition with oxygen and promote the transfer of heat from the flames to the surrounding walls of the heating system (heat exchanger), leaving as essential components of the waste gas carbon dioxide (CO₂) and water vapor (H₂O_{steam}) and a small proportion of unburnt components in the ash.

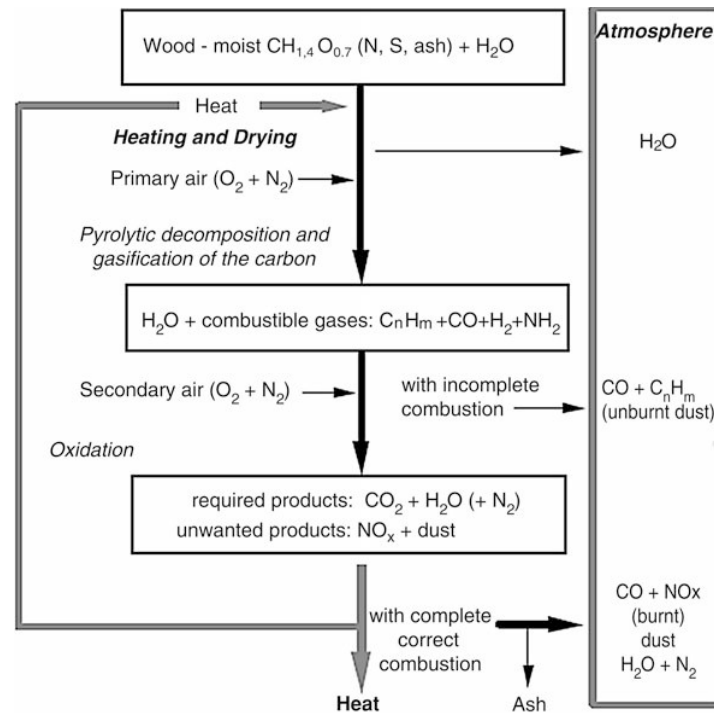


Figure 2.5. Combustion characteristics of wood (Döring, 2013).

The combustion processes described occurring simultaneously in the various areas of the fuel as a function of the local temperature, as the speed of the reaction depends mainly on the size of the fuel parts and on the temperature in the furnace (Döring, 2013).

For automatically fed heating systems, the processes described above takes place in parallel at any given time as new fuel is continuously supplied to the combustion chamber and there is already degassed fuel in the form of charcoal present and burning. Attempting to reconstruct the thermochemical combustion process with respect to the thermal decomposition of the molecular structure of the biomass, the irreversible destruction of the first macromolecules begins with the fuel being heated within a temperature range of between 150 and 200 °C as described in Figure 2.6. The thermal decomposition is depending on the rate of heating and the raw material. The percentages by weight of the gaseous decomposition products (such as CO_2 , H_2O , CH_4 etc.) released during this process are determined by the proportions of cellulose, hemicellulose and lignin specific to the raw material. In the case of wood, after it has passed through a temperature range of approximately 320–340 °C, about 30% loss in weight can already be registered, reaching a maximum release of gases and vapors (breaking down of volatile components) at 400 °C and also of the breaking down of cellulose, which ends at about 450 °C. The weight loss of biomass is about 70%. Thus, as the biomass is heated

further, the remaining lignin is broken down up to a temperature of about 400 °C, followed by the oxidation (combustion) of the charcoal (Döring, 2013).

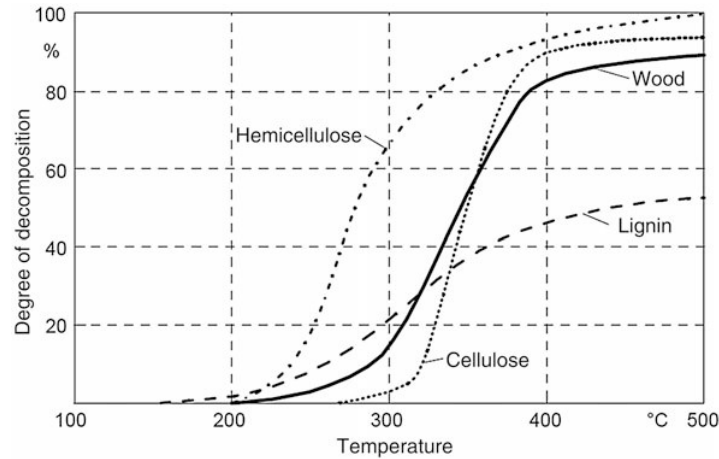


Figure 2.6. Thermal decomposition of wood as a function of temperature with its cellulose, hemicellulose and lignin components (Döring, 2013).

2.3.2.2 Biomass combustion systems

There are three general modes of combustion for most solid fuels including biomass materials as described by Loo and Koppejan (2008):

1. Grate (fixed or moving) combustors, which are generally applied in domestic, and small and medium-sized industrial/commercial applications;
2. Fluidized bed combustors, of the bubbling bed and circulating types, which are commonly used for medium-sized industrial/commercial applications and
3. Pulverized fuel combustors, which are mostly applied in large industrial and utility applications.

These modes of combustion are rarely used for 100% biomass firing, and the interest is mainly in the co-firing of biomass in large coal-fired boilers.

2.3.3 Parameters influencing biomass combustion

Amongst variables that influence the combustion behavior of biomass the most important are: grate size, excess air, residence time, and primary and secondary air ratio.

2.3.3.1 Grate size

Grate size is one of the important parts in the design of a pellet boiler, in order to be thermally efficient and with reduced emissions. The main criterion for designing the cross section area of the grate is that

it has to be able to devolatilize the fuel at the rate equal to the fuel supply (Ribeiro *et al.*, 2019). The authors studied the influence of three different grate sizes in the combustion of the biomass pellets in a 25 kW boiler. This study shows that the smaller grates would be unbalanced with fuel supply rate greater than the combustion rate, while the larger ones showed that the burner was capable to operate at any load without being overloaded of pellets. Even though, a reduction on the grate size (cross section 135 x 95 mm) with the rectangular shape, obtained a very good CO emission level, while overload of burner became an important problem mainly at full load (Ribeiro *et al.*, 2019). Yin *et al.* (2008) states that in the fuel bed, the propagation of the flame fronts determines the releasing of volatiles and affects the heat output from a given grate area and the stability of combustion.

2.3.3.2 Excess air ratio

The combustion occurs, as the fuel requires the presence of a given amount of air (oxygen). For the condition of stoichiometric combustion (where all fuel is burned completely), the excess air ratio (λ) equals to 1 (Hansen *et al.*, 2009). The percentage of excess air in the combustion is another indicator of the proportion of air in the mixture and the percentage of air exceeding the stoichiometric amount is defined in Eq. (2.11) (Ribeiro, 2012). An optimum excess air ratio is required for each system as stated by Burkhard and Russell (2010), where higher excess air ratios will result in a decreased combustion temperature and lower excess air ratios will result in inadequate mixing conditions.

In practice, combustion will always take place with excess air ($\lambda > 1$), since it is impossible to achieve complete combustion with a stoichiometric amount of air. In Table 2.3 the typical excess air figures are shown along with the corresponding oxygen content left in the flue gas (Hansen *et al.*, 2009). In addition, the excess air ratio figure is to a great extent dependent on the combustion technology and to some extent on the fuel. In wood combustion, the amount of excess air ratio when burning wood pellets is typically lower than when combusting wood chips. Hansen *et al.* (2009) stated that the best combustion of wood fuels is attained at an excess air ratio (λ) value between 1.4 and 1.6, while Yin *et al.* (2008) reveal that in the type of grate-firing, the overall excess air for most biomass fuels is normally set to 25% or above.

Table 2.3. Typical excess air ratio (λ) and the resulting of air content in the flue gas.(Hansen *et al.*, 2009).

	Excess air ratio (λ)	O ₂ , dry (%)
Fireplace, open	> 3	> 14
Wood stove	2.1-2.3	11-12
District heating, wood chips	1.4-1.6	6-8
District heating, wood pellets	1.2-1.3	4-5
Power plant producing heat, wood dust	1.1-1.2	2-3

2.3.3.3 Residence time

The correlation between CO burnout and residence time in an ideal stirring reactor is depicted in Figure 2.7. It shows that the higher the combustion temperature and the oxygen content, the lower the residence time necessary to reach high CO burnout rate. The residence time is a function of the combustion chamber volume and combustion gas flow, swirl. The design of the combustion chamber has to guarantee the high residence times as well at high load operation and to avoid undesirable conditions (e.g. dead zones, insufficient mixing, etc.) (Burkhard and Russell, 2010).

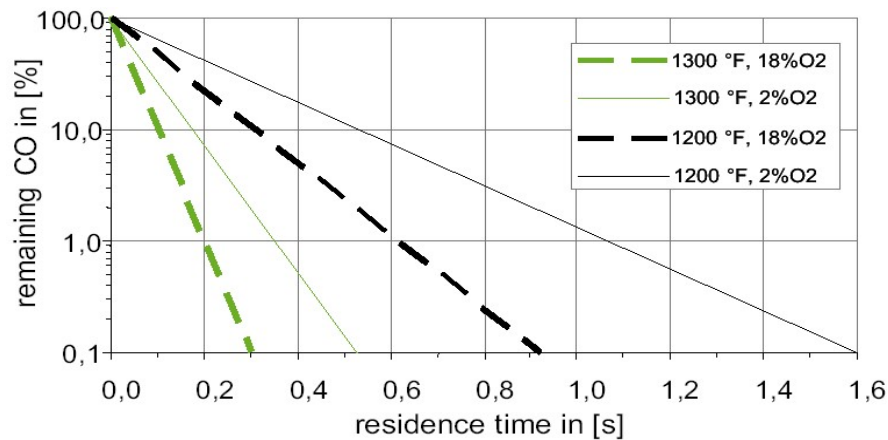


Figure 2.7. CO remaining as a function of residence time, combustion temperature and oxygen concentration in an ideal stirring reactor (Leuckel and Roemer, 1979).

2.3.3.4 Primary and secondary air ratio

Air staging method is based in the principle that the primary and secondary combustion air is injected in clearly separated zones or combustion chambers (Burkhard and Russell, 2010). The design of an air supply system for primary air and secondary air, plays a very important role in the efficient and complete combustion of biomass (Yin *et al.*, 2008). In this, the primary air is introduced through the fuel bed under the grate to promote its devolatilization, and secondary air is supplied above the grate or downstream of PA to complete the fuel oxidation (Ribeiro *et al.*, 2019). In addition, the split ratio of

primary air to secondary air tends to be 40/60 in modern grate-fired boilers burning biomass, instead of 80/20 in older units (Yin and Li, 2017), as older boilers are troublesome due to the lack of good flow measurement devices and monitoring equipment. Meanwhile, modern grate-fired boilers have four key elements such as a fuel feeding system, a grate assembly, a secondary air (including over-fire air) system and an ash discharge system (Yin *et al.*, 2008).

2.3.4 Combustion temperature

Pastre (2002) states that incomplete combustion is mainly the result of low combustion temperatures, short residence times, bad mixing conditions with oxygen (or oxygen shortage) or combinations of these effects. The combustion temperature is influenced by several parameters such as moisture content (Oberberger and Thek, 2010), pellet length (Sikanen and Vilppo, 2012), and excess air ratio (Burkhard and Russell, 2010; Loo and Koppejan, 2008). High moisture content will decrease the combustion efficiency, the lower heating value and combustion temperature (Oberberger and Thek, 2010). The pellet length has also a significant effect on the combustion temperature, as increasing the pellets length, the average burning temperature is decreasing up to 31% (Sikanen and Vilppo, 2012). Among others parameters, a low combustion temperature results in incomplete combustion (Loo and Koppejan, 2008), and unburned fuel will exit through the chimney (Hansen *et al.*, 2009). In addition, the necessary combustion temperature, which is approximately 900-1,000 °C, is sustained partly by the right design of the combustion chamber relative to the fired amount of wood pellets and partly by matching the amount of air to the amount of fuel that is used (Hansen *et al.*, 2009). The theoretical combustion temperature as a function of moisture content and excess air ratio is shown in Figure 2.8 (Burkhard and Russell, 2010). This can be explained by the effectiveness of the fuel and oxygen mixing, which is controlled by turbulence in the combustion zone. Whereas the turbulence is primarily influenced by the flow velocity of the combustion air. With increasing in the flow velocities, the mixing of fuel and air becomes increasingly ideal. This condition again results in lower amounts of air needed for the combustion and thus higher combustion temperatures.

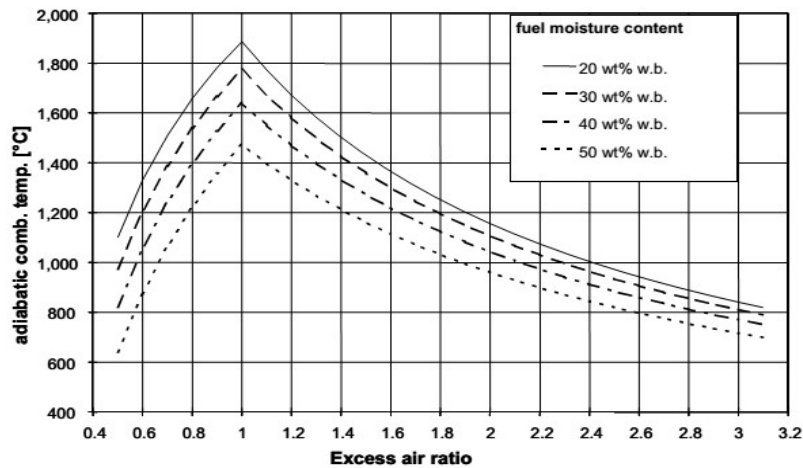


Figure 2.8. The relationship between the adiabatic combustion temperature and the excess air ratio (Nussbaumer, 1989).

2.3.5 NO_x

Nitrogen oxides (NO_x) are a generic term for the sum of all nitrogen based gasses, from NO to NO₂. The NO_x gasses are unwanted because NO_x is a greenhouse gas and it contributes to the acidification of precipitation (Hansen *et al.*, 2009). In addition, NO and NO₂ are the most hazardous of nitrogen oxides (ATSDR, 1975). Nitrogen oxides are produced partly during the combustion of fuels with nitrogen content (e.g. bio-fuels) and also in the boiler room by the nitrogen that is injected during combustion with the combustion air. Hansen *et al.* (2009) addressed the influence of the design and size of the boiler combustion chamber on the emission of nitrogen oxides. It is not possible to give completely plain guidelines for the design of boilers with low NO_x emission but the main trends are (Hansen *et al.*, 2009; Burkhard and Russell, 2010):

- High content of N in the fuel gives increased NO_x emissions;
- High combustion temperatures contribute to high NO_x emissions;
- Conversion of NO to NO₂ in the atmosphere;
- Some NO_x may be formed from nitrogen in the air given certain conditions.

Regarding the thermal route of NO_x formation, this can be mitigated by reducing the primary air supply to the fuel bed and by recirculation of the exhaust gases back into the combustion chamber in order to lower the temperature and the oxygen content. Hansen *et al.* (2009) discuss the influence of fuel type in the NO_x emissions in a small scale boiler (Table 2.4).

Table 2.4. Typical NO_x emission in small scale boiler, normalized by the thermal output.
(Hansen *et al.*, 2009).

Fuel	Emission (NO _x)	Unit
Wood pellet	130-300	mg/MJ
Straw	130-300	mg/MJ
Fuel oil	75	mg/MJ
Natural gas	50-100	mg/MJ

As stated in the previous section, NO_x emissions from biomass increase with increasing N content in the fuel and with increasing combustion oxygen concentration (Pastre, 2002). The author referred that in line with the fuel nitrogen content, furnace design and operating conditions are significant parameters that influence the NO_x emissions from boilers. It is also referred that there exists a trade-off between NO_x emissions and those of unburnt hydrocarbons (UHC) and carbon monoxide. The decrease in the excess air ratio or oxygen concentration will result in lower NO_x emissions but in increased emissions of UHC and CO. In fact, efficiency increases as the excess air ratio decreases until the losses due to incomplete combustion become too high. Recently the development of burners and stoves has been focused on achieving low emissions of UHC (Pastre, 2002).

In order to decrease NO_x emissions, both primary and secondary methods are used. In a primary method, an air staged combustion can be operated, which corresponds to a combustion air at two (or three) levels. At the first level (primary air), oxygen deficiency conditions are created such as the primarily formed nitrogen compounds can be reduced to molecular nitrogen (N₂) if the residence time is sufficient. Secondary air (or tertiary air in some cases) is supplied downstream in the furnace after the reducing zone to enable complete burnout of hydrocarbons and CO (Pastre, 2002). As secondary methods they consist in flue gas cleaning techniques, such as non-catalytic reduction, or selective non-catalytic reduction. Combined, a maximum 60-95% reduction can be achieved. The secondary methods can be applied but usually only for the larger combustion units. Table 2.5 shows the Austrian limiting values for emissions defined by ÖNORM EN 303-5 for automatically and manually fed furnaces that are fired with solid biomass fuels (Oberberger and Thek, 2010).

Table 2.5. Emissions limits defined by ÖNORM EN 303-5.
(Oberberger and Thek, 2010).

Feed system	CO	NO _x ²⁾	OGC	Dust	Unit
Manual	1,100	150	80	60	mg/MJ ¹⁾
Automatic	500 ³⁾	150	40	60	mg/MJ ¹⁾
Manual ⁴⁾	2,460	330	180	135	mg/Nm ³
Automatic ⁴⁾	1,120 ³⁾	330	90	135	mg/Nm ³

where: 1) Relating to LHV of the fuel; 2) Applicable only in wood furnaces; 3) At partial load of 30% nominal load the limiting value may be exceeded by 50%; 4) Conversion of mg/MJ to mg/Nm³ (Oberberger and Thek, 2010), valid for dry flue gas and 10 vol.% O₂.

2.3.6 Ashes

Ash results from solid biomass combustion and is the remaining mass after all the fuel is completely burned. Wood usually has only a few tenths of an ash percent. The temperature affects the formation of ash, as typically the ash begins to soften at 1,200 °C and becomes fluid at 1,300 °C, although this varies significantly between fuels. Table 2.6 shows ash melting temperature for a wide variety of fuels (Pastre, 2002). Ash needs to be well treated in the combustion of solid fuel, in order to minimize slagging, fouling, erosion, and corrosion (Borman and Ragland, 1998). Loo and Koppejan (2008) said that ash-forming elements are present in biomass as salts, bound in the carbon structure (inherent ash) or they are attendant as mineral particles from dirt and clay introduced into the biomass fuel during harvest or transport (entrained ash). Thus, the compounds in inherent ash are homogeneously dispersed in the fuel and are much more mobile compared to the compounds in entrained ash and, therefore, readily volatile and available for reactions in burning char.

Figure 2.9 shows the mechanisms involved in ash formation in biomass combustion. A fraction of the ash forming compounds in the fuel is devolatilized and released to the gas phase, during combustion. This depends on the fuel characteristics, the gas atmosphere, and the combustion technology in use (Loo and Koppejan, 2008). For example, high combustion temperatures and a reducing atmosphere have been reported to enhance the devolatilization of the environmentally relevant heavy metals such as Zn, Pb, and Cd.

Table 2.6. Ash melting temperature for a range of fuels (Pastre, 2002).

Temperature (°C)	Coal	Wood chips	Wood chips 2	Pine sawdust	Spruce chips	Wheat straw	Wheat straw 2	Grey straw
Fusion temperature	1,100	1,210	1,144	1,150	1,340	848	1,056	950
Softening temperature		1,225	1,172	1,180	1,410	956	1,122	1,100
Hemispherical stage		1,250	1,222	1,200	1,700	1,107	1,161	
Melting point	1,400	1,275	1,300	1,225	1,700	1,241	1,232	

The main elements in the biomass ash are potassium, calcium, sulphur, chlorine, silicon, and phosphorus (Magdziarz *et al.*, 2016). Several studies have been conducted in improving the biomass combustion in a furnace by minimizing the problem occurring during the combustion due to ashes. Amongst the problems caused by the slagging and fouling of ash, include reduced heat transfer, corrosion, and erosion, which increased the probability of shutdown for maintenance and cleaning

(Fang and Jia, 2012). Reducing the ash formation during the combustion, adding an additive is one method beside the fuel mixing and leaching out the problematic elements from fuels before combustion (Wang *et al.*, 2012). This study revealed that through the application of additives this will influence the chemical binding as the most important route to convert problematic ash elements into high-temperature stable substances.

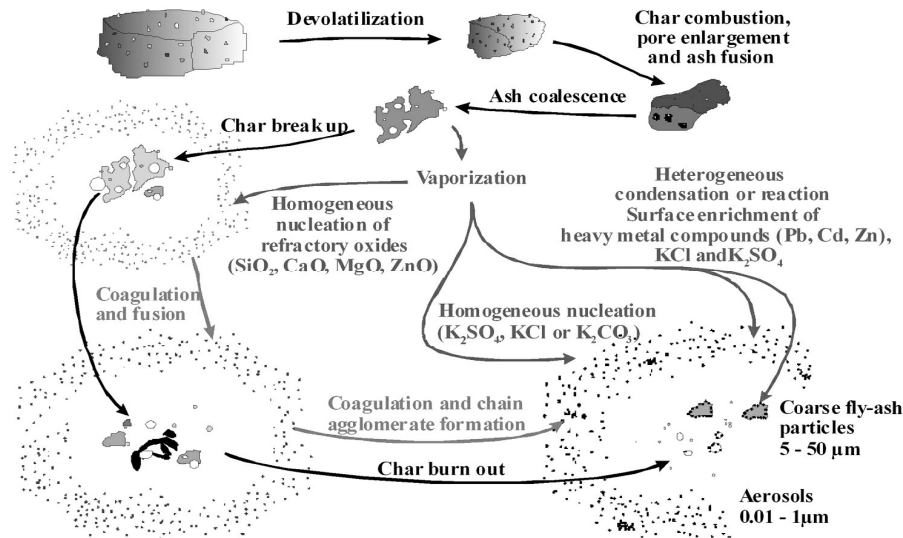


Figure 2.9. Ash formation mechanisms in biomass combustion (Haslinger *et al.*, 2004).

A study on the particle formation mechanisms and the influence of different operating parameters on the particle emissions in a wood pellets combustion under fixed-bed conditions was conducted by Wiinikka and Gebart (2004). This study describes that the particles released from this combustion are formed in three different mechanisms namely coarse fly ash particles ($>10\mu\text{m}$) (released by mechanical ejection from the fuel bed), submicrometer-sized fly ash particles (produced from the vaporization and nucleation of ash minerals) and, submicrometer-sized soot particles (produced from incomplete combustion). These different particles are produced from mechanical ejection from the fuel bed, the vaporization, and nucleation of ash minerals, and incomplete combustion respectively.

2.4 Fuel devolatilization

Devolatilization or volatile release is defined as an early stage occurring upon fuel particle feeding in a combustor. Devolatilization is an endothermic step where the heat is needed from the environment. In addition, devolatilization can be controlled either thermally, or by particle size and shape (Miccio *et al.*, 2013). Several parameters related to the devolatilization are presented as follows.

2.4.1 Thermogravimetric analysis (TGA)

Thermogravimetric analysis is a useful tool used to determine the devolatilization rate of material in releasing the mass including the volatile matter during the thermal process and its fraction of volatile components. The decreasing of mass occurs under controlled conditions and the thermal process is taking place, with increasing temperature or time. Based on the mass evolution (Calvo *et al.*, 2014) on the TGA curve three stages are identified. In the first phase weight loss takes place due to the moisture release (20 to 130 °C). The second stage corresponds to the devolatilization of the hemicellulose and cellulose components and their respective ignition (from 160 to 400 °C), and the third – the residual lignin decomposition and char formation (from 420 to 600 °C), (Ferreira, 2016; Paulauskas *et al.*, 2015). The weight losses for the thermal degradation of the biomass constituents including hemicellulose, cellulose and lignin components can be seen in Ferreira (2016). The mass loss and DTG curves of pine sawdust are depicted in Figure 2.10. From Figure 2.10, it could be explained as follows: 1) moisture released; 2) maximum heat release; 3) burnout (Indicated by the point immediately before reaction ceases, when the rate of weight loss is down to 1%/min) (Ferreira, 2016), 4), 5) and 6) is first, second and third region respectively (Yorulmaz and Atimtay, 2009); 7) initial decomposition (referred to the beginning of the weight loss and it is defined as the temperature at which the rate of weight loss reaches 1%/min after the initial moisture loss peak in the DTG curve); 8) temperature and maximum combustion rate at first peak; 9) temperature and maximum combustion rate at the second peak (Ferreira, 2016).

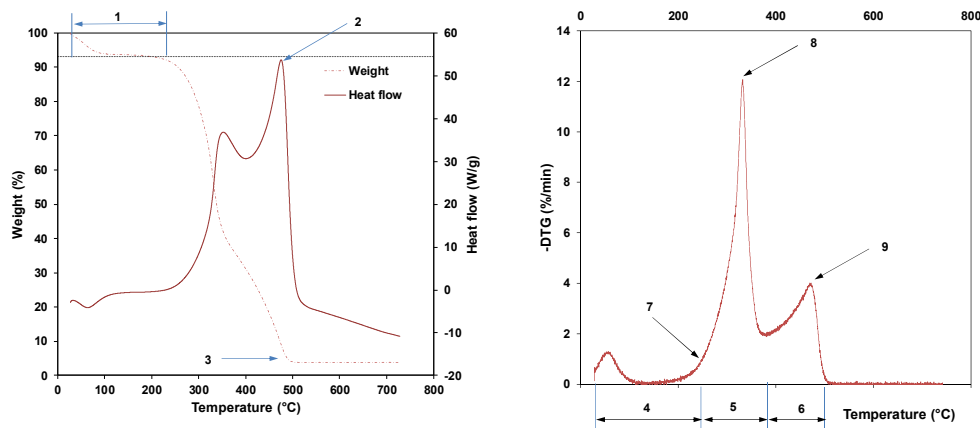


Figure 2.10. Mass loss and DTG curves for pine sawdust.

2.4.2 Mechanism of devolatilization

The devolatilization occurs after moisture release (drying) (Miccio *et al.*, 2013) when the temperature rises; the solid fuel begins to decompose and releasing volatiles as long as the drying of small fuel particle or a zone within the large particle is completed (Borman and Ragland, 1998). The devolatilization is referred to as the pyrolysis stage since the volatiles flow out of the solid through the pores and external oxygen cannot penetrate into the particle. The rate of devolatilization and pyrolysis products depends on the temperature and the type of fuel.

2.4.3 The influence of variables on devolatilization

Several variables influence the devolatilization on solid fuel such as temperature, particle size, and heating rate. The influence of those parameters on devolatilization was analyzed by using the TGA technique.

2.4.3.1 Influence of temperature

Temperature is one of the determined parameters on the devolatilization. Increasing in the temperature enhance the thermal decomposition of the material. Previous studies revealed that, depending on the fuel type, the devolatilization occurs between 180 °C and 360 °C (Ferreira, 2016), including for pine wood. Previous study shows that the thermal decomposition of Brassica pellet starts at 150 °C, and Poplar pellet starts to decompose at about 225 °C (Granada *et al.*, 2013). In addition, the main devolatilization occurs at a maximum rate between 300 and 340 °C, and is mainly completed at about 400 °C.

2.4.3.2 Influence of particle size

The particle size has an influence on the devolatilization rate (Daouk *et al.*, 2015; Harun *et al.*, 2009). The study conducted by Daouk *et al.* (2015) showed that increasing the diameter of pine wood particles produces a short delay in the TG and DTG curves. In addition, the result obtained from Harun *et al.* (2009) also shows that increasing the particle size the total degradation, activation energy and pre-exponential factor decreased in both first and second reaction zones. Boriouchkine *et al.* (2014) also revealed that larger particle size has higher maximum mass loss rate when compared to smaller particles with two different wood content: pure spruce wood particles and mostly content of bark respectively. In addition, this indicates that samples are comprised of components with different reaction kinetics.

2.4.3.3 Influence of heating rate

This technique of applying a heating rate in TG devices is that preheating the sample to a given temperature (T_0) followed by starting the experiment with a fixed nominal heating rate (β), as in Eq. (2.16) (Ebrahimi-Kahrizsangi and Abbasi, 2008).

$$T = T_0 + \beta \cdot t \quad (2.16)$$

Using different heating rates on pine wood particle shows that the duration of devolatilization is shorter when compared to drying and char combustion and decreases with the increasing heating rate. During the initial decomposition, the temperature is also decreasing with the increased heating rate. While the maximum combustion rate is increasing as a result of decreasing of the residence time of the sample in the furnace, and thermal decomposition was shifted to a higher magnitude with increasing of heating rate. The shift of curves to the right indicated that the weight losses occur at increasing temperatures (Garcia-Maraver *et al.*, 2015).

3. MATERIALS AND METHODS

This chapter describes the materials and methods applied throughout the experiment: wood pellets, boiler, small scale reactor, and TGA device. The combustion of pellets in a furnace evaluates:

- Thermogravimetric analysis of wood particles;
- Mass loss of pellets and the devolatilization of species in wood pellets;
- The fuel/air supply and the relationship with the fuel bed.

3.1 Combustion facility

The schematic diagram of the test facility used in this study is presented in Figure 3.1. It consists of: the boiler unit (including heat exchanger pipes, combustion chamber and fuel grate), the ventilator, fuel storage, external cooling loop, the gas analyzer unit and computer and the data acquisition unit. The fuel is transported from the fuel storage tank by means of screw and is supplied on top of the combustion chamber by gravity. The ventilator drafts the air into the combustion chamber by primary and secondary air pipes working below atmospheric pressure. A vacuum pump was used to extract a sample of exhaust gas into the gas analyzer for measurement purposes. Before entering the vacuum pump, the sample was cooled and filtered in order to remove any moisture and particles. The computer unit, including a National Instrument data acquisition board, was used to monitor and control all the system. Each component of the facility will be explained in the following sections.

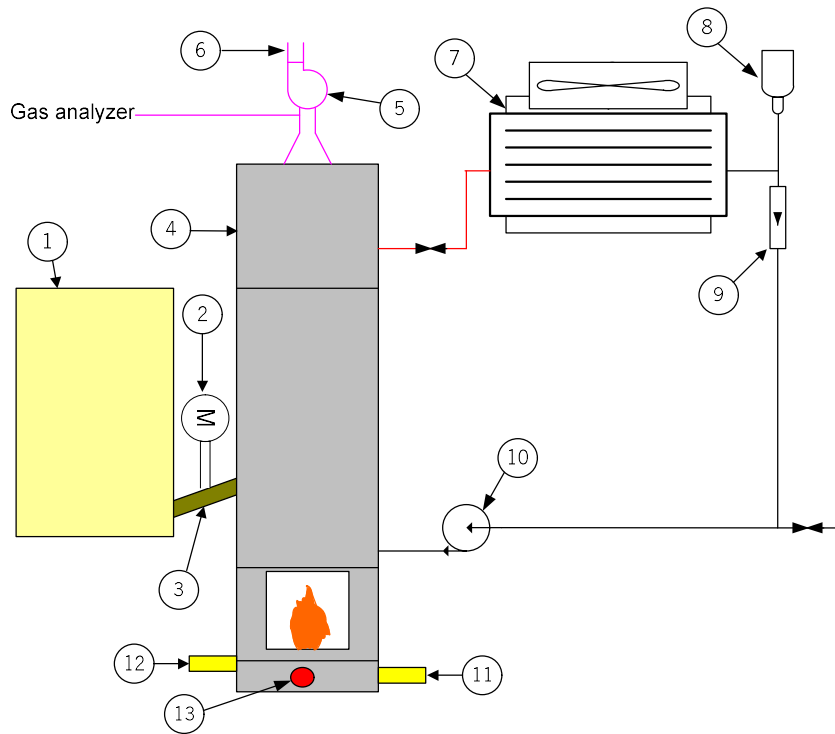


Figure 3.1. Experimental diagram.

Notes:

- | | | |
|--------------------------|-------------------------------|-------------------------|
| 1. Pellets storage tank. | 6. Stack. | 10. Water pump. |
| 2. Feeding motor. | 7. Air cooler heat exchanger. | 11. Primary air tube. |
| 3. Feed auger. | 8. Expansion vessel. | 12. Secondary air tube. |
| 4. Boiler. | 9. Flow meter. | 13. Ignition coil. |
| 5. Ventilator. | | |

The nominal load of the boiler in this study was set at 20 kW. The boiler is 126.8 cm height and with a width of 42.64 cm and 35.1 cm in depth. The combustion chamber is 53 cm in height and with a cross section 30 cm x 25.3 cm. The combustion chamber is lined with the slabs of fire clay in order to increase the temperature inside the combustion chamber and avoid cold walls that would lower the combustion rates and lead to incomplete combustion. Useful heat is transferred to water by means of a double pass heat exchanger made up of 20 pipes buried inside the ± 80 L water tank. Those included: 14 pipes with 38 cm height, 4 cm diameter, in three rows of 5, 4, and 5 pipes as depicted in Figure 3.2; and 6 pipes in the back with 90.5 cm height and 4 cm diameter.



Figure 3.2. Heat exchanger pipes, bottom view.

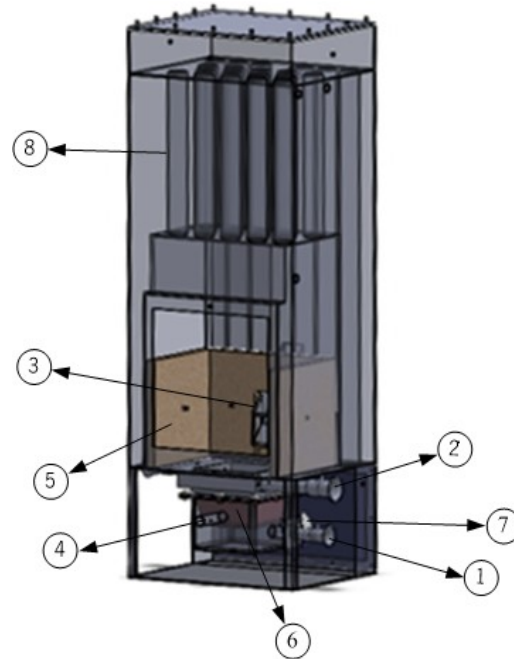


Figure 3.3. Boiler unit.

- | | |
|------------------------|---------------------|
| 1. Primary air tube. | 5. Fire clay slabs. |
| 2. Secondary air pipe. | 6. Grate. |
| 3. Fuel inlet. | 7. Exhaust. |
| 4. Ignition coil. | 8. Heat exchanger. |

The total air flow rate is set by adjusting the ventilator draft and the primary/secondary air split is adjusted by throttling the primary air supply. The whole unit is covered by a jacket of rock wool to minimize the heat losses to the outside. The grate is installed underneath the combustion chamber and lock into place by screws. The grate is covered by the metal box and a sealing material (rock wool) was applied in the connection parts to prevent uncontrolled air entrance on those parts during operation. The primary air pipe is installed underneath and the secondary air is installed above the grate. The ignition coil is in the front of the grate box and the fuel inlet is on the top of the grate. The full scale of the boiler is described in Figure 3.3.

The grate applied in this study was of rectangular shape, can be easily changed and three different cross sections areas according to the study were used. The grate model is schematically described in Figure 3.4, where 1 and 4 are primary and secondary air orifice (4 mm diameter) respectively, 2 is primary air orifice on the bottom (3 mm width), 3 is the ignition hole and 5 is secondary air inlet. The grate design can be seen in Annex (Figure A.1).

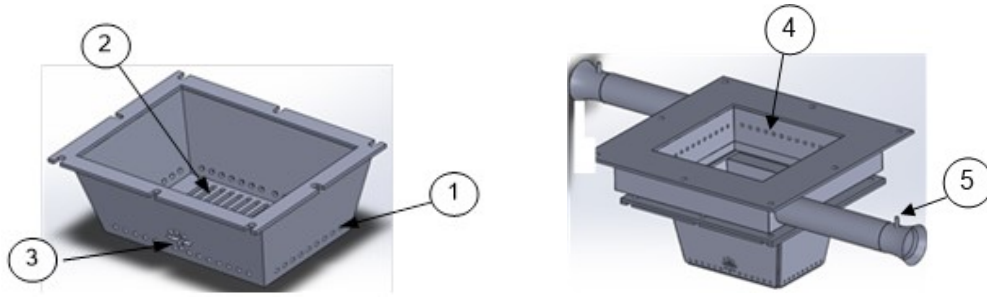


Figure 3.4. Grate unit.

The suction ventilator (working frequency between 0 – 60 Hz) was installed in the exhaust duct to draft the air into the grate through primary and secondary air pipes, and also to release the exhaust through the stack. The thermal load is removed from the boiler through a cooling loop. In this, a circulating pump (maximum flow rate of 500 L/h) drives the cooling water through an air-cooled heat exchanger and back to the boiler. The flow rate is controlled by a valve and measured by a calibrated rotameter.

3.2 Measurement techniques

To conduct the experimental program, the operating parameters that needed to be determined include the excess air, thermal load, the split ratio of primary and secondary air, and the grate area. Also, the value of the mass flow rate of air and fuel were determined.

3.2.1 Flow rate and velocity measurement

Several measurement devices are applied to measure the flow rate of liquids and gases flowing through pipes or ducts such as orifice plate, venturi and nozzle meter. The incompressible steady fluid flow in a horizontal pipe of diameter (D) that is constricted to a flow area of diameter (d), is shown in Figure 3.5. The mass balance and the Bernoulli equations applied to the flow from section (1) to section (2) can be written as in Eq. (3.1) and (3.2) respectively, and in Eq. (3.3).

Mass balance:

$$\rho_1 A_1 v_1 = \rho_2 A_2 v_2 \quad (3.1)$$

When $\rho_1 = \rho_2$, equation 3.1 becomes $A_1 v_1 = A_2 v_2$

Bernoulli equation ($z_1 = z_2$):

$$\frac{p_1}{\rho g} + \frac{v_1^2}{2g} = \frac{p_2}{\rho g} + \frac{v_2^2}{2g} \quad (3.2)$$

Combining Eqs. 3.1 and 3.2 and solving for velocity v_2 gives obstruction (with no loss):

$$v_2 = \sqrt{\frac{2(p_1 - p_2)}{\rho(1 - \beta^4)}} \quad (3.3)$$

β being the diameter ratio (d/D). Regarding the flow past the obstruction, where there are some pressure losses taking place due to frictional effects, become inevitable. Thus, a correction factor, or discharge coefficient (C_d), which is experimentally determined, must be considered. The flow rate calculated for obstruction flow meters can be expressed as in Eq. (3.4) (Cengel and Cimbala, 2006).

$$\dot{Q} = A_0 \cdot C_d \sqrt{\frac{2(p_1 - p_2)}{\rho(1 - \beta^4)}} \quad (3.4)$$

where, $A_0 = A_2 = \pi d^2 / 4$, C_d depends on the β and the Reynolds number, Re . The experimentally determined data for C_d , for the flow meter, is expressed in Eq. (3.5) (Cengel and Cimbala, 2006).

$$C_d = 0.5959 + 0.0312\beta^{2.1} - 0.184\beta^8 + \frac{91.71\beta^{2.5}}{Re^{0.75}} \quad (3.5)$$

Regarding the pressure generating in a pipe or channel, a detector such as a pressure transducer is used to record the oscillation in pressure. The manometer or pressure transducer shown in Figure 3.6 is simply measuring the pressure difference $p_1 - p_2$.

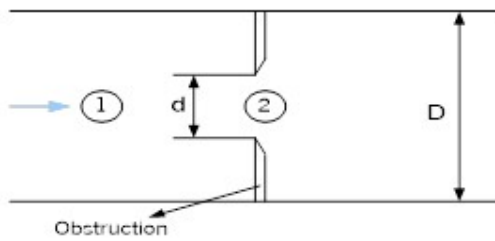


Figure 3.5. Flow through a constriction in a pipe.



Figure 3.6. Pressure transducer.

The excess air ratio (λ) applied in this study is set at 1.5, 1.7, and 2.1. In determining the excess air ratio, the experiment was conducted to obtain the average value of oxygen on the gas analyzer and the reading was introduced into the calculation sheet in the excel file to compute the excess air ratio (λ). This is calculated in Eqs. (3.6 – 3.8), which is referred to as the stoichiometry condition of pine wood.

$$\lambda = \frac{(-x + \%O_{2,x} - (\%O_{2,m_C})/12)}{((\%O_{2,x} + \%O_{2,y}) - x)} \quad (3.6)$$

where,

$$x = (m_C / 12 + m_H / 4) - (m_O / (2 \times 16)) + m_S / 32 \quad (3.7)$$

$$y = x 3.76 + (m_N / 28) \quad (3.8)$$

$\%m_C, \%m_H, \%m_O, \%m_N, \%m_S$ are the mass percentage in the fuel for carbon, hydrogen, oxygen, nitrogen, and sulphur respectively, while $\%O_2$ is the percentage of oxygen in the flue gas.

3.2.2 The split ratio of primary and secondary air

The primary and secondary air flow rates are measured by special made inlet ports. These ports are of a bell mouth shape and machined from an aluminum billet. This shape provides a smooth, frictionless flow whose pressure drop (monitored by a pressure tapping at the throat) is related to the volumetric flow rate by a simple equation (Eq. 3.9). In this equation, the discharge coefficient can be neglected, as it is very close to 1.

$$\dot{Q} = \pi d^2 / 4 \sqrt{\frac{2 \Delta p}{\rho}} \quad (3.9)$$

To obtain the best combination of primary and secondary air split ratio within an acceptable pressure drop range, the tube diameter of 21 mm and 26 mm were installed on both primary and secondary inlet channels respectively. The schematic diagram of the primary and secondary air tubes is present in Figure 3.7. The inlet tubes for primary and secondary air were manufactured and calibrated during a previous project on the same boiler. Three different split ratio (SR) were selected including 20/80, 30/70 and 37/63 for every different geometry of the grate and air flow rate applied in this study (Table 3.1).

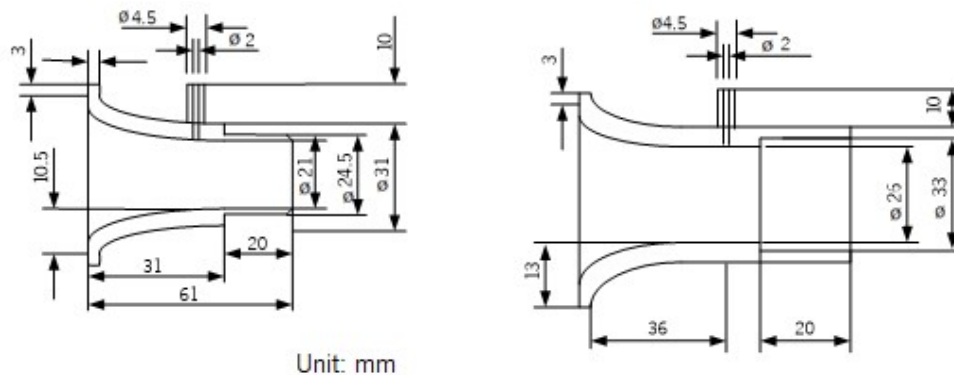


Figure 3.7. Primary and secondary air tube.

Table 3.1. Study parameters.

No.	Power (kW)	Time		Mass fuel (kg/h)	Total mass of air (kg/h) and λ			PA : SA
		on	off		1.5	1.7	2.1	
1	10	8	12	2.11	18.52	20.94	25.86	20 : 80 30 : 70 37 : 63
2	13	7	6	2.74	24.02	27.22	33.62	
3	16	13	6	3.37	29.56	33.50	41.38	

In Table 3.1 the columns with the on/off time refer to the feeding patterns that were defined for each one of the desired power levels.

3.2.3 Fuel mass flow measurement

To measure the mass flow of fuel (wood pellets), a digital mass scale was used, as shown in Figure 3.8 with an accuracy of ± 0.1 kg. The mass flow of fuel is the ratio of the mass difference of wood pellets measured over a period of time. The mass flow of fuel was then given by Eq. (3.10).

$$\dot{m}_f = \frac{m_i - m_f}{\Delta t} \quad (3.10)$$

where, \dot{m}_f is fuel mass flow rate, m_i is initial mass, m_f is final mass, and Δt is time at m_i and m_f .



Figure 3.8. Digital mass scale.

The thermal load or power selected for this study was set at 10, 13, and 16 kW. This value was determined based on the pre-experimental observation and the result obtained from the previous study shows that medium power (12 kW) produced less CO emissions (Ribeiro *et al.*, 2013). However, the method for setting the power level of the boiler is not based on the direct measurement by the scale as explained below. The feeding mechanism was switched on continuously for a large period of time and the total mass of pellets was measured by weight difference. In this way, the average value of the pellet mass flux was calculated. This value was assumed to determine the length of time that the feeding mechanism is set on which is interrupted by more active periods as in a ON/OFF scheme. Based on the experiment and the previous study conducted by Ribeiro (2012) shown that the time interval for the

power of 20 kW is 20 s ON and 3 s OFF. By regulating the operating time on the LabVIEW program, then the desired power can be determined. By recording the parameters including the initial mass and final mass of pellets loaded to the boiler, the initial and final time and heating value of wood pellets. Theoretically, the power or thermal load (P) is calculated based on the mass of the fuel rate feeding (\dot{m}_{fd}), the time interval ($t_{ON, OFF}$), the heating value of pellets (LHV) and efficiency (η). The example of the time interval for 5 s (ON/1) and 3 s (OFF/0) is presented in Figure 3.9. These time intervals are introduced into the formulation to obtain the power which is equal to 18.42 kW (Eq. 3.11). This means that another 1.58 kW needs to be added to obtain 20 kW, to have the same value with the result obtained from the experiment. This occurs as the result of the feed auger is still running when the engine is already instructed to stop.

$$P = \dot{m}_{fd} \frac{t_{ON}}{(t_{ON} + t_{OFF})} \text{LHV} \cdot \eta \quad (3.11)$$

Taking into account $t_{ON} = 5$ s; $t_{off} = 3$ s for the measured fuel feeding rate ($\dot{m}_{fd} = 4.46$ kg/h) and assuming the LHV = 17,100 kJ/kg the power will be 14.82 kW.

$$= 4.46 \frac{\text{kg}}{\text{h}} \cdot \frac{5}{(5+3)} \cdot 17100 \frac{\text{kJ}}{\text{kg}} \cdot \eta = 13.24 \text{ kW} , \text{ then, } 13.24 \text{ kW} + 1.58 \text{ kW} = 14.82 \text{ kW}.$$

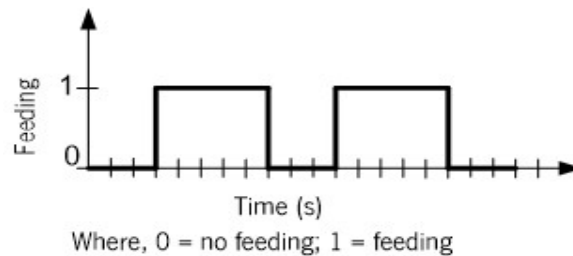


Figure 3.9. Time interval for pellet feeding (5 s ON and 3 s OFF).

3.2.4 Temperature measurement

The temperature field can be measured by thermocouples, which are pairs of junctions between two different metals. A voltage, approximately proportional to the temperature difference between the two junctions, is induced known as thermoelectrical effect. Usually, different metal combinations are used depending on the temperature range and sensitivity that needs to be acquired (for instance, platinum/platinum-rhodium or tungsten/tungsten-molybdenum) (Warnatz *et al.*, 2001).

The thermocouple location in the boiler is described in Figure 3.10. The reference numbers described on the boiler are recorded in the excel file. The temperature characteristics for some standard thermocouple materials shows in Figure 3.11 (Morris and Langari, 2012) and type K thermocouple (chromel-alumel) was used to measure the temperature in the grate (see Figure 3.12). The standard of thermocouple type can be seen in Annex (Table A.2) (AN107).

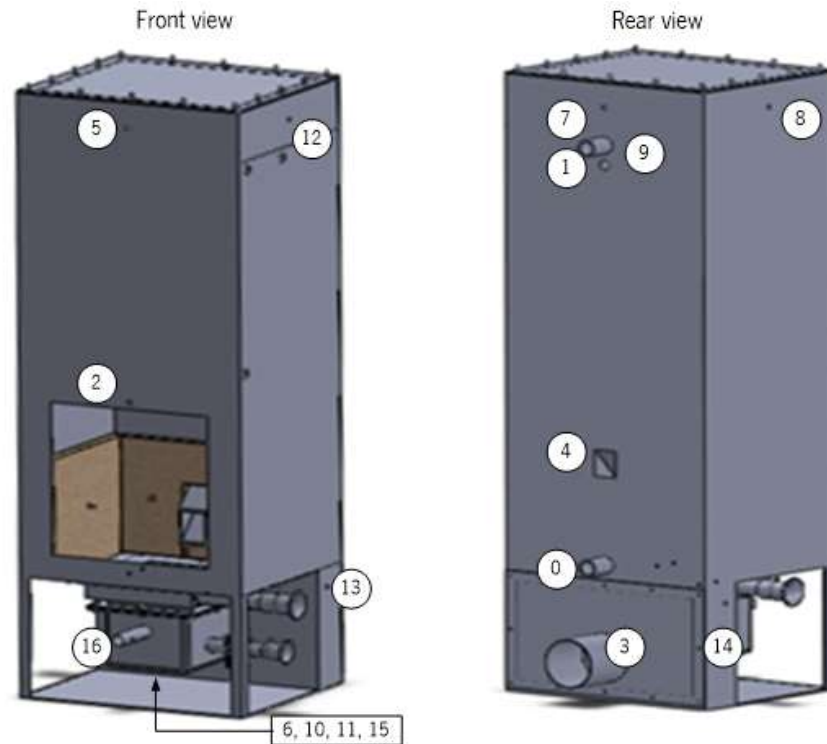


Figure 3.10. Thermocouple location on the boiler.

Legend:

- | | | |
|------------------------|----------------------|--------------------------|
| 0. Cold water. | 6. T at 25 mm. | 12. Water HE top center. |
| 1. Hot water. | 7. Chamber top back. | 13. Plain exit right. |
| 2. Combustion chamber. | 8. Chamber top left. | 14. Plain exit left. |
| 3. T exhaust. | 9. Water HE outlet. | 15. T at 5 mm. |
| 4. Pellets inlet. | 10. T at 60 mm. | 16. Ignition. |
| 5. Chamber top front. | 11. T at 15 mm. | |

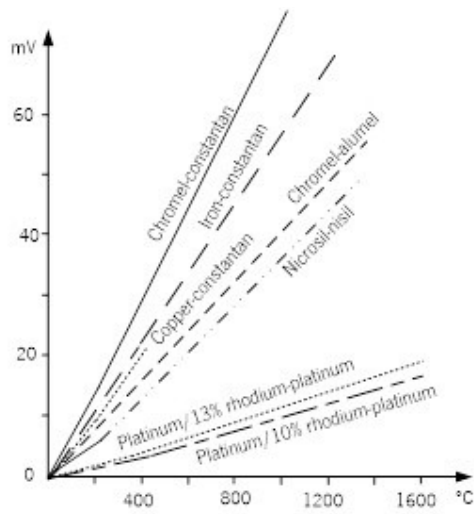


Figure 3.11. Temperature characteristics for some standard thermocouple materials (Morris and Langari, 2012).



Figure 3.12. Type K thermocouple installed in the fuel bed.

In this study, the temperature in the fuel bed was measured in four different positions such as 5, 15, 25 and 60 mm. The thermocouples were introduced from the bottom of the grate as shown in Figure 3.13.



Figure 3.13. Thermocouple unit.

3.2.5 Data collection

After the experimental is terminated, the data were collected and transferred into the excel worksheet for subsequent analysis. The data is later organized into tables and graphs to enable the analysis, including:

- 1) The influence of the grate dimensions, excess air, the thermal load and the split ratio of primary and secondary air on the fuel bed temperature, gas emission, boiler efficiency and ashes on the grate.

- 2) The influence of the different parameters on the stability of the fuel bed.

Sample preparation

All the experiments were carried out with pellets whose properties are fully listed in Annex A (Table A.3). The pellet is certified according to the ENPlus standard which is rated as A1 class pellets, (see characteristics of A1 class in Annex A (Table A.1)). The most relevant properties are summarized in Table 3.2.

Table 3.2. Properties of pine wood pellets.

Proximate analysis (wt.%, as received)		Ultimate analysis (wt.%, dry ash free)	
Moisture	6.9	Carbon	50.8
Volatile matter	77.80	Hydrogen	5.39
Ash	0.6	Nitrogen	1.55
Fixed carbon	14.70	Sulphur	0.037
Lower Heating Value (MJ/kg)	17.1	Oxygen	42.22

3.3 Flue gas analyzer

The schematic diagram of the flue gas analyzer unit is presented in Figure 3.14. The gas sample is extracted from the stack by means of a vacuum pump. Before entering the gas analyzer, the sample is cooling down in the heat dissipation loop. In order to prevent the moisture from entering the gas analyzer, the water was condensed in the condensation tube. The filter is used to prevent the unnecessary particles flowing to the gas analyzer. The gas analyzer is a set of sensors used for the measurement of the gases. It contains infrared carbon dioxide and visible spectrum oxygen detectors and connects to any PowerLab* data acquisition system or any device that records an analog signal. The gas analyzer measures carbon dioxide, oxygen, nitrogen oxides, and carbon monoxide concentration according to its specification (ADInstruments). The gas analyzer is show Figure 3.15, and the full assembly measurement unit in Figure 3.16.

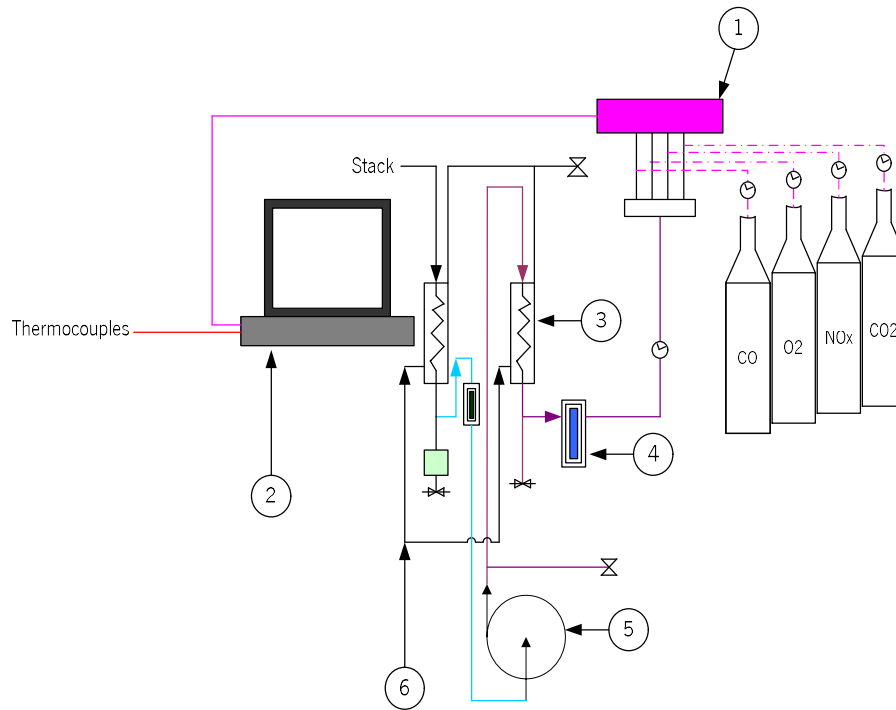


Figure 3.14. Flue gas analyzer scheme.

Notes:

- | | | |
|-----------------------------|------------------|-----------------|
| 1. Flue gas analyzer. | 3. Cooling loop. | 5. Vacuum pump. |
| 2. Data acquisition system. | 4. Filter. | 6. Water inlet. |



(a)



(b)

Figure 3.15. (a) Multi-gas analyzer 9000, and (b) NOx gas analyzer.

Species are measured in a sample diluted with a variable % of oxygen. It is standard procedure to normalize that concentration to a fixed dilution of oxygen, which for biomass application is 13% O₂. In order to correct the concentration of a given species (X_i), diluted to a certain concentration of oxygen in

the exhaust gases (%O₂) for a reference oxygen level (%O_{2ref}) one follows the conversion equation (3.12), (Turns, 2000; Ribeiro, 2012).

$$X_i @ \%O_{2ref} = X_i @ \%O_2 \frac{N_{mix} @ \%O_2}{N_{mix} @ \%O_{2ref}} \quad (3.12)$$

where, X_i is the corrected concentration of a given species (ppm), N_{mix} represents the sum of the number of moles of all species in the exhaust (kmol), considered here in a dry gas, i.e. an absent of water and considering that H₂, CO and other pollutants present in the exhaust gases are in negligible quantity. The mole fraction of dry corrected to a specific O₂ is defined as following (Eq. 3.13).

$$N_{mix,dry} = 4.76 \left[\frac{C_x + (1 - \%O_{2,dry}) H_y / 4}{1 - 4.76 \%O_{2,dry}} \right] - H_y / 4 \quad (3.13)$$

where, %O_{2,dry} the concentration of O₂ in the exhaust (%), C_x and H_y is the proportion of mole carbon and hydrogen (kmol).



Figure 3.16. Gas emissions collection unit.

Before starting the experiment, one should run the calibration of the gas analyzer. The gas analyzer was calibrated with a nitrogen-diluted reference gas with concentrations for CO = 5,000 ppm; O₂ = 20%, CO₂ = 10%, while NO_x is set at 3,000 ppm. To conduct the calibration of the gas analyzer one can

follow the detailed calibration procedure in Annex B. After the calibration of the measurement tools, then one can follow the experimental procedure in Annex B to perform the experiment.

3.4 Data acquisition and control system

3.4.1 Data acquisition mechanism

A data acquisition and control system was used to control and monitor the system to work properly. All the systems are integrated and programmed in a language of LabVIEW 8.6 to perform the operating system. The data acquisition used in this system was developed in the Department of the Mechanical Engineering University of Minho. The data acquisition and control system applied in the boiler is made up of several instruments including a controller of the National Instruments, a relay rack, and a power supply. The schematic diagram of the data acquisition and control system of the boiler is depicted in Figure 3.17. The National Instrument control system is composed of various elements as described here.

- 1) Chassis: Model PXI-1052 which functions as a motherboard, where all the remaining modules are connected, and possible to connect up to 4 PXI and 8 SCXI modules.
- 2) Controller: Works as a computer on the system using the Windows XP operating system. The model is PCI-8105 and based on the processor of Intel Core Duo with 512 MB of RAM and 60 GB hard drive.
- 3) Acquisition board: Consists of a PXI-6259 model board which allows the connection of other more specific boards including PCI, PCI Express, PXI, PXI Express, and USB. It has 32 inputs and 4 analog outputs with 16 bits and also has 48 inputs/outputs. The board also allows being demultiplexing in several more specific modules, such as a thermocouple, analog input, and the digital output module. After demultiplexing, the board also provides several functions, which emits the output voltage signals variable from 0-10 V DC. In order to be able to be used directly, then it was connected to a CB-68LP terminal board.
- 4) Thermocouple module: Consists of a specific SCXI-1102 module for reading the thermocouple incorporating a cold joint reading. The thermocouple module has 32 channels with a low pass filter of 2 Hz per channel and a protector from the highest tension of more than ± 42 V. This module is coupled with a terminal of SCXI-1303 model.

- 5) Analog input module: Consists of SCXI-1100, which provides the input of 32 analog channels of ± 10 V. The connections are fitted with the terminal board and paired with the SCXI-1300 module.
- 6) Digital input module: Consists of a model board of SCXI-1162, which provides 32 digital channels and also paired with the SCXI-1326 terminal box.
- 7) Digital output module: Consists of a model board of SCXI-1163, which provides 32 digital channels, with the voltages of between 0 and 5 V which depends on the power supply applied from an outside source. This module is also paired with a terminal board of SCXI-1326.

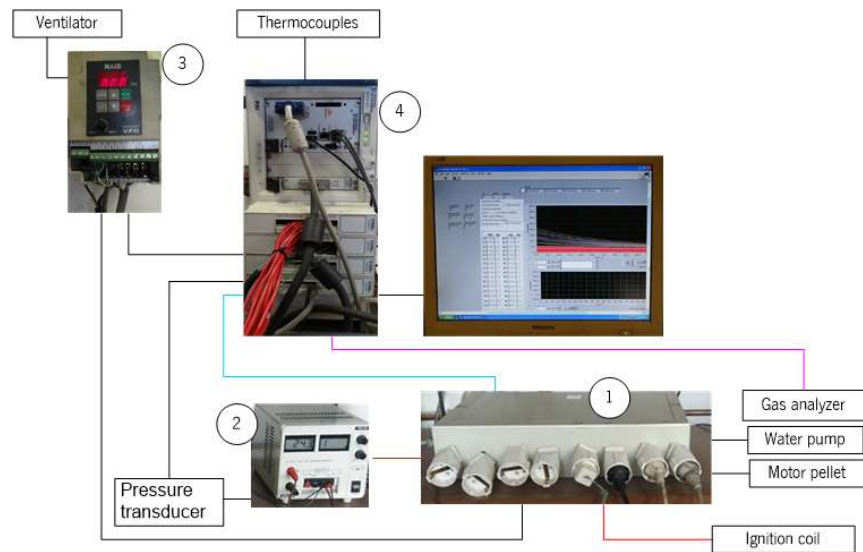


Figure 3.17. Schematic diagram of data acquisition system.

The main components are integrated as follows:

- 1) The relay frame: allows a separate power supply to the various devices operating with a 230 V AC voltage of the control devices with a voltage of 5 V DC. The relays are activated by a voltage of 24 V DC and the National Instruments control system operates at 5 V DC, the relay box is also incorporated with a voltage transforming circuit from 5 to 240 V DC.
- 2) The power supply: it is used in the system has two direct outputs of 5 and 12 V DC and an adjustable output, in this case, it is set to 24 V DC. This source feeds not only the digital output board with 5 V DC and the relay box with 24 V DC but also the pressure sensors used in the nozzles and in the orifice board that require 5 V DC power.
- 3) The control of the fan speed: it was made of an inverter with a programmable frequency. This inverter (brand NAIS), has a digital input 0/5 V DC that corresponds to the order of ON-OFF and was connected to the SCXI-1163 digital output board. It has a variable input of 0 to 10 V

DC that allows the frequency regulation of the motor. This input was connected to the variable output of 0-10 V DC available on the board of PXI-6259 through the CB-68LP terminal board.

- 4) Data acquisition system.

3.4.2 LabVIEW

LabVIEW is an object based programming language created by National Instruments. The program logics work on the principle of the data flow, which is treated and manipulated through pre-defined blocks of primary functions, which can be edited simultaneously with exit orders. The logic gives this language an optimal effect of data acquisition and processing as well as control and automation. The application developed for the experimental installation in order to acquire, manipulate, register and export the data received from the various transducers and analyzers. Besides, the application also allows the boiler to be controlled in a completely “manual mode” or by signals received by transducers, namely temperature “automatic mode”. The user interface is simple and allows the experimentalist to define the various parameters in the beginning and end of the tests, such as temperature reading, gas emissions, amongst others. The temperature reading and the corresponding the thermocouple location was presented in Figure 3.10, while other parameters including the gas emissions reading are presented in Table 3.3. The reading data are saved automatically and ready to convert into the excel sheet for the analysis process. In addition, the LabVIEW is also very useful in order to visualize and monitor graphically and in a real-time the parameters investigated during the experiment. The LabVIEW 8.6 and the user interface are shown Figure 3.18.

Table 3.3. Parameters reading in data acquisition.

Channel	Reading parameters
0	%O ₂
1	CO
2	CO ₂
3	NO _x
4	-
5	-
6	SA Tube
7	PA Tube
8	-
9	-

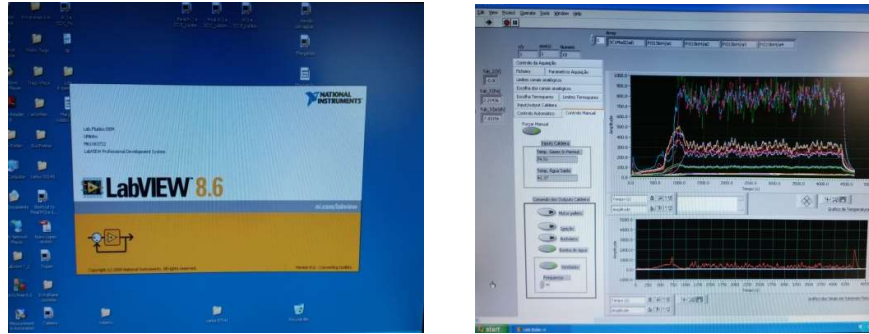


Figure 3.18. The LabVIEW 8.6 and the user interface.

3.5 Uncertainty analysis

The error in a measurement is a result of a difference between the measured value (x) and the true value (ASME, 1998). The difference between the two is the total measurement error (δ). There are two components of total measurement error: systematic error and random error. Since the measurement observation is the combination of the true value of the parameter and the total measurement error, then there is an inherent uncertainty in the use of the measurement to represent the true value. The random error is the portion of the total measurement error that varies in a repeated measurement of the true value. The systematic error is the portion of the total measurement error that remains constant in repeated measurements of the true value. The uncertainty caused by random errors can be solved by repeating the measurements (Oliveira, 2016). The total systematic errors, the elemental systematic error can be calibrated out, while those which are negligible, ignored, unknown and whose limits must be estimated (ASME, 1998). The schematic example to describe the comparison between random and systematic errors by using the target practice board is presented in Figure 3.19. Through the target practice board, the random and systematic error can be explained within four scenarios as follows (Oliveira, 2016):

- (a) High precision with small systematic error and high accuracy with small random error;
- (b) Low precision with large systematic error and high accuracy with small random error;
- (c) High precision with small systematic error and low accuracy with large random error;
- (d) Low precision with large systematic error and low accuracy with large random error.

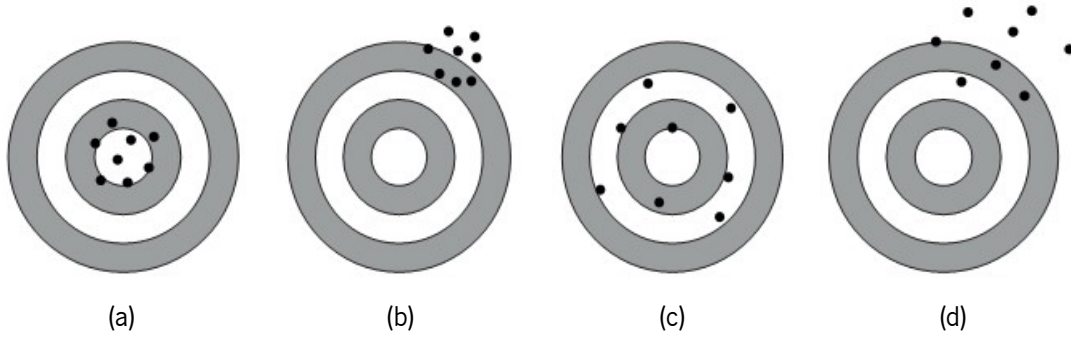


Figure 3.19. Comparison of the random and systematic errors, using the example of target practicing (Oliveira, 2016).

Regarding the uncertainty due to the random error, since the random of error introduces the variation or scatter in repeated measurements of a parameter, the uncertainty may be estimated by inspection of the measurement scatter. The population standard deviations (σ) is a measure of the scatter about the true population mean (μ) caused by the random error. Equation 3.14 represents the interval for a normal distribution including approximately 95% of the population (ASME, 1998).

$$\mu \pm 2\sigma \quad (3.14)$$

Since the sample standard deviation (S_x) is more accurate for small values of measurement number (n), thus it is preferable in comparison to the population standard deviation (Oliveira, 2016). The sample standard deviation is calculated by the following equation (Eq. 3.15) (ASME, 1998).

$$S_x = \sqrt{\sum_{i=1}^n \frac{1}{n-1} (x_i - \bar{x})^2} \quad (3.15)$$

where \bar{x} is the mean of the individual measurement x_i given by equation 3.16,

$$\bar{x} = \frac{1}{n} \sum_{i=1}^n x_i \quad (3.16)$$

The estimated standard deviation of the sample mean ($S_{\bar{x}}$) is calculated by equation 3.17,

$$S_{\bar{x}} = \frac{S_x}{\sqrt{n}} \quad (3.17)$$

The uncertainty which is defined as an interval, about the measured include the probability of the true value with the interval as given by equation 3.18,

$$R = \bar{x} \pm U \quad (3.18)$$

where U is called uncertainty or error or margin of error in the measurement of x , and for the convenience, U is always defined to be positive $(\bar{x} + U)$ (Taylor, 1997). In terms of uncertainty for a 95% confidence interval, the uncertainty is calculated through the Standard Deviation of the Mean by an expansion factor (B). Factor B is obtained from the t-student distribution table for 95% and using the degrees of freedom (df), where $df = n - 1$ (Oliveira, 2016). The expansion factor (B) is defined in equation 3.19.

$$U = S_{\bar{x}} \cdot B \quad (3.19)$$

Then the experimental data can be calculated by two simple rules (see Eq. 3.20) based on the size of n .

$$2 \leq n < 5: \quad U = (x_{\max} - x_{\min}) / 2 \quad (3.20a)$$

$$n > 5: \quad U = S_{\bar{x}} \cdot B \quad (3.20b)$$

In the experimental tests, the random error can be solved by repeating the measurement number in which the value of the parameters recorded in the long running boiler. The systematic error of the measurements was solved by calibrating the systems or gas analyzer before doing the measurement.

To know the combustion efficiency, instead of analysing the gaseous and particulate emissions, the calculation of the boiler efficiency through a heat exchanger is of a great interest for commercialization of the investigated biofuels (Lajili *et al.*, 2015). The boiler efficiency is calculated according to the NF EN 303-5 standard as conducted by Lajili *et al.* (2015).

3.6 Operation system

Correct knowledge on how to operate the system is an important part before doing any experiment. In order to formalize the experimental methodology, a step-by-step procedure sheet was developed as a guideline to operate the boiler (see Annex B). The experimental procedure includes calibration of the measurement devices, running the system and safety issues. The general information for operating the boiler in this study can be explained as follows.

3.6.1 Feeding procedure

During the feeding process before the ignition, the thermal load of wood pellets should be set at approximately 10 kW and the air flow rate at $9.4 \times 10^{-3} \text{ m}^3/\text{s}$ (23.8 Hz at the controller). While during the ignition process, if the accumulation of smoke is observed without combustion then the airflow should be gradually increased up to $1.62 \times 10^{-2} \text{ m}^3/\text{s}$ (40 Hz) to initiate the combustion. After the

combustion is initiated, set the power to 7 kW and it will require approximately 5 minutes for the combustion to reach the a stable state condition before adjusting for the required power. This sequence is introduced to avoid the instability of combustion during the start-up phase which can compromise the combustion process.

To initiate the combustion, pellets were supplied to the top of the grate by the auger. The ignition coil was installed close to the grate to allow the hot air entering to the grate after passing through the ignition coil. The boiler was provided with two-stage air channels including primary and secondary air channel. On the primary air channel, most of the air was introduced at the bottom of the grate through orifices of rectangular shape (3 mm x 26 mm), and some air was also introduced at the bottom side of the grate through orifices of 4 mm diameter. Regarding secondary air flow, orifices with a diameter of 4 mm were located on the top of the grate, 92 mm above the fuel bed. Meanwhile, the numbers of the orifices are determined based on the cross sections area of the grate.

3.6.2 Measurement condition

The gas analyzer was used to measure the CO, O₂, CO₂, and NO_x composition, and the CO was corrected to 13% of O₂. In each experiment, the boiler was running for 4 hours. If instabilities and irreversible build up of pellets on the grate were observed the boiler was shut down. The temperatures inside the fuel bed were measured in the center of the grate at four different heights. The temperature on the hot and cold water pipes was also recorded which enabled to calculate the boiler efficiency.

3.6.3 Operating conditions for wood pellets combustion

This section presents the set of operating conditions of the boiler which was used throughout this work. It includes the thermal load, excess air (EA), grate area (GA), and the primary/secondary split ratio (SR) applied. This boiler has the minimum and maximum thermal load in the range of 7 – 20 kW (Ribeiro *et al.*, 2013). When operating the boiler at maximum thermal load (20 kW), the boiler should be operated with the excess air ratio > 1.4 otherwise the fuel will be overload as the consumption of wood pellets is lower than fuel flow rate. On the other hand, at a lower thermal load (7 kW) the boiler should be operated with the excess air ratio above 1.7; otherwise, the fuel cannot be burned well, yielding high levels of smoke. In addition, this condition will create condensation in the chimney as a result of the low temperature in the exhaust gases which is below to dew point. The set of thermal loads applied in this study is presented in Table 3.4.

Specially designed air pipes are included in the boiler to provide the primary air through the grate to promote the devolatilization of fuel (Ribeiro *et al.*, 2019), and maintain the char combustion while the secondary air on the top for the purpose of efficient mixing with volatile gases to complete the fuel oxidation. With this combination, the minimum and maximum SR for primary to secondary air is 11/89 and 37/63 respectively. At lower SR, less air supply on the primary section will slow down the burning process (Ribeiro *et al.*, 2019), which results in poor combustion.

Regarding the grate area, this boiler is manufactured with rectangular shape grate fitting, where the cross-section area can be changed. The larger grate section area is 120 x 120 mm and the height can be adjusted between 50 - 70 mm, but the optimum grate height should be around 60 mm. Three different sizes (cross section area) were applied in this experiment, which will be described later.

Table 3.4. Thermal load.

Excess air (%)	Thermal load (kW)		
	10	13	16
50	a,b,c	a,b,c	a,b,c
70	a,b,c	a,b,c	a,b,c
110	a,b,c	a,b,c	a,b,c

Notes: a = SR 20/80; b = SR 30/70; c = SR 37/63.

3.7 TGA device

To observe the thermal decomposition of pine wood, the TGA technique was performed in Laboratory of Metallurgy of the University of Minho. The TA Instruments SDT 2960 simultaneous DSC-TGA instrument is presented in Figure 3.20. In the TGA test, different parameters can be assessed to investigate the thermal decomposition of the biomass material such as particle size, material, heating rate, flow rate, and diluting gas. To conduct the TGA test the wood pellets were milled into dust and sieved into different batches, according to the particle size desired. The temperature in the TGA test was set to a maximum of 750 °C, as at this range (above 700 °C) fuel samples display similar behavior regardless of the diluting gas (Yuzbasi and Selçuk, 2011). In differential scanning calorimetry (DSC) measurement, the reading temperature was measured based on the temperature difference between the empty cup (reference cup) and the cup with the samples (sample cup). Thus, a difference in heat flow between the sample cup and reference cup is measured using thermocouples in the balance arms. The SDT 2960 provides differential thermal analysis data with the high ΔT sensitivity (0.001 °C) and allows the detection of small endothermic and exothermic transitions, the results being expressed either in °C or μV . As far as the TGA is concerned, weight is measured by a taut-band meter movement by using an

infrared light-emitting diode source and a pair of photo-sensitive diodes. The taut-band meter movement is located at the rear of each balance arm to measure the weight change of the sample (www.artisan-tg.com).



Figure 3.20. DSC-TGA device unit.

3.7.1 Experimental procedure

From this TGA data, the kinetics reaction of the pellets was calculated by using the change in the extent of reaction (α). Meanwhile, the rate of the chemical reaction (k) is calculated by applying an Arrhenius equation (Ferreira, 2016). Then, the kinetic properties of biomass fuels under non-isothermal conditions are calculated by applying the Coast-Redfern equation (Ebrahimi-Kahrizsangi and Abbasi, 2008) which is an integral method and involves the thermal degradation mechanism as described in Aboulkas and Harfi (2008). The schematic diagram of the procedure followed in the TGA experiment is depicted in Figure 3.21.

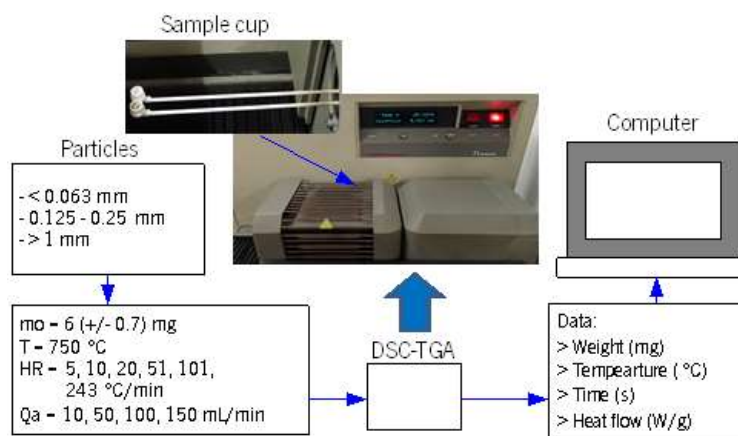


Figure 3.21. TGA experiments procedure.

3.7.2 Sample preparation

Regarding the TGA experiment, 6 mm diameter wood pellets were milled into dust by means of a hammer and a knife mill. The knife mill, with a sieve limit of 2 mm of diameter has a processing capacity between 0.2 to 50 kg/h and a power of 1.5 kW (Ferreira, 2016), is presented in Figure 3.22.



Figure 3.22. Knife mill device.

Once milled, the ground dust passed through a sieving device with the vibration unit to separate the wood particles, as presented in Figure 3.23. The resulting batches were organized into three different classes: < 0.063 mm, 0.125 – 0.25 mm and > 1 mm. Figure 3.24 shows a sample of the original pellets and the three size classes resulting from the milling/sieving operation. The properties are listed in Table 3.2.



Figure 3.23. Calibrated sieving machine and vibration unit.



Figure 3.24. Pellets and pine wood particles.

3.7.3 Operating conditions for TGA experiment

To conduct the TGA analysis for the various particle sizes, air flow and heating rates were determined. Three particle sizes including smaller than 0.063 mm, 0.125 - 0.25 mm and larger than 1 mm were used with a heating rate of 5, 10, 20 and 51 °C/min. In addition, heating rates of 101 and 243 °C/min were applied but only for particle size between 0.125 - 0.25 mm. In this set of experiments, the air flow rate was always maintained at 100 mL/min. Besides, air flow rates of 10, 50, 100 and 150 mL/min were also applied for the three different classes of particle size and the heating rate was maintained at 10 °C/min. Pine wood particles with the initial mass of approximately 6 mg were used. This TGA device can be operated up to a maximum temperature of 1,500 °C, and a heating rate up to approximately 250 °C/min. The size of the particles are limited to 6 mm, the sample weight to 50 mg and the air flow rate to 150 mL/min. Before introducing the sample, the equipment was set to the desired value. The device was running as the setting conditions applied and terminated automatically as the sample is fully combusted. In addition, the duration of the experiment depends on the heating rate and diluting temperature applied, as the heating rate increased a shorter time is required for the combustion to be completed.

3.8 Mass loss experiments

To conduct the mass loss and elemental analysis in order to understand the behavior of wood pellets combustion, a small scale reactor was used. This experiment was conducted mostly in the Laboratory of Foundry where the reactor was located. A preliminary set of experiments was carried out at the Energy and Fluids Laboratory by using a reactor with a temperature range limited up to 250 °C (see Figure 3.25 (a1)) with a setting of 144, 191, and 225 °C. This set of experiments was developed as a test basis for the experimental procedure. The second set of experiments was carried out in a small scale reactor with a thermal capacity of 1.36 kW and a temperature range up to 1,150 °C. The testing temperatures were defined at 264, 351, 444, 541, 650 and 734 °C. This reactor is 100 mm diameter, 170 mm height (see Figure 3.25 (a2)); the cup is 30 mm diameter and 33 mm height (see Figure 3.25 (b)), and scale with 10 mg accuracy as shown in Figure 3.25 (c).



Figure 3.25. (a) The small scale reactor, (b) Cup, and (c) Scale.

3.8.1 Experimental procedure

To understand the mass loss of the burning pellets, a small holding cup was used in the experiments. Before conducting the mass loss experiment, the cup was preheated for a period of time, until its temperature was uniform. By applying the transient lump capacity equation one could assess the adequacy of the preheating stage. To compare the experimental data with the transient equation

calculation, then the thermocouple was attached to the surface of the holding cup. From this test it could be concluded that the time required for the cup to reach its equilibrium temperature is 15 minutes. Once this condition was attained, one could proceed with the mass loss experiment.

After a series of preliminary tests, the procedure converged to the following steps (see Figure 3.26).

1. Set up the desired temperature. To set the desired temperature one needs to measure the actual internal temperature instead of the scale reading. By introducing the thermocouple into the reactor with the data logger, the correct temperature can be obtained.
2. Preheat the reactor. Start preheating the reactor for the experiment.
3. Prepare the sample. To obtain the weight of the sample, the scale with 10 mg accuracy was used.
4. Introduce the sample. After 15 minutes of the preheating time, introduce the sample into the reactor.

To obtain the accuracy result then the test was conducted for 3 times for one piece of data.

The holding cup was the subject of a series of tests in order to ensure that it had no influence upon the results. The selected design consisted of a light stainless steel mesh that combined lightness and an “open” structure to enable the fast response of the sample inside the reactor.

After the test is terminated, the sample with the cup is weighted. The mass loss was obtained from the difference between the cup with the sample and the empty cup weighted at approximately 7 minutes after the preheat state.

3.8.2 Elemental analysis of pellets

At selected times, the sample was removed from the reactor and rapidly cooled down. Then the elemental analysis was conducted to the solid sample in order to understand the devolatilization of the pellets. The elemental analysis was determined at different temperature and time as applied for the mass loss experiment. The elemental analysis was carried out in CVR (*Centro para a Valorização de Resíduos*) Guimarães, using a CHN/CHNS Carbon/Hydrogen/Nitrogen/Sulfur/Oxygen determinators. To ensure reproducibility this elemental analysis the sample is prepared with the same method as for the mass loss experiment. Figure 3.26 describes the experiments procedure for mass loss and elemental analysis.

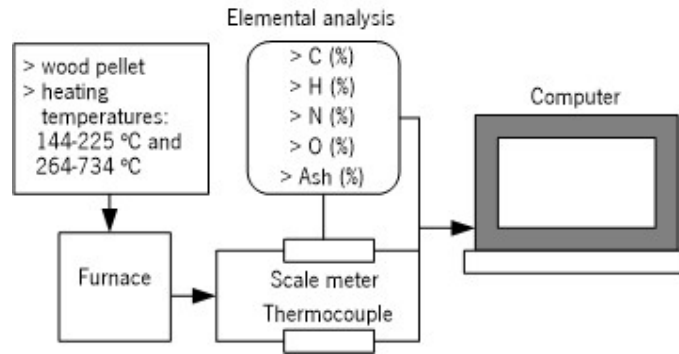


Figure 3.26. Experimental diagram of mass loss and elemental analysis.

3.8.3 Temperature profile of the pellets

To understand the temperature profile of the pellets during the pellets burning, then the single pellet experiment can be implemented. Pellets with a diameter of 6 mm were drilled along its axis (orifice 1.35 mm) and a Type K thermocouple (1.25 mm) was introduced through the pellet to measure its core temperature. From this experiment, the temperature profile in the center of a wood pellet can be obtained and compared with the analytical profile for different heating using a simple model for 1D transient conduction in a cylinder (Cengel, 2002). The reactor used to conduct this experiment is depicted in Figure 3.25 (a1).

3.8.4 Moisture content of pellets

The mass loss of dry and wet pellets can also be conducted as a function of time and temperature. To remove the moisture content, then the pellets were placed in the reactor (Figure 3.25 (a1)) at a constant controllable temperature. The moisture content of the pellets can be observed by measuring the mass loss at a different times such as 1, 12, 24 and 208 hours at 105 °C. The moisture content value is recorded when it reaches the constant value with the minimum time applied. To conduct the experiment, first set the internal temperature of the reactor at 105 °C for a period of 24 hours. This procedure is in accordance with standard SS 18 71 20 (Hansen *et al.*, 2009).

3.8.5 Sample preparation

The pine wood pellets with 6 mm diameter, 12 - 15 mm length, 2.08 – 3.94 g weight and in each test three pellets were used. The samples were weighted once before the test was started. The properties of pine wood pellets were presented in Table 3.2, and they are fairly uniform from a large batch supplied by the manufacturer, as it is a certified product. In developing the elemental analysis there are several

methods used in sample preparation including Gel Capsule method, Thin Foil method, Manual preparation and using the Foiler. The Manual method was followed (Leco, 2007):

1. Place the sample cup holder on the balance.
2. Place foil into the sample cup holder and tare the balance.
3. Remove the foil and the sample cup holder from balance and add sample to foil.
4. Place the sample cup holder and foil on the balance and weigh.
5. Remove the foil from the sample cup holder twist to seal.

Enter the mass in the spreadsheet or automatically by pressing print on the balance.

4. TGA ANALYSIS OF PINE WOOD PARTICLES

This chapter discusses the thermal decomposition and kinetics of pine wood particles using the TGA technique. Several parameters were evaluated in this study including the heating rate, air flow rate, and particle sizes. The properties of pine wood pellets used in this study were previously presented in Table 3.2.

4.1 Test conditions

In conducting the TGA tests, a wide combination of air flow and heating rates was applied. From the batches selected by sieving (see section 3.7.2) three particle sizes were tested: smaller than 0.063 mm, in the range 0.125 - 0.25 mm and larger than 1 mm. In this way a broad band of the sizes could be evaluated. Regarding the heating rate, four levels were selected for all the samples: 5, 10, 20 and 51 °C/min. In addition, heating rates of 101 and 243 °C/min were applied for the middle particle size (0.125 - 0.25 mm). This represent, the upper limit that could be tested with the present apparatus. In this set of experiments the air flow rate was maintained at 100 mL/min. Besides, air flow rates of 10, 50, 100 and 150 mL/min were applied for the three different classes of particle size while the heating rate was kept at 10 °C/min. Each sample had an initial mass of approximately 6 mg.

4.2 Thermal decomposition of pine wood particles

The TGA and the derivative thermogravimetric curve (DTG) profiles directly obtained during the experiments enable the identification of various key temperatures, such as: initial decomposition (T_{id}), peak (T_{max}) and burnout (T_b) temperatures. T_{id} corresponds to the beginning of the weight loss and it is defined as the temperature at which the rate of weight loss reaches 1%/min after the initial moisture loss peak in the DTG profile. T_{max} is the point at which the maximum reaction rate occurs. T_b is identified when the last peak comes to the end and the temperature at which the sample is completely oxidized. It is taken as the point immediately before reaction ceases, when the rate of weight loss is down to 1%/min (Ferreira, 2016; Yuzbasi and Selçuk, 2011). The ignition temperature (T_i) is obtained by applying the TG-DTG tangent methods (Magalhães *et al.*, 2017; Li *et al.*, 2006). Furthermore, these experiments enable the identification of the combustion rate and the heat released at different temperatures and times. All this information allows characterizing the thermal decomposition of the pine wood samples. From the mass loss rate data, the ignition index (D) and combustion index (S) are obtained through Eqs. 4.1 and 4.2 respectively (Vamvuka and Sfakiotakis, 2011).

$$D = \frac{R_{\max}}{t_{mr} \cdot t_j} \quad (4.1)$$

R_{\max} is the maximum combustion rate, t_{mr} and t_j is the time that corresponds to maximum combustion rate and the ignition time that corresponds to ignition temperature T_j respectively.

$$S = \frac{R_{\max} \cdot R_a}{T_j^2 \cdot T_b} \quad (4.2)$$

where R_a is the average mass loss rate and T_b is the burnout temperature.

4.2.1 Influence of the heating rate

Figures 4.1, 4.2 and 4.3 (a), dashed lines, allows to identify the three different stages of biomass combustion: moisture loss, volatile matter loss, and char residue loss. This section discusses the thermal decomposition of pine wood particles using the TGA analysis. The weight loss (%), specific heat flow (W/g) and rate of mass loss (%/min) for the different particle size at various heating and air flow rates were examined. The weight loss and heat flow data are grouped in the same figure on the *l.h.s*. In it, the dashed line represents the mass loss and the solid line refers to the heat flow. The graph on the *r.h.s* refers to the rate of mass loss. The colors in both graphs are matched. Following the procedure described above, the data obtained at various heating rates for the three particle sizes are summarized in Tables C.1 through C.3 (see Annex C). These data include the most relevant variables that identify the various transitions occurring during the couplet combustion of biomass. It is possible to observe that the heating rate affects the weight loss curves. The figures also include a horizontal line at the moisture content of the samples ($\approx 7\%$). As can be observed in the Figures 4.1, 4.2 and 4.3 (b) that, the thermal decomposition, for all particle sizes examined, starts at approximately 260 °C for low heating rates and, at 211 °C for high heating rates, see Tables C.1, C.2 and C.3. Therefore, as the heating rate increases, the initial decomposition temperature decreases. This can be explained that, at low heating rates (< 10 °C/min), the initial decomposition starts at a higher temperature because the heating release was taking place at a slower rate and allows enough time for water to be removed completely from the sample. But at higher heating rates (> 20 °C/min), the initial decomposition starts at a lower temperature because as the faster heating there is not enough time for the moisture to be fully removed from the sample; the drying phase is controlled by the water diffusion inside the biomass structure. This was indicated by the mass loss of the sample that is below 7% after the initial decomposition. A major loss of mass follows, where the main devolatilization occurs with a maximum combustion rate between 319 to 365 °C for particles smaller than 0.063 mm, 321 to 401 °C for

particles between 0.125 and 0.25 mm and, 321 to 369 for particles larger than 1 mm. From these figures, it can be seen that, as the particle size and the heating rate increase, the maximum combustion rate increases although, the effect of the heating rate is much stronger. This condition could be a result of the total time of the sample in the furnace which decreases with increasing heating rate.

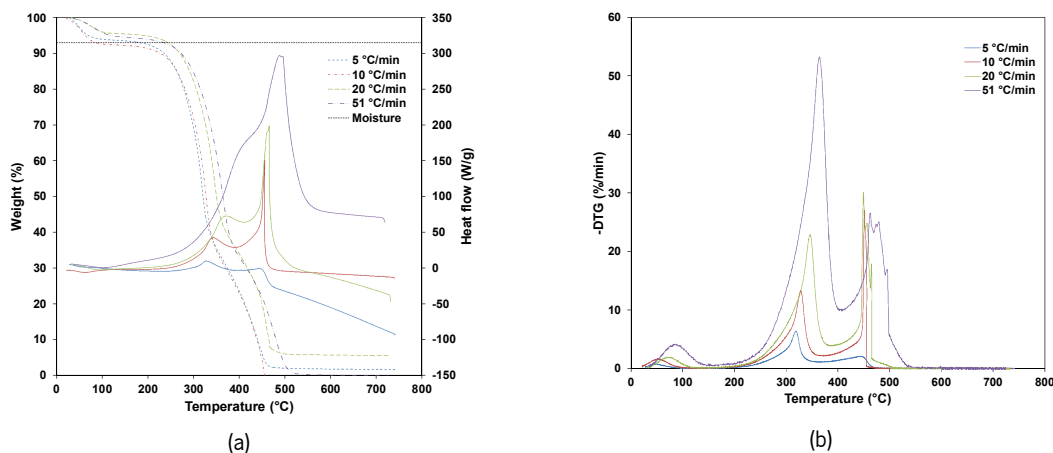


Figure 4.1. (a) Weight loss and heat flow, and (b) Rate of mass loss (particles smaller than 0.063 mm).

The data show that the heat flow increases with the heating rate, which according to Kok and Özgür (2013) is due to thermal lag. During the thermal decomposition, it is possible to identify two different exothermic reaction regions. The first region is associated with the combustion of light volatile matters which provides the reactivity to biomass fuels, while the second region is associated with the combustion of char (Kok and Özgür, 2013). Consequently, heat, in general, is released between approximately 300 °C and 500 °C, reaching the highest value in the vicinity of 450 °C, for all pine wood particles analyzed at lower heating rates (5, 10 and 20 °C/min). However, for higher heating rates, as is the case at 243 °C/min, the temperature range is higher reaching 700 °C and the highest value close to 680 °C. This is due to the higher thermal gradient inside the particles, and then the char combustion is completed later at a higher temperature.

Therefore, according to the DTG curves, as depicted in Figures 4.1, 4.2 and 4.3 (b), when the heating rate is increased, the thermal decomposition was shifted to a higher magnitude. The reason for these shifts is due to different heat transfer and kinetic rates, delaying the sample decomposition. In addition, the intensity of degassing and the thickness of the gas cushion around the particle increase and may temporarily slow down the heat flux inside the particle (Kluska *et al.*, 2019).

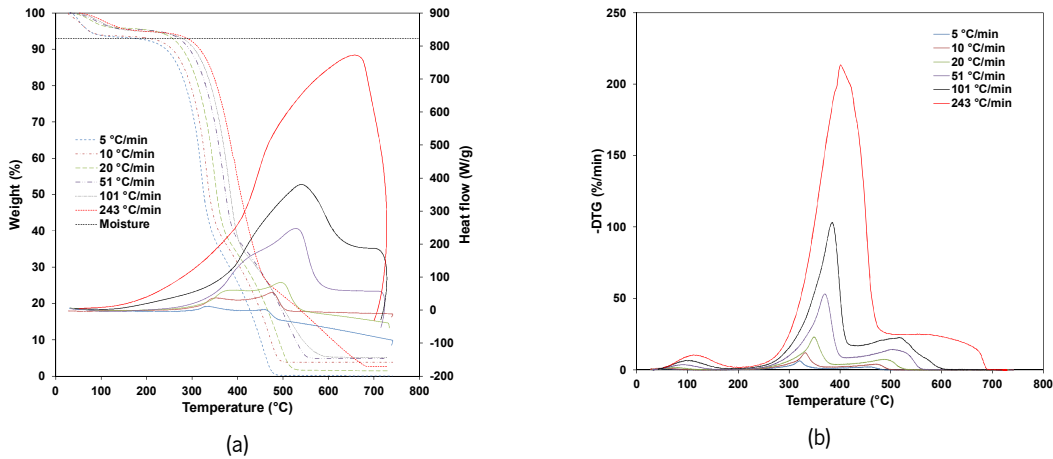


Figure 4.2. (a) Weight loss and heat flow, and (b) Rate of mass loss (particles between 0.125 - 0.25 mm).

Another effect is that heat transfer is not as effective and efficient at slower heating rates and, therefore, the minimum heat required for cracking of the particles is reached later, at higher temperatures (Mani *et al.*, 2010). Conversely, at lower heating rates, the heating of the pine wood samples occurs more slowly, yielding a more effective heat transfer to the inside of the particles and, as a consequence, the cracking takes place more efficiently.

The heat flow increases with the higher heating rate and the temperature at which the maximum heat flow occurs shift to the higher value which corresponds to the char combustion stage where the volatiles are almost completely oxidized.

Figures 4.1, 4.2 and 4.3 (b) describe the peak temperature for the various heating rates applied. The lower the peak temperature the easier the ignition of the pine wood particles will be. The combustion reactivity is proportional to the height of the DTG peak so that it is clear that higher heating rates correspond to the most reactive of combustion.

In Figures 4.2 and 4.3 (a) (for particles of medium and large sizes), at high heating rates, only one peak is visible. This is because at a high heating rate the heat release was very high, the material reaches a given temperature in a shorter time and the thermal decomposition starts earlier than at a low heating rate (Kluska *et al.*, 2019), as indicated by the initial decomposition temperature (see Table C.1 – C.3). For example at a heating rate of 243 °C/min, combustion is completed in less than 4 minutes. It is also observed that, as the heating rate increases, there is a shift to higher temperatures for the initiation of decomposition process (Kluska *et al.*, 2019). In addition, this increase in temperature is independent of the particle size which suggests that temperature gradients inside the sample push the initiation of the decomposition to higher temperatures. This is because at a high heating rate the yield of volatile materials was higher and it occurs during the first stage of volatiles combustion while it delayed the

thermal degradation process (Vamvuka and Sfakiotakis, 2011), due to the increase in thermal gradient inside the sample at a higher heating rate. This is indicated by the value of the ignition and burnout temperatures (Table C.1 – C.3) that shifted to the higher values. This observation is in agreement with the work by Vamvuka and Sfakiotakis (2011) and Kok and Özgür (2013). Shen *et al.* (2009) stated that a high heating rate will not give sufficient time for heat to be transferred to the center of the particle and leave a high-temperature gradient within the particle. In addition, increase the heating rate increases the residue at the end of the experiments as revealed by Mani *et al.* (2010). This feature is not observed in the present work which shows that there is no consistent trend as far as the heating rate is concerned.

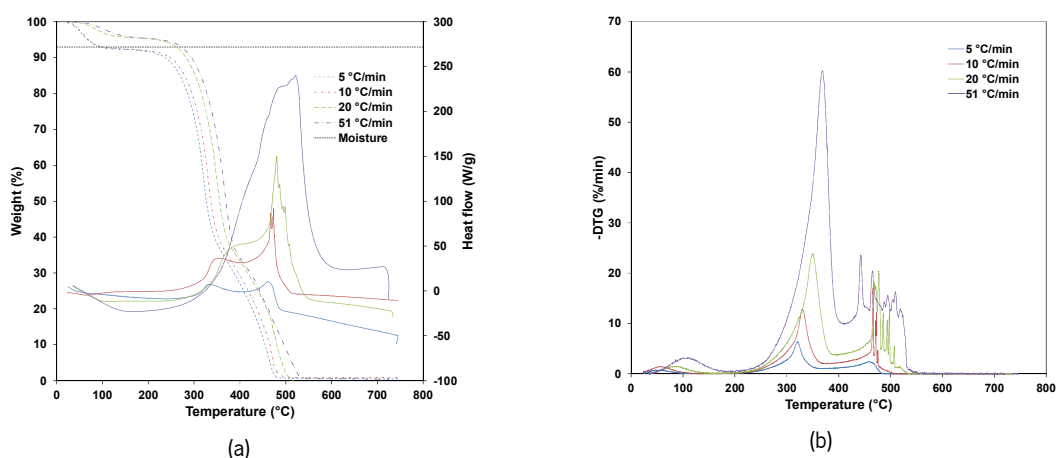
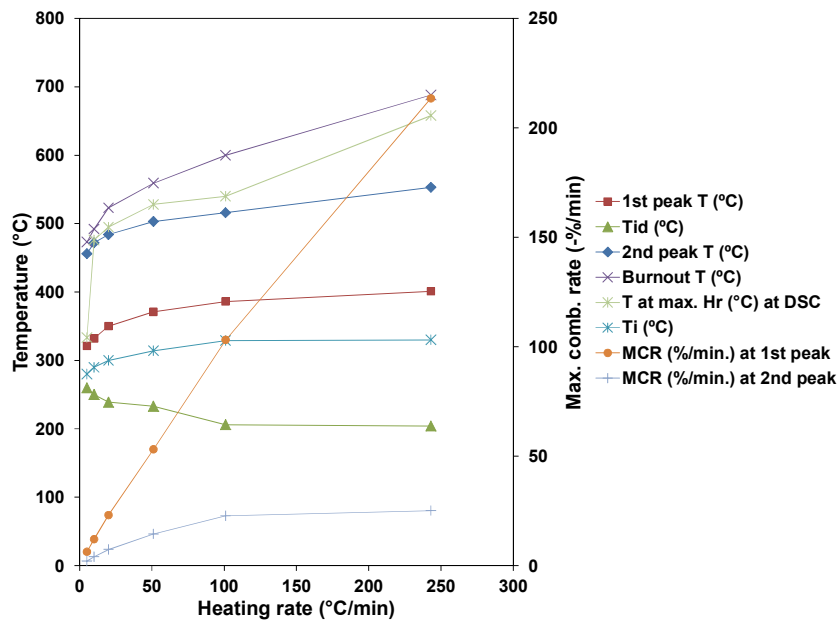


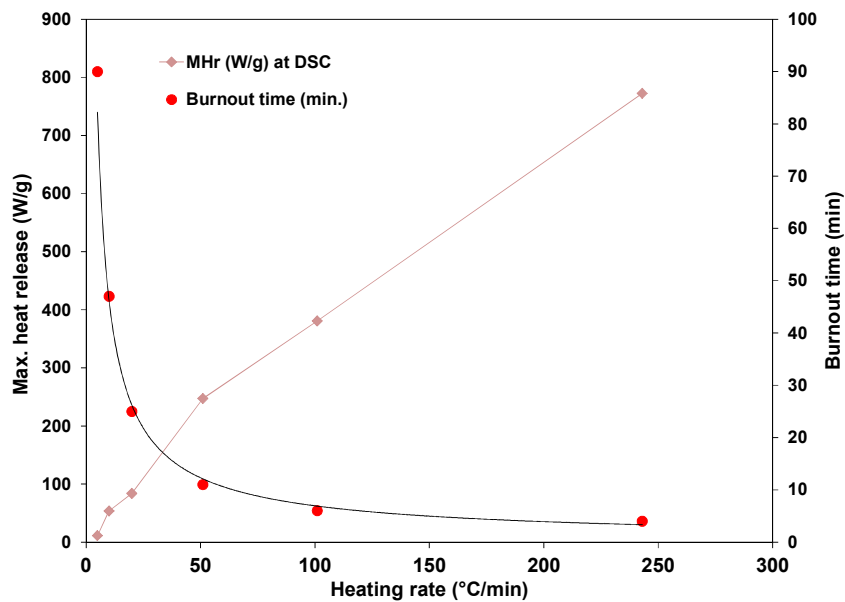
Figure 4.3. (a) Weight loss and heat flow, and (b) Rate of mass loss (particles larger than 1 mm).

It is important to note that this trend was observed for all particle sizes. Meanwhile, the remaining mass (the mass that is observed based on the heating rate and temperature applied) (Table C.1 – C.3) shows a different trend or inconsistent behavior which may be influenced by the uncertainty either from the instruments or random selection of the testing sample from the bulk of the material (see Figure 4.4 for particle 0.125 – 0.25 mm). Figure 4.4 also presents the combustion characteristic referred to Table C.2, which indicates that the parameters such as the initial decomposition temperature (see Figure 4.4 (a)) and burnout time tends to decrease as increasing of the heating rate compared to the other parameters applied (see Figure 4.4 (b)). Such behavior is also observed for other particle sizes: < 0.063 mm and > 1 mm. Figure 4.4 (b) also shows that when increasing the heating rate, there is limited for the heating rate that may be due to the thermal gradient. Since the composition of the sample which may be varied with either more ash or volatile compositions. This condition may also be observed for different air flow rates (Table C.6 – C.8), (in Annex C), after the burnout time the remaining mass show an inconsistent pattern. One would expect that once the combustion is completed only the ashes were

present. However one may observe that the data shows a wide variation and also, not a clear trend (Figure 4.4 (c)). This may be due to either from the selection of the testing sample or uncertainty in the instruments as stated before. To verify the randomness hypothesis, three tests with the same conditions at 10 °C/min, 100 mL/min and middle particle size range (0.125 and 0.25 mm) were conducted (see Figure 4.5). The figure obviously shows the different values of the remaining mass obtained as an indication of the effect of the randomness in the sample. One has also to refer that all other parameters (included in Table C.2) were verified. This observation may point to the hypothesis of sample randomness.



(a)



(b)

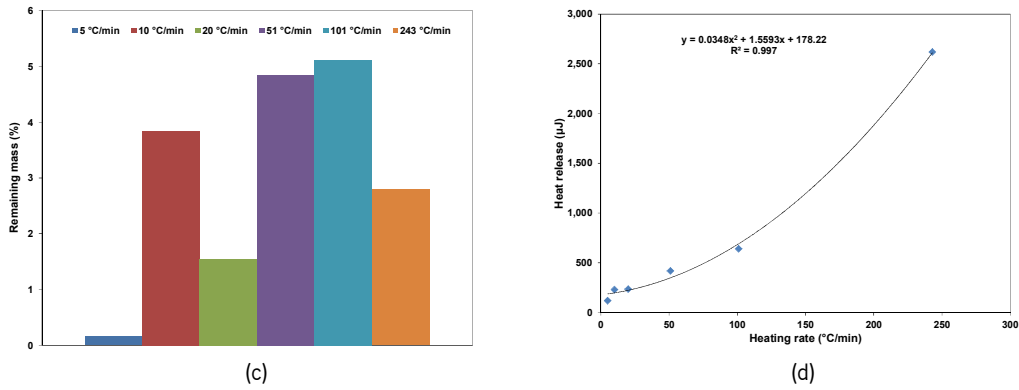


Figure 4.4. The combustion behavior test at different heating rates for particles between 0.125 – 0.25 mm: (a) Max. comb. rate and temperature at various conditions, (b) Max. heat release and burning time, (c) Remaining mass, and (d) Heat release.

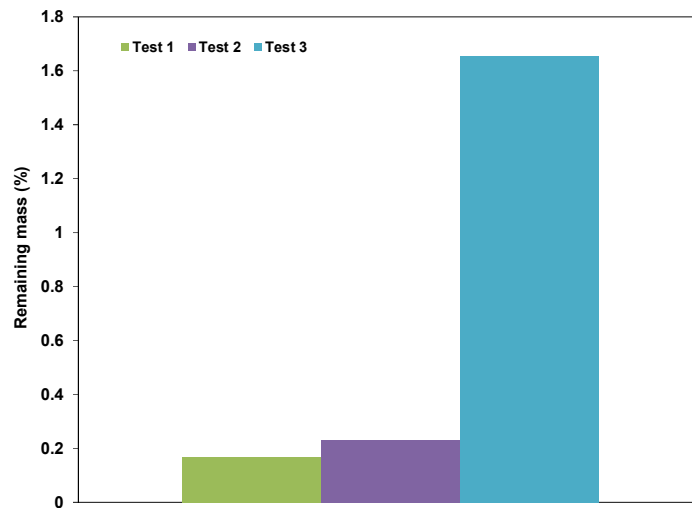
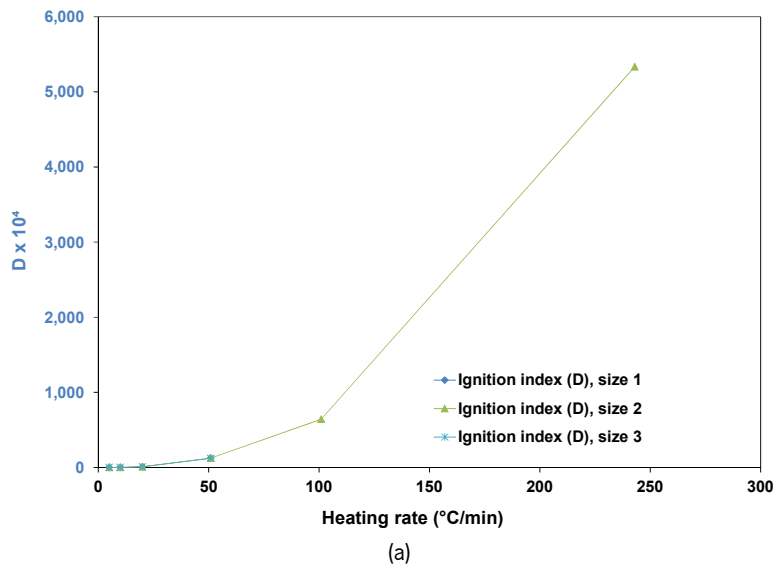


Figure 4.5. The remaining mass of the three tests in the same condition with middle particles size.

Mass loss through the conversion process was calculated on the basis of three different stages that are defined by the characteristic temperatures identified in the TGA curve (Magalhães *et al.*, 2017). While the first stage refers to the decomposition of the fuels before ignition, the second stage is associated with the main combustion stage, and the third stage concerns char combustion. The mass loss in the first stage was calculated between the initial decomposition (T_{id}) and to the ignition temperature (T_i). The second stage is bounded by the first peak after moisture release in DTG curves. The third stage corresponds up to the temperature of the second peak in DTG curves. The mass losses in such three stages at different heating rates and particle sizes are presented in Table C.4 (see Annex C). This shows that the total mass loss increases with increasing heating rate as the amount of lignin that is converted into char is reduced. This observation is in agreement with the results presented by Hoekstra *et al.*

(2012). The value of mass loss in the first stage indicates that at a high heating rate the mass loss is higher than at a low heating rate for all particles. Table C.4 shows that most of the mass loss occurs in the second stage which accounts for approximately 50% of the total mass loss. This corresponds to the combustion of light volatile matters (Kok and Özgür, 2013).

Following the procedure previously described the ignition (D) and combustion (S) indexes are summarized in Table C.5 (see Annex C), for different heating rates. The results show that the ignition index is correlated with the ignition temperature. The better ignition performance was observed at a higher ignition index, for all particles sizes. The value of the combustion index also follows a similar trend (see Figure 4.6 (a, b)), where the value increases with the heating rate for all particle sizes. The figures also show that there is no significant effect of the particle sizes on the ignition and combustion indexes.



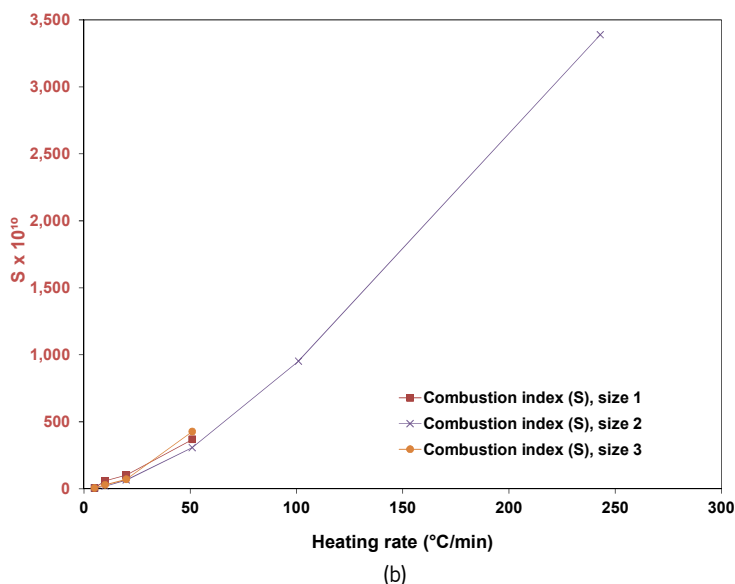


Figure 4.6. Combustion parameters of the pine wood particles at different heating rates: (a) Ignition index, and (b) Combustion index.

4.2.2 Influence of air flow rate

Figures 4.7, 4.8 and 4.9 show the weight loss (%), heat flow (W/g) and the rate of mass loss (%/min) for the three pine wood particle sizes examined at four different air flow rates (10, 50, 100 and 150 mL/min), the heating rate was set at 10 °C/min.

The dashed lines in Figure 4.7 (a), show the weight loss for particles smaller than 0.063 mm. It is possible to see that the mass loss plot have a similar behavior at different air flow rates. However, after the devolatilization stage, there are differences in mass loss rate. In this way, with middle air flow rates, 50 and 100 mL/min, the mass loss occurred earlier when compared with other air flow rates. These differences can be seen in the DTG curves in Figure 4.7 (b) in the second peak for the 100 mL/min air flow rate. Therefore, at 100 mL/min, during the char combustion, the mass loss increased and, consequently, in the heat flow curve (continuous line in Figure 4.7 (a)), it is possible to see that more heat was released at 100 mL/min during the devolatilization and char combustion stages. For particles between 0.125 and 0.25 mm similar results were obtained (Figure 4.8). However, during char combustion, the mass loss is independent of the air flow rate, as can be seen in Figure 4.8 (b) and, the heat flow decreases significantly when compared with the results presented previously at 100 mL/min. Furthermore, as can be seen in Figure 4.8 (a), a higher heat flow was observed at 100 mL/min.

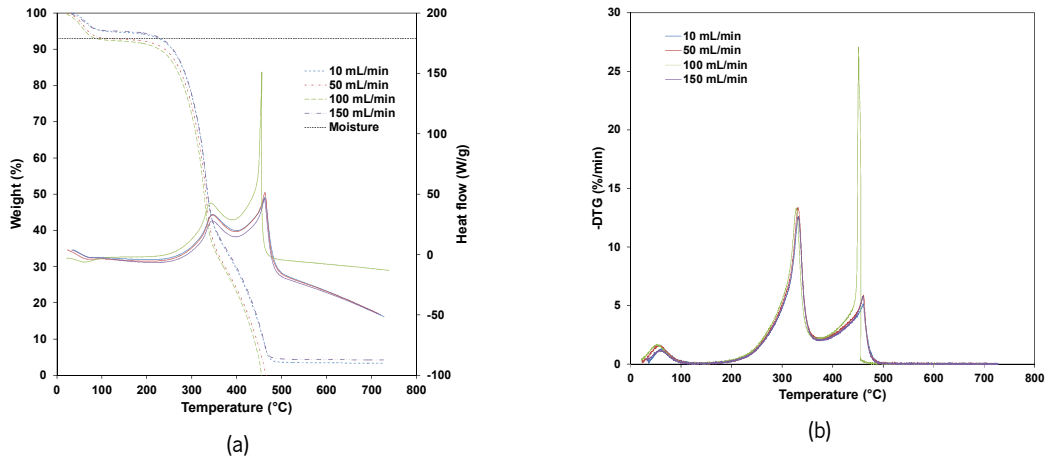


Figure 4.7. (a) Weight loss and heat flow, and (b) Rate of mass loss (particles smaller than 0.063 mm).

Figure 4.9 presents the results of the experimental data for the particles larger than 1 mm. As can be seen in Figure 4.9 (a), at 10 and 100 mL/min the mass loss during the drying process occurred earlier and, during devolatilization and char combustion the mass is slower at 150 mL/min.

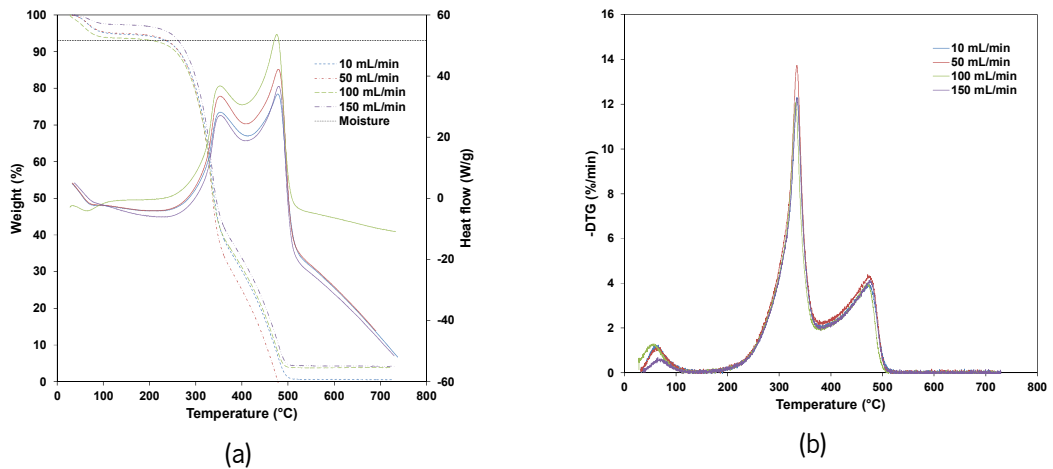


Figure 4.8. (a) Weight loss and heat flow, and (b) Rate of mass loss (particles between 0.125 and 0.25 mm).

Figure 4.9 (b) shows, at the second peak, a trend similar to that observed for particles below 0.063 mm in diameter. However, the second peak occurred at 100 mL/min but also at 10 mL/min and 150 mL/min.

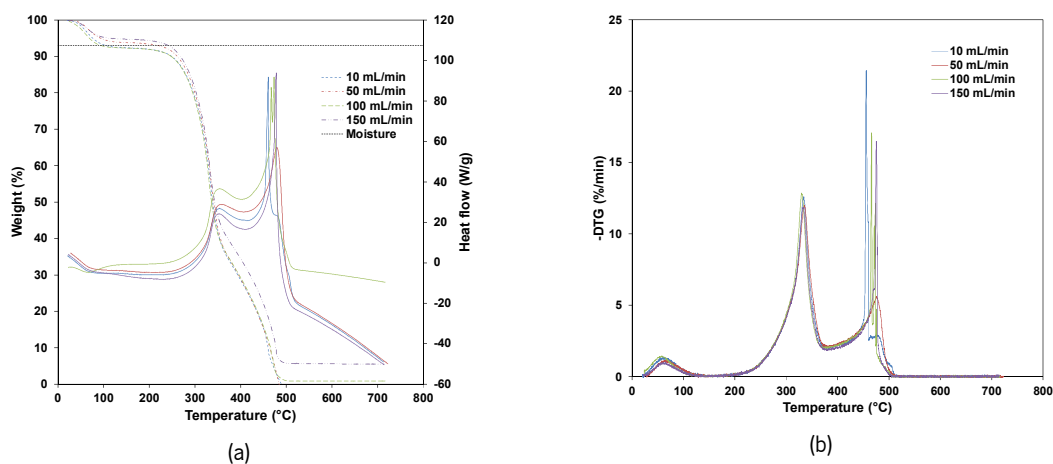


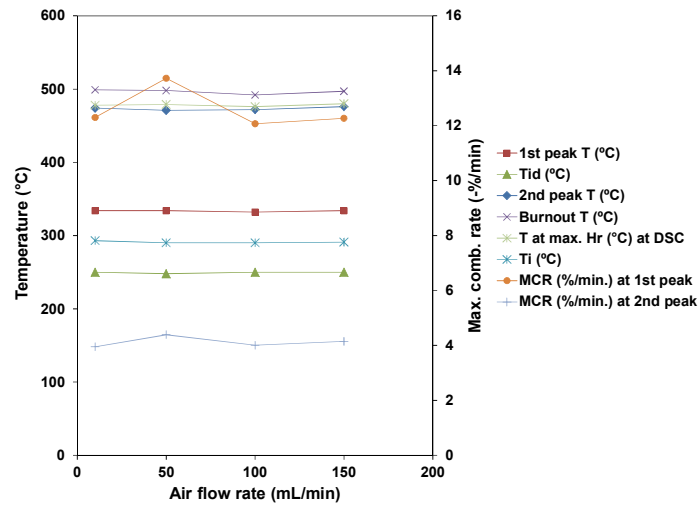
Figure 4.9. (a) Weight loss and heat flow, and (b) Rate of mass loss (particles larger than 1 mm).

Consequently, the heat flow (Fig. 4.9 (a)) displays a higher value at the second peak for 10, 100 and 150 mL/min. It should be noted that although the maximum heat flow peak is higher in the case of particles smaller than 0.063 mm at 100 mL/min, more heat was released in the experiments with particles greater than 1 mm, for various air flow rate in this study except at 50 mL/min. Therefore, as could be expected, more energy is released with increasing the particle size at different air flow rates.

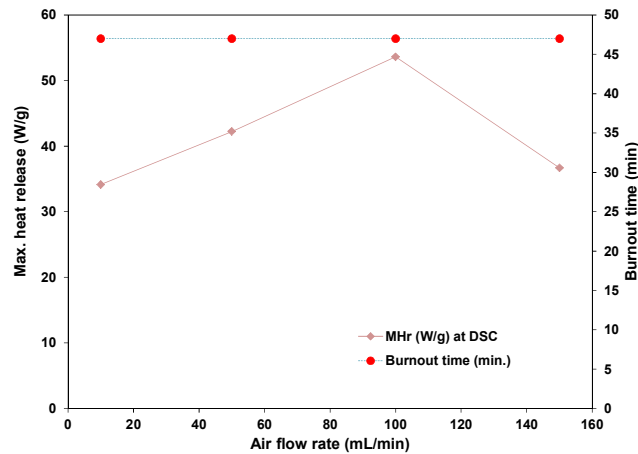
Following the procedure described earlier in this chapter, the main thermal parameters from the TGA curve are summarized in Table C.6 through C.8 (see Annex C), depending upon the particle size. From these results, it can be said that there is a negligible influence of the air flow rate on the thermal decomposition of the biomass particles. The main devolatilization occurs at a maximum combustion rate between 328 to 332 °C for particles smaller than 0.063 mm, 332 to 334 °C for particles between 0.125 - 0.25 mm and, 330 to 335 °C for particles larger than 1 mm. In this value, it can be seen that, as the particles size and the air flow rates increase, the maximum combustion rate increases slightly. This may result from the surface area of the particle, where an increase in surface area of the particles minimizes mass and heat transfer limitations and improves conversion efficiency (Manouchehrinejad *et al.*, 2018).

Another feature is that for a heating rate of 10 °C/min the air flow rate has no influence on the relationship between the moisture release temperature and the initial decomposition temperature. That is, at this heating rate the drying stage is fully completed before the devolatilization commences. Only at very high flow rates the temperatures converge (see Table C.6 – C.8). In fact, the influence of the gas flow rate is negligible as depicted in Figure 4.10 for most of the variables of interest, taking the data with the particles with a diameter between 0.125 and 0.25 mm. Figure 4.10 (b) shows that the burnout time is almost constant for different air flow rates, but the MHR is increasing with air flow rates and then

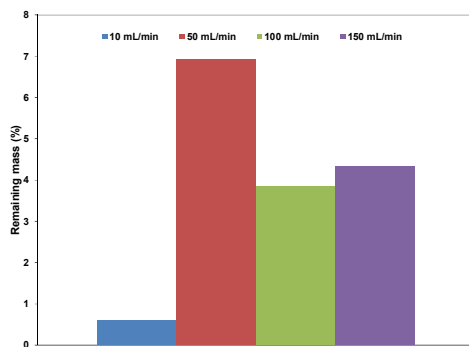
significantly decreasing at 150 mL/min. This indicates that the heat release is higher at 50 and 100 mL/min for different air flow rates (see Figure 4.10 (d)), the same behavior being observed for particles < 0.063 mm and > 1mm.



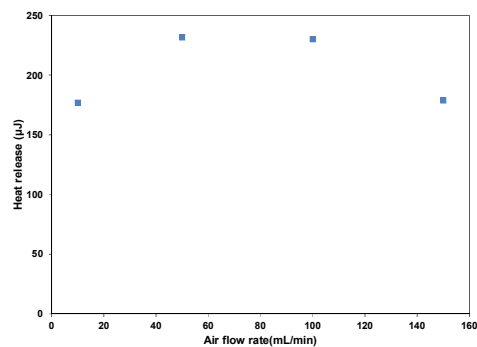
(a)



(b)



(c)



(d)

Figure 4.10. The combustion behavior test at different air flow rates for particles between 0.125 – 0.25 mm: (a) Max. comb. rate and temperature at various conditions, (b) Max. heat release and burning time, (c) Remaining mass, and (d) Heat release.

Again, the remaining mass shows (Fig. 4.10 (c)) a wide variability that is not consistent with the composition of biomass. Following the procedure applied above for the mass loss calculation in the three different stages, the influence of air flow rate and particle size is presented in Table C.9 (see Annex C). It shows, that the mass loss in the first, second and third stage for all particles is between 7.62 - 9.16%, 46.25 - 53.40%, 28.87 - 36.56 respectively. The total mass loss for three particles size indicates that higher mass loss and lower residues were obtained for an air flow rate of 50 mL/min. While the total mass losses and unaccounted substances (the mass difference between the total mass loss and ash with 100% that is observed within the three stages) are between 85.63 - 98.23% and 1.17 - 13.77% respectively.

Table C.10 (see Annex C) presents the different air flow rates on combustion parameters of the pine wood particles. The results show that for different air flow rates the value for the ignition index (D) and combustion index (S) on the ignition temperatures were observed with no consistent trend (see Figure 4.11). This trend indicates that different air flow rates have no significant contribution to ignition performance.

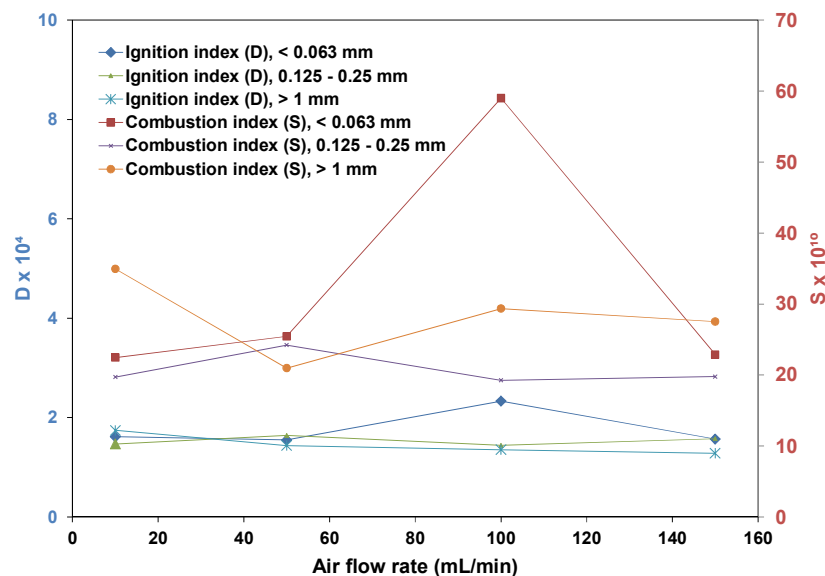


Figure 4.11. Combustion parameters of the pine wood particles at different air flow rates.

4.2.3 Influence of particle size

Figure 4.12 – 4.15 shows the influence of particle size for various heating rates while the air flow rate is kept at 100 mL/min. The figures show the mass loss (dashed lines) and heat flow (solid lines). Overall

the influence of the particle size is of small magnitude. The mass loss for three different particles size has the same behavior, even though the mass loss for small particles (< 0.063 mm) occurs earlier compared to the middle and larger particles size. This result is in agreement with that obtained by Neves *et al.* (2011). The amount of char produced by small particles (< 0.063) tends to be lower when compared with middle size and larger particles. However, at a certain heating rate (such as 20 °C/min, see Table C.4), (in Annex C), the middle and larger particles size have the lower residues. This condition indicates that particles may contain components with different reaction kinetics as suggested by Boriouchkine *et al.* (2014). The heat flow for three different particles in Figure 4.12 (a) – 4.15 (a) shows that for a heating rate at 5 °C/min the middle and larger particles have a high heating release, but the opposite was observed for the heating rate of 10 °C/min. In addition, the small particles release heat earlier or at a lower temperature than the larger sizes. During the experiment, the heat release for three different particles size at a low heating rate (< 10 °C/min) is between 300 °C and 500 °C while for the high heating rate (> 20 °C/min) is between 320 °C and 580 °C. This indicates that at a high heating rate the heat release was taking place later and at a higher temperature due to the sample inertia. Figure 4.12 (b) – 4.15 (b) show DTG for three different particles size at every heating rate. It is observed that at a low heating rate (5 °C/min), the mass loss rate was more uniform both in the second and third stage combustion compared to that observed at a heating rate above 10 °C/min. This condition shows that for different particles size, at a lower heating rate the combustion is more efficient than at a higher heating rate.

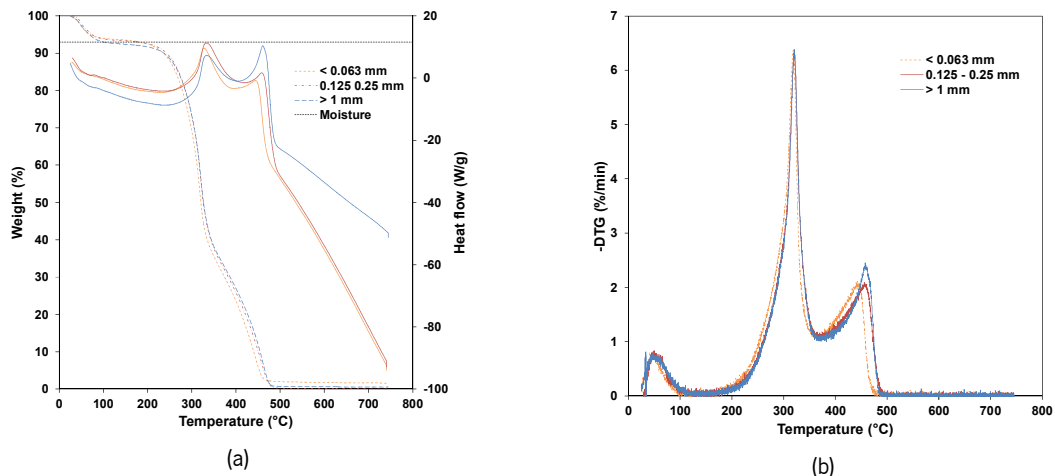


Figure 4.12. (a) Weight loss and heat flow, and (b) Rate of mass loss (for heating: 5 °C/min).

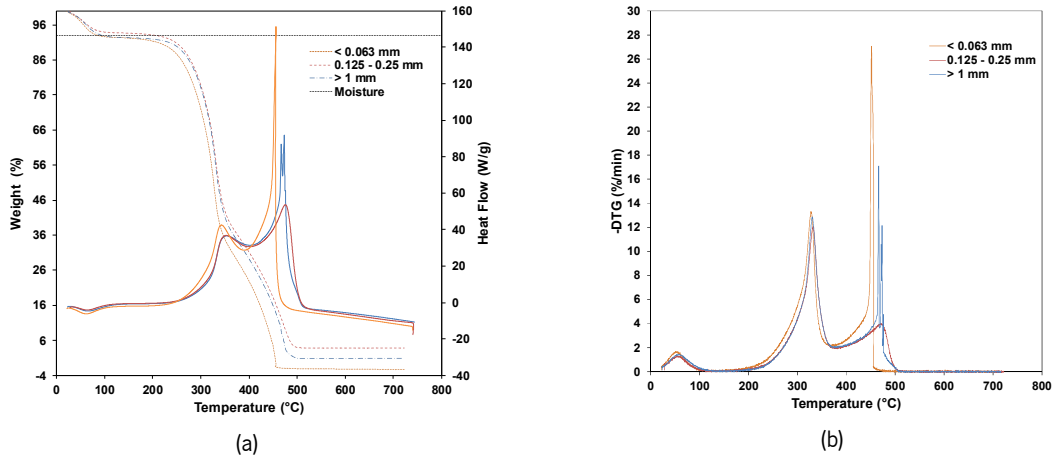


Figure 4.13. (a) Weight loss and heat flow, and (b) Rate of mass loss (for heating: 10 °C/min).

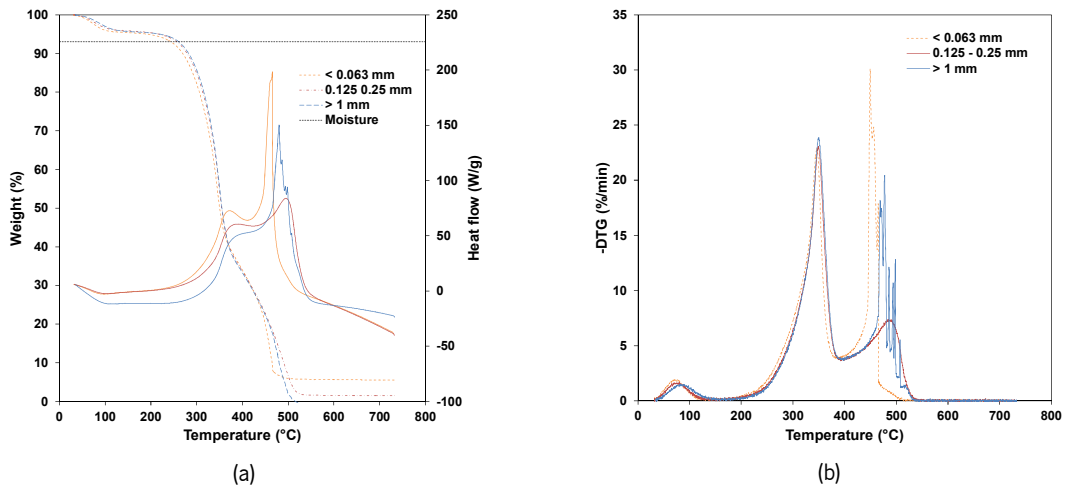


Figure 4.14. (a) Weight loss and heat flow, and (b) Rate of mass loss (for heating: 20 °C/min).

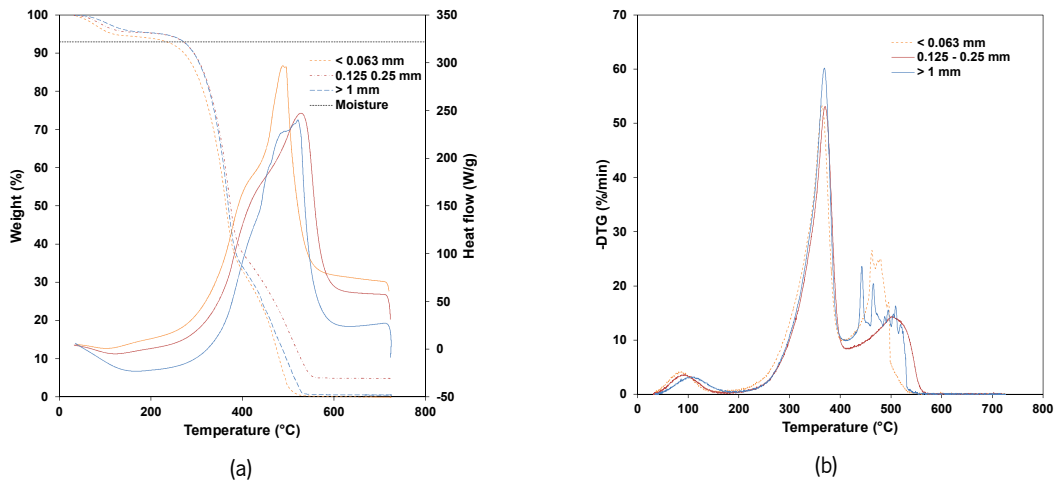
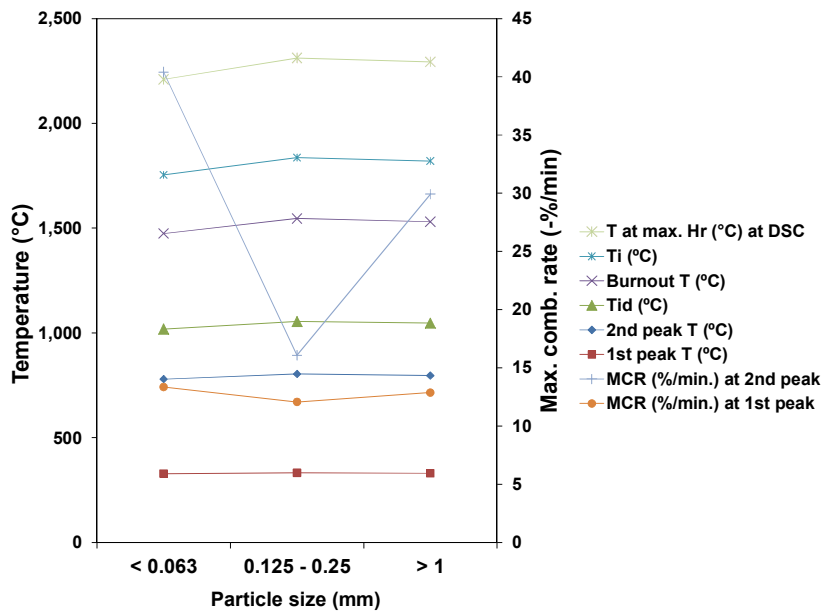
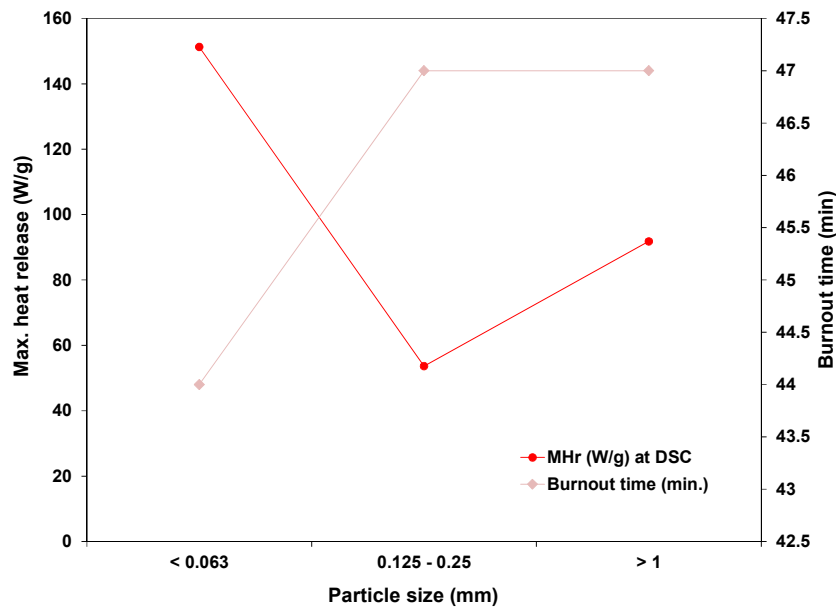


Figure 4.15. (a) Weight loss and heat flow, and (b) Rate of mass loss (for heating: 51 °C/min).

Figure 4.16 presents the combustion characteristic for different particle sizes at 10 °C/min and 100 mL/min. Figure 4.16 (a) shows that except for MCR for the 1st and 2nd peaks all the parameters are lower for the smaller particle and have an almost constant value for the middle and larger particle sizes. The MCR at 2nd peak (Figure 4.16 (a)) and MHR (Figure 4.16 (b)) tend to have the same behavior. The remaining mass (Figure 4.16 (c)) shows the same pattern for the different heating and air flow rates. The heat release (Figure 4.16 (d)) for different particle sizes shows inconsistent behavior which may indicate that there is no influence of the particle sizes on the amount of heat release.



(a)



(b)

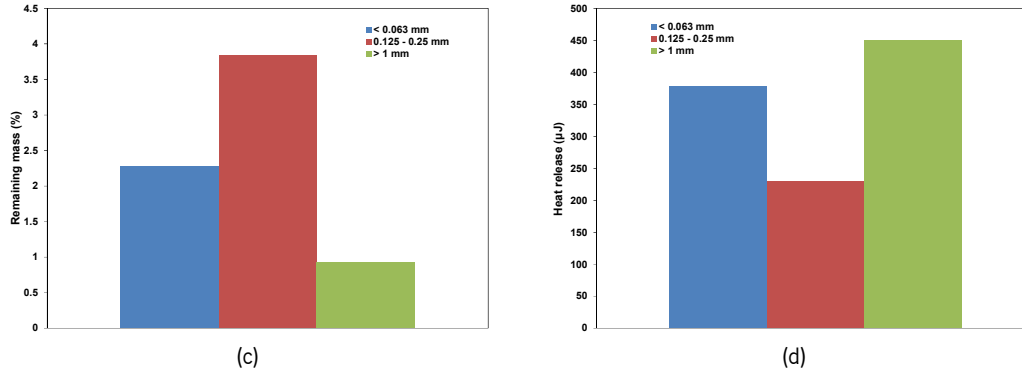


Figure 4.16. The combustion behavior test at different particle sizes for the heating rate 10 °C/min and air flow rate 100 mL/min: (a) Max. comb. rate and temperature at various conditions, (b) Max. heat release and burning time, (c) Remaining mass, and (d) Heat release.

4.3 Kinetic analysis of pine wood particles

From the TGA data the kinetic parameters can be derived using the 1st order Coats-Redfern equation (Ebrahimi-Kahrizsangi and Abbasi, 2008) as described by Eqs. (4.3, 4.4 and 4.5). For the calculation of the thermal kinetics, the Coats-Redfern equation is an appropriate method to be applied (Garcia-Maraver *et al.*, 2015; Wang *et al.*, 2012). The kinetics of the solid reactions is calculated by using the change in the extent of reaction (α) given by Eq. (4.3), (Ebrahimi-Kahrizsangi and Abbasi, 2008):

$$\alpha = \frac{m_i - m_t}{m_i - m_f} \quad (4.3)$$

where m_i is the initial mass, m_t is sample mass at time t , and m_f is the mass at the end of the reaction. The rate of the chemical reaction k is given by an Arrhenius type equation (Eq. 4.4):

$$k = A \cdot \exp\left(\frac{-E}{RT}\right) \quad (4.4)$$

where E is the activation energy (kJ/mol), T is the absolute temperature (K), R is the universal gas constant (kJ/kmol.K), and A is the pre-exponential factor (min^{-1}). In order to calculate the kinetic properties of biomass fuels under non-isothermal conditions, the Coats-Redfern equation is applied. This is an integral method and involves the thermal degradation mechanism as described by Aboulkas and Harfi (2008) through Equation (4.5):

$$\ln\left[-\frac{\ln(1-\alpha)}{T^2}\right] = \ln\left(\frac{AR}{\beta E}\right) - \left(\frac{E}{RT}\right) \quad (4.5)$$

where β is the heating rate (K/min). According to Eq. (4.5), a plot of the term in left side versus $1/T$ corresponds to a straight line in a $-\ln$ plot whose slope is $-E/R$ and an intercepts at $\ln(AR / \beta E)$, from which the values of E and A can be obtained. Figure 4.17 depicts the application of the method for one case. This method can be applied separately to either the second or the third stages (defined by the first temperature and second temperature peaks respectively) or to the overall temperature range (Ferreira, 2016). In defining the combustion stages several authors have different procedures. Magalhães *et al.* (2017) considered three stages with the first stage defined between the initial decomposition and ignition temperature, and the second and third stages are characterized by the first and second peak release. Moisture release stage is not considered. Mani *et al.* (2010) followed by Daouk *et al.* (2015), and Ferreira (2016) amongst others considered three stages including dehydration, volatile combustion, and char combustion. Shen *et al.* (2009) considered two different stages to define the kinetic model which includes a first stage and second stages associated to solid combustion (char and gas), and char combustion (gas and ash) respectively. The kinetic analysis procedure applied in this study followed the method used by Mani *et al.* (2010). In this study, the linear correlation factor shows a good result mostly for the second and third stages ($R^2 > 0.90$), while for the total combustion the fitting is poorer ($R^2 < 0.85$) for more data examined.

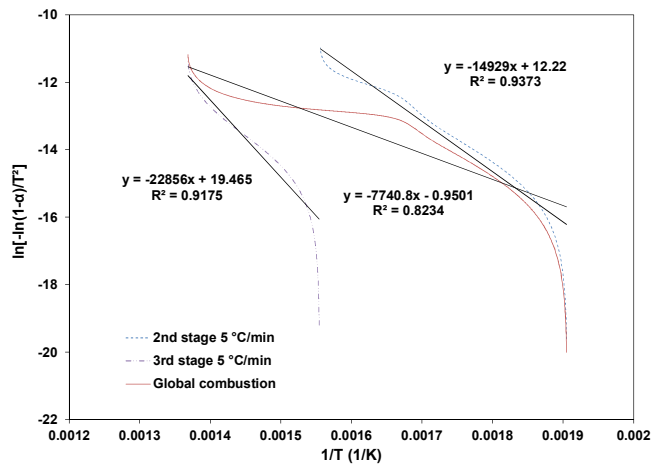
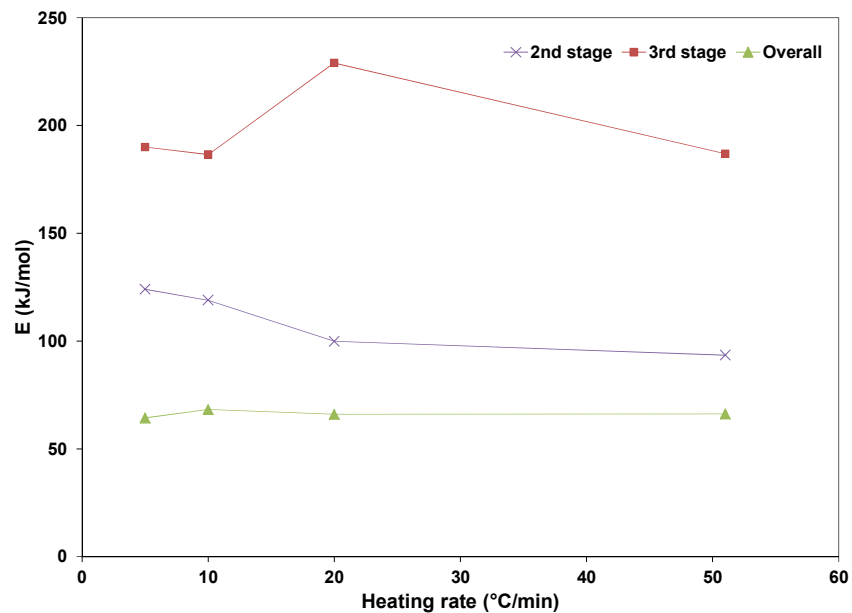


Figure 4.17. Kinetic parameter for three different stages at particle size is 0.063 mm, HR is 5 °C/min, and the air flow rate is 100 mL/min.

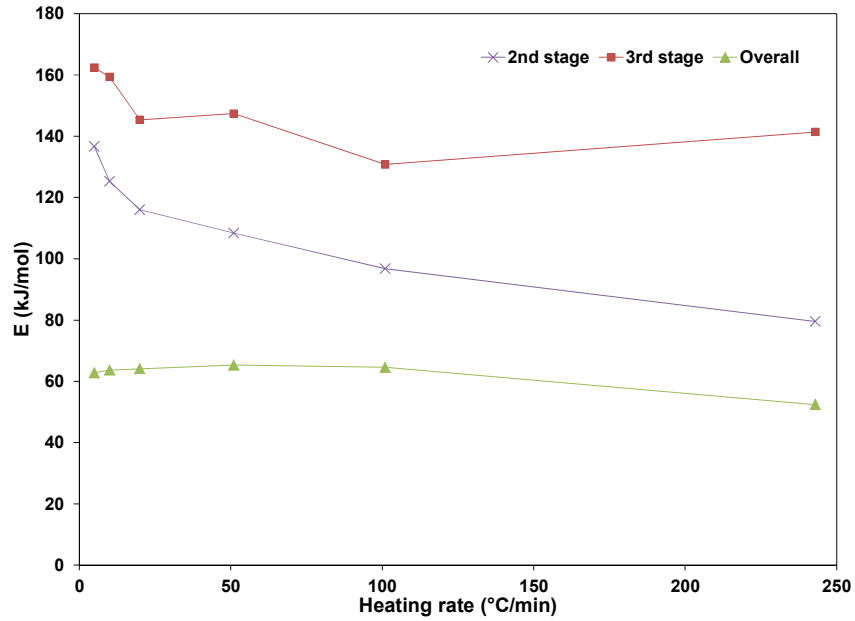
4.3.1 Influence of the heating rate

Table C.11 – C.13 (see Annex C) present the kinetic parameters for the combustion of pine wood particles at different heating rates for particles < 0.063 mm, 0.125 - 0.25 mm, and > 1 mm respectively.

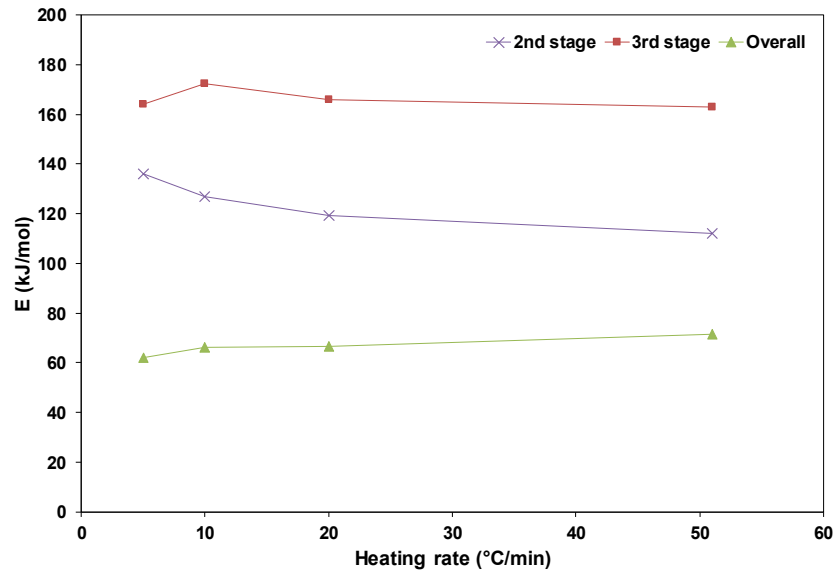
Figure 4.18 shows that the value for activation energy for three different particle sizes at different heating rates have the same behavior. The value for activation energy in the second stage decreases with increasing heating rate. In the third stage, the activation energy tends to decrease and oscillate with an increase in the heating rate. While in overall combustion the activation energy slightly decreases with an increase in the heating rate, which can be seen more clearly for particles < 0.125 and 0.25 mm. As stated by Mani *et al.* (2010) that at a lower heating rate the heat transfer is more effective and efficient, and it provides better heat transfer inside the particle (Mishra and Mohanty, 2018). In addition, the higher activation energy indicates a slower reactivity (Garcia-Maraver *et al.*, 2015). Dhyani *et al.* (2018) also stated that a higher value of activation energy indicated the presence of strong chemical bonding in the chemical species, and inversely. This condition is observed for all different particle sizes. While in the overall combustion the activation energy for particles size 0.125 - 0.25 mm at the highest heating rate (243 °C/min) the activation energy is lower than others, which is associated with the highest reactivity.



(a)



(b)



(c)

Figure 4.18. Activation energy vs heating rates for particles: (a) < 0.063 mm, (b) 0.125 - 0.25 mm, and (c) > 1 mm.

4.3.2 Influence of the air flow rate

Tables C.14 through C.16 (see Annex C) present the kinetic parameters for the combustion of pine wood particles at four different air flow rates for particles < 0.063 mm, 0.125 and 0.25 mm, and > 1 mm respectively. The influence of air flow rate on the activation energy for different particles sizes is

presented in Figure 4.19. It shows that the value for activation energy for three different particle sizes at different air flow rates presents the same behavior. The value of activation energy in the second stage and overall combustion is not too much different. In the third stage for different particle sizes, the activation energy does not show a clear trend. In addition, only the smallest of the particles show an activation energy that is significantly different from the other sizes, for the 2nd and 3rd stages, although the influence on the overall value is negligible. From the data it is observed that in the 2nd stage (early step of devolatilization at lower temperature) the smaller particles are the most reactive while the large ones exhibit the highest activation energy. As the presence of lignin is associated with lower decomposition rates (Burhenne *et al.*, 2013) one expects that a fine grinding of biomass may break the larger molecules of lignin and, so, contribute to a higher reactivity. Harun *et al.* (2009) stated that less collision occurs by increasing the particle sizes and therefore slower reaction will take place thus causing the thermal degradation characteristics and kinetic parameters to decrease regardless of the reaction zones.

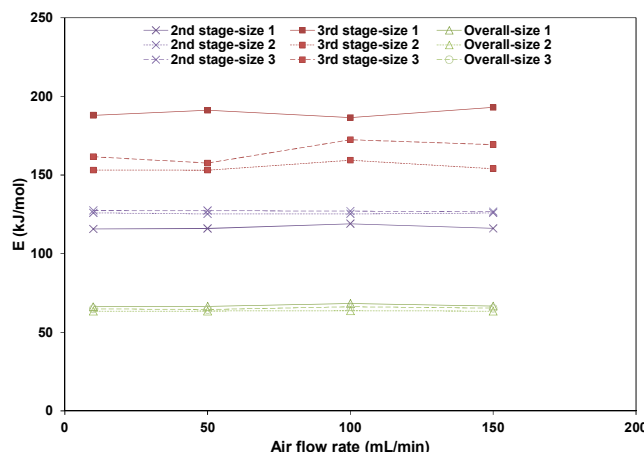
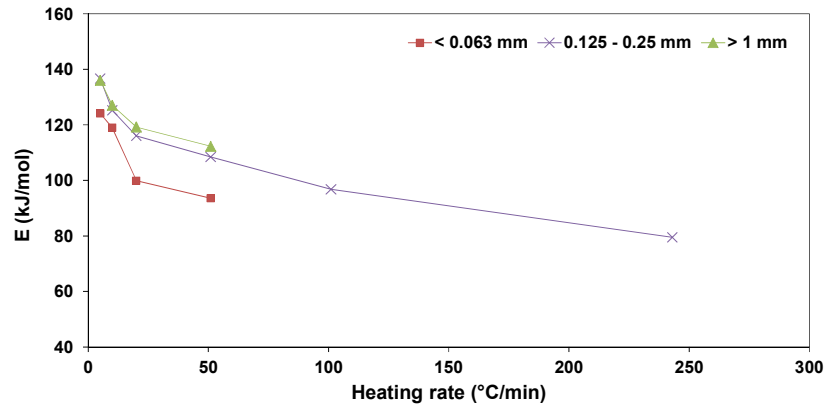


Figure 4.19. Activation energy vs air flow rates for particles: (a) < 0.063 mm (size 1), (b) 0.125 - 0.25 mm (size 2), and (c) > 1 mm (size 3).

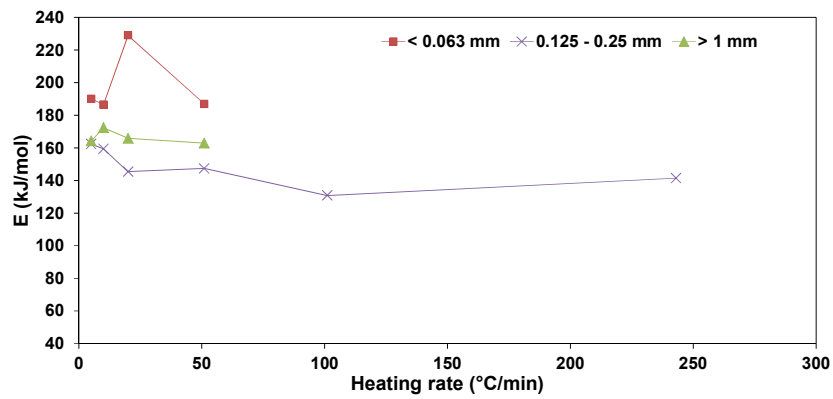
4.3.3 Influence of particle size

The effect of the particle sizes on the combustion reactivity is presented in Figure 4.20. The influence of the particles size on the combustion reactivity at different heating rates show that on the second stage the small particles have a higher reactivity and increasing as the increasing of the heating rates, but the higher reactivity in the third and total stages of combustion was observed for middle particles size. The activation energy tends to decrease as the increase of the heating rates, mostly in all the combustions

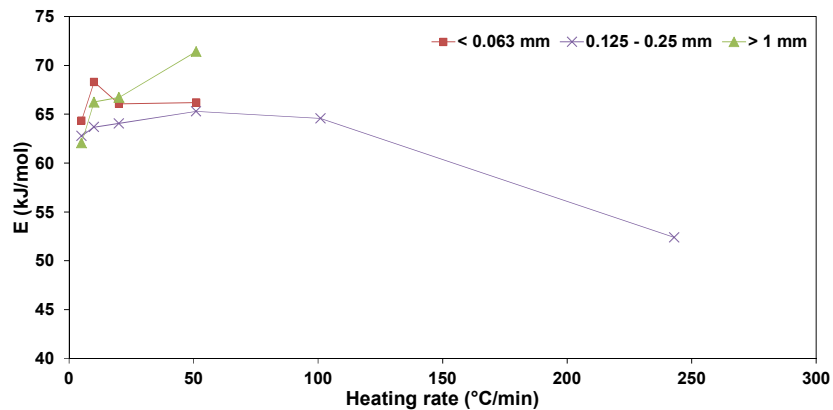
stages as can be seen for middle size particles, this result is similar with the result obtained by Shen *et al.* (2009). The influence of particles size on the combustion reactivity at different air flow rates show almost the same behavior, where the reactivity is slightly constant for each stage.



(a)



(b)



(c)

Figure 4.20. Activation energy vs heating rates for three particles size: (a) 2^{nd} stage, (b) 3^{rd} stage, and (c) Total combustion.

5. MASS LOSS AND ELEMENTAL ANALYSIS OF PINE WOOD PELLETS IN A SMALL SCALE REACTOR

This chapter discusses the mass loss of wood pellets performed in a small scale reactor designed to investigate the influence of temperature in the devolatilization of wood pellets. This investigation is based on the determination of mass loss and composition as a function of time. In this way one can obtain information of the devolatilization process in a commercial grade fuel.

5.1 Test conditions

The experimental apparatus and procedure were previously described (see Chapter 3, section 3.8). Basically, a pellet sample was heated on a constant temperature environment and, at specific time intervals, the sample mass loss and the elemental composition (based on the proximate and ultimate analysis) were measured. The data were obtained at different ambient temperatures: 264, 351, 444, 541, 650 and 734 °C and at time intervals of 30, 60, 120, 180, 240, 300, 600, 900, 1,200 and 3,600 s. The properties of pine wood pellets used in this study were presented in Table 3.2.

A preliminary set of experiments was carried out on an alternative test facility, whose temperature was limited to a maximum of 250 °C. Although the scope of such experiments is limited, they provided the basis for fine tuning the procedure. The methods and results are detailed in Annex D.

5.2 Results and discussion

5.2.1 Mass loss of wood pellets

The mass loss of wood pellets was calculated as the difference of the initial mass and final mass (Eq. 5.1).

$$m_l = m_i - m_f \quad (5.1)$$

where m_l is a mass loss, m_i is the initial sample mass, m_f is the final mass of the sample.

The mass loss as a function of time and temperature is presented in Figure 5.1. The temperature reported is the actual temperature inside the reactor, because it was observed a gap between the set up and actual temperatures. The horizontal dotted line, at 84.7%, represents the percentage of volatile matter for the pine wood pellets, on wet basis (see Table 3.2).

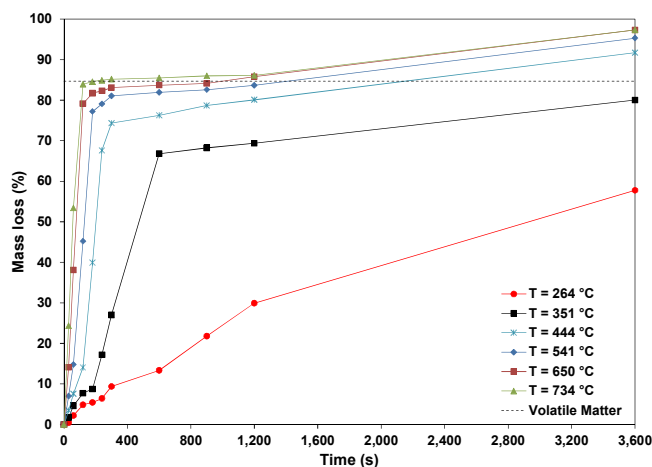


Figure 5.1. Mass loss of wood pellets vs time at temperature 264 – 734 °C.

The data plotted show that the mass loss increases for any specific temperature; the higher the temperature, the faster the pellets volatilize. The results also show that most of the devolatilization occurs in the first 5 minutes of the process, depending on the temperature. For very low temperature (264 °C) the mass loss occurs at a very slow rate, as the experiment was extended for over one hour. In any case this temperature is above the one that defines the initial decomposition of biomass (204 – 261 °C) (including hemicellulose and lignin), as shown in Chapter 4. This observation is in agreement with the TGA tests which have shown that the reaction kinetics is very slow at such low temperatures. Because of the slow devolatilization process, at the lowest temperatures (264 – 351 °C) the data show a kink in the rate of mass loss, where a leveling of the mass precedes the devolatilization process. Because this stabilization is in the range of 7 – 8%, it suggests that the drying process is independent of the fuel devolatilization and these are two distinct phases. At higher temperatures (which will induce a higher heating rate) such separation is not evident. The TGA data also corroborates this observation. For the highest temperatures (650 – 734 °C) it is observed that most of the volatile matter is released within the first 2 minutes, as the mass loss approaches the percentage of volatile matter, 84.7%. After approximately 1 hour, the mass loss at 650 and 734 °C converges to the same value ($\approx 97\%$), which means that all the volatile gases have been released and the remaining substances are ashes, and the remaining unburned fixed Carbon which is about 3%.

In order to investigate the influence of the initial moisture of the pellets and the transition between the drying and devolatilization phases, a set of tests was carried out with dry pellets. The experiments were limited to the initial 240 s of the process and the results are presented in Figure 5.2. From the data one may observe that the initial mass loss is due to the moisture release as the rate of mass is higher for

wet pellets than that for dry pellets. Water diffusion is more effective which is more evident for low temperature (low heat rate). In fact for the lowest temperature (264 °C) the dry pellets do not lose any mass at all in the initial 240 s. Because this temperature is above initial decomposition temperature, the fuel volatiles will eventually be released as one can conclude from the data represented in Figure 5.1. As the pellet is brought into higher temperature, the fuel volatiles are released and the presence of water inside the pellet structure delays the fuel devolatilization due to the phase change enthalpy. With the temperature increase (and so the heat rate), the fuel devolatilization (mass loss observed in dry pellets) increases at a higher rate, and earlier in the process. For the highest testing temperatures the temperature rise is so fast (high heat rate) that dry pellets appear to devolatilize faster than wet pellets even in the initial stages of reaction. Because of the sampling procedure, at 30 s (1st data point) we are not able to capture the initial moisture release from the biomass. This observation is in agreement with the results obtained with the TGA. Eventually in the long run all the samples (wet and dry) converge for the same rate of mass loss as all the moisture should have been released by this time.

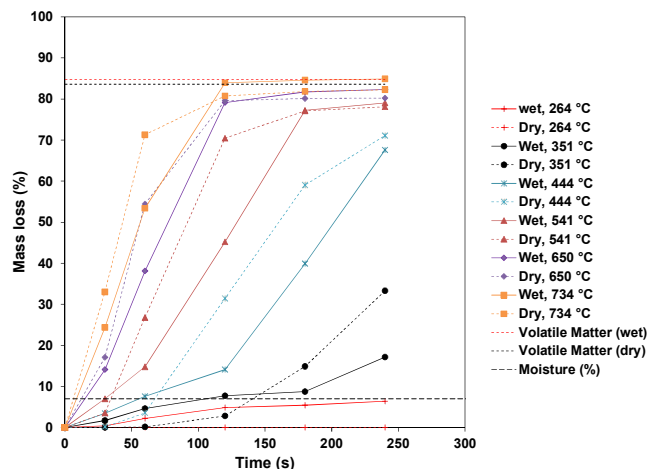


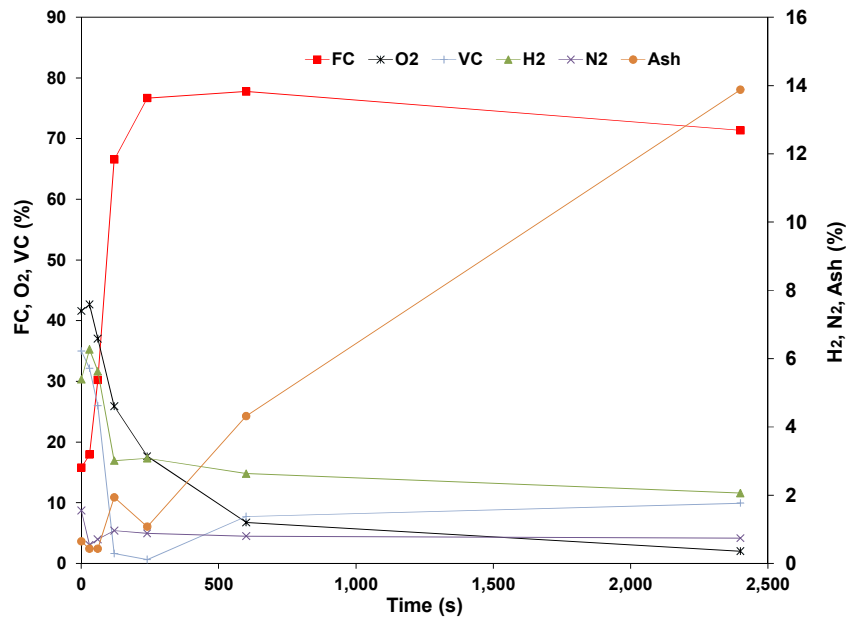
Figure 5.2. Mass loss of dry and wet pellets.

The temperature range between 400 – 700 °C includes the primary and secondary pyrolysis where volatile gases are released including water, tar, permanent gas, and char, while the range of 700 – 800 °C is referred as the gasification phase (Neves *et al.*, 2011).

5.2.2 Elemental analysis of wood pellets

The structure of biomass is composed of Cellulose (cell walls of biomass material), $(C_6H_{10}O_5)_n$ which represents 40 to 45%; Hemicellulose $((C_5H_8O_4)_n$ abundant in SO_4 , Cl , NO_3 and $Si(OH)_4$) represents 20

to 35% of the dry weight of wood and Lignin ($C_{11}H_{12}O_4$)_n representing 15 to 30% of the dry weight of wood (Borman and Ragland, 1998). The elemental analysis was conducted over time at different temperatures. By applying the same test for the mass loss experiment, then the result of the elemental analysis can be obtained. Figure 5.3 presents the preliminary test to observe the behavior of the elemental composition during the combustion of wood pellets in a small scale reactor with the temperature range of 1,150 °C, in order to determine the time length required for the other samples.



(a)

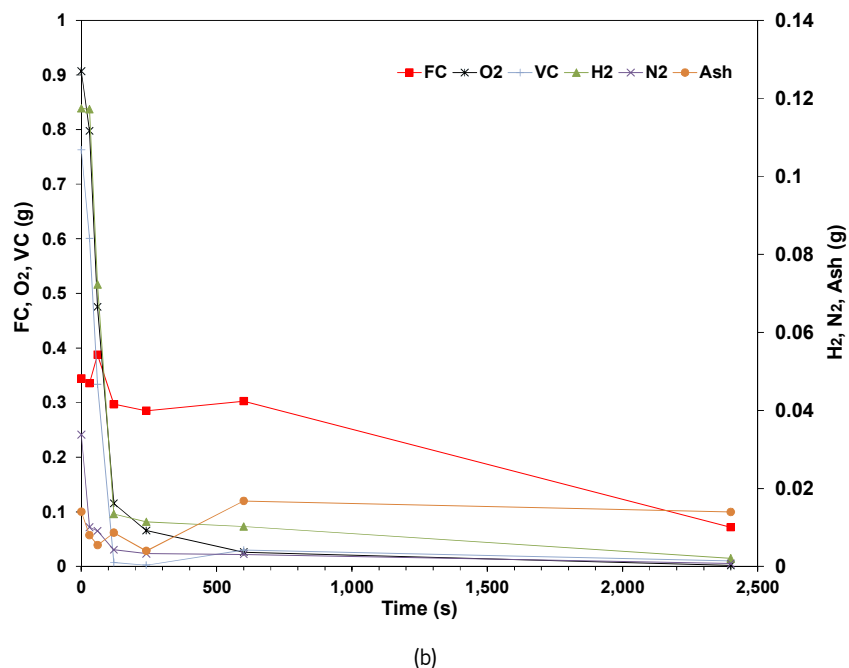


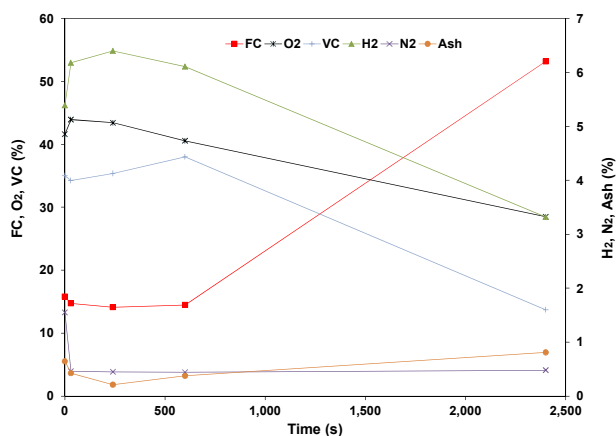
Figure 5.3. Elemental analysis of wood pellets at $T = 650\text{ }^{\circ}\text{C}$: (a) in percentage, and (b) in gram.

For each data point in the relationship between the mass loss and temperature, the composition of the remaining fuel was determined in terms of volatiles (C, H, N, O), fixed Carbon and ash. The results are presented in Figure 5.3 as a mass ratio (a) and as the total mass (b). The data in Figure 5.3 (b) shows that the volatile matter is released in a very short time (at this temperature within the initial 4 – 5 min) while the ratio of fixed Carbon and ash steadily increases and, later in the oxidation process, constitutes most of the remaining matter Figure 5.3 (a). After about 5 minutes there are no significant changes in the gas composition which means that only the char combustion is taking place. It is also observed that the rate of conversion for the volatile is similar for all compounds, although Nitrogen shows a higher rate of conversion.

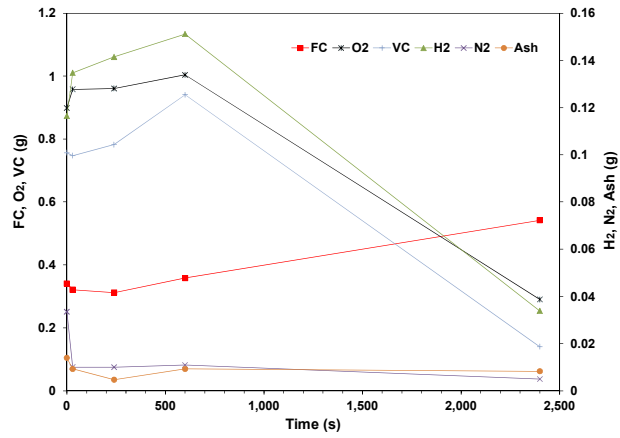
After approximately 10 min, it is observed a steady reduction of volatiles which, on the long run, approaches zero coupled with a much slow oxidation of fixed Carbon. The ash content remains approximately constant, within the accuracy of the instrumentation.

Because the mass loss occurs in the early stage, all subsequent tests are analyzed for that period. Figures 5.4 through 5.9 depict the influence of temperature in the devolatilization process. In these, the time scale was adjusted according to the total reaction time in order to highlight the initial decomposition phase. As mentioned, the tests were carried out at 264, 351, 444, 541, 650 and 734 $^{\circ}\text{C}$.

From the data, it can be concluded that the rate of mass loss increases with the temperature. This increase in the reaction kinetics coefficient is in agreement with the results obtained with TGA. In all, the pattern is similar to that described above: the volatiles are released at a similar rate although Nitrogen shows a higher diffusion coefficient. Looking at the data on a mass basis, it is observed that the mass of fixed Carbon increases during the initial devolatilization phase before its subsequent oxidation in the later stages of the devolatilization. This suggests that there is Carbon diffusion from the volatile fraction to the fixed fraction. This mechanism occurs over a period of time that is inversely proportional to the testing temperature. Taking into consideration that the heating rate is dependent upon the testing temperature one may postulate that the diffusion between the volatile and fixed fractions of Carbon occurs at low temperature. Also, it can be concluded that this time is directly correlated with the devolatilization of other volatiles, such as O, N and H. Taking as an example, a temperature of 444 °C (see Fig. 5.6) the maximum mass of fixed Carbon occurs at approximately 240 s which is the time frame for the nearly complete devolatilization of the volatile matter occurring at the same time. This is observed for all the other test conditions. This time is correlated with the testing temperature in Figure 5.10. where dT is the temperature difference between the reactor and the initial temperature. The data also suggests that the time for Carbon migrating to the fixed fraction tends to level off at high heating rates.

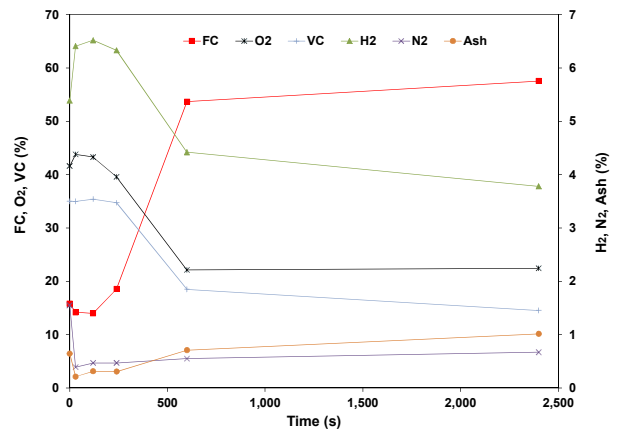


(a)

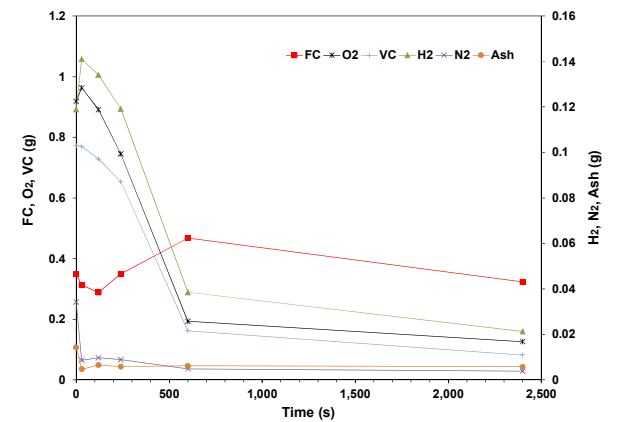


(b)

Figure 5.4. Elemental analysis of wood pellets at T = 264 °C: (a) in percentage, and (b) in gram.

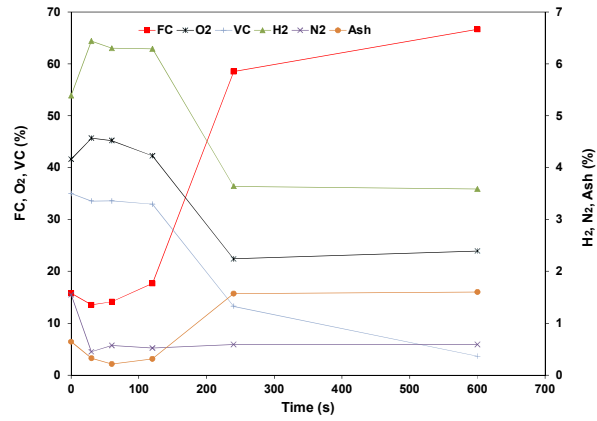


(a)

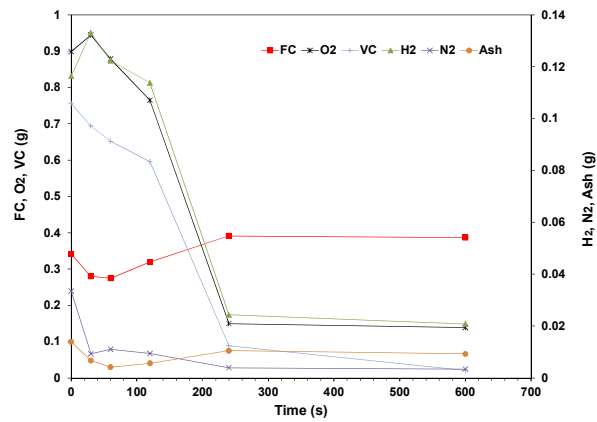


(b)

Figure 5.5. Elemental analysis of wood pellets at T = 351 °C: (a) in percentage, and (b) in gram.

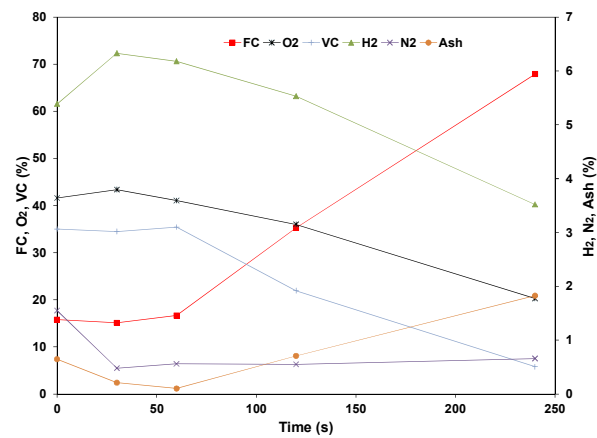


(a)



(b)

Figure 5.6. Elemental analysis of wood pellets at $T = 444\text{ }^{\circ}\text{C}$: (a) in percentage, and (b) in gram.



(a)

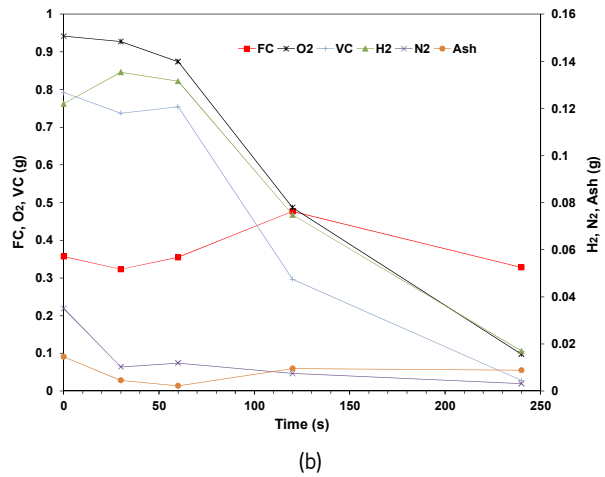


Figure 5.7. Elemental analysis of wood pellets at $T = 541\text{ }^{\circ}\text{C}$: (a) in percentage, and (b) in gram.

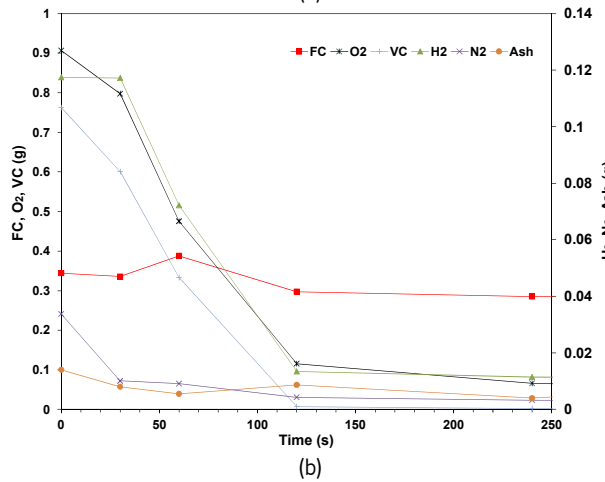
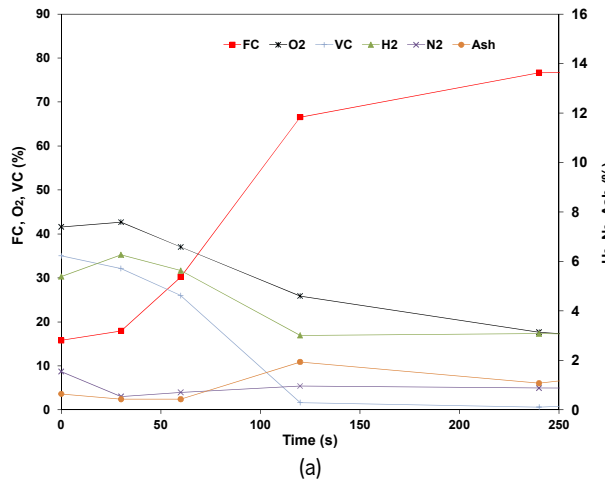


Figure 5.8. Elemental analysis of wood pellets at $T = 650\text{ }^{\circ}\text{C}$: (a) in percentage, and (b) in gram.

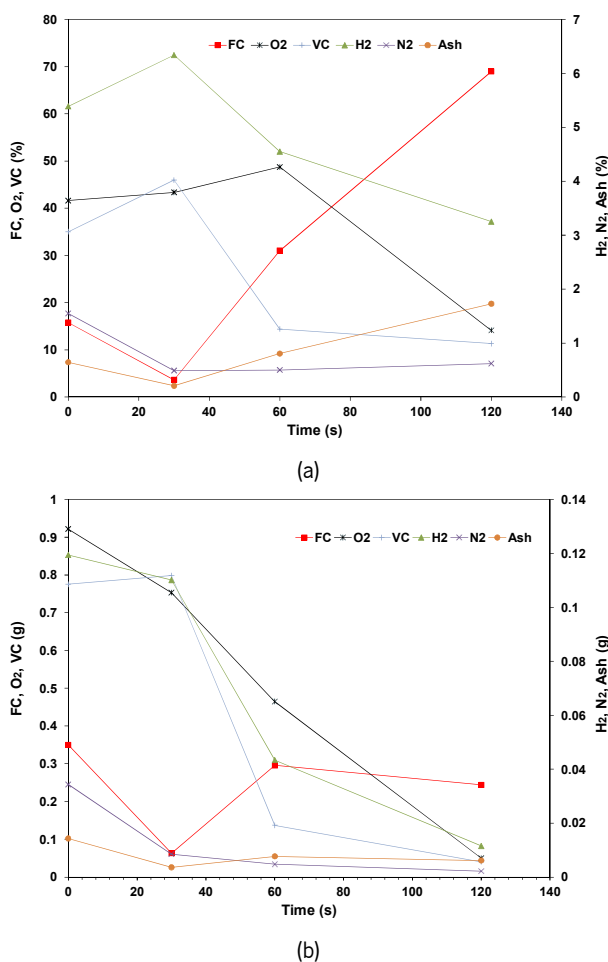


Figure 5.9. Elemental analysis of wood pellets at $T = 734$ °C: (a) in percentage, and (b) in gram.

Obviously, the total Carbon will decrease with time as it is being oxidized. This is observed in Figure 5.11 where the total mass of Carbon is made dimensionless with the initial mass of Carbon. It shows that the mass loss of Carbon at different temperatures changes with the time. This change corresponds to the initial loss of some low molecular weight of Carbon compounds present in the biomass (extractives) as well as thermal decomposition of hemicellulose, lignin and at a higher temperatures of the cellulose. According to Yeo *et al.* (2019), these compounds start to decompose at 320 K and undergo several different stages and temperature ranges. The decomposition of hemicellulose, cellulose and lignin starts at a temperature between 500 - 600, 575 - 700, and 320 - 1,100 K respectively. The decomposition of these compounds is dependent on the temperature and residence time. When the temperature or residence time increases, the carbonaceous structure is more stable also undergoing bond cracking and subsequent mass loss observed at a slower rate. Madzaki *et al.* (2016) also stated that the high volatile matter content of the biochar is due to the decomposition of cellulose,

hemicellulose and lignin. Therefore the data suggests that some of the Carbon released from hemicellulose and lignin is fixed into the cellulose structure. Figure 5.11 also shows that at 264 °C the total mass of carbon is increasing in early stages. This may be explained as for short residence time dehydration reactions takes place, which contributes to the elimination of oxygen and hydrogen in particular. For the higher temperatures this effect is not noticeable as it is compensated by the faster elimination of fixed carbon.

The data for species concentration in the sample, presented as a fraction of sample mass, as shown in Figure 5.4 (a) through 5.9 (a), depicts the variation in concentration resulting from the species diffusion out of the biomass. Therefore some are expected to increase in concentration if their rate of volatilization is lower than others. However, if one looks at the actual mass (Figure 5.4 (b) through 5.9 (b)) it is observed that H and O show an increase in the total mass present in the sample in the early stages of the devolatilization process, once the only source of Oxygen and Hydrogen is the moisture of biomass. Our hypothesis is that during the drying phase the O and H from the water are integrated into the O and H in the biomass. The time scale for the H and O is the same; that is, the maximum mass occurs at approximately the same time. In fact, the maximum in O and H mass occurs within the time frame of the drying phase (see Figure 5.2).

In order to prove this hypothesis, a complementary set of tests was developed. In this, the tests were conducted at 264 °C and limited in time for the initial 4 min of the devolatilization process. The samples were removed from water moisture by drying them according to standard SS 18 71 20 (Hansen *et al.*, 2009). The results are presented in Figure 5.12 in terms of species concentration (a) and on a mass basis (b). The analysis was limited to O and H. The results clearly show that with the dry pellets the mass of H and O always decreases which validates the hypothesis that in the drying phase some of the O and H is transferred from the water to the biomass structure.

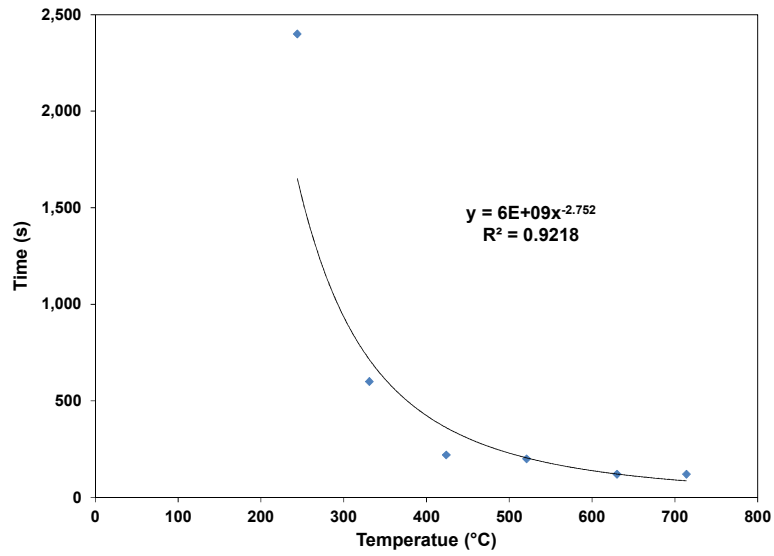


Figure 5.10. Fixed Carbon profile at different temperature during the combustion.

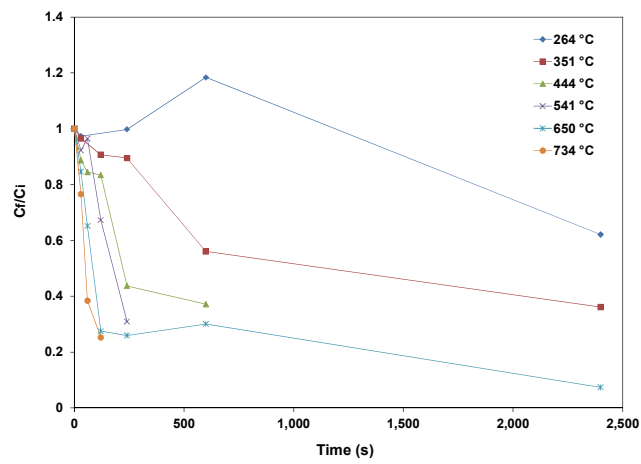
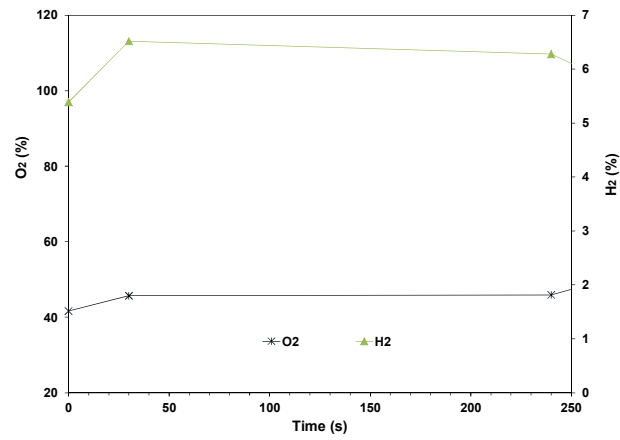
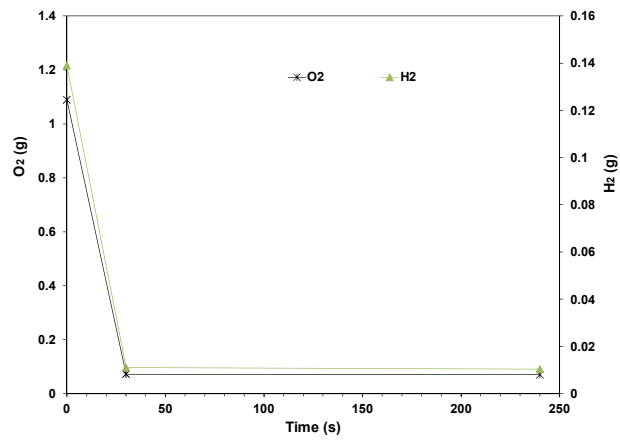


Figure 5.11. Carbon ratio for different temperature.



(a)



(b)

Figure 5.12. O₂ and H₂ concentration of dry pellets for the temperature of 264 °C at 30 s and 4 min (a) in percentage, and (b) in gram).

6. EMISSIONS AND TEMPERATURE MEASUREMENT IN A FIXED BED COMBUSTOR

This chapter describes the combustion characteristics of pine wood pellets in a 20 kW boiler. This boiler is installed in the laboratory of Heat and Fluids, School of Engineering at the University of Minho. Different parameters were studied including Power, grate area (GA), excess air (EA), and split ratio of primary and secondary air (SR). Pine wood pellets with 6 mm diameter were used, whose properties are the same as presented in Table 3.2. Several parameters were measured and determined, which include: emissions (CO, CO₂, O₂, and NO_x); fuel bed temperature; thermal efficiency; the ashes agglomeration and combustion instability were also observed. The Taguchi method (TM) was applied to plan the experimental program, with the parameters investigated in this study, which includes: GA, SR, thermal load (Power), and EA. In the Taguchi method, the analysis of variance (ANOVA) was used to analyze the experimental results. This chapter begins with a general overview of the experimental results and finishes with a statistical analysis based on the TM application.

6.1 Test conditions

In the experimental analysis, several parameters are recorded and calculated including gas emissions, fuel bed temperature, thermal efficiency, bottom ashes, and combustion instability (see Chapter 3). The efficiency of the boiler was calculated based on the temperature difference of the cold and hot water in the inlet and outlet of the heat exchanger.

To conduct the experimental analysis several parameters need to be determined including excess air ratio in three levels (1.5, 1.7, and 2.1), thermal load/Power (10, 13, and 16 kW), air split ratio in three levels as well (20/80, 30/70, and 37/63), and three different grate areas (see Table 6.3). The determination of the parameters is presented below:

6.1.1 Excess air

By running the boiler and recording the value of the oxygen on the gas analyzer, the value of excess air can be obtained, see Eq. (3.6 – 3.8), (section 3.2.1). This procedure was used by various authors such as Wang *et al.* (2015) - excess air 1.0-1.3; Ribeiro (2012) - excess air 1.9, 2.3, and 2.7. The result of the reading based on the oxygen percentage is presented in Table 6.1.

Table 6.1. O₂ content and excess air coefficient.

O ₂ (%)	λ
6.52 - 7.42	1.45 - 1.54
8.29 - 8.99	1.65 - 1.74
9.67 - 10.23	1.85 - 1.94
10.78 - 11.24	2.05 - 2.14
11.26 - 11.68	2.15 - 2.24

6.1.2 Thermal load calculation

The thermal load (P) is calculated based on the different mass flow rate of pellets during the experiment, as presented in the following equation:

$$P = \dot{m}_f \cdot \text{LHV}(\text{kW}) \quad (6.1)$$

where P is Power (kW), \dot{m}_f is fuel mass flow rate (kg/s) and LHV is a lower heating value of fuel (kJ/kg).

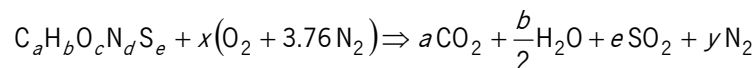
The stoichiometric air fuel ratio ($\text{AFR}_{\text{stoic}}$) for the wood pellets combustion in this study is 5.85, which obtained based on the chemical composition of the pine wood, as presented in Table 6.2.

Table 6.2. Chemical composition of pine wood pellets.

	C	H	O	N	S
Mass percentage (%)	50.80%	5.39%	42.22%	1.55%	0.037%
Molar mass (kg/kmol)	12	1	16	14	32
	a	b	c	d	e
Mole (kmol)	4.23	5.39	2.64	0.11	0.001

The calculation for the stoichiometric air fuel ratio ($\text{AFR}_{\text{stoic}}$) is as follows.

Wood combustion:



where a, b, c, d, and e relate to the moles' fraction of each constituent of the fuel knowable by elemental chemical analyzes.

$$x = a + \frac{b}{4} - \frac{c}{2} + e = 4.26 \text{ kmol}$$

$$y = x(3.76) + (0.11 / 2) = 16.08 \text{ kmol}$$

Mass of air for 100 kg of fuel (m_a)

$$m_a = x(M_{O_2} + 3.76M_{N_2}) = 4.26(32 + 3.76 \times 28) = 585 \text{ kg}$$

Stoichiometric air fuel ratio (AFR_{stoic})

Air fuel ratio is given by:

$$AFR_{\text{stoic}} = \left(\frac{m_a}{m_f} \right)_{\text{stoic}} = \left(\frac{m_a}{100} \right)_{\text{stoic}} = 5.85 \text{ kg}_a/\text{kg}_f$$

When we apply the excess air coefficient (λ), the air mass flow rate is calculated. For example for 50% excess air ($\lambda = 1.5$), the AFR_{real} is:

$$AFR_{\text{real}} = AFR_{\text{stoic}} \cdot \lambda = 5.85 \times 1.5 = 8.78$$

For a thermal load of 10 kW, ($m_f = 2.11 \text{ kg/h}$). The air flow rate is calculated by $m_a = m_f \cdot AFR_{\text{real}}$,

which yields $m_a = 18.53 \text{ kg/h}$.

To set a specific value for the thermal load a calibration procedure was implemented in which the feeding mechanism was set at a varying on-off pattern and the corresponding mass flow rate was determined by measuring the mass of pellets over a period of time, assuming a LHV of 17,100 kJ/kg. In this way, the thermal loads were set to 10, 13, and 16 kW.

6.1.3 Split ratio

The split ratio of primary and secondary air in this study was set to 20/80, 30/70, and 37/63. While Yin *et al.* (2008) revealed that the value of the split ratio of primary and secondary air tends to be 40/60 in modern grate fired boilers burning biomass and 80/20 in older units. (Ribeiro, 2012) also applied three different split ratio including 10/90, 30/70, and 50/50.

6.1.4 Grate size

Three different grates of rectangular shape were tested in this study as presented in Table 6.3. Ribeiro *et al.* (2019), in a boiler of similar configuration, has applied three different grate size (cross section area): 135 x 135, 135 x 115, and 135 x 95 mm.

Table 6.3. Grate area.

No.	Size (mm x mm)	h (mm)
1	90 x 75	61
2	115 x 75	
3	115 x 96	

Height, h , represents the distance from the grate surface to the top of the grate.

6.2 Experimental plan

As mentioned the Taguchi method was applied in this project. The Taguchi method is a method developed to optimize the process of engineering experimentation. This method was developed as a response to minimizing the expenditure of resources in the production processes. It is also very important in resolving the quality issues as well (Roy, 2010), and was of great impact in the development of the Japanese industry. In analyzing the experimental results, the data obtained are treated according to an analysis of variance/ANOVA (Ferreira, 2008) and one obtain one or more from the following three objectives: (1) determine the trend of influence of factors and interactions under study, (2) identify the significant factors and their relative influences on the variability of results and, (3) establish the best or the optimum condition for a product or a process, along with an estimate of contribution of individual factors and a prediction of expected response under the optimum conditions (Roy, 2010). The application of Taguchi method in the planning of experimental projects makes it possible to significantly reduce the amount of tests, and to evaluate the influence of several parameters considered in a particular process (Ferreira, 2008). In addition, it also allows to confirm the importance and relative weight of each parameter in a particular response or outcome expected.

In the Taguchi method, multiple parameters (factors) and several values of these parameters (factor levels) are arranged according to standard orthogonal arrays, enabling a dramatic decrease in full-factorial trial experiments (Liu *et al.*, 2019). As described by Ferreira (2008) there are three phases in applying the method: 1) selection of factors and eventual interaction; 2) planning of the experiment; 3) analysis and interpretation of the results. In addition, to allow the evaluation of the influence of each parameter, it is important to emphasize that for the experimental plan at least 3 levels should be applied for each parameter in the study. With this experimental plan, then the test plan matrix to be used is the orthogonal matrix L₂₇, which consists of 27 experiments and 13 columns.

6.2.1 Levels

In this study, four parameters including grate area (GA), the split ratio of primary and secondary air (SR), thermal load (Power), and excess air (EA) were considered to be the most dominant in the combustion of wood pellets in a boiler rated at 20 kW thermal. In order to reduce the time and experimental effort, the Taguchi method was applied to develop experimental planning. In this experiment, the values of the parameters and three different levels for each parameter were selected as presented in Table 6.4.

Table 6.4. Factor and Level of the experimental plan, using the Taguchi method.

Factor		Level		
		1	2	3
A	Power (kW)	10	13	16
B	Excess air (%)	50	70	110
C	Grate area (mm²)	90 x 75	115 x 75	115 x 96
D	Split ratio (P/S)	20/80	30/70	37/63
Grate height 61 (mm)				

As shown in Table 6.4, 4 parameters with 3 levels were used for each variable, then by applying the Taguchi method, the number of experiment runs is 27. The Notation of a Taguchi orthogonal array can be written as L₂₇ (3¹³). In this notation 27 is the number of the experimental runs, 3 is the number of levels and 13 is the number of experimental factors. Furthermore, the L₂₇ matrix with 13 columns can be used for the study of 7 factors and three interactions, where each interaction requires two columns (see Table 6.5) (Ferreira, 2008). Then, these values were introduced into an excel file to obtain the relationship between the variables.

Table 6.5. Matrix L₂₇, with indication parameter (1, 2, 5, 10), interaction (3, 4, 6, 7, 8, 11), and independent (9, 12, 13) (Ferreira, 2008).

Test	Power (kW)	EA (%)			GA (mm ²)				SR				
	A	B	AxB	4	C	AXC	BxC	e	D	BxC	e	e	
	1	2	3	4	5	6	7	8	9	10	11	12	13
1	1	1	1	1	1	1	1	1	1	1	1	1	1
2	1	1	1	1	2	2	2	2	2	2	2	2	2
3	1	1	1	1	3	3	3	3	3	3	3	3	3
4	1	2	2	2	1	1	1	2	2	2	3	3	3
5	1	2	2	2	2	2	2	3	3	3	1	1	1
6	1	2	2	2	3	3	3	1	1	1	2	2	2
7	1	3	3	3	1	1	1	3	3	3	2	2	2
8	1	3	3	3	2	2	2	1	1	1	3	3	3
9	1	3	3	3	3	3	3	2	2	2	1	1	1
10	2	1	2	3	1	2	3	1	2	3	1	2	3
11	2	1	2	3	2	3	1	2	3	1	2	3	1
12	2	1	2	3	3	1	2	3	1	2	3	1	2
13	2	2	3	1	1	2	3	2	3	1	3	1	2
14	2	2	3	1	2	3	1	3	1	2	1	2	3
15	2	2	3	1	3	1	2	1	2	3	2	3	1
16	2	3	1	2	1	2	3	3	1	2	2	3	1
17	2	3	1	2	2	3	1	1	2	3	3	1	2
18	2	3	1	2	3	1	2	2	3	1	1	2	3
19	3	1	3	2	1	3	2	1	3	2	1	3	2
20	3	1	3	2	2	1	3	2	1	3	2	1	3
21	3	1	3	2	3	2	1	3	2	1	3	2	1
22	3	2	1	3	1	3	2	2	1	3	3	2	1
23	3	2	1	3	2	1	3	3	2	1	1	1	2
24	3	2	1	3	3	2	1	1	3	2	2	3	3
25	3	3	2	1	1	3	2	3	2	1	2	1	3
26	3	3	2	1	2	1	3	1	3	2	3	2	1
27	3	3	2	1	3	2	1	2	1	3	1	3	2

6.2.2 Plan of tests

From the experiments, several parameters are recorded including the gas emissions (CO, NO_x, O₂, and CO₂), and the temperature of the fuel bed measured at four different positions (5, 15, 25 and 60 mm from the bottom) in the center of the fuel bed. The experimental data and experimental figures are presented in Annex E (Table E.1 and Figure E.1). In a combustion process, the parameter that better describes the combustion quality is the CO emission. Meanwhile, during the long run combustion, as the CO value could fluctuate and increasing significantly with the fuel bed (FB) rise, then the CO considered in this study is recorded before the occurrence of those instabilities in the FB.

According to Ferreira (2008), for the optimization process, the deviation to the optimal value depends on the dispersion of results. Thus, the analysis of variance (ANOVA) is based on the mean and variance of each test. ANOVA provides the dispersion present in a specific set of data, identifying their origins and evaluating the contribution of each data to the total dispersion. This method allows us to test the significance of the effects relatively to the random error, also known as noise. The combustion procedure used in this study, follows the experimental procedure described above and used for all tests.

As mentioned, the response parameter used was the concentration of CO, corrected for 13% O₂, and the temperature measured at four different heights inside the fuel bed: 5, 15, 25, and 60 mm.

The data obtained from the experiment was transformed into a signal-to-noise ratio (S/N) to measure the deviation of quality of parameters from the desired values. The S/N ratio is always < 0. A higher value ratio corresponds to a better quality characteristic of the parameter observed (Babu *et al.*, 2014); the values close to zero indicating the best conditions (Thanakiatkrai and Welch, 2011). In the Taguchi method, three types of characteristic performance are selected in the analysis, include the-larger-the-better, the-smaller-the-better, and the-nominal-the-better (on-target-better) (Liu *et al.*, 2019; Thanakiatkrai and Welch, 2011). In the analysis of variance for CO, the calculation for signal/noise was selected the small-the-better (see Eq. 6.2) and for temperature was the-nominal-the-better (see Eq. 6.3) (Ferreira, 2008).

$$S/N = -10 \log \left(\bar{X}^2 + \sigma_x^2 \right) \quad (6.2)$$

$$S/N = -10 \log \left(\sigma_x^2 \right) \quad (6.3)$$

where \bar{X} is the average value of the data and σ_x^2 is variance. The final plan of experiments and value of responses, according to the Taguchi method is presented in Table 6.6.

Table 6.6. The experiments plan and value of responses, according to the Taguchi method.

No	A		B		C		D		Emission					Fuel bed temperature (°C)					Total air (m ³ /h)
	Power (kW)	EA (%)	EA (%)	GA (mm ²)	SR (P/S)	O ₂ (%)	CO (ppm)	NOx (ppm)	CO ₂ (%)	η (%)	5 mm	15 mm	25 mm	60 mm	T _{cham} (°C)	TaHE (°C)	PA (m ³ /h)		
1	10	50	50	90 x 75	20/80	5.83	395	36.12	18.13	63.92	582	791	811	678	393	255	2.90	14.71	
2	10	50	50	115 x 75	30/70	6.69	149	31	13.42	74.96	700	983	933	572	404	321	4.45	14.93	
3	10	50	50	115 x 96	37/63	2.79	1,042	47.3	2.11	71.07	744	864	838	633	398	217	4.29	11.74	
4	10	70	70	90 x 75	30/70	8.34	143	64.3	13	72.63	627	931	916	624	413	324	5.04	16.91	
5	10	70	70	115 x 75	37/63	4.88	452	67.06	12.66	77.67	687	1,009	907	648	432	325	4.85	13.25	
6	10	70	70	115 x 96	20/80	8.25	157	58.67	13.08	69.25	691	855	853	514	407	298	3.30	16.72	
7	10	110	110	90 x 75	37/63	10.82	474	62	11.5	83.02	542	877	925	612	433	377	7.75	21.19	
8	10	110	110	115 x 75	20/80	10.87	209	49.44	10.4	81.16	630	961	983	765	439	321	4.17	21.11	
9	10	110	110	115 x 96	30/70	10.77	370	25.78	9.48	83.85	656	929	849	546	425	310	6.25	20.98	
10	13	50	50	90 x 75	37/63	6.75	110	54.94	13.58	87.08	626	1,039	1,012	741	493	333	7.20	19.67	
11	13	50	50	115 x 75	20/80	6.37	126	74.04	15.59	74.03	700	929	907	647	475	337	3.77	19.10	
12	13	50	50	115 x 96	30/70	6.5	128	37.69	14.38	86.01	699	951	957	631	478	335	5.69	19.11	
13	13	70	70	90 x 75	20/80	8.33	109	73.3	14.39	91.57	676	985	968	848	528	369	4.32	21.86	
14	13	70	70	115 x 75	30/70	8.32	228	37.12	11.78	88.85	651	1,006	986	753	505	362	6.54	21.94	
15	13	70	70	115 x 96	37/63	8.29	262	70	12.93	91.77	627	913	866	542	493	365	8.11	22.17	
16	13	110	110	90 x 75	30/70	10.5	134	32.46	10.11	87.26	619	1,054	1,041	831	509	389	7.87	26.41	
17	13	110	110	115 x 75	37/63	10.84	314	29.2	9.71	87.36	556	1,076	1,049	820	507	389	10.07	27.51	
18	13	110	110	115 x 96	20/80	10.03	234	63.34	11.44	85.61	710	1,032	987	630	483	375	5.00	25.31	
19	16	50	50	90 x 75	30/70	6.57	213	79.31	13.32	83.18	668	1,007	1,043	783	546	421	7.13	23.93	
20	16	50	50	115 x 75	37/63	6.39	190	69.92	14.66	91.32	640	984	995	576	577	431	8.65	23.64	
21	16	50	50	115 x 96	20/80	6.53	219	80.9	13.9	87.02	695	1,086	1,016	788	546	414	4.67	23.67	
22	16	70	70	90 x 75	37/63	8.30	356	74.1	13.1	87.19	576	1,023	1,078	719	567	433	9.88	27.01	
23	16	70	70	115 x 75	20/80	8.25	111	72.91	11.69	86.65	699	1,068	1,064	867	558	423	5.28	26.77	
24	16	70	70	115 x 96	30/70	8.44	267	38.8	12.28	90.2	681	1,003	972	606	541	410	8.11	27.21	
25	16	110	110	90 x 75	20/80	10.77	227	62.33	8.4	80.99	689	1,089	1,083	947	520	435	6.60	33.44	
26	16	110	110	115 x 75	30/70	10.83	282	31.85	9.6	86.7	649	1,092	1,060	692	539	420	10.05	33.71	
27	16	110	110	115 x 96	37/63	10.93	447	32.61	9.33	84.79	577	825	626	606	516	406	12.49	34.13	

6.3 Combustion of wood pellets

This section presents the ignition condition, the emission characteristics, the thermal efficiency, instability, and the ash formation and agglomeration.

6.3.1 Ignition conditions

The ignition process is accomplished by a 37 W electrical resistance. The ignition takes about 7–9 minutes, depending on several conditions such as thermal load, ambient temperature, primary air flow rate, and grate area. Ribeiro *et al.* (2019) stated that the ignition rate in pellet fuel bed is a function of the PA supply rate. In this study, for ignition purposes, the thermal load of wood pellets should be set at approximately 10 kW and the air flow rate need to be set at $9.4 \times 10^{-3} \text{ m}^3/\text{s}$. For smaller grates (for example 90 mm x 75 mm), the thermal load of wood pellets needs to be reduced and can be set at approximately 7.36 kW at the same air flow rate.

The relationship of ignition rate and fuel supply, and PA mass flow rate through the GA is presented in Figure 6.1, with the maximum ignition rate of $0.08 \text{ kg}/\text{m}^2\cdot\text{s}$ (Ribeiro *et al.*, 2019; Ronnback *et al.*, 2001). It presents the overall combustion with the maximum fuel supply of approximately 13 kW based on the Ronnback *et al.* calculation (Ronnback *et al.*, 2001). It relates the combustion rate with the primary air flux. Both these quantities are based on the grate area. The data are organized accordingly to the power level of the boiler. It clearly suggests that for most of the conditions tested the grate is small for the fuel flux. The condition is more evident for the higher power levels that were tested.

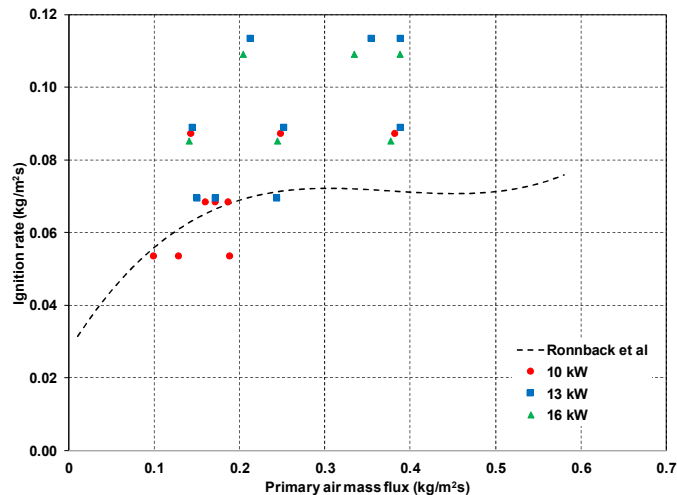


Figure 6.1. Specific ignition rate and fuel supply for three different GA as function of the PA mass flow.

6.3.2 Emission characteristics

Emissions were measured automatically at the chimney by a “Multi gas analyzer 9000” (CO, O₂, and CO₂), and NO_x by “NO_x gas analyzer” (see Chapter 3).

The volatile fuels from the bed combustion are assumed to be light hydrocarbons (modelled as methane), heavy hydrocarbon (tar modelled as C_xH_y), carbon monoxide (CO) and hydrogen (H₂). In addition, the effluent gases also include: H₂O and N₂ (Klason and Bai, 2007).

Figure 6.2 shows, as an example, the gas emissions during a run at 13 kW with the excess air of 70%, the P/S split ratio of 37/63 and a grate area 115 mm x 96 mm, referred as test number 15 (TN15). The input parameter and the average value of gas emission and temperature in the fuel bed recorded are presented in Table 6.7 and Table 6.8. The rising of fuel bed means that the feeding rate of wood pellets is unbalanced by the mass loss rate. This leads to the fuel bed increasing gradually up to 60 mm or, overflowing the grate. After the fuel bed rising, the combustion becomes unstable which is followed by an increase in CO emissions. The thermal efficiency of the boiler obtained for TN15 was 91.77%, with the cold and hot water temperature on heat exchanger being 36 °C and 68 °C respectively. As shown in Figure 6.2 all gases were measured continuously, except for NO_x that was measured within about 12 – 15 minutes during the test. In this study, the emissions fluctuate due to the several conditions such as temperature, the gas residence time (ratio of volume of the combustion chamber/gas flow), turbulence and excess air, which are decisive for the optimization of the combustion process (Kraiem *et al.*, 2016).

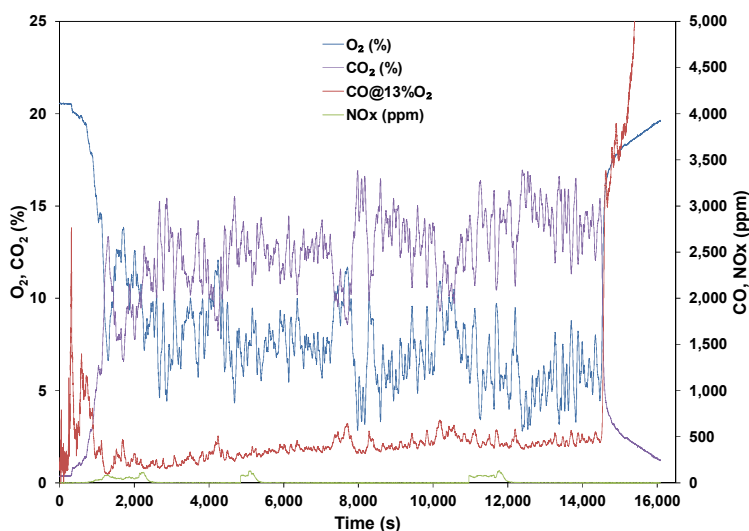


Figure 6.2. Gas emissions profiles for TN15.

Table 6.7. The input parameter for TN15.

Parameter	Value
T ambient (°C)	19
Fuel flow rate (kg/h)	2.75
Primary air flow rate (m ³ /h)	8.11
Secondary air flow rate (m ³ /h)	14.06

Table 6.8. The experimental data for TN15.

Parameter	Before FB rising	After FB rising	Overall	T _{fb} (°C)
O ₂			8.29 %	627 (5 mm)
CO (13% O ₂)	262 ppm	427 ppm	390 ppm	913 (15 mm)
NO _x			70 ppm	866 (25 mm)
CO ₂			12.93 %	542 (60 mm)

6.3.3 The thermal efficiency

The boiler efficiency is calculated according to the NF EN 303-5 standard as follows Eq. (6.4) (Lajili *et al.*, 2015):

$$\eta_b = \frac{P_n}{P_i} \cdot 100 \quad (6.4)$$

$$P_n = m_w \cdot C_w \cdot \Delta T_w \quad (6.5)$$

$$P_i = m_f \cdot \text{LHV} \quad (6.6)$$

where, η_b is the boiler efficiency (%), P_n is the nominal useful boiler power (kW), P_i is the power input (kW), m_w is the water mass flow rate (kg.s⁻¹), C_w C_{pw} is the heat capacity of water (kJ.kg⁻¹.K⁻¹), ΔT_w

is the difference temperature of water in the exchanger (K) and m_f is the fuel mass flow rate (kg.s⁻¹).

Figure 6.3 shows the thermal efficiency obtained for the different conditions of the combustion. This experiment shows that the thermal efficiency is always above 60%. For tests TN13, TN15, TN20 and TN24, the efficiency was above 90% as presented in Table 6.9.

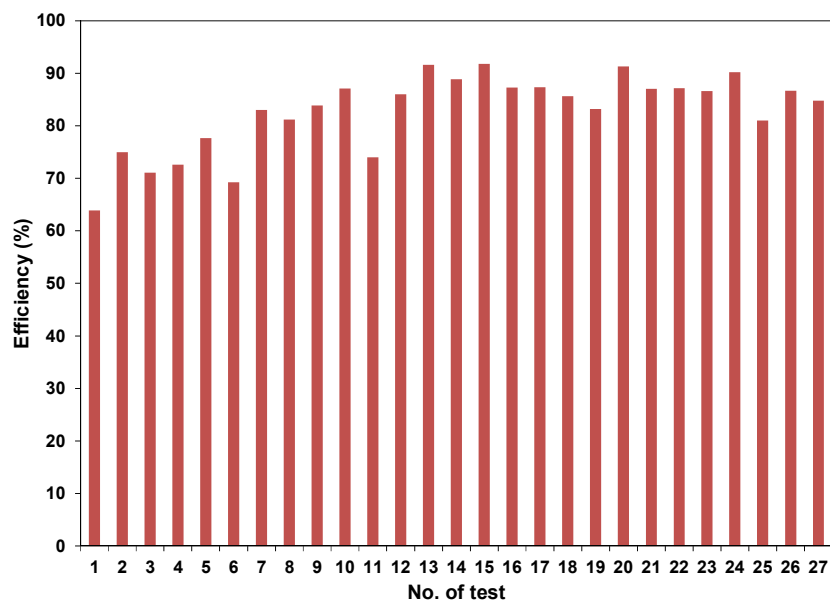


Figure 6.3. The efficiency obtained for each test.

From the data it appears that on average the efficiency tends to occur at the lowest power level (runs 1 through 9) particularly for low SR.

Table 6.9. Highest thermal efficiency experiments.

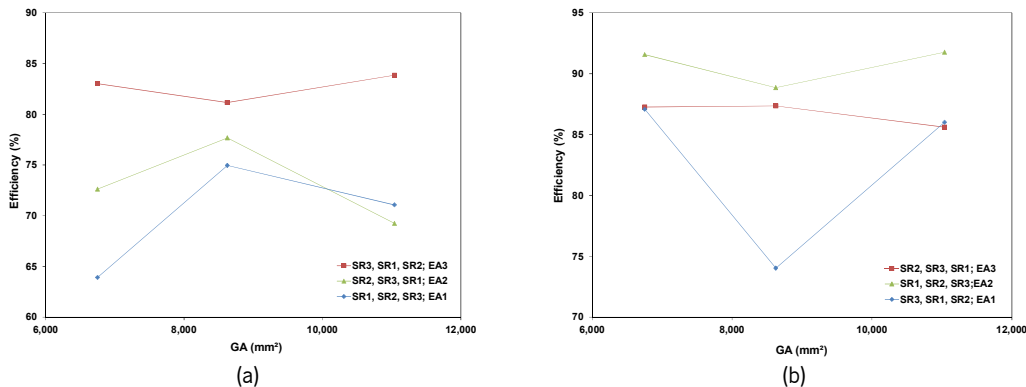
	TN15	TN13	TN20	TN24
Power (kW)	13	13	16	16
EA (%)	70	70	50	70
GA (mm ²)	115 x 96	90 x 75	115 x 75	115 x 96
SR	37/63	20/80	37/63	30/70
O ₂ (%)	8.29	8.33	6.39	8.44
CO before FB rising	262	109	190	267
CO after FB rising	427	262	212	325
CO average	390	252	204	302
NO _x (ppm)	70	73.3	69.92	38.8
CO ₂ (%)	12.93	14.39	14.65	12.28
η (%)	91.77	91.57	91.32	90.2

Figure 6.4 shows the relationship between GA and thermal efficiency at different Power, SR, and EA. Figure 6.4 (a) shows that at 10 kW with 50% of EA (EA1) the efficiency was higher for the combination of middle GA (GA2) with middle SR (SR2), the same behavior for 70% of middle EA (EA2) with the combination of GA2 with higher SR (SR3). For 110% of EA (EA3), the thermal efficiency was higher for the combination of smaller GA (GA1) with SR3, and larger GA (GA3) with middle SR (SR2). Figure 6.4 (a) shows that at lower Power, the best combination of the parameter is either EA3-GA1-SR3 or EA3-

GA3-SR2 in order to produce higher combustion efficiency. This means that at a lower Power requires a higher EA during the combustion of wood pellets. As in fact, lower Power produce lower devolatilization rate, then higher EA requires to burn up the fuel; the opposite may be observed for higher Power levels (see Figure 6.4 (c)).

Figure 6.4 (b) shows that at 13 kW with 50% of EA the thermal efficiency was higher for the combination of smaller GA (GA1) with SR3, and larger GA (GA3) with middle SR (SR2). The same behavior was observed for 70% of EA (EA2) referred to the combination of GA1 with lower SR (SR1) and GA3 with higher SR (SR3). For 110% of EA, the thermal efficiency was slightly higher referred for GA1 and GA2, with the combination of GA1 with SR2 and GA2 with SR3 respectively. Figure 6.4 (b) shows that at middle Power, the best combination of the parameter is either EA2-GA1-SR1 or EA2-GA3-SR3 in order to produce the highest combustion efficiency.

Figure 6.4 (c) shows that at 16 kW with different SR and 50% of EA, the thermal efficiency was higher at middle GA with the combination of GA2 and SR3, the same behavior for 110% of EA (EA3) with the combination of GA2 with middle SR (SR2). For 70% of EA, the thermal efficiency was higher for the combination of GA3 with SR2. Figure 6.4 (c) shows that the best combination of the parameter is EA1-GA2-SR3. This means that at a higher Power, a lower EA and middle GA with higher SR are suitable to produce higher combustion efficiency. From the figures the higher efficiency (above 90%) is obtained for three different GA. The data indicates that an efficient combustion can be obtained with any grate, providing the operational parameters (EA, SR) are properly adjusted for any specific power level, which is in line with the result obtained from Verma *et al.* (2013). Higher efficiencies cannot be obtained at higher EA due to stuck losses, as stated by Serrano *et al.* (2013) that the excess air in the boiler reduces the boiler efficiency. The high efficiency could be related to the low CO emission during combustion (Arranz *et al.*, 2015).



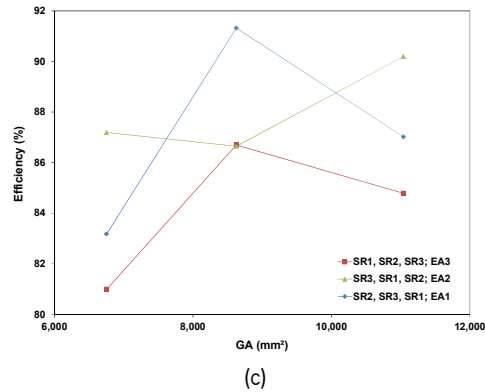


Figure 6.4. Relationship between efficiency and GA with different EA and SR: (a) At 10 kW, (b) At 13 kW, and (c) At 16 kW.

6.3.4 Combustion instability

During the course of the various tests, it was observed that instabilities could occur over long runs. These were identified with a sudden rise in the fuel bed height that would lead to an increase in emissions and, ultimately, to a collapse of the combustion. This is a reason why boiler manufacturers introduced a control strategy that, periodically, clean the fuel bed. Table 6.10 presents the experimental and a qualitative assessment of the combustion behavior for the 27 tests. In the table $t_{av,ins}$ is average time (moment) when the instability starts to occur and t_{run} is the running time duration of the test. The data in Table 6.10 shows that the majority of the experiments experienced instability which is indicated by the fuel bed rising and increasing in the CO emissions. The instability occurs as an indication of the poor combination of the parameters applied which result in a high CO concentration as referred to TN1 and TN3. The instability is mostly linked of the fuel bed rising which may be a consequence of the lower combustion rate (accumulation of unburned pellets on the grate). The instability may also occur as a result of the poor combination of the parameters applied which is referred mostly to the GA.

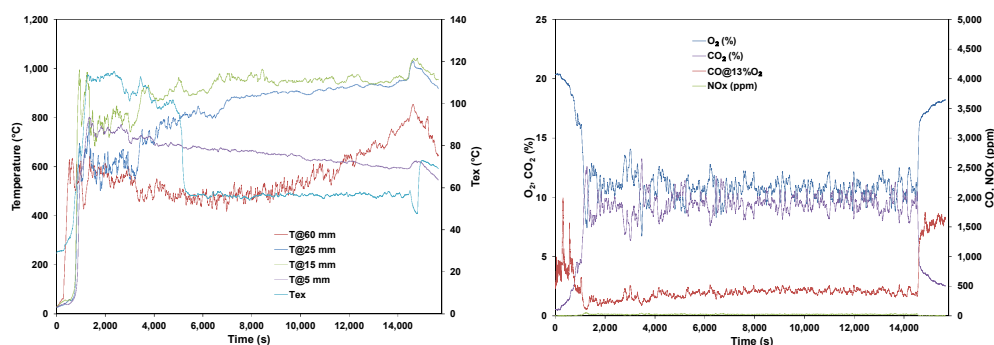
Table 6.10. Stability and instability combustion condition of the experiment identified.

Test.	P (kW)	EA (%)	GA (mm ²)	SR	t _{av,ins} (s)	t _{run} (s)	Indication	CO after (ppm)	Description
TN1	10	50	90 x 75	20/80	2,300	4,500	High CO	1,830	Poor combustion: Instability, FB rising, and condensation.
TN2	10	50	115 x 75	30/70	3,600	5,500	Fuel bed rising	217	Instability and condensation.
TN3	10	50	115 x 96	37/63	2,500	4,500	High CO	1,985	Poor combustion: high CO, noisy, flame instability and condensation.
TN4	10	70	90 x 75	30/70	3,500	5,500	Fuel bed rising	334	Instability.
TN5	10	70	115 x 75	37/63	6,600	8,900	Fuel bed rising	847	Noise and condensation.
TN6	10	70	115 x 96	20/80	4,500	6,000	Fuel bed rising	470	Instability and condensation.
TN7	10	110	90 x 75	37/63	8,600	14,400	Fuel bed rising	561	Instability and condensation.
TN8	10	110	115 x 75	20/80	5,000	14,400	Fuel bed rising	282	Instability, noise and condensation.
TN9	10	110	115 x 96	30/70	14,400	14,400	-	415	Stable combustion.
TN10	13	50	90 x 75	37/63	2,700	5,000	Fuel bed rising	149	Instability and condensation.
TN11	13	50	115 x 75	20/80	3,200	5,400	Fuel bed rising	787	Instability and condensation.
TN12	13	50	115 x 96	30/70	6,500	9,000	Fuel bed rising	176	Instability and noise.
TN13	13	70	90 x 75	20/80	2,800	10,000	Fuel bed rising	262	Instability and condensation.
TN14	13	70	115 x 75	30/70	5,400	12,000	Fuel bed rising	490	Instability.
TN15	13	70	115 x 96	37/63	14,400	14,400	Fuel bed rising	427	Noise.
TN16	13	110	90 x 75	30/70	3,100	7,500	Fuel bed rising	218	Instability.
TN17	13	110	115 x 75	37/63	6,000	14,400	Fuel bed rising	213	Small instability.
TN18	13	110	115 x 96	20/80	7,200	14,400	Fuel bed rising	395	Noise.
TN19	16	50	90 x 75	30/70	2,900	6,100	Fuel bed rising	246	Instability.
TN20	16	50	115 x 75	37/63	14,400	14,400	-	212	Stable combustion.
TN21	16	50	115 x 96	20/80	5,800	14,400	Fuel bed rising	350	Small instability.
TN22	16	70	90 x 75	37/63	5,200	8,000	Fuel bed rising	413	Instability and noise.
TN23	16	70	115 x 75	20/80	4,100	11,000	Fuel bed rising	242	Small instability.
TN24	16	70	115 x 96	30/70	8,000	14,400	Fuel bed rising	325	Small instability.
TN25	16	110	90 x 75	20/80	2,400	6,000	Fuel bed rising	341	Instability.
TN26	16	110	115 x 75	30/70	7,400	14,400	Fuel bed rising	492	Instability.
TN27	16	110	115 x 96	37/63	14,400	14,400	-	544	Small noise.

The instability may be identified in some cases from a phenomenon such as noise, the increasing of CO emissions, and the increasing of the fuel bed which can be observed directly or from the increasing of the temperature at 60 mm above the fuel bed. The noise occurs as a result of vortex generation (associated with a higher pressure drop) and oscillation in the air flow rate. This may result from the accumulation of pellets on the grate which blocks the primary air entrance or also a larger GA that may create a low velocity of the primary air flow through the grate. Yazdanpanah *et al.* (2011) stated that the pressure drop is caused by pellet size, geometry of container cross-section, and air flow rate. The authors revealed that pressure drop increases with the air flow rate and smaller wood pellet. Regarding the geometry of the container cross-section, Ray *et al.* (2004) stated that the pressure drop increases with a packed fill versus a loose fill.

Condensation is an indication of the dropping of the exhaust temperature (the profile of the exhaust temperature can be seen in Annex E (Figure E.1)), even though, among those experiments, TN9 and TN20 are considered as stable combustion examples since there was no indication of the instability during the 4 hours running (see Figure 6.5). This is an indication of the good combination parameters applied in this study. In general, from the instability data and the result data, one can conclude that the middle size grate is the optimum grate. Meanwhile, Figure 6.6 (a) shows that after the fuel bed rising (as indicated by the temperature profile in 60 mm) the experiment was terminated because the instability was very high, which is coupled with a sharp increase of CO. However, as illustrated by Figure 6.6 (b) one test was extended for 4 hours because the system shifted to another stable condition.

The instability of exhaust temperature can result from poor combustion in the grate that produces low temperature (see Figure 6.6 (a)). However, the increasing of the exhaust temperature may relate to the higher air flow rate (higher EA) that may expel more heat to the exhaust pipe (see Figure 6.7 (a)). The same condition may also be obtained for SR, as increasing the SR contributes to the increasing of the exhaust temperature (e.g. see Figure 6.7 (b) test at 70% of EA and at a middle SR).



(a)

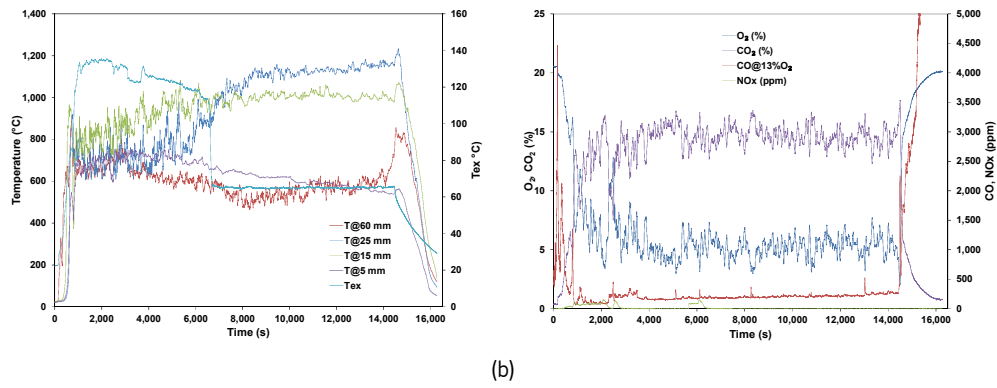


Figure 6.5. Temperature and emissions profiles for (a) TN9, and (b) TN20.

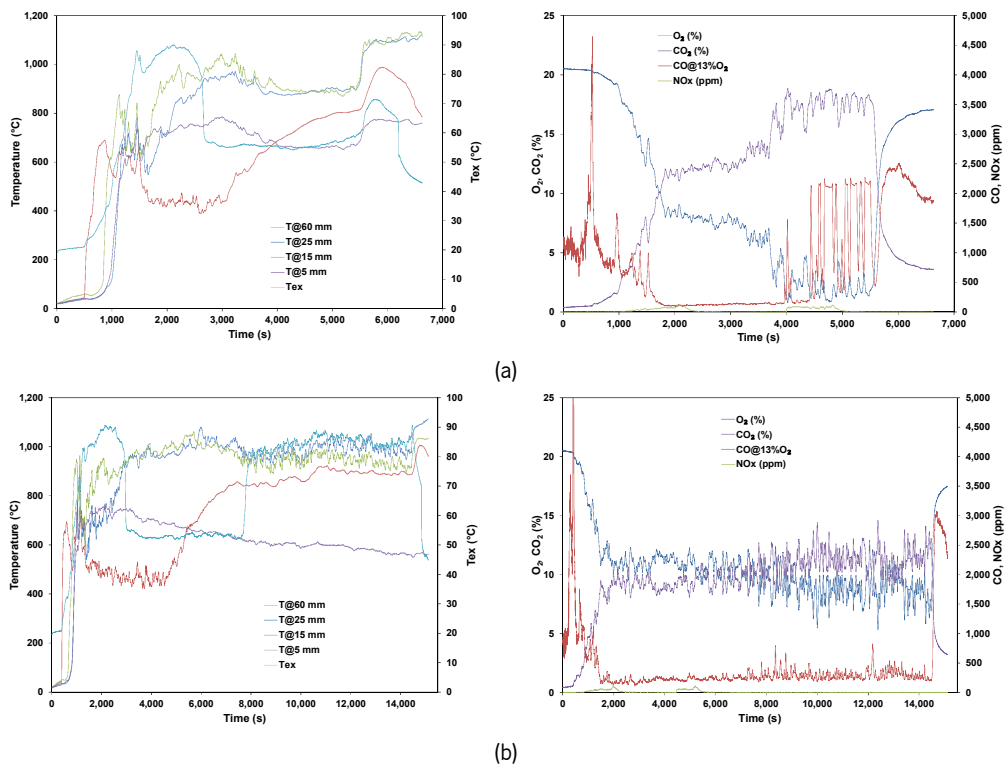


Figure 6.6. Temperature and emissions profiles for (a) TN11, and (b) TN8.

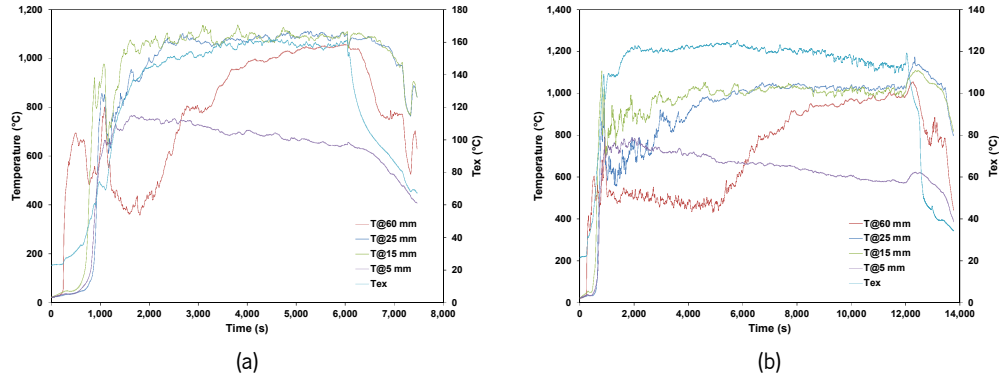


Figure 6.7. Temperature profiles for (a) TN25, and (b) TN14.

Figure 6.8 shows that the shorter the instability time ($t_{av,ins}$), the earlier the instability was observed and when $t_{av,ins} = t_{run}$ means there is no instability (fuel bed rising) during the combustion of the wood pellets (e.g. TN9, TN20, and TN27). Figure 6.8 (a, b, and c) show that in a certain combination of Power, EA and GA create an early instability, such as a small GA with a middle or higher Power and a lower EA (e.g. TN10 and TN19). Meanwhile, the SR ratio has no significant influence on the instability since the same trend was observed for different SR.

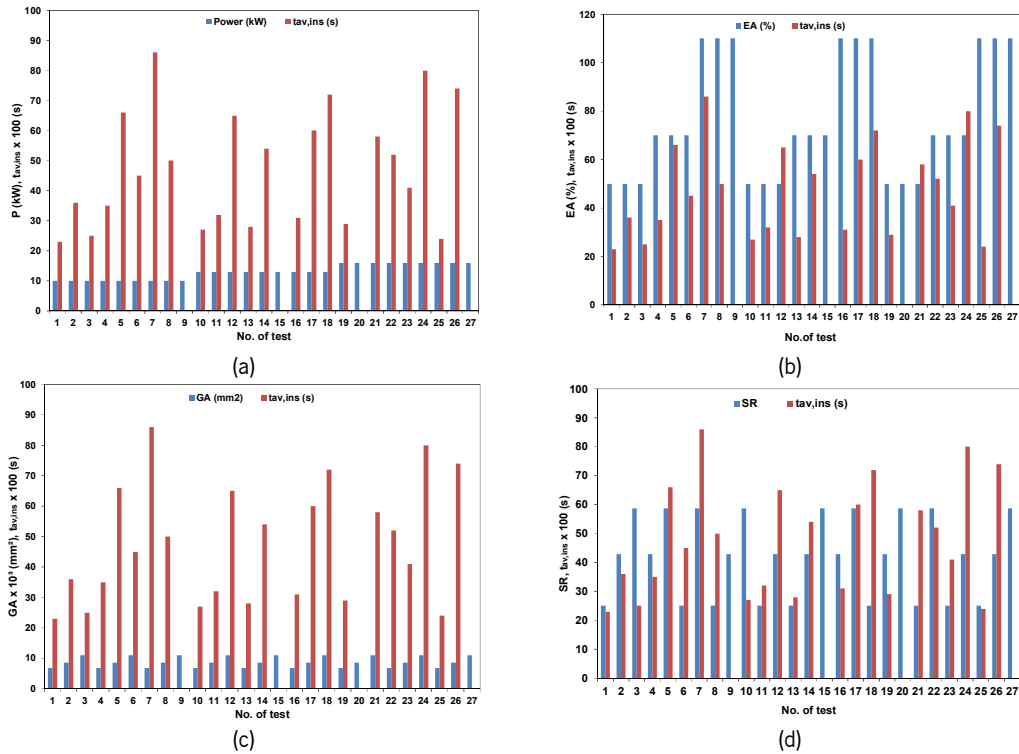


Figure 6.8. Combustion characteristics on the instability.

6.3.5 Ashes formation and agglomeration

Subsequently to each experimental run, the ashes were collected from the bottom of the grate. A high resolution frame was collected, and the *ImageJ* software was used to measure the size of the aggregated ashes. They were measured based on the larger size of its agglomeration. Generally speaking, ash formation and agglomeration depends upon the burner and fuel types (Öhman *et al.*, 2004). It was observed that the agglomeration of the ashes occurred when the boiler was operated at a high load and high-temperature condition (Roy *et al.*, 2013). Dibdiakova *et al.* (2015) reveal that the chemical composition of the ashes from the combustion of a pine tree contains mostly Ca, K, Mg, Mn, P, and Si, and the melting process of the ashes started in the temperature range of 930-965 °C. For red pine, the ash deformation temperatures are over 1,100 °C (Fang and Jia, 2012). In addition, the remaining mass as fixed Carbon and ashes or unburned substances after the combustion of these wood pellets is about 3%.

The size of the ashes agglomeration is presented in Annex E (Figure E.2). This study revealed that, besides several conditions mentioned before that have an influence on the ashes agglomeration, the duration of the combustion is also determinant for the agglomeration of the ashes. For example, the combustion of pine wood pellets with TN2 (10 kW, EA 50%, and SR 30/70) with a duration time of 5,500 s has almost no agglomeration above 3 mm in size, but only show their sintering. The degree of sintering is mostly an effect of the composition of the fuel ash (Öhman *et al.*, 2004). Moreover, when the time of the combustion is less than 5,500 s, the ashes agglomeration is less than 10 mm in size. Incidentally, the largest size of the ashes agglomeration was referred to TN26 (16 kW, EA 110%, and SR 30/70) which is 59 mm and the duration time is 14,400 s (\approx 4 h).

Figure 6.9 (a-d) shows that from the parameters applied (P, EA, GA, and SR) the middle and higher level tend to increase the ash accumulation size. The high fuel bed temperature and long running time have also increased the ash accumulation size (see Fig. 6.9 (e, f)). The large residence time (longer running of the boiler) of wood pellet combustion also produces more ashes agglomeration. These conditions indicate that the agglomeration of the ashes is as a function of time and temperature. In addition, Ribeiro *et al.* (2014) also stated that the ash agglomeration is mostly related to the changing of the chemical elements ratio due to vaporization of the more volatile species.

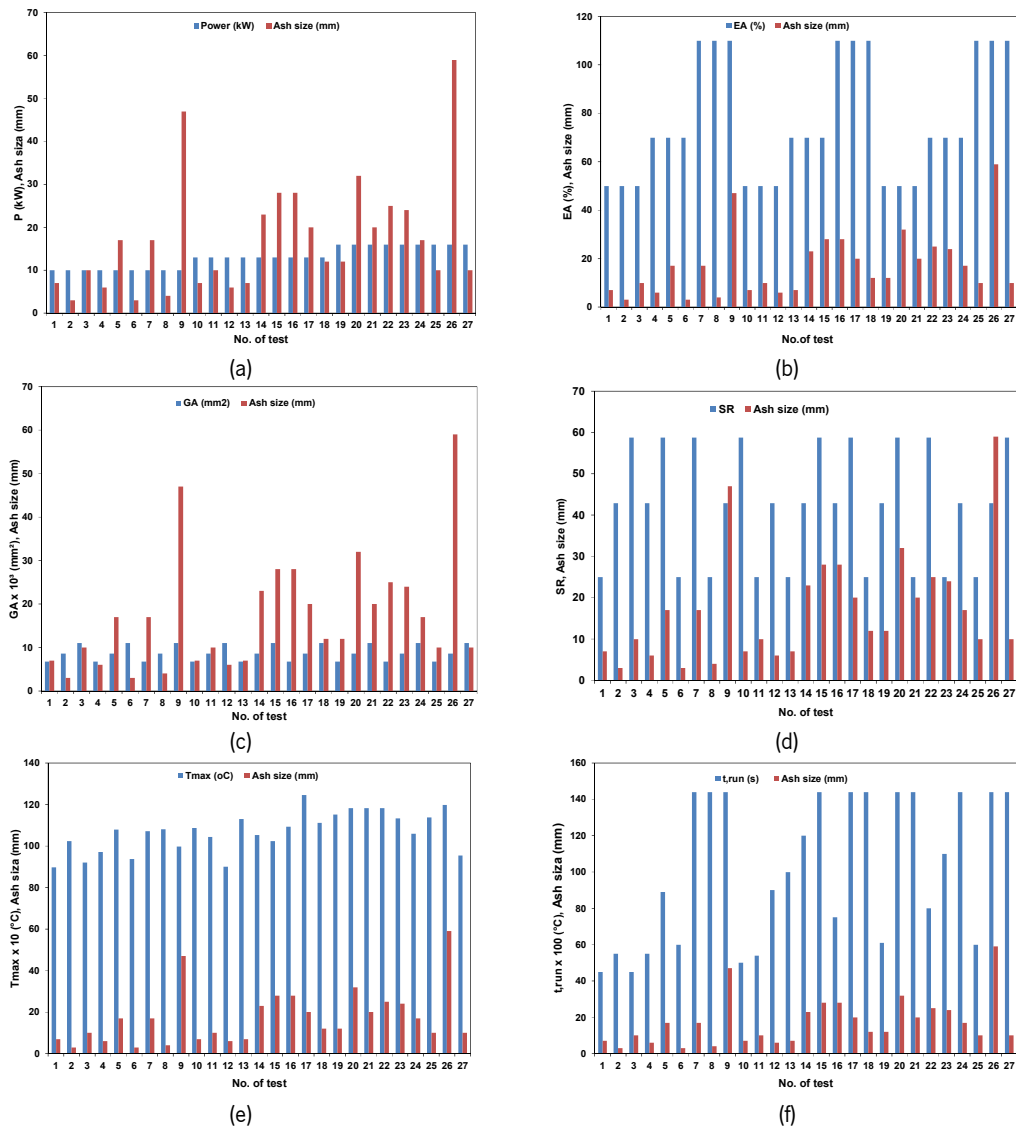


Figure 6.9. Combustion characteristics on the ashes.

6.4 CO emissions

CO is a key indicator of the combustion quality. The influence of different conditions on CO emissions is presented as follows.

6.4.1 Overview of CO emissions

CO emissions during the test presents a fluctuated behavior, which can be caused by the intermittent feeding system (screw conveyor). During the feeding process fresh wood pellets drop on the combusting bed, causes a sudden heating of the particles and a sharp reduction of the temperature of the surrounding fuel and produce a high amount of CO (Gómez *et al.*, 2016). The high CO emission also

indicates imperfect combustion conditions and poor energy efficiency and are caused by inadequate mixing of air and combustible gases, a too short residence time at sufficiently high temperature, high moisture content (Olsson, 2006a; Ravichandran, 2013) or poor furnace design (Ravichandran, 2013). At high loads and low excess oxygen there are mixing limitations that will increase the CO emissions. On the other hand higher excess oxygen and lower load result in more CO emissions as gas temperature decreases (Roy *et al.*, 2013). Very low and high burn rates will also increase CO emission factors (Fachinger *et al.*, 2017). According to Serrano *et al.* (2013) the CO emissions decrease with EA and SA. Overall, the CO emission ranged between 109 and 1,042 ppm. The lowest CO emissions were measured before the fuel bed rising: is 109, 110 and 111 ppm with thermal efficiency 91.57%, 87.08%, and 86.65% referred to TN13, TN10, and TN23 respectively. The lowest CO emission and higher efficiency obtained indicated the good combination of the parameters observed (A2-B2-C1-D1).

6.4.2 ANOVA analysis of CO emissions

The S/N indices are determined for each response value analyzed in this study. The mean values of the S/N indices for each of the three levels of each parameter or interaction on CO are presented in Table 6.11. The last line of each table shows the maximum value of the difference between the averages of the indices for each of the parameters. These results evaluate the relative weight of influence of each parameter on the response value.

Based on the analysis of Table 6.11 it is verified that the split ratio (SR) index (parameter D, dif. = 5.56) has the highest contribution to CO reduction, followed by parameter A (Power, dif. = 5.16), the interaction of parameters Power and EA (dif. = 3.12), parameter C (GA, dif. = 2.91) and parameter B (EA, dif = 2.60). There is a parameter that was not identified, whose influence is higher than that of the interaction of parameters Power and EA, GA, and EA. This indication is supported by the value of the left-hand column of the SR value. This result may show the influence of parameters that were not considered but make some significant contribution to the process.

Table 6.12 presents the analysis based only on the mean values of the CO concentration for each parameter. The data confirms the trend observed by the analysis of the S/N indices, on how to minimize the response value. The data show that the most important is SR with the difference about 207 ppm, followed by Power at 194 ppm, and other unidentified parameters (column 10 is identified as "e") at 144 ppm.

Table 6.11. Mean values of S/N index and maximum differences between levels on CO.

S/N	P		EA		GA		SR						
	A	B	AxB	C	AxC	BxC	D	e					
1	-49.87	-46.81	-48.68	-49.22	-46.44	-47.01	-48.61	-47.41	-47.20	-45.34	-48.16	-47.97	-48.60
2	-44.71	-46.46	-46.10	-46.70	-46.54	-46.29	-47.41	-46.53	-45.90	-46.09	-46.22	-47.14	-46.13
3	-47.76	-49.06	-47.54	-46.41	-49.35	-49.03	-46.31	-48.39	-49.22	-50.90	-47.94	-47.22	-47.60
diff.	5.16	2.60	3.12		2.91	2.74		2.17	3.32	5.56		0.83	2.47

Table 6.12. Analysis of the relative contribution of the parameters based on the mean concentration of CO.

Average	P		EA		GA		SR						
	A	B	AxB	C	AxC	BxC	D	e					
1	376.8	285.8	333.5	349.0	240.1	246.7	290.4	245.4	249.3	198.6	284.5	272.4	288.5
2	182.7	231.8	230.1	228.5	229.1	232.8	247.8	236.0	211.6	212.6	220.6	245.5	233.5
3	256.9	298.9	252.9	239.0	347.2	337.0	278.2	335.1	355.5	405.3	311.4	298.6	294.4
diff.	194.1	67.2	120.5		118.2	104.2		114.5	143.9	206.7		53.1	60.9

Figure 6.10 shows the dependence of the response with the different parameters, for the various levels of analysis. These data allow to observe the evolution through the three levels for each one of the parameters in the CO concentration. Figure 6.10 (a) shows that at a medium Power (13 kW) CO emission is the lowest observed for the three power levels. Meanwhile, Figure 6.10 (b, c, and d) show that the CO emission is lower at the lower level of the parameter applied and increases with the increasing of the EA, GA, and SR respectively. This means that increasing those parameters create more unburned substances that contribute to the CO emission.

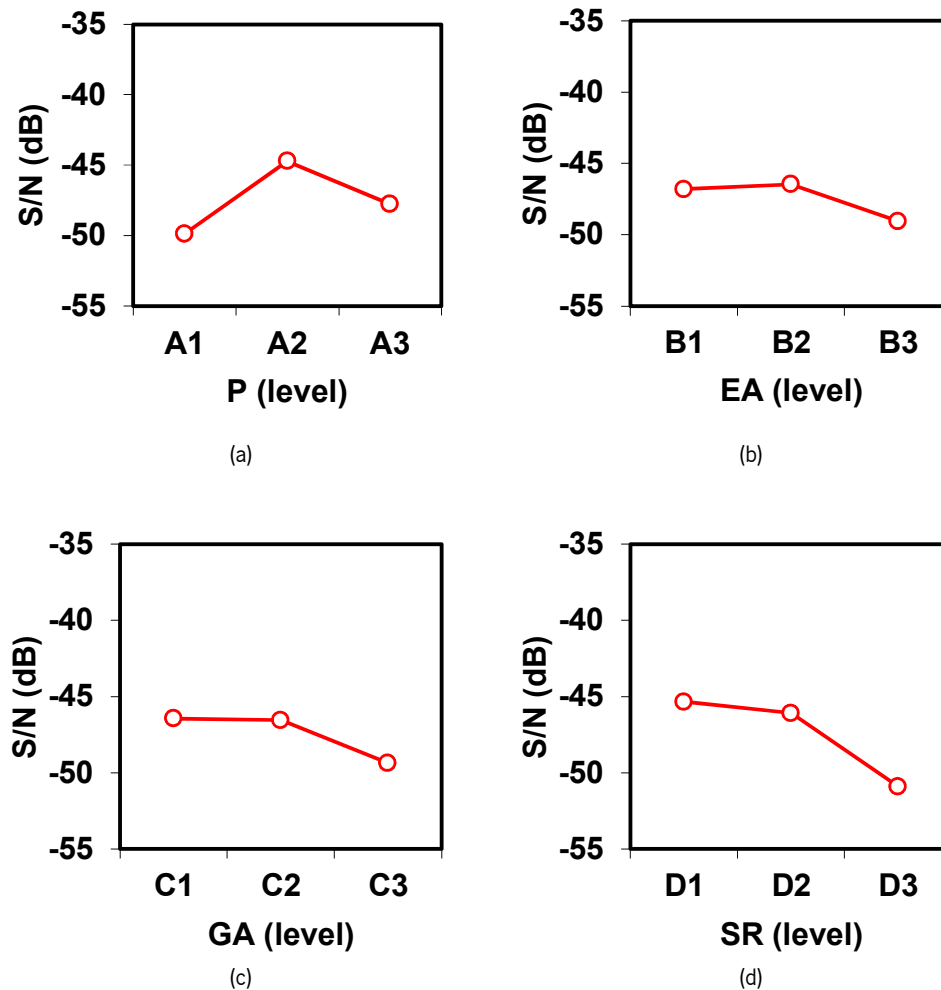


Figure 6.10. Individual influence of factors on the response (CO).

Figure 6.11 presents the interaction between all parameters on CO. From these graphs, we can identify that there is an important interaction between middle Power and lower EA (Figure 6.11 (a)), and between middle Power and lower GA (Figure 6.11 (b)). Based on Figure 6.11 and the value of

maximum differences between levels on CO (Table 6.11), then the best combination to reduce the variance (more stable and best result) is A2-B1-C1-D1.

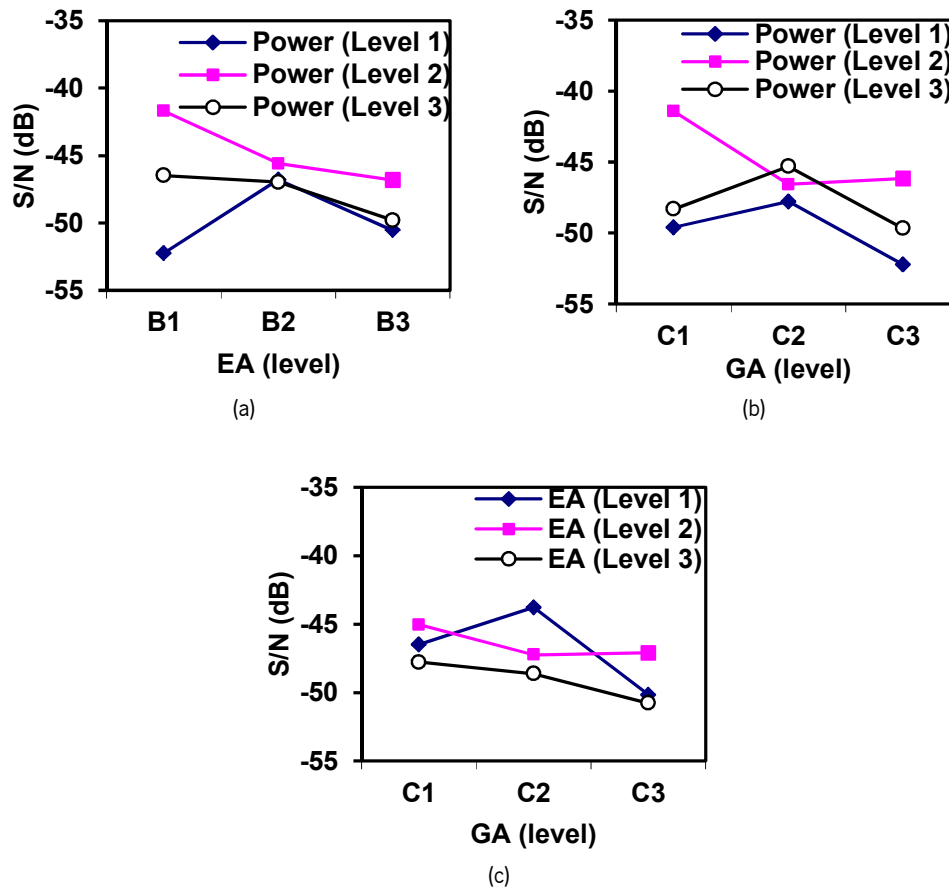


Figure 6.11. Indices of interaction between factors on CO.

In the analysis of variance (ANOVA) the F test (ratio between the variance of a parameter and the variance of the error) is used (Table 6.13). When F and the level of confidence become sufficiently high (confidence = $1 - \text{risk}(\alpha)$; α is also referred to as level of significance, representing the probability (or risk) of accepting that the effect or interaction is significant, when this hypothesis is false), it can be said that two variances are considered to be different. This means that the variance associated with this (factor) is statistically different from the error variance, i.e.: the influence of this parameter in the response is significant. To determine whether an F value of two variances are statistically high, one should consider: the level of confidence required, the degrees of freedom associated with the variance of the sample in the numerator and the degrees of freedom (df) associated with the sample variance in the denominator. The value of F critical is then compared with the F value of a ratio of sample variances. The analysis of variance is a more objective and quantifiable test, allowing conclusions which

are not possible with the simple analysis of the means or S/N indices. Table 6.14 presents the statistical calculation of the F critical according to the level of risk α (1%, 5%, and 10%), for the final configuration of Table 6.13. This method of analysis was previously applied by Ferreira (2008).

Table 6.13. ANOVA worksheet for CO.

ANOVA	P	EA		GA				SR			Error calculation	
	1	2	3 & 4	5	6 & 7	8 & 11	9	10	12	13	error exp.	Total
	A	B	AxB	C	AxC	BxC	e	D	e	e		
df	2	2	4	2	4	4	2	2	2	2	22	26
sq	121.14	35.84	73.10	49.06	60.09	36.08	50.35	163.76	3.74	27.84	336.09	620.99
var	60.57	17.92	18.28	24.53	15.02	9.02	25.18	81.88	1.87	13.92	15.28	23.88
pool	n	s	s	s	s	s	s	n	s	s	n	
F	3.96							5.36				
sq'	90.59							133.20			397.20	620.99
%	14.59							21.45			63.96	100.00

In Table 6.13 only the parameters that contribute significantly to the reduction of CO concentration are identified. After applying the analysis of variance, from Table 6.13 it is verified that the F value associated to parameter D (SR), is higher than the critical value for the confidence index (risk $\alpha = 0.05$) but less than $\alpha = 0.01$, calculated for the same number of degrees of freedom ($df = 2$). From these results, we can conclude that, with a confidence index greater than 95%, it can be stated that the SR intensity contributes about 21% for the reduction of CO concentration. It is the same condition, for the F value associated with Power, which is higher than the value for $\alpha = 0.05$. This means that the confidence index is the same as the previous parameter referred to the SR. Then, it can be said that, with a confidence index of over 95%, the influence of Power contributes about 15% for the reduction of CO concentration.

Table 6.13 allows us to conclude that the main effect comes from the SR followed by Power (A). However, the value associated with the experimental error is 63.96%. This value is indeed significant and deserves careful consideration, as it has a dimension to mask the influence of the most significant parameters. In practice, this error can be the result of several factors: important parameter not considered in the study, unsuitability of the chosen levels, misadjust with the level of factors, and any deficiency in the control of the chosen parameters or instabilities in the operation as stated by Ferreira (2008).

Table 6.14. ANOVA F critic calculation for CO.

F critic		
	Degree of freedom	
Nominator	2	4
Denominator	22	22
α		
0.10	2.56	2.22
0.05	3.44	2.82
0.01	5.72	4.31

6.5 Temperature in fuel bed

6.5.1 Temperature profile in fuel bed

The temperature profile (Fig. 6.12) was measured for the same experimental setting TN15, presented before (Fig. 6.2). The temperature measurements during the test showed a fluctuating behavior as a consequence of the feeding system (Fig. 6.12). When the feeding is taking place, the fresh wood pellets come into contact with the thermocouples thus causing the decreasing of the temperature (Daouk *et al.*, 2017). Average temperature measurement in fuel bed indicated that the highest temperature was observed at 15 mm followed by 25 mm, 5 and 60 mm in height. These values indicated that the highest combustion rate was taking place in a layer between 15 and 25 mm from the bottom. At 5 mm, which is close to the bottom of the grate, the temperature was low as a result of fresh air supply into the grate. In addition, the low temperature at 60 mm indicates that in that region there was a mixing of devolatilization material with secondary air entering above the grate.

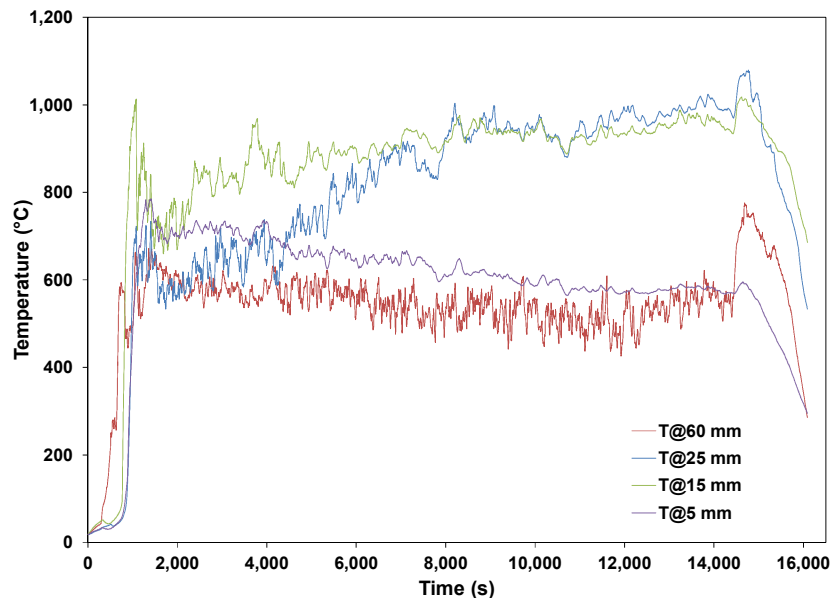


Figure 6.12. Temperature profiles for TN15.

Figure 6.13 presents the temperature profile for experiment TN17. The temperature profile, especially at 60 mm shows that there are two different equilibrium conditions. The first equilibrium did take place at time $< 5,400$ s and the second equilibrium started at $t > 9,000$ s. The equilibrium occurs when the feeding rate of wood pellets is equal to the mass loss rate. While, the slope of the temperature profile at 60 mm, starting within $5,000 - 7,000$ s, is the condition where the fuel bed was rising. The fuel bed was rising because the feeding rate of wood pellets being higher than the mass loss rate. This phenomenon occurs as a result of the cross sectional area of the grate, the thermal load, and the excess air applied. A combination of such factors will cause the feeding rate of wood pellets being higher than mass loss rate, which starts the accumulation of wood pellets on the grate and increases the thickness of the fuel bed.

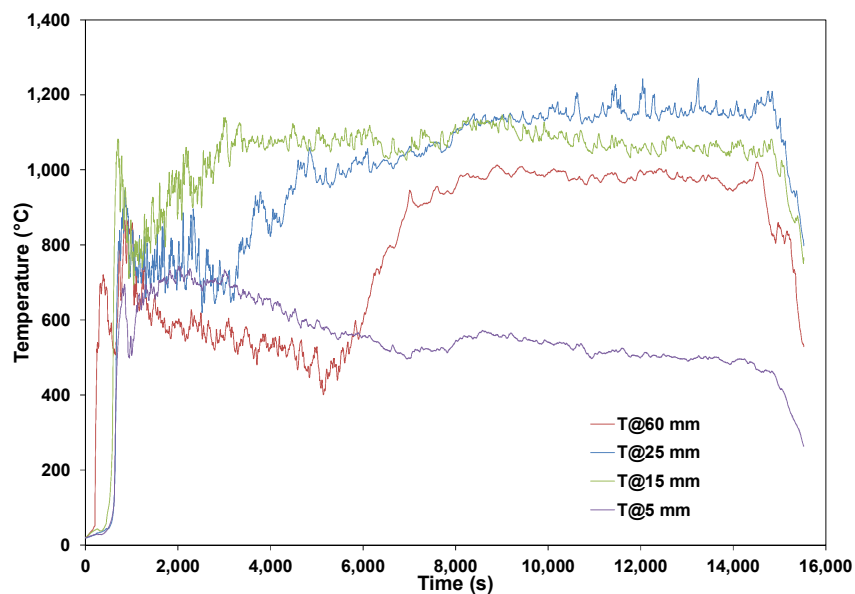


Figure 6.13. Temperature profiles for TN17.

6.5.2 Temperature profile after the shut off of the boiler

The temperature profile in Figure 6.14 was measured at 13 kW, with the excess air of 50%, and a primary and secondary air split ratio of 37/63, with the grate area 90 mm x 75 mm (TN10), (the figure on the *r.h.s.* is a magnification of that on the *l.h.s.*). This temperature profile was observed after the fuel feeding was stopped. During this period, the pellets were burned and reached the highest temperature of 1,284 °C at 25 mm. This temperature peak was achieved as the result of the combination of two things: low excess air (lower oxygen and condition close to stoichiometry) and stopping of fuel supply (Roy *et al.*, 2013). In fact, cutting off the fresh supply of fuel, removes a heat sink in the combustion

bed, which combined with the heat release of the existing fuel, leads the temperature surge. This can be indicated by the lower exhaust gas temperature (see Figure 6.15) for TN10 and TN12 which is more visible. The lower excess air (EA) will minimize the thermal losses by the stack (Ribeiro *et al.*, 2019). Another reason is, when the feeding was stopped, the combustion rate reached the maximum rate causing the devolatilization and heat release to increase, and the thermal decompositions were shifted to the higher magnitude.

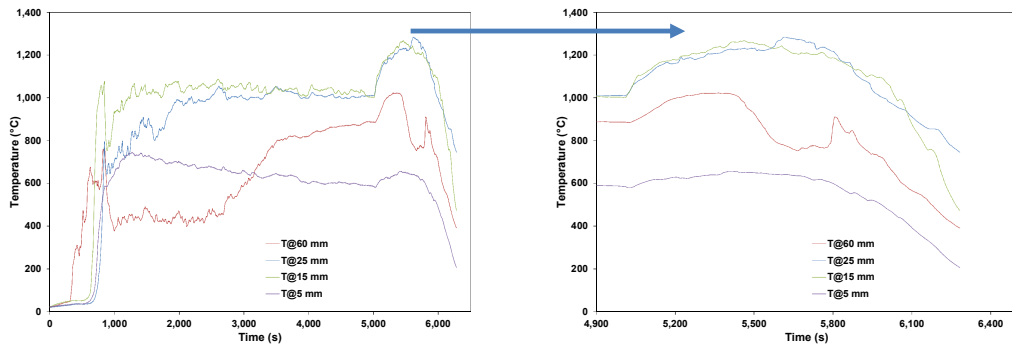


Figure 6.14. Temperature profiles for TN10.

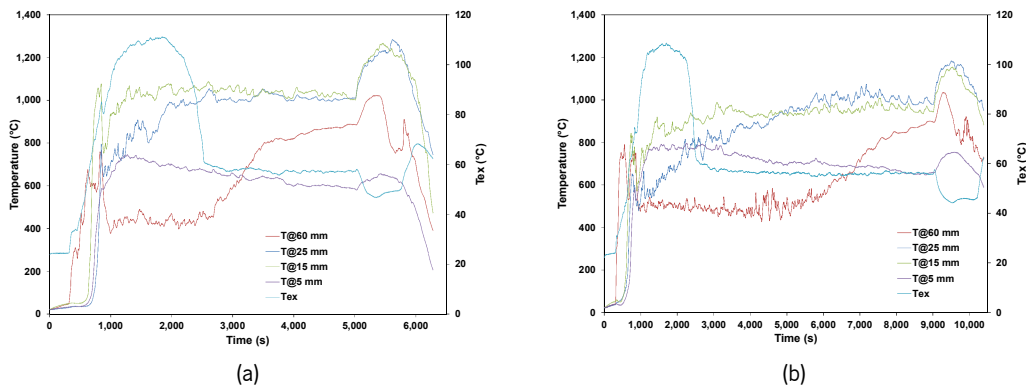


Figure 6.15. Temperature profiles for (a) TN10, and (b) TN12.

Moreover, the heating up of the particle occurs at a faster rate which enhanced the combustion temperature during this period (Silva *et al.*, 2018). According to Vicente *et al.* (2016), a high temperature in the fuel bed is related to rich fuel mixture conditions.

6.5.3 ANOVA analysis on temperature

The mean values of the S/N indices for each of the three levels of each parameter or interaction on fuel bed temperature are presented in Table 6.15 – 6.18. The last line of each table shows the maximum

value of the difference between the averages of the indices for each of the parameters. These results evaluate the relative weight of influence of each parameter on the response value.

Table 6.15 – 6.18 present the mean value of S/N index and the maximum difference between levels on the temperature at a different height in fuel bed. For temperature at 5 mm, it is verified that excess air (EA) has the highest contribution to increasing of temperature, followed by a Power, SR, and the interaction of parameters Power and EA, and parameter GA. For temperature at 15 mm the highest contribution is the interaction of parameters EA and GA, SR, and one unidentified parameter (column 10) followed by another unidentified parameter (column 14), the interaction of Power and EA, and Power and GA. For temperature at 25 mm the highest contribution is from the parameter SR, followed by interaction of parameters Power and EA, GA, the interaction of Power and GA, and two unidentified parameters (column 13 and 10). For temperature at 60 mm, the highest contribution is from parameter SR, followed by interaction of parameters Power and EA, GA, one unidentified parameter (column 13), and the interaction of EA and GA.

Table 6.15. Mean values of S/N index and maximum differences between levels on T at 5 mm.

S/N	EA		GA		AxC		BxC		SR		
	A	B	C		AxC	BxC	D	e	D	e	
1	-30.06	-29.42	-31.85	-30.46	-31.35	-32.96	-31.38	-32.35	-32.79	-31.30	-31.20
2	-31.51	-33.97	-30.77	-32.35	-31.92	-31.52	-33.32	-31.91	-29.68	-31.82	-33.34
3	-34.28	-32.46	-33.23	-33.04	-32.59	-31.37	-31.16	-31.59	-33.38	-32.73	-31.31
diff.	4.22	4.55	2.78	2.76	1.61	2.16	0.75	3.70	2.14	0.59	

Table 6.16. Mean values of S/N index and maximum differences between levels on T at 15 mm.

S/N	EA		GA		AxC		BxC		SR		
	A	B	C		AxC	BxC	D	e	D	e	
1	-30.28	-29.43	-30.15	-29.92	-29.81	-29.96	-30.25	-30.87	-30.97	-29.96	-30.11
2	-29.19	-31.70	-28.90	-30.13	-29.38	-30.86	-32.54	-28.07	-27.95	-29.66	-31.54
3	-31.61	-29.95	-32.03	-31.03	-31.89	-30.26	-28.29	-32.14	-32.16	-31.47	-29.44
diff.	2.42	2.27	3.13	1.67	2.51	4.25	4.08	4.21	2.10	3.77	

Table 6.17. Mean values of S/N index and maximum differences between levels on T at 25 mm.

S/N	EA		GA		AxC		BxC		SR		
	A	B	C		AxC	BxC	D	e	D	e	
1	-33.92	-33.04	-34.88	-34.52	-35.85	-34.80	-34.84	-34.31	-30.65	-33.52	-35.55
2	-33.05	-34.57	-30.59	-34.06	-31.77	-34.50	-34.94	-32.20	-33.45	-33.59	-35.54
3	-35.69	-35.05	-37.19	-34.08	-35.03	-33.37	-32.88	-36.15	-38.56	-35.55	-31.57
diff.	2.64	2.01	6.60	5.66	4.08	2.67	3.95	7.91	3.98	2.65	

Table 6.18. Mean values of S/N index and maximum differences between levels on T at 60 mm.

S/N	P		EA		GA		AxC		BxC		SR		e
	A	B	AxB	C	AxC	BxC	D	e	D	e			
1	-39.81	-40.91	-42.35	-38.53	-40.39	-41.47	-41.25	-40.66	-42.49	-41.15	-39.95	-41.34	
2	-42.78	-41.38	-40.50	-42.60	-41.51	-42.15	-40.26	-41.98	-43.28	-39.79	-43.91	-41.98	
3	-41.51	-41.81	-41.25	-42.96	-42.20	-40.47	-42.59	-41.46	-38.33	-43.15	-40.23	-40.77	
dif.	2.97	0.90	4.43	4.42	1.80	3.36	1.31	4.95	3.96	1.21			

Table 6.19. (a) Analysis of the relative contribution of the parameters on the mean temperature at 5 mm.

Average	P		EA		GA		AxC		BxC		SR		e
	A	B	AxB	C	AxC	BxC	D	e	D	e			
1	651.0	672.6	651.9	655.0	622.9	641.8	623.3	634.5	629.5	674.7	650.8	651.7	643.4
2	651.5	657.2	660.7	654.8	656.9	654.6	665.3	651.4	652.8	661.1	654.3	649.1	645.5
3	652.7	625.5	642.7	645.5	675.5	658.9	666.6	669.4	673.0	619.6	650.3	654.5	666.4
dif.	1.7	47.1	18.1	52.6	43.3	34.9	43.5	55.1	5.5	23.0			

Table 6.19. (b) Analysis of the relative contribution of the parameters on the mean temperature at 15 mm.

Average	P		EA		GA		AxC		BxC		SR		e
	A	B	AxB	C	AxC	BxC	D	e	D	e			
1	911.2	959.4	988.3	949.7	977.4	959.8	947.1	970.8	938.9	977.3	967.4	979.7	980.6
2	998.4	977.0	968.8	1003.9	1012.1	993.9	996.6	958.0	1012.7	995.2	965.3	999.3	958.6
3	1019.6	992.9	972.1	975.6	939.8	975.5	985.6	1000.4	977.7	956.8	996.5	950.2	990.1
dif.	108.4	33.5	54.1	72.3	49.5	42.4	73.8	38.4	49.1	31.4			

Table 6.19. (c) Analysis of the relative contribution of the parameters on the mean temperature at 25 mm.

Average	P		EA		GA		AxC		SR		e	
	A	B	AxB	C	AxC	BxC	D	e				
1	890.5	945.7	974.9	907.9	986.3	953.3	912.0	960.9	925.5	963.4	954.5	948.3
2	974.8	956.5	924.4	978.5	987.1	939.7	981.9	917.7	976.5	973.1	952.7	983.4
3	992.9	956.0	958.9	971.9	884.9	965.2	964.4	979.6	956.3	921.8	985.0	920.3
dif.	102.4	10.8	70.6		102.2	69.9		67.2	51.1	51.3		63.2

Table 6.19. (d) Analysis of the relative contribution of the parameters on the mean temperature at 60 mm.

Average	P		EA		GA		AxC		SR		e	
	A	B	AxB	C	AxC	BxC	D	e				
1	621.3	672.2	706.3	696.8	753.6	650.4	681.5	682.3	674.8	742.5	700.0	676.7
2	716.0	680.1	672.1	690.4	704.5	711.6	693.1	641.0	716.4	671.1	649.6	694.9
3	731.6	716.5	690.4	681.6	610.7	706.9	694.2	745.5	677.6	655.2	724.4	699.8
dif.	110.3	44.4	34.2		142.9	61.2		104.5	41.6	87.2		31.0

The temperature behavior on the fuel bed at 5, 15, 25, and 60 mm is presented here. Table 6.19 (a-d) presents the analysis based only on the mean values of temperature at 5, 15, 25, and 60 mm observed for each parameter.

➤ **Behavior of the fuel bed temperature at 5 mm**

Figure 6.16 shows the evolution of S/N for temperature with the different parameters, for the various levels of analysis at 5 mm. The temperature decreases as Power increases which may result from the accumulation of wood pellets at higher Power. The parameters EA and GA have almost the same behavior, which shows that lower levels yield higher temperatures. This means that at higher EA and GA provided more air into the grate that may reduce the temperature. For SR, the higher temperature was observed at middle SR.

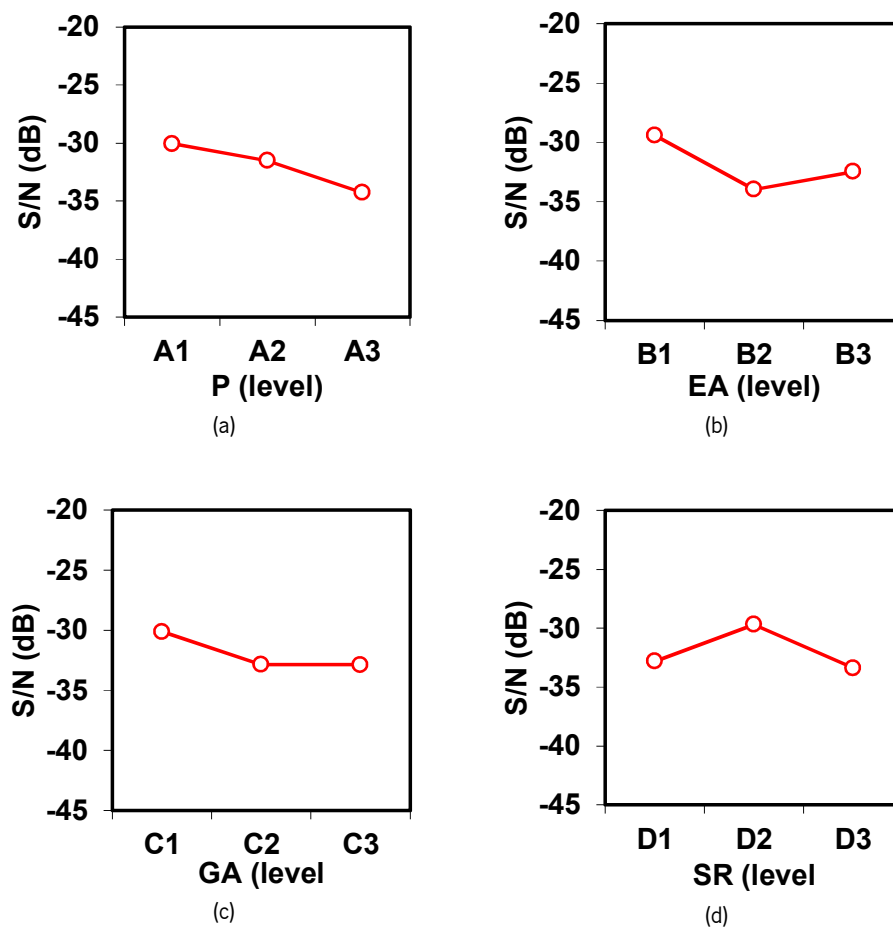


Figure 6.16. Individual influence of factors on the temperature at 5 mm.

Figure 6.17 presents the interaction between all parameters for the temperature at 5 mm. From these graphs, we can identify that there is an important interaction between lower Power and lower EA (Figure 6.17 (a)), and between lower power and lower GA (Figure 6.17 (b)). Based on Figure 6.17 and the value of maximum differences between levels on temperature (Table 6.15), then the best combination to reduce the variance (more stable and best result) is A1-B1-C1-D2.

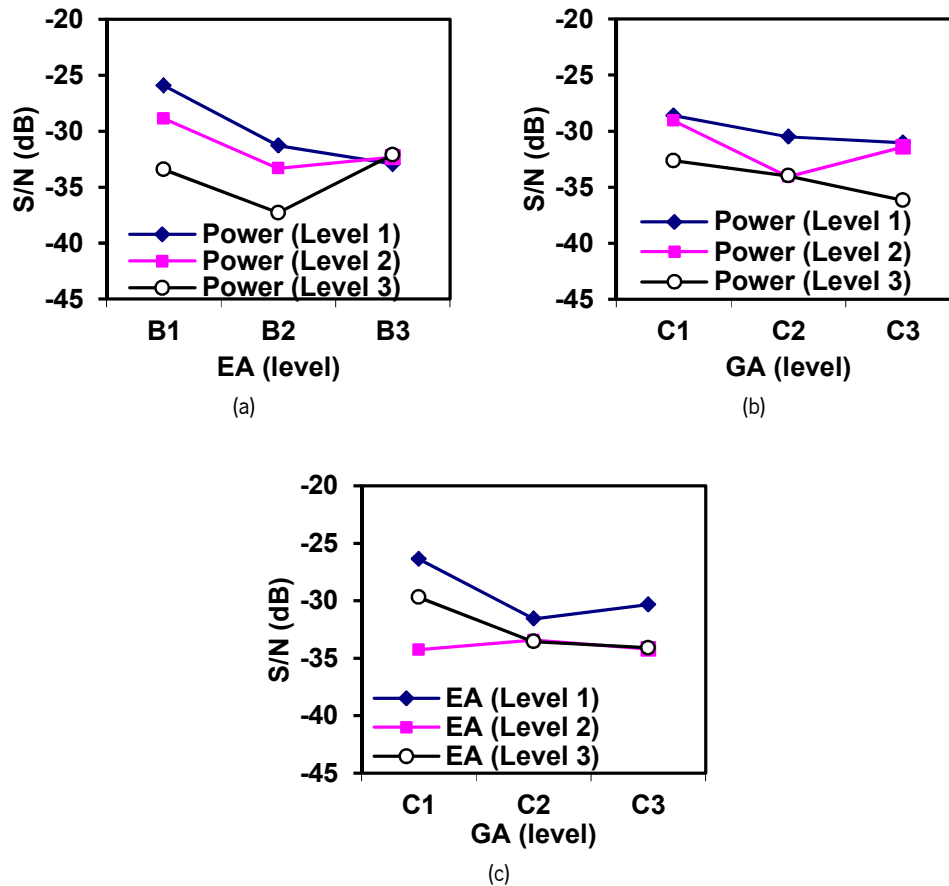


Figure 6.17. Indices of interaction between factors (T at 5 mm).

Table 6.21 presents the statistical calculation of the F critical according to the level of risk α (1%, 5%, and 10%), for the final configuration of Table 6.20.

Table 6.20. ANOVA worksheet for the temperature at 5 mm.

ANOVA	P	EA		GA				SR			Error calculation	
	1	2	3 & 4	5	6 & 7	8 & 11	9	10	12	13	error exp.	Total
	A	B	AxB	C	AxC	BxC	e	D	e	e		
df	2	2	4	2	4	4	2	2	2	2	20	26
sq	82.68	96.86	59.83	45.39	20.76	34.80	2.57	71.08	26.11	1.71	191.17	441.79
var	41.34	48.43	14.96	22.70	5.19	8.70	1.28	35.54	13.06	0.85	9.56	16.99
pool	n	n	s	s	s	s	s	n	s	s	n	
F	4.32	5.07						3.72				
sq'	63.56	77.74						51.96			248.52	441.79
%	14.39	17.60						11.76			56.25	100.00

After applying the analysis of variance, from Table 6.20 it is verified that except for GA, the F value associated to all parameters (Power, EA, and SR) is higher than the critical value for the confidence index (risk $\alpha = 0.05$), calculated for the same number of degrees of freedom ($df = 2$). This means that with a confidence greater than 95%, the Power, EA, and SR contribute to change in temperature at 5 mm about 14%, 18%, and 12% respectively. Table 6.20 allows us to conclude that the main effect parameter is the EA, Power, and SR respectively. The value associated with the experimental error is 56%.

Table 6.21. ANOVA F critic calculation for the temperature at 5 mm.

F critic		
	Degree of freedom	
Nominator	2	4
Denominator	20	20
α		
0.10	2.59	2.25
0.05	3.49	2.87
0.01	5.85	4.43

➤ Behavior of the fuel bed temperature at 15 mm

Figure 6.18 shows the evolution of S/N for temperature with the different parameters, for the various levels of analysis at 15 mm. It presents a similar behavior, where the higher temperature is observed at the middle level, but the opposite occurs for the EA. Meanwhile, the temperature decreases with the increasing of GA.

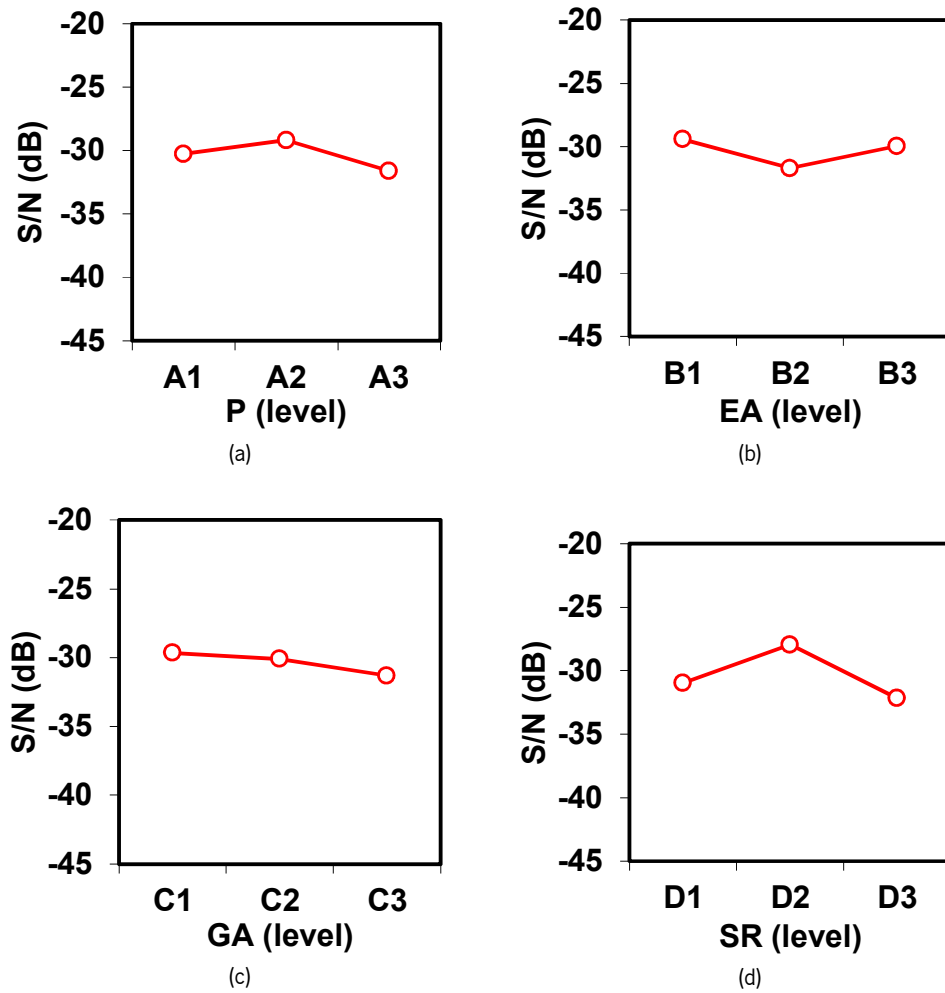


Figure 6.18. Individual influence of factors on the temperature at 15 mm.

Figure 6.19 presents the interaction between all parameters for the temperature at 15 mm. From these graphs, one can identify a strong interaction between middle Power and lower EA (Figure 6.19 (a)), and between middle Power and lower GA (Figure 6.19 (b)). Based on Figure 6.19 and the value of maximum differences between levels on temperature (Table 6.16), the best combination to reduce the variance is A2-B1-C1-D2.

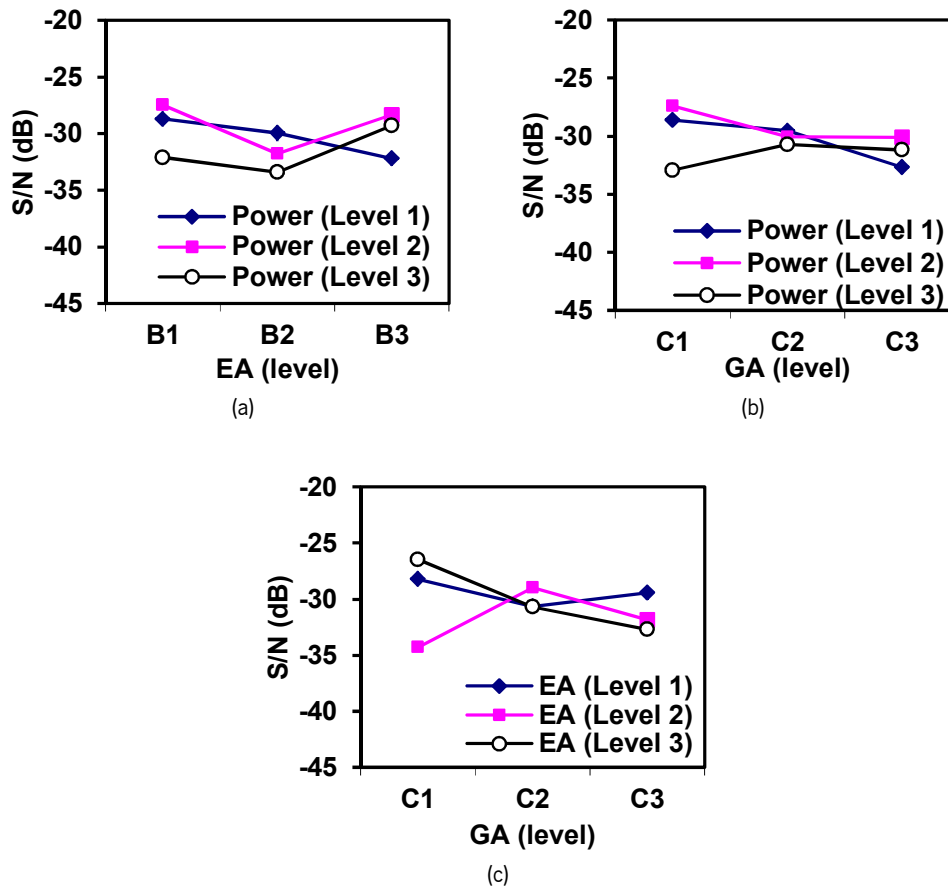


Figure 6.19. Indices of interaction between factors (T at 15 mm).

Table 6.23 presents the statistical calculation of the F critical according to the level of risk α (1%, 5%, and 10%), for the final configuration of Table 6.22.

Table 6.22. ANOVA worksheet for the temperature at 15 mm.

ANOVA	P	EA		GA			SR				Error calculation	
	1	2	3 & 4	5	6 & 7	8 & 11	9	10	12	13	error exp.	Total
	A	B	AxB	C	AxC	BxC	e	D	e	e		
df	2	2	4	2	4	4	2	2	2	2	26	26
sq	26.46	25.55	50.77	13.48	36.10	98.48	78.36	84.93	20.69	65.89	500.69	500.69
var	13.23	12.77	12.69	6.74	9.02	24.62	39.18	42.47	10.35	32.94	19.26	19.26
pool	s	s	s	s	s	s	s	s	s	s	n	
F												
sq'											500.69	500.69
%											100.00	100.00

After applying the analysis of variance, from Table 6.22 it is verified that there is no significant influence of the parameters observed on the temperature at 15 mm, for $\alpha=0.05$.

Table 6.23. ANOVA F critic calculation for the temperature at 15 mm.

F critic		
	Degree of freedom	
Nominator	2	4
Denominator	26	26
α		
0.10	2.52	2.17
0.05	3.37	2.74
0.01	5.53	4.14

➤ Behavior of the fuel bed temperature at 25 mm

Figure 6.20 presents the evolution of S/N for temperature with the different parameters, for the various levels of analysis at 25 mm. It shows that the higher temperature is observed at middle Power. For parameters, EA, GA, and SR, the temperature tends to decrease with the increasing of the parameters observed, but the SR has the most significant influence.

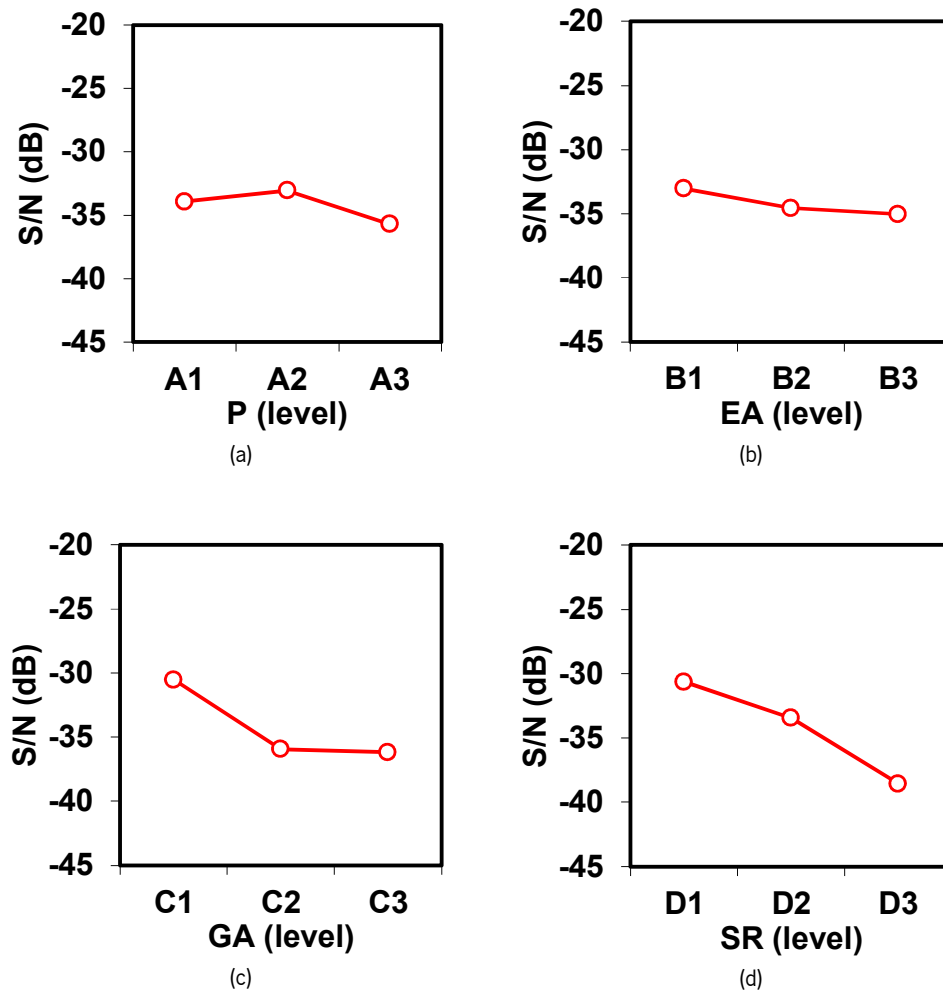


Figure 6.20. Individual influence of factors on the temperature at 25 mm.

Figure 6.21 presents the interaction between all parameters for the temperature at 25 mm. From these graphs, we can identify that there is an important interaction between middle Power and lower EA (Figure 6.21 (a)), and between middle Power and lower GA (Figure 6.21 (b)). Based on Figure 6.21 and the value of maximum differences between levels on temperature (Table 6.17), the best combination to reduce the variance is A2-B1-C1-D1.

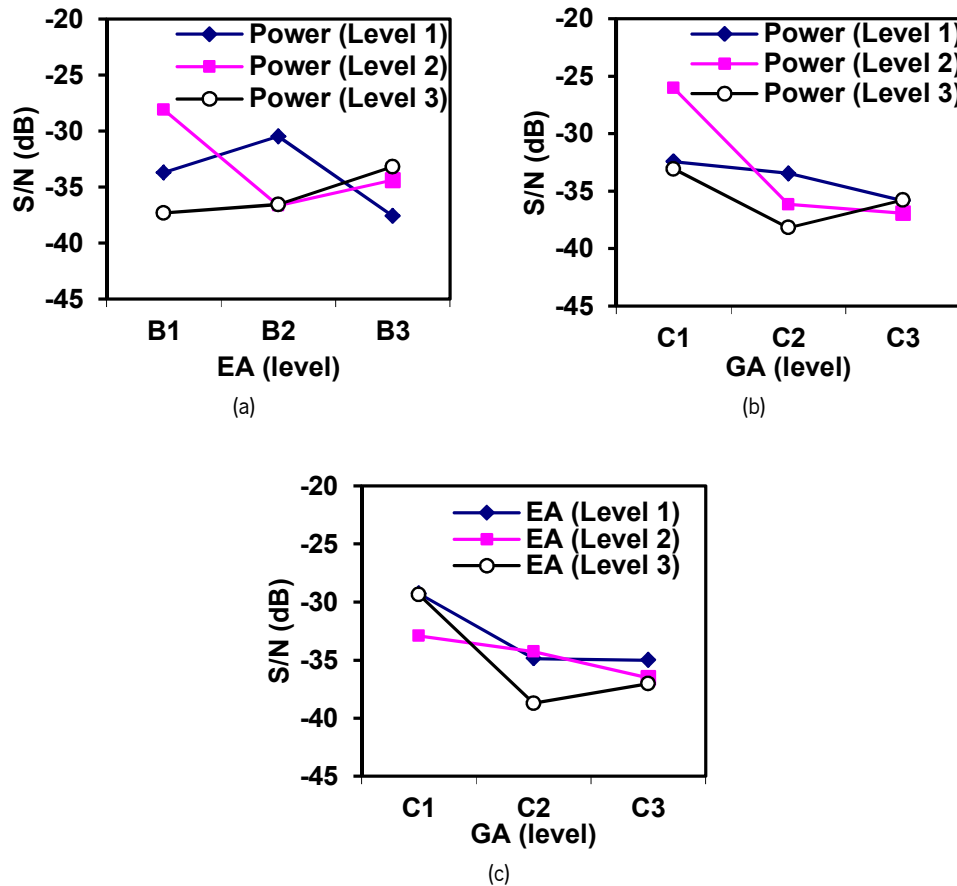


Figure 6.21. Indices of interaction between factors (T at 25 mm).

Table 6.25 presents the statistical calculation of the F critical according to the level of risk α (1%, 5%, and 10%), for the final configuration of Table 6.24.

Table 6.24. ANOVA worksheet for the temperature at 25 mm.

ANOVA	P	EA		GA				SR			Error calculation	
	1	2	3 & 4	5	6 & 7	8 & 11	9	10	12	13	error exp.	Total
	A	B	AxB	C	AxC	BxC	e	D	e	e		
df	2	2	4	2	4	4	2	2	2	2	24	26
sq	32.70	19.80	202.88	184.40	94.17	48.08	70.46	289.84	94.74	34.30	781.51	1071.35
var	16.35	9.90	50.72	92.20	23.54	12.02	35.23	144.92	47.37	17.15	32.56	41.21
pool	s	s	s	s	s	s	s	n	s	s	n	
F								4.45				
sq'								224.71			846.64	1071.35
%								20.97			79.03	100.00

After applying the analysis of variance, from Table 6.24 it is verified that the F value associated to parameter D (SR), is higher than the critical value for the higher confidence index (risk $\alpha = 0.05$), calculated for the same number of degrees of freedom ($df = 2$). This means that, with a confidence index greater than 95%, it can be stated that the SR intensity contributes about 21% for the temperature variation at 25 mm. Table 6.24 allows us to conclude that the main effect parameter is the SR. The value associated with the experimental error is 79%.

Table 6.25. ANOVA F critic calculation for the temperature at 25 mm.

F critic		
	Degree of freedom	
Nominator	2	4
Denominator	24	24
α		
0.10	2.54	2.19
0.05	3.40	2.78
0.01	5.61	4.22

➤ Behavior of the fuel bed temperature at 60 mm

Figure 6.22 shows the evolution of S/N for temperature with the different parameters, for the various levels of analysis at 60 mm. It shows that a higher temperature is observed at a lower Power. The temperature decreases with the increasing of EA. The GA and SR have the same behavior, where the temperature increases with the increasing of those parameters.

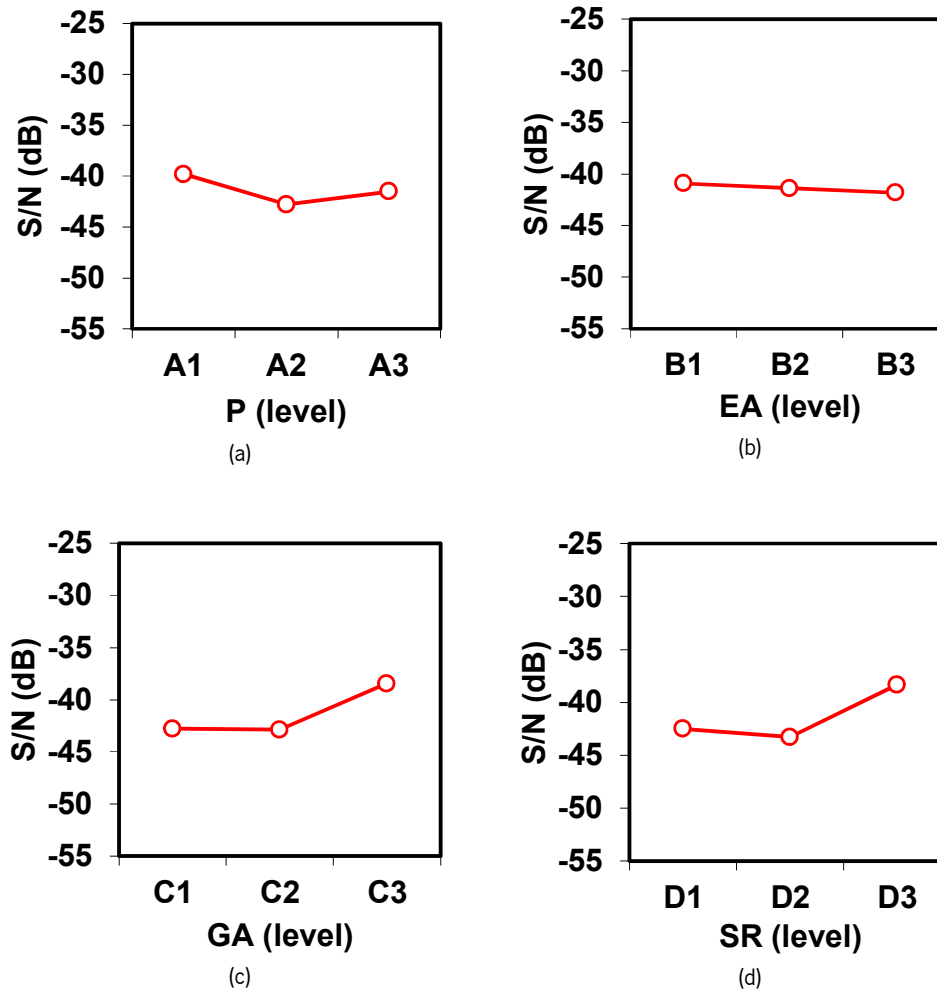


Figure 6.22. Individual influence of factors on the temperature at 60 mm.

Figure 6.23 presents the interaction between all parameters for the temperature at 60 mm. From these graphs, we can identify that there is an important interaction between lower Power and lower EA (Figure 6.23 (a)), and between lower Power and higher GA (Figure 6.23 (b)). Based on Figure 6.23 and the value of maximum differences between levels on temperature (Table 6.18), the best combination to reduce the variance is A1-B1-C3-D3.

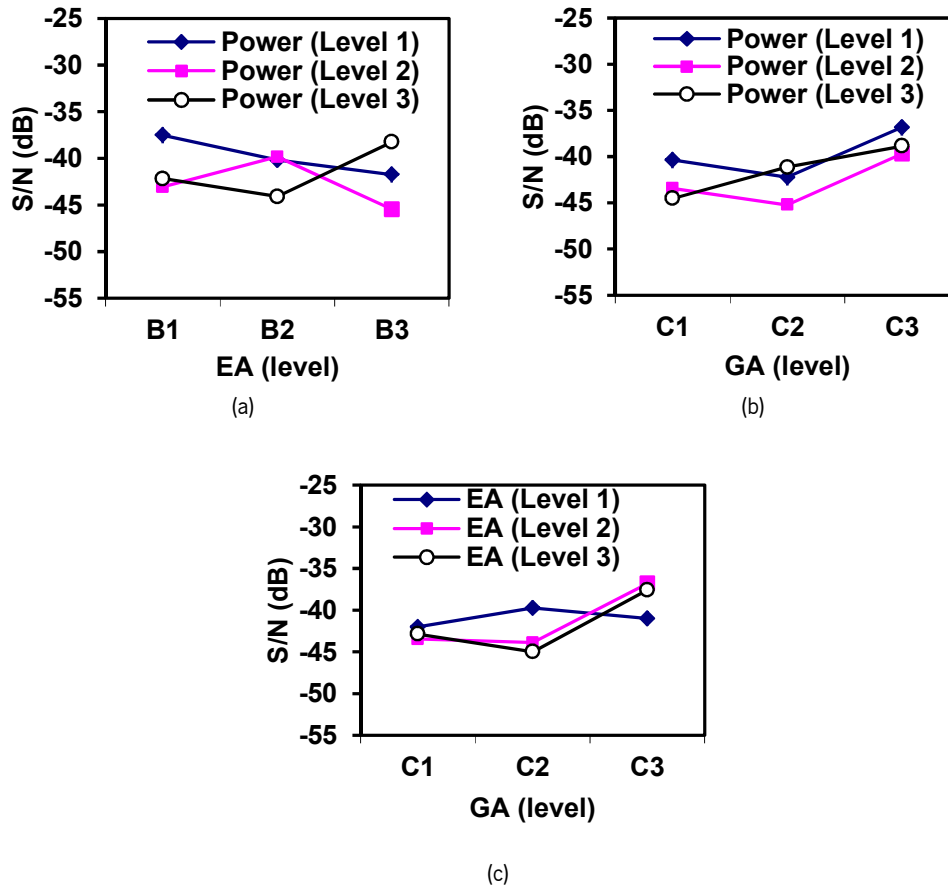


Figure 6.23. Indices of interaction between factors (T at 60 mm).

Table 6.27 presents the statistical calculation of the F critical according to the level of risk α (1%, 5%, and 10%), for the final configuration of Table 6.26.

Table 6.26. ANOVA worksheet for the temperature at 60 mm.

ANOVA	P	EA		GA				SR			Error calculation	
	1	2	3 & 4	5	6 & 7	8 & 11	9	10	12	13	error exp.	Total
	A	B	AxB	C	AxC	BxC	e	D	e	e		
df	2	2	4	2	4	4	2	2	2	2	10	26
sq	40.03	3.61	124.45	114.92	27.68	75.84	7.85	127.37	87.84	6.60	45.75	616.20
var	20.02	1.80	31.11	57.46	6.92	18.96	3.93	63.68	43.92	3.30	4.57	23.70
pool	n	s	n	n	s	n	s	n	n	s	n	
F	4.38		6.80	12.56		4.14		13.92	9.60			
sq'	30.88		106.15	105.77		57.54		118.22	78.69		118.95	616.20
%	5.01		17.23	17.16		9.34		19.18	12.77		19.30	100.00

After applying the analysis of variance, from Table 6.26 it is verified that the F value associated to the parameters GA, SR, and one unidentified parameter (column 10) is higher than the critical value for the higher confidence index (risk $\alpha = 0.01$), and F value is above the critical value for the confidence index

(risk $\alpha = 0.05$) to Power, the interaction of Power and EA, and interaction of EA and GA, calculated for the same number of degrees of freedom ($df = 2$). This means that, with a confidence greater than 99%, the GA, SR, and one unidentified parameter (column 10) contribute to change in temperature at 60 mm about 17%, 19%, and 13% respectively. For the Power, the interaction of Power and EA, and interaction of EA and GA, with a confidence greater than 95% it contributes about 5%, 17%, and 9% respectively. Meanwhile, the value associated with the experimental error is 19%.

Table 6.27. ANOVA F critic calculation for the temperature at 60 mm.

F critic		
	Degree of freedom	
Nominator	2	4
Denominator	10	10
α		
0.10	2.92	2.61
0.05	4.10	3.48
0.01	7.56	5.99

From the best combination of the parameters influencing CO and temperature, one can identify that the only parameter that gives the lowest variance at the same level is the EA, which is at the first level (B1). Considering that the most important temperature is the one in the core of the fuel bed (at 15 and 25 mm), the best combination to reduce variance is A2-B1-C1 which gives the best result for 15 and 25 mm. In addition, the D parameter (SR) should be at level 2 (D2) for $h = 15$ mm and level 1 (D1) for $h = 25$ mm. From the description above the best combination for CO is the same that reduces the variance of temperature at 25 mm height in the core of fuel and is representative of the whole burning process of wood pellets in this boiler.

The parameters that influence the mean value can be different from those who influence the variance, and the Taguchi method helps to identify those parameters. The parameters that may change the mean value of temperature at a different height (see Table 6.19) include: at 5 mm is SR and GA ($\Delta T = 55.1$ °C and 52.6 °C); at 15 mm is Power ($\Delta T = 108.4$ °C); at 25 mm is Power and GA ($\Delta T = 102$ °C) and at 60 mm is GA and Power ($\Delta T = 142.9$ °C and 110.3 °C). Other parameters that could influence but were not identified (indicated by the high value of error) might be pellets specification and volume of the combustion chamber.

Table 6.28 presents the overall influences of the parameters applied in this study on the temperature at a different height. The data show that the most influencing parameter on the temperature at different height is the SR which is contributing to about 12%, 21%, and 19% at 5, 25, and 60 mm respectively.

The second parameter influencing the temperature is Power, which contributes approximately 14% and 5% at 5 and 60 mm.

Table 6.28. The overall influences of the parameters on fuel bed temperature.

Height (mm)	P	EA		GA				SR		
	1	2	3 & 4	5	6 & 7	8 & 11	9	10	12	13
	A	B	AxB	C	AxC	BxC	e	D	e	e
5	14.39%	17.60%						11.76%		
15										
25								20.97%		
60	5.01%		17.23%	17.16%		9.34%		19.18%	12.77%	

➤ **The results based on the best combination parameters according to ANOVA analysis.**

Regarding the ANOVA analysis, it was concluded that the best combination parameters for CO and the temperature in the core of the fuel bed (referred to 25 mm) have the same combination parameters. The results of this test are presented in Figure 6.24 and the mean value of CO and temperature are presented in Table 6.29. Figure 6.24 shows that the test run for less than 4,500 s has a consequence of the fuel bed rising which was followed by the high concentration of CO. Thus the results show this is not a stable condition. This may be caused by the high error from the experiments and also by unidentified parameters which were not considered in the tests such as the size of the combustion chamber and type of biomass fuel. The combustion chamber size may influence on the heat radiation and convection from the wall. Ahn and Jang (2018) stated that an increase in the aspect ratio of the combustion chamber contributes to complete combustion. While the different heating value of the biomass fuel may influence the behavior of the combustion including the temperature, particle, and tar as revealed by Buchmayr *et al.* (2015), Mediavilla *et al.* (2009). According to Buchmayr *et al.* (2015), the heating value of the volatiles leaving the fuel bed is strongly dependent on fuel moisture and primary air ratio. If temperature and particle are increasing with the primary air ratio and for biomass with low fuel moisture, then a high heating value product is generated.

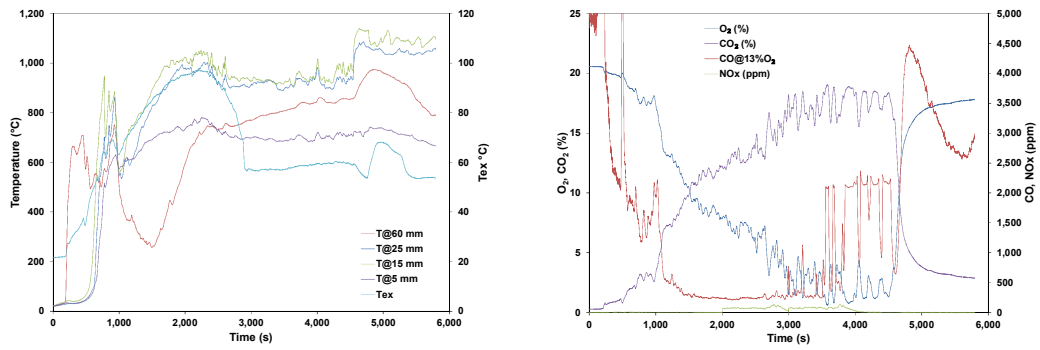


Figure 6.24. Temperature and emissions profiles for A2-B1-C1-D1.

Table 6.29. Mean value and variance of the best combination parameters (A2-B1-C1-D1).

	CO (ppm)	Temperature (°C)			
		5 mm	15 mm	25 mm	60 mm
Mean value	237	699	939	916	800
Variance	152	101	353	251	1,390

7. CLOSURE

7.1 Conclusions

This chapter presents the main conclusions that can be drawn from the work developed over the course of this project including the: mass loss and kinetic analysis using TGA techniques; mass loss and elemental analysis in a small scale reactor; emissions and temperature measurement in a fixed bed combustor.

- The combustion experiments were carried out in a purpose built boiler with the capability to control the fuel rate and primary/secondary air split.
- A small reactor was developed and an experimental procedure devised to investigate the devolatilization process of pine wood pellets under controllable conditions.
- TGA analysis shows that the thermal decomposition for all the particle sizes examined, starts at a higher temperature for low heating rates and the opposite was obtained at a higher heating rate. The maximum combustion rate increase with the particle size and the heating rate, but the heating rate has a stronger influence. The heat flow also increases with the heating rate. In addition, at a higher heating rate (243 °C/min), the combustion took place in a very short time. The results also revealed that there is no significant influence of air flow rate. The ignition and burnout temperatures, ignition and combustion indexes increase with the heating rate.
- The activation energy decreases with increasing heating rate, and the highest reactivity is observed at higher heating rates. There is no significant influence of the air flow rate on the kinetic parameters of wood particles combustion. The middle and small size particles have higher reactivity which increases with the heating rate.
- The mass losses increase for any specific temperature and the higher the temperature, the faster the pellets volatilize. Devolatilization occurs at a very slow rate for low temperatures. The maximum mass loss obtained at the highest temperature (650 and 734 °C), for 1 hour test, leveled off at about 97% with the remaining substances include fixed carbon and ashes being about 3%. Mass loss of dry pellets increases with the temperature and at a higher temperature, the dry pellets devolatilize faster than wet pellets.
- The elemental results show that the volatile matter is released in the early stages while the ratio of fixed carbon and ash steadily increases. The rate of conversion for the volatile is similar for all compounds, though Nitrogen shows a higher rate of conversion. The mass of fixed carbon

increases due to the Carbon diffusion from the volatile fraction. The decomposition of these compounds is dependent on the temperature and residence time applied.

- The total Carbon decreases with time as it is being oxidized and the species concentration in the sample is expected to increase in concentration if their rate of volatilization is lower than others. The results for dry pellets show that the mass of H and O always decrease which indicates that in the drying phase some of the O and H is transferred from the water to the biomass structure. In addition, the decomposition of biomass is related to hemicellulose, cellulose and lignin, which starts at different temperatures and stages.
- The lowest CO emission obtained in this study measured before the fuel bed rising, was 109 ppm with thermal efficiency of 91.57%. From the Taguchi plan of experiments, the split ratio (SR) contributes 21.45% to CO reduction, followed by power with 14.59%. The data show that the medium power (13 kW) has the highest efficiency or lowest CO emissions than at both lower (10 kW) and higher power (16 kW). The EA, GA, and SR have the same tendency on the efficiency and CO emissions, where at a lower and middle value of those parameters has higher efficiency. The parameter that gives the lowest variance at the same level is the EA at the first level or a lower EA.
- The temperature magnitude in fuel bed on the average values indicated that the highest temperature was observed at 15 mm followed by 25, 5 and 60 mm in height. The most important parameter contributing to the fuel bed temperature is the SR and Power.
- This study revealed that the ashes agglomerations were influenced by the duration of the combustion and the temperature of the fuel bed. The largest size of the ashes agglomeration was referred to TN26 (16 kW, EA 110%, and SR 30/70) which is 59 mm and the duration time is 14,400 s (\approx 4 h).
- The instability during the combustion occurs since the fuel bed rising as the accumulation of the unburned wood pellets on the grate caused the slow combustion rate and pressure drop, which creates noise and disturbances. Instability creates poor combustion resulting in a rise of CO and possible condensation in the boiler.

7.2 Future work

The development of the present work opened a few lines of opportunities that are worth pursuing in the near future. In brief:

- The results show that the influence of the grate size is not yet properly addressed and other sizes (and, possibly, different configurations) could be investigated.
- The size of the combustion chamber is a variable that, based on the ANOVA analysis, appears to be of the utmost relevance. One possible development would be the investigation of the influence of the combustion chamber size on the performance of the boiler.
- The analysis of mass loss and devolatilization of pellets can be applied to other materials (such as waste biomass from agriculture or forestry) or commercial fuels such as wood chips.
- The data presented in this thesis refers to air as the ambient atmosphere. It would be worth investigating the use of an inert atmosphere in order to analyze separately the influence of temperature.
- The data regarding the mass loss and devolatilization of pellets could be extended and correlated with time and temperature in order to build sub models as a gas phase input to be used in the CFD modeling of boilers.

REFERENCES

- ABA Japan (2002), "Asian Biomass Handbook Part 2. Biomass resources", In Asian Biomass Handbook, pp. 12–80.
- Aboulkas, A. and Harfi, K.El (2008), "Study of the kinetics and mechanisms of thermal decomposition of Moroccan Tarfaya oil shale and its kerogen", *Oil Shale*, vol. 25, pp. 426–443.
- Adams, D. (2013), "Sustainability of biomass for co-firing, IEA Clean Coal Centre", Available at: <http://www.iea-coal.org.uk/documents/83254/8869/Sustainability-of-biomass-for-cofiring,-CCC/230>.
- ADInstruments, "Gas Analyzer Owner's Guide", Available at: http://cdn.adinstruments.com/adi-web/manuals/Gas_Analyzer_ML206_OG.pdf.
- Ahn, J. and Jang, J.H. (2018), "Combustion characteristics of a 16 step grate-firing wood pellet boiler", *Renewable Energy*, vol. 129, pp. 678–685.
- Alakoski, E.; Jämsén, M.; Agar, D.; Tampio, E. and Wihersaari, M. (2016), "From Wood Pellets to Wood Chips, Risks of Degradation and Emissions from the Storage of Woody Biomass - A Short Review," *Renewable and Sustainable Energy Reviews*, vol. 54, pp. 376–383.
- AN107, A., "Practical Thermocouple Temperature Measurements", p. 8. Available at: <http://www.dataforth.com/catalog/pdf/an107.pdf>.
- Arranz, J.I.; Miranda, M.T.; Montero, I.; Sepúlveda, F.J. and Rojas, C.V. (2015), "Characterization and combustion behaviour of commercial and experimental wood pellets in South West Europe", *Fuel*, vol. 142, pp. 199–207.
- Arshanitsa, A.; Akishin, Y.; Zile, E.; Dizhbite, T.; Solodovnik, V. and Telysheva, G. (2016), "Microwave treatment combined with conventional heating of plant biomass pellets in a rotated reactor as a high rate process for solid biofuel manufacture", *Renewable Energy*, vol. 91, pp. 386–396.
- ASME (1998), "Test Uncertainty", p. 112. Available at: <https://www.asme.org/products/codes-standards/ptc-191-1998-test-uncertainty>.
- Babu, J.; Dutta, A. and Kumaraswamy, A. (2014), "Experimental Studies on Effect of Temperature and Strain Rate on Deformation Behaviour of Ti-6Al-4V using Taguchi Method", vol. 6, pp. 1121–1130.
- Barrette, J.; Thiffault, E.; Achim, A.; Junginger, M.; Pothier, D. and Grandpré, L. (2017), "A financial analysis of the potential of dead trees from the boreal forest of eastern Canada to serve as feedstock for wood pellet export. *Applied Energy*", vol. 198, pp. 410–425.
- Bioenergy Europe (2018), "International trade fair for innovative energy supply".
- Bishop, G.N. (2001), "Native tree of Georgia", Georgia Forestry Commission, p. 98.

- Bjerg, J.; Aden, R.; Ogand, J.A.; Arrieta, J.A.; Hahlbrock, A.; Holmquist, L.; Kellberg, C.; Klip, W.N; Koch, J.; Langnickel, U.; Nielsen, C.; Rising, A.; Rizkova, M.; Rookmaaker, J.; Ryckmans, Y.; Ryymin, R.; Shier, C.; Sochr, D.; Tatar, T. and Tolley, A. (2011), "Biomass 2020: Opportunities, Challenges and Solutions", p. 72.
- Boman, C. (2005), "Particulate and gaseous emissions from residential biomass combustion", Umea Universitet.
- Boriouchkine, A.; Sharifi, V.; Swithenbank, J. and Jämsä-Jounela, S.L. (2014), "A study on the dynamic combustion behavior of a biomass fuel bed", *Fuel*, vol. 135, pp. 468–481.
- Borman, L.G. and Ragland, W.K. (1998), "Combustion engineering", McGraw-Hill, international edition.
- Bu, C.; Leckner, B.; Chen, X.; Pallarès, D.; Liu, D.; Gómez-Barea, A.; Liu, D. and Pallarès, D. (2015), "Devolatilization of a single fuel particle in a fluidized bed under oxy-combustion conditions. Part A: Experimental results", *Combustion and Flame*, vol. 162, pp. 797–808.
- Buchmayr, M.; Gruber, J.; Hargassner, M. and Hochenauer, C. (2015), "Experimental investigation of the primary combustion zone during staged combustion of wood-chips in a commercial small-scale boiler", *Biomass and Bioenergy*, vol. 81, pp. 356–363.
- Burhenne, L.; Messmer, J.; Aicher, T. and Laborie, M.P. (2013), "The effect of the biomass components lignin, cellulose and hemicellulose on TGA and fixed bed pyrolysis", *Journal of Analytical and Applied Pyrolysis*, vol. 101, pp.177–184.
- Burkhard, E. and Russell, N. (2010), "European Wood-Heating Technology Survey: An Overview of Combustion Principles and The Energy And Emissions Performance Characteristics Of Commercyally Available Systems In Austria, Germeny, Denmark, Norway. And Sweden".
- Calvo, A.I.; Tarelho, L.A.C.; Alves, C.A.; Duarte, M. and Nunes, T. (2014), "Characterization of operating conditions of two residential wood combustion appliances", *Fuel Processing Technology*, vol. 126, pp. 222–232.
- Cengel, A.Y and Cimbala, J. (2006), "Fluid mechanics: fundamentals and applications", McGraw Hill, 1st edition.
- Cengel, A.Y. (2002), "Heat Transfer a Practical Approach", McGraw-Hill, 2nd edition.
- Chum, H.L. and Overend, R.P. (2001), "Biomass and renewable fuels", *Fuel Processing Technology*, vol. 71, pp. 187–195.
- Ciferno, J.P. and Marano, J.J. (2002), "Benchmarking biomass gasification technologies for fuels, chemicals and hydrogen production", US Department of Energy, National Energy, p. 58.

- Daouk, E.; Van de Steene, L.; Paviet, F.; Martin, E.; Valette, J. and Salvador, S. (2017), "Oxidative pyrolysis of wood chips and of wood pellets in a downdraft continuous fixed bed reactor", *Fuel*, vol. 196, pp. 408–418.
- Daouk, E.; Van de Steene, L.; Paviet, F. and Salvador, S. (2015), "Thick wood particle pyrolysis in an oxidative atmosphere", *Chemical Engineering Science*, vol. 126, pp. 608–615.
- Demirbas, M.F.; Balat, M. and Balat, H. (2009), "Potential contribution of biomass to the sustainable energy development", *Energy Conversion and Management*, vol. 50, pp. 1746–1760.
- Dhyani, V.; Kumar Awasthi, M.; Wang, Q.; Kumar, J.; Ren, X.; Zhao, J.; Chen, H.; Wang, M.; Bhaskar, T. and Zhang, Z. (2018), "Effect of composting on the thermal decomposition behavior and kinetic parameters of pig manure-derived solid waste", *Bioresource Technology*, vol. 252, pp. 59–65.
- Dibdiakova, J.; Wang, L. and Li, H. (2015), "Characterization of Ashes from *Pinus Sylvestris* forest Biomass", *Energy Procedia*, vol. 75, pp. 186–191.
- Dinu, R. (2006), "Wood pellets combustion with rich and diluted air in HTAC furnace", The Royal Institute of Technology, Stockholm.
- Döring, S. (2013), "Power from pellets: Technology and applications", Springer, p. 223.
- Ebrahimi-Kahrizsangi, R. and Abbasi, M.H. (2008), "Evaluation of reliability of Coats-Redfern method for kinetic analysis of non-isothermal TGA", *Transactions of Nonferrous Metals Society of China*, vol. 18, pp. 217–221.
- Ehrig, R. and Behrendt, F. (2013), "Co-firing of imported wood pellets - An option to efficiently save CO₂ emissions in Europe?", *Energy Policy*, vol. 59, pp. 283–300.
- Euh, S.H.; Kafle, S.; Choi, Y.S.; Oh, J.H. and Kim, D.H. (2016), "A Study on the Effect of Tar Fouled on Thermal Efficiency of a Wood Pellet Boiler: A Performance Analysis and Simulation Using Computation Fluid Dynamics," *Energy*, vol. 103, pp. 305–312.
- European Pellet Council, 2015. ENplus Quality Certification Scheme Part 3: Pellet Quality Requirements. EN plus Handbook (UK Pellet Council-Handbook), (August), p.10. Available at: <https://www.enplus-pellets.eu/en-in/resources-en-in/technical-documentation-en-in.html#handbook>.
- Faaij, A.; Schlamadinger, B.; Solantausta, Y. and Wagener, M. (2002), "Large Scale International Bio-Energy Trade", *Proceed. 12th European Conf. and Technology Exhibition on Biomass for Energy, Industry and Climate Change Protection, Amsterdam*, 17–21 June.

- Fachinger, F.; Drewnick, F.; Gieré, R. and Borrmann, S. (2017), "How the user can influence particulate emissions from residential wood and pellet stoves: Emission factors for different fuels and burning conditions", *Atmospheric Environment*, vol. 158, pp. 216–226.
- Fang, X. and Jia, L. (2012), "Experimental study on ash fusion characteristics of biomass", *Bioresource Technology*, vol. 104, pp. 769–774.
- Fernandes, U.; Guerrero, M.; Millera, Á.; Bilbao, R.; Alzueta, M.U. and Costa, M. (2013), "Oxidation behavior of particulate matter sampled from the combustion zone of a domestic pellet-fired boiler", *Fuel Processing Technology*, vol. 116, pp. 201–208.
- Ferreira, M.E.C. (2008), "Atomização Efervescente na Combustão de Óleos Usados", PhD Thesis, University of Minho.
- Ferreira, P. (2016), "Combustion of alternative biomass fuels in a domestic boiler and in a large-scale furnace", PhD Thesis, University of Minho.
- Ferreira, P.T.; Ferreira, M.E.C. and Teixeira, J.C.F. (2014), "Analysis of Industrial Waste in Wood Pellets and Co-combustion Products", *Waste and Biomass Valorization*, vol. 5, pp. 637–650.
- Ferreira, S.; Monteiro, E.; Brito, P. and Vilarinho, C. (2017), "Biomass resources in Portugal: Current status and prospects", *Renewable and Sustainable Energy Reviews*, vol. 78, pp. 1221–1235.
- Flagan, R.C. and Seinfeld, J.H. (1988), "Fundamentals of Air Pollution Engineering", Prentice Hall.
- Gao, H.B.; Qu, Z.G.; He, Y.L. and Tao, W.Q. (2012), "Experimental study of combustion in a double-layer burner packed with alumina pellets of different diameters", *Applied Energy*, vol. 100, pp. 295–302.
- Garcia-Maraver, A.; Perez-Jimenez, J.A.; Serrano-Bernardo, F. and Zamorano, M. (2015), "Determination and comparison of combustion kinetics parameters of agricultural biomass from olive trees", *Renewable Energy*, vol. 83, pp. 897–904.
- Garcia-Maraver, A.; Rodriguez, M.L.; Serrano-Bernardo, F.; Diaz, L.F. and Zamorano, M. (2015), "Factors affecting the quality of pellets made from residual biomass of olive trees", *Fuel Processing Technology*, vol. 129, pp. 1–7.
- Garcia-Maraver, A.; Zamorano, M.; Fernandes, U.; Rabaçal, M. and Costa, M. (2014), "Relationship between fuel quality and gaseous and particulate matter emissions in a domestic pellet-fired boiler", *Fuel*, vol. 119, pp. 141–152.
- Ghodke, P. and Mandapati, R.N. (2019), "Investigation of particle level kinetic modeling for babul wood pyrolysis", *Fuel*, vol. 236, pp. 1008–1017.

- Di Giacomo, G. and Taglieri, L. (2009), "Renewable energy benefits with conversion of woody residues to pellets. *Energy*", vol. 34, pp. 724–731.
- Gómez, M.A.; Porteiro, J.; Cuesta, D.; Patiño, D. and Míguez, J.L. (2016), "Numerical simulation of the combustion process of a pellet-drop-feed boiler", *Fuel*, vol. 184, pp. 987–999.
- Gómez, M.A.; Porteiro, J.; Patiño, D. and Míguez, J.L. (2014), "CFD modelling of thermal conversion and packed bed compaction in biomass combustion", *Fuel*, vol. 117, pp. 716–732.
- Gómez, M.A.; Porteiro, J.; Patiño, D. and Míguez, J.L. (2015), "Fast-solving thermally thick model of biomass particles embedded in a CFD code for the simulation of fixed-bed burners", *Energy Conversion and Management*, vol. 105, pp. 30–44.
- González, J.F.; Ledesma, B.; Alkassir, A. and González, J. (2011), "Study of the Influence of the Composition of Several Biomass Pellets on the Drying Process," *Biomass and Bioenergy*, vol. 35, pp. 4399–4406.
- Granada, E.; Eguía, P.; Comesaña, J.A.; Patiño, D.; Porteiro, J. and Miguez, J.L. (2013), "Devolatilization behaviour and pyrolysis kinetic modelling of Spanish biomass fuels", *Journal of Thermal Analysis and Calorimetry*, vol. 113, pp. 569–578.
- Guo, F. and Zhong, Z. (2018), "Optimization of the co-combustion of coal and composite biomass pellets", *Journal of Cleaner Production*, vol. 185, pp. 399–407.
- Hall, D.O. and Rao, K.K. (1999), "Photosynthesis", *Studies in Biology*, Cambridge University Press, 6th edition.
- Han, J.; Kim, H.; Minami, W.; Shimizu, T. and Wang, G. (2008), "The effect of the particle size of alumina sand on the combustion and emission behavior of cedar pellets in a fluidized bed combustor", *Bioresource Technology*, vol. 99, pp. 3782–3786.
- Hansen, M.T.; Jein, A.R.; Hayes, S. and Bateman, P. (2009), "English Handbook for Wood Pellet Combustion", *Pelletsatlas*, p. 86.
- Harun, N.Y.; Afzal, M.T. and Shamsudin, N. (2009), "Reactivity Studies of Sludge and Biomass Combustion", *International Journal of Engineering*, vol. 3, pp. 413–425.
- Haslinger, W.; Padinger, R.; Wörgetter, M. and Spitzer, J. (2004), "Austrian research and development of novel solid biofuels and innovative small-scale biomass combustion systems", 2nd World Conference and Exhibition on Biomass for Energy, Industry and Cl.
- Hoekstra, E.; Van Swaij, W.P.M.; Kersten, S.R.A. and Hogendoorn, K.J.A. (2012), "Fast pyrolysis in a novel wire-mesh reactor: Decomposition of pine wood and model compounds", *Chemical Engineering Journal*, vol. 187, pp. 172–184.

- Hoogwijk, M. and Graus, W. (2008), "Global potential of renewable energy sources: A Literature assessment", EcoFys, p. 45.
- Jenkins, D. (2010), "Wood Pellet Heating Systems", The Earthscan Expert Handbook for Planning, Design and Installation, Earthscan, p. 126.
- Klason, T. and Bai, X.S. (2007), "Computational study of the combustion process and NO formation in a small-scale wood pellet furnace", *Fuel*, vol. 86, pp. 1465–1474.
- Kluska, J.; Ronewicz, K. and Kardaś, D. (2019), "Characteristics of single wood particle pyrolysis using particle image velocimetry", *International Journal of Thermal Sciences*, vol. 135, pp. 276–284.
- Kok, M.V. and Özgür, E. (2013), "Thermal analysis and kinetics of biomass samples", *Fuel Processing Technology*, vol. 106, pp. 739–743.
- Kokko, A. (2012), "Bio Coal Market Perspectives in Europe", Pöyry.
- Kraiem, N.; Lajili, M.; Limousy, L.; Said, R. and Jeguirim, M. (2016), "Energy recovery from Tunisian agri-food wastes: Evaluation of combustion performance and emissions characteristics of green pellets prepared from tomato residues and grape marc", *Energy*, vol. 107, pp. 409–418.
- Kruggel-Emden, H. and S. Wirtz, V.S. (2013), "An experimental investigation of mixing of wood pellets on a forward acting grate in discontinuous operation", *Chemical Engineering Science*, vol. 233, pp. 261–277.
- Kumar, A.; Gupta, P. and Kumar, R. (2008), "Modelling and experimental studies on pyrolysis of biomass particles", vol. 81, pp. 183–192.
- Lajili, M.; Jeguirim, M.; Kraiem, N. and Limousy, L. (2015), "Performance of a household boiler fed with agropellets blended from olive mill solid waste and pine sawdust", *Fuel*, vol. 153, pp. 431–436.
- Leco, C. (2007), "Instruction Manual: CHN/CHNS Carbon/Hydrogen/Nitrogen/Sulfur/Oxygen determinators".
- Leuckel, W. and Roemer, R. (1979), "Schadstoffe aus Verbrennungsprozessen; VDI-Bericht Nr. 346; VDI Verlag Duesseldorf.
- Li, X.G.; Ma, B.G.; Xu, L.; Hu, Z.W. and Wang, X.G. (2006), "Thermogravimetric analysis of the co-combustion of the blends with high ash coal and waste tyres", *Thermochimica Acta*, vol. 441, pp. 79–83.
- Liu, X.; Zhou, Y.; Li, C.-Q.; Lin, Y.; Yang, W. and Zhang, G. (2019), "Optimization of a New Phase Change Material Integrated Photovoltaic/Thermal Panel with The Active Cooling Technique Using Taguchi Method", *Energies*, vol. 12, pp. 1022.

- Loo, S. van and Koppejan, J. (2008), "The Handbook of Biomass Combustion and Co-firing", Earthscan.
- Madzaki, H.; Karimghani, W.A.W.AB.; Nurzalikharebitanim and Azilbaharialis (2016), "Carbon Dioxide Adsorption on Sawdust Biochar", *Procedia Engineering*, vol. 148, pp. 718–725.
- Magalhães, D.; Kazanç, F.; Riaza, J.; Erensoy, S.; Kabaklı, Ö. and Chalmers, H. (2017), "Combustion of Turkish lignites and olive residue: Experiments and kinetic modelling", *Fuel*, vol. 203, pp. 868–876.
- Magdziarz, A.; Dalai, A.K. and Koziński, J.A. (2016), "Chemical composition, character and reactivity of renewable fuel ashes", *Fuel*, vol. 176, pp. 135–145.
- Mani, T.; Murugan, P.; Abedi, J. and Mahinpey, N. (2010), "Pyrolysis of wheat straw in a thermogravimetric analyzer: Effect of particle size and heating rate on devolatilization and estimation of global kinetics", *Chemical Engineering Research and Design*, vol. 88, pp. 952–958.
- Manouchehrinejad, M.; Giesen, I. and Mani, S. (2018), "Grindability analysis of torrefied wood chips and wood pellets", *Fuel Processing Technology*, vol. 182, pp. 1–35.
- McKendry, P. (2002), "Energy production from biomass (part 1): overview of biomass. *Bioresource Technology*", vol. 83, pp. 37–46.
- Mediavilla, I.; Fernández, M.J. and Esteban, L.S. (2009), "Optimization of pelletisation and combustion in a boiler of 17.5 kWth for vine shoots and industrial cork residue", *Fuel Processing Technology*, vol. 90, pp. 621–628.
- Melkior, T.; Barthelemy, C. and Bardet, M. (2017), "Inputs of solid-state NMR to evaluate and compare thermal reactivity of pine and beech woods under torrefaction conditions and modified atmosphere", *Fuel*, vol. 187, pp. 250–260.
- Miccio, F.; Russo, S. and Silvestri, N. (2013), "Assessment of the devolatilization behavior of fuel pellets in fluidized bed", *Fuel Processing Technology*, vol. 115, pp. 122–129.
- Milne, T.A.; Elam, C.C. and Evans, R.J. (2002), "Hydrogen from Biomass State of the Art Research Challenges", National Renewable Energy Laboratory Golden, CO USA.
- Mishra, R.K. and Mohanty, K. (2018), "Pyrolysis kinetics and thermal behavior of waste sawdust biomass using thermogravimetric analysis", *Bioresource Technology*, vol. 251, pp. 63–74.
- Monedero, E.; Portero, H. and Lapuerta, M. (2015), "Pellet blends of poplar and pine sawdust: Effects of material composition, additive, moisture content and compression die on pellet quality", *Fuel Processing Technology*, vol. 132, pp. 15–23.

- Morris, A.S. and Langari, R. (2012), "Measurement and instrumentation: Theory and application", ELSEVIER, 1st edition.
- Neves, D.; Thunman, H.; Matos, A.; Tarelho, L. and Gómez-Barea, A. (2011), "Characterization and prediction of biomass pyrolysis products", *Progress in Energy and Combustion Science*, vol. 37, pp. 611–630.
- Nichols, J.D. and Vanclay, J.K. (2012), "Domestication of native tree species for timber plantations: key insights for tropical island nations", *International Forestry Review*, vol. 14, pp. 402–413.
- Nunes, L.J.R.; Matias, J.C.O. and Catalão, J.P.S. (2016), "Biomass combustion systems: A review on the physical and chemical properties of the ashes", *Renewable and Sustainable Energy Reviews*, vol. 53, pp. 235–242.
- Nunes, L.J.R.; Matias, J.C.O. and Catalão, J.P.S. (2013), "Energy recovery from cork industrial waste: Production and characterisation of cork pellets", *Fuel*, vol. 113, pp. 24–30.
- Nussbaumer, T. (2008), "Biomass Combustion In Europe Overview On Technologies And Regulations", NYSERDA.
- Nussbaumer, T. (1989), "Schadstoffbildung bei der Verbrennung von Holz", Dissertation, ETH Zuerich.
- Obernberger, I. and Thek, G. (2010), "The pellet handbook: The production and thermal utilisation of biomass pellets", Earthscan, p. 549.
- Öhman, M.; Nordin, A.; Hedman, H. and Jirjis, R. (2004), "Reasons for slagging during stemwood pellet combustion and some measures for prevention", *Biomass and Bioenergy*, vol. 27, pp. 597–605.
- Öhman, M.; Boman, C.; Hedman, H.; Nordin, A. and Boström, D. (2004), "Slagging tendencies of wood pellet ash during combustion in residential pellet burners", *Biomass and Bioenergy*, vol. 27, pp. 585–596.
- Oliveira, R.F. (2016), "Study and development of a holding chamber for inhalation", PhD Thesis, University of Minho.
- Olsson, M. (2006a), "Residential Biomass Combustion– Emissions Of Organic Compounds To Air From Wood Pellets And Other New Alternatives", PhD Thesis, Chalmers University of Technology.
- Olsson, M. (2006b), "Wheat straw and peat for fuel pellets-organic compounds from combustion", *Biomass and Bioenergy*, vol. 30, pp. 555–564.
- Pa, A.; Bi, X.T. and Sokhansanj, S. (2013), "Evaluation of wood pellet application for residential heating in British Columbia based on a streamlined life cycle analysis", *Biomass and Bioenergy*, vol. 49, pp. 109–122.

- Pastre, O. (2002), "Analysis of the technical obstacles related to the production and utilisation of fuel pellets made from agricultural residues", *Altener*, p. 51-107.
- Paulauskas, R.; Džiugys, A. and Striūgas, N. (2015), "Experimental investigation of wood pellet swelling and shrinking during pyrolysis", *Fuel*, vol. 142, pp. 145–151.
- Pirraglia, A.; Gonzalez, R.; Saloni, D. and Denig, J. (2013), "Technical and economic assessment for the production of torrefied ligno-cellulosic biomass pellets in the US", *Energy Conversion and Management*, vol. 66, pp. 153–164.
- Pozzobon, V.; Salvador, S.; Bézian, J.J.; El-Hafi, M.; Le Maout, Y. and Flamant, G. (2014), "Radiative pyrolysis of wet wood under intermediate heat flux: Experiments and modelling", *Fuel Processing Technology*, vol. 128, pp. 319–330.
- Qiu, G. (2013), "Testing of flue gas emissions of a biomass pellet boiler and abatement of particle emissions", *Renewable Energy*, vol. 50, pp. 94–102.
- Rabaçal, M.; Fernandes, U. and Costa, M. (2013), "Combustion and emission characteristics of a domestic boiler fired with pellets of pine, industrial wood wastes and peach stones", *Renewable Energy*, vol. 51, pp. 220–226.
- Ravichandran, P. (2013), "Assessing Alternative Options for Energy Cost Reduction in Greenhouse Industry", Master Thesis, Dalhousie University.
- Ray, S.J.; Pordesimo, L.O. and Wilhelm, L.R. (2004), "Airflow resistance of some pelleted feed", vol. 47, pp. 513–519.
- Ribeiro, P.E.A.; Vilarinho, C.; Ferreira, M.E.C.; Seabra, E.; Fraga, L.G. and Teixeira, J.C.F. (2019), "Strategies for the Design of Domestic Pellet Boilers", in: *Innovation, Engineering and Entrepreneurship*, vol. 505, 2019, pp. 668–674.
- Ribeiro, P.E.A.; Teixeira, J.C.F. and Ferreira, M.E.C. (2014), "Ash Sintering in a Biomass Pellet Boiler", in *ASME 2013 International Mechanical Engineering Congress and Exposition Volume 8A: Heat Transfer and Thermal Engineering*.
- Ribeiro, P.E.A.; Ferreira, M.E.C. and Teixeira, J.C.F. (2013), "Desenvolvimento de uma caldeira a pellets de madeira dedicada ao aquecimento doméstico", University of Minho.
- Ribeiro, P.E.A. (2012), "Aglomeración de Cinzas numa Caldeira a Pellets – Influência da Temperatura e do Fluxo de Ar", Master Thesis, University of Minho.
- Ronnback, M.; Axell, M. and Gustavsson, L. (2001), "Combustion processes in a biomass fuel bed—experimental results", In: *Progress in Thermochemical Biomass Conversion*.

- Rosillo-Calle, F. (2007), "The Biomass Assessment Handbook Bioenergy for a Sustainable Environment", Earthscan, 1st edition.
- Roy, M.M.; Dutta, A. and Corscadden, K. (2013), "An experimental study of combustion and emissions of biomass pellets in a prototype pellet furnace", *Applied Energy*, vol. 108, pp. 298–307.
- Roy, R.K. (2010), "A Primer on The Taguchi method", SME, Second edition.
- Rybak, W.; Moroń, W.; Czajka, K.M.; Kisiela, A.M.; Ferens, W.; Jodkowski, W. and Andryjowicz, C. (2017), "Co-combustion of unburned carbon separated from lignite fly ash", *Energy Procedia*, vol. 120, pp. 197–205.
- Ryu, C.; Yang, Y.B.; Khor, A.; Yates, N.E.; Sharifi, V.N. and Swithenbank, J. (2006), "Effect of fuel properties on biomass combustion: Part I. Experiments - Fuel type, equivalence ratio and particle size", *Fuel*, vol. 85, pp. 1039–1046.
- Saidur, R.; Abdelaziz, E.A.; Demirbas, A.; Hossain, M.S. and Mekhilef, S. (2011), "A review on biomass as a fuel for boilers", *Renewable and Sustainable Energy Reviews*, vol. 15, pp. 2262–2289.
- Salema, A.A. and Afzal, M.T. (2015), "Numerical simulation of heating behaviour in biomass bed and pellets under multimode microwave system", *International Journal of Thermal Sciences*, vol. 91, pp. 12–24.
- Saygin, D.; Gielen, D.J.; Draeck, M.; Worrell, E. and Patel, M.K. (2014), "Assessment of the technical and economic potentials of biomass use for the production of steam, chemicals and polymers", *Renewable and Sustainable Energy Reviews*, vol. 40, pp. 1153–1167.
- Serrano, C.; Portero, H. and Monedero, E. (2013), "Pine chips combustion in a 50 kW domestic biomass boiler", *Fuel*, vol. 111, pp. 564–573.
- Shen, D.K.; Gu, S.; Luo, K.H.; Bridgwater, A.V. and Fang, M.X. (2009), "Kinetic study on thermal decomposition of woods in oxidative environment", *Fuel*, vol. 88, pp. 1024–1030.
- Sikanen, L. and Vilppo, T. (2012), "Small Scale Pilot Combustion Experiments with Wood Pellets – The Effect of Pellet Length", *The Open Renewable Energy Journal*, vol. 5, pp. 1–6.
- Silva, J.; Fraga, L.G.; Ferreira, M.E.C.; Chapela, S.; Porteiro, J.; Teixeira, S.F.C.F. and Teixeira, J.C.F. (2018), "Combustion Modelling of a 20 kW Pellet Boiler", in *Proceedings, ASME International Mechanical Engineering Congress and Exposition (IMECE)*, p. 9.
- Soria-Verdugo, A.; Garcia-Gutierrez, L. M.; Blanco-Cano, L.; Garcia-Hernando, N. and Ruiz-Rivas, U. (2014), "Evaluating the accuracy of the Distributed Activation Energy Model for biomass devolatilization curves obtained at high heating rates", *Energy Conversion and Management*, vol. 86, pp. 1045–1049.

- Sultana, A. and Kumar, A. (2012), "Ranking of biomass pellets by integration of economic, environmental and technical factors", *Biomass and Bioenergy*, vol. 39, pp. 344–355.
- Suzdalenko, V.; Gedrovics, M.; Zake, M.; Barmina, I. and Lickrastina, A. (2012), "The Effect of Swirling Flow on Co-Firing Process of Wood Pellets and Propane", LEI.
- Taylor, J. (1997), "Introduction to Error Analysis, the Study of Uncertainties in Physical Measurements", University Science Books, 2nd edition.
- Thanakiatkrai, P. and Welch, L. (2012), "Using the Taguchi method for rapid quantitative PCR optimization with SYBR Green I", *International Journal of Legal Medicine*, vol. 126, pp. 161–165.
- Thomson, H. and Liddell, C. (2015), "The suitability of wood pellet heating for domestic households: A review of literature", *Renewable and Sustainable Energy Reviews*, vol. 42, pp. 1362–1369.
- Thrän, D.; Seidenberger, T.; Zeddies, J. and Offermann, R. (2010), "Global biomass potentials - Resources, drivers and scenario results", *Energy for Sustainable Development*, vol. 14, pp. 200–205.
- Tilay, A.; Azargohar, R.; Drisdelle, M.; Dalai, A. and Kozinski, J. (2015), "Canola meal moisture-resistant fuel pellets: Study on the effects of process variables and additives on the pellet quality and compression characteristics", *Industrial Crops and Products*, vol. 63, pp. 337–348.
- Turns, S. (2000), "An Introduction To Combustion: Concepts and Applications", , McGraw Hill, 2nd edition.
- U.S. Department of Health and Human Services: Agency for Toxic Substances and Disease Registry, 1975. Nitrogen Oxides (NO, NO₂, and others) CAS 10102-43-9; UN 1660 (NO) CAS 10102-44-0; UN 1067 (NO₂) UN 1975 (Mixture). Agency for Toxic Substances and Disease Registry (ATSDR), 1660(2), pp.1–20. Available at: <http://www.atsdr.cdc.gov/MHMI/mmg175.pdf>.
- Vamvuka, D. and Sfakiotakis, S. (2011), "Combustion behaviour of biomass fuels and their blends with lignite", *Thermochimica Acta*, vol. 526, pp. 192–199.
- Verma, V.K.; Bram, S.; Delattin, F. and De Ruyck, J. (2013), "Real life performance of domestic pellet boiler technologies as a function of operational loads: A case study of Belgium", *Applied Energy*, vol. 101, pp. 357–362.
- Vicente, E.D.; Tarelho, L.A.C.; Teixeira, E.R.; Duarte, M.; Nunes, T.; Colombi, C.; Gianelle, V.; da Rocha, G.O.; de la Campa, A.S. and Alves, C.A. (2016), "Emissions from the combustion of eucalypt and pine chips in a fluidized bed reactor", *Journal of Environmental Sciences*, vol. 42, pp. 246–258.
- Vicente, E.D. and Alves, C.A. (2018), "An overview of particulate emissions from residential biomass combustion", *Atmospheric Research*, vol. 199, pp. 159–185.

- Wang, L.; Hustad, J.E.; Skreiberg, Ø.; Skjevraak, G. and Grønli, M. (2012), "A critical review on additives to reduce ash related operation problems in biomass combustion applications", *Energy Procedia*, vol. 20, pp. 20–29.
- Wang, M. and Dunn, J.B. (2015), "Comments on Avoiding Bioenergy Competition for Food Crops and Land by Searchinger and Heimlich," Argonne National Laboratory, p. 9.
- Wang, Q.; Zhao, W.; Liu, H.; Jia, C. and Xu, H. (2012), "Reactivity and Kinetic Analysis of Biomass during Combustion", *Energy Procedia*, vol. 17, pp. 869–875.
- Wang, Y.; Shao, Y.; Matovic, M.D. and Whalen, J.K. (2015), "Exploring switchgrass and hardwood combustion on excess air and ash fouling/slugging potential: Laboratory combustion test and thermogravimetric kinetic analysis", *Energy Conversion and Management*, vol. 97, pp. 409–419.
- Wang, Y.; Tan, H.; Wang, X.; Du, W.; Mikulčić, H. and Duić, N. (2017), "Study on extracting available salt from straw/woody biomass ashes and predicting its slugging/fouling tendency", *Journal of Cleaner Production*, vol. 155, pp. 164–171.
- Warnatz, J.; Maas, U. and Dibble, R.W. (2001), "Combustion: Physical and Chemical Fundamentals, Modeling and Simulation, Experiments, Pollutant Formation", Springer, 3rd edition. Available at: <http://link.springer.com/10.1007/978-3-662-04508-4>.
- Wiinikka, H. and Gebart, R. (2004), "Critical parameters for particle emissions in small-scale fixed-bed combustion of wood pellets", *Energy and Fuels*, vol. 18, pp. 897–907.
- www.artisan-g.com, SDT 2960 Simultaneous DSC-TGA including DTA capabilities, (888), pp.1–8.
- Yazdanpanah, F.; Sokhansanj, S.; Lau, A.K.; Lim, C.J.; Bi, X. and Melin, S. (2011), "Airflow versus pressure drop for bulk wood pellets", *Biomass and Bioenergy*, vol. 35, pp. 1960–1966.
- Yeo, J.Y.; Chin, B.L.F.; Tan, J.K. and Loh, Y.S. (2019), "Comparative studies on the pyrolysis of cellulose, hemicellulose, and lignin based on combined kinetics", *Journal of the Energy Institute*, vol. 92, pp. 27–37.
- Yin, C. and Li, S. (2017), "Advancing grate-firing for greater environmental impacts and efficiency for decentralized biomass/wastes combustion", *Energy Procedia*, vol. 120, pp. 373–379.
- Yin, C.; Rosendahl, L.A. and Kær, S.K. (2008), "Grate-firing of biomass for heat and power production", *Progress in Energy and Combustion Science*, vol. 34, pp. 725–754.
- Yorulmaz, S.Y. and Atımtay, A. (2009), "Investigation of combustion kinetics of treated and untreated waste wood samples with thermogravimetric analysis", *Environmental Earth Sciences*, vol. 90, pp. 939–946.

- Yuzbasi, N.S. and Selçuk, N. (2011), "Air and oxy-fuel combustion characteristics of biomass/lignite blends in TGA-FTIR", *Fuel Processing Technology*, vol. 92, pp. 1101–1108.
- Zhu, C.; Liu, S.; Liu, H.; Yang, J.; Liu, X. and Xu, G. (2015), "NO_x emission characteristics of fluidized bed combustion in atmospheres rich in oxygen and water vapor for high-nitrogen fuel", *Fuel*, vol. 139, pp. 346–355.

ANNEXES

A. Biomass characteristics and experimental auxiliary

This section presents the biomass characteristic and biomass standard for different classes, the thermocouple standardization nomenclature and grate design.

Table A.1. Threshold values of the most important pellet parameters based on ISO 17225-2 (European Pellet Council, 2015).

Property	Unit	ENplus A1	ENplus A2	ENplus B	Testing Standard ¹¹⁾
Diameter	mm	6 ± 1 or 8 ± 1			ISO 17829
Length	mm	3.15 < L ≤ 40 ⁴⁾			ISO 17829
Moisture	w-% ²⁾	≤ 10			ISO 18134
Ash	w-% ³⁾	≤ 0.7	≤ 1.2	≤ 2.0	ISO 18122
Mechanical Durability	w-% ²⁾	≥ 98.0 ⁵⁾	≥ 97.5 ⁵⁾		ISO 17831-1
Fines (< 3,15 mm)	w-% ²⁾	≤ 1.0 ⁶⁾ (≤ 0.5 ⁷⁾)			ISO 18846
Temperature of pellets	°C	≤ 40 ⁸⁾			
Net Calorific Value	kWh/kg ²⁾	≥ 4.6 ⁹⁾			ISO 18125
Bulk Density	kg/m ³ ²⁾	600 ≤ BD ≤ 750			ISO 17828
Additives	w-% ²⁾	≤ 2 ¹⁰⁾			-
-Nitrogen	w-% ³⁾	≤ 0.3	≤ 0.5	≤ 1.0	ISO 16948
Sulfur	w-% ³⁾	≤ 0.04	≤ 0.05		ISO 16994
Chlorine	w-% ³⁾	≤ 0.02		≤ 0.03	ISO 16994
Ash Deformation Temperature ¹⁾	°C	≥ 1200	≥ 1100		CEN/TC 15370-1
Arsenic	mg/kg ²⁾	≤ 1			ISO 16968
Cadmium	mg/kg ³⁾	≤ 0.5			ISO 16968
Chromium	mg/kg ³⁾	≤ 10			ISO 16968
Copper	mg/kg ³⁾	≤ 10			ISO 16968
Lead	mg/kg ³⁾	≤ 10			ISO 16968
Mercury	mg/kg ³⁾	≤ 0.1			ISO 16968
Nickel	mg/kg ³⁾	≤ 10			ISO 16968
Zinc	mg/kg ³⁾	≤ 100			ISO 16968

1) ash is produced at 815 °C.

2) as received.

3) dry basis.

4) a maximum of 1% of the pellets may be longer than 40 mm, no pellets longer than 45 mm are allowed.

5) at the loading point of the transport unit (truck, vessel) at the production site.

- 6) at factory gate or when loading truck for deliveries to end-users (*Part Load Delivery and Full Load Delivery*).
- 7) at factory gate, when filling pellet bags or sealed Big Bags.
- 8) at the last loading point for truck deliveries to end-users (*Part Load Delivery and Full Load Delivery*).
- 9) equal \geq 16.5 MJ/kg as received.
- 10) the amount of additives in production shall be limited to 1.8 w-%, the amount of post-production additives (e.g. coating oils) shall be limited to 0.2 w-% of the pellets.
- 11) As long as the mentioned ISO standards are not published, analyses shall be performed according to related CEN standards.

Table A.2. Standard thermocouple types (AN107).

Type	Materials*	Typical Range (°C)
T ^{1, 2}	Copper (Cu) vs Constantan	-270 to 400
J ^{1, 3}	Iron (Fe) vs Constantan	-210 to 1,200
K	Chromel vs Alumel	-270 to 1,370
E	Chromel vs Constantan	-270 to 1,000
S	(Pt-10%Rh) vs Pt	-50 to 1,768
B	(Pt-13% Rh) vs (Pt-6%Rh)	0 to 1,820
R	(Pt-13%Rh) vs Pt	-50 to 1,768
N	(Ni-Cr-Si) vs (Ni-Si-Mg)	-270 to 1,300

*** Material definitions:**

- Constantan, alloy of Nickel (Ni) - Copper (Cu)
- Chromel, alloy of Nickel (Ni) - Chromium (Cr)
- Alumel, alloy of Nickel (Ni) and Aluminum (Al)
- Magnesium (Mg), base element
- Platinum (Pt), base element
- Nickel (Ni) a base element
- Silicon (Si), a base element
- Chromium (Cr), a base element
- Iron (Fe), a base element
- Rhodium (Rh), a base element

Notes

1. Both the L and U Type thermocouples are defined by DIN Standard 43710; however, they are not as frequently used in new installations as the more popular T and J Type thermocouple standards.
2. The U Type thermocouple is similar to the popular standard T Type.
3. The L Type thermocouple is similar to the popular standard J Type.

Table A.3. Physical and chemical properties of wood pellets.

Element	Value	Unit
Moisture content	6.9	%
Ash content at 800 °C	0.6	%
Volatile matter at 550 °C	77.80	%
Lower heating value	17.1	(MJ/kg)
Nitrogen	1.55	% dry base
Carbon	50.9	% dry base
Hydrogen	5.39	% dry base
Oxygen	42.22	% dry base
Sulfur	0.037	% dry base
Bulk Density	0.598	(g/cm ³)
Cl	0.001	%
Cr	0.004	%
Cu	0.002	%
Mn	0.011	%
Ni	0.004	%
Al	0.033	%
Fe	0.023	%
K	0.067	%
Na	0.01	%
Si	0.043	%
P	0.014	%
Ti	0.002	%
Mg	0.058	%
Ca	0.097	%
Zn	0.001	%

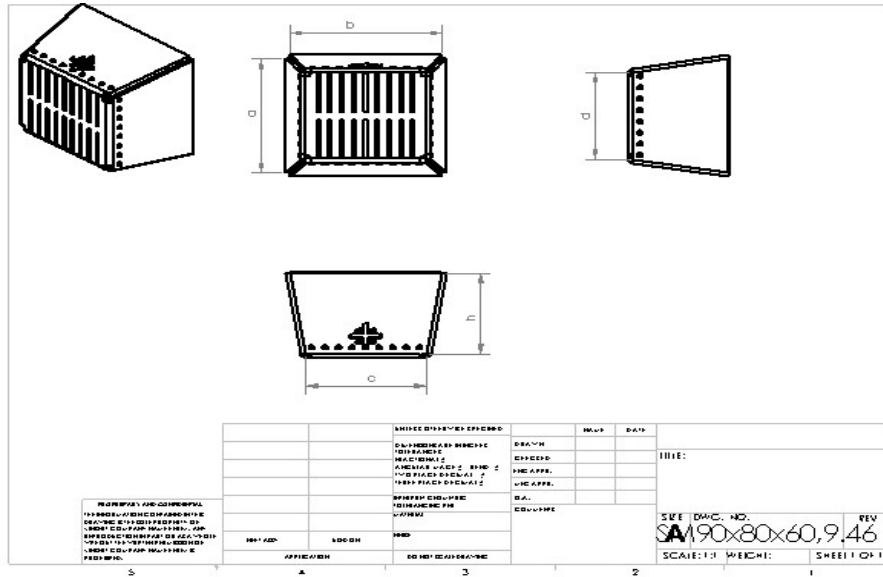


Figure A.1. Grate design.

where:

h = Height of grate = 61 mm.

c = Length bottom of grate (mm).

d = Width bottom of grate (mm).

Cross section area, $A = c \times d$.

B. Experimental procedure

In order to safely and repeatably operate the test facility it is recommended that a sequence of steps are followed by the operator. These involve verification, calibration of the gas analyzer, experimental and turn off phases.

B.1 Verification of the boiler

1. Turn on the computer.
2. Turn on the ventilator and cooling loop ventilator.
3. Open the program/acquisition and click on "Run program".
4. Turn on the power supply.
5. Select the acquisition control and select start manual and check all the devices to make sure they are working properly by introducing the frequency of the ventilator to ± 20 Hz.
6. The water pump runs automatically and check if the water flow rate is between 400-600 L/h (≈ 500 L/h).
7. If the water pump is properly working, then turn off acquisition and close the program to clean all the previous data.

B.2 Calibration of gas analyzer

1. Turn on the vacuum pump.
2. Turn on the gas analyzer, switch to sample mode and wait ± 10 -15 minutes before proceeding to calibration.
3. For the calibration and operation purposes of multi-gas analyzer (CO, CO₂, O₂ and NO_x):
 - 3.1 Check if the sample flow rate within the minimum and maximum range on the digital flow meter in the gas analyzer display. Adjust the by-pass valve on gas conditioning circuit if necessary.
 - 3.2 Open all the gas bottles and press the "CAL" button on all displays and wait until it finishes. Press the "ZERO" button to check the zero value on the gas analyzer. Press the "SPAN" button on all displays to check gas concentration at bottle (e.g. for CO = $\pm 5,000$ ppm, O₂ = 20%, CO₂ = 10% and NO_x = 3,000 ppm. Pay attention to gas analyzer SPAN scale). If there's some drift on Zero and Span values, repeat calibration. After finish click on "SAMP" to turn to sample mode and start reading. Close all the bottles except Nitrogen bottle, that should be always on during the operation

4. For the calibration and operation purposes of NO_x analyzer:
 - 4.1 Turn on the dedicated vacuum pump and ionizer,
 - 4.2 In the heating device, adjust the collecting pipe temperature for a value above exhaust gases temperature, to prevent condensation,
 - 4.3 For calibration, open NO_x, O₂ and N₂ calibration bottles. Follow procedure number 3.
5. For NO_x analyzer, N₂ and O₂ bottles should remain open during all the operation.

B.3 Experimental phase

1. Turn on the water in the cooling system of the gas analyzer.
2. Plug in the scale to the mains supply.
3. Open the program/acquisition and click on “Run program”.
 - 3.1 Select the parameters in *canais analógicos* (0-9).
 - 3.2 Select the parameters in *termopares* (e.g: 0-16). Depends on the number of thermocouples installed.
 - 3.3 Adjust the ignition time to start after 95 s.
 - 3.4 Adjust the initial feeding start from low feeding (exp. 4 on, 8 off) after the combustion is stabilized start with the mass flow rate required for feeding.
 - 3.5 Adjust the temperature for turn off the ignition (≈ 110 °C).
 - 3.6 Adjust the temperature for automatic feeding (≈ 100 °C), after the combustion is taking place but no pellets is supplied, then decrease the feeding temperature (reduce to ≈ 60 °C).
 - 3.7 Adjust water pump On/Off temperatures. Set 5 °C/4 °C to keep it always turned on.
 - 3.8 Introduce the initial and feeding flow rate to 23.8 Hz.
 - 3.9 Run the acquisition on “*modo automático*”.
4. Once the combustion starts then introduce the real data for the experiment.
5. For safety issues during the test, follow the safety issues (see B.5).
6. After finishing the experiment, shut down the equipment by following the “turn off procedure” (see B.4).

B.4 Turn off procedure

1. Select the manual mode.
2. Press the manual/ *forçar* manual and set the ventilator value to 20–30 Hz.

3. Wait until water temperature falls to below 40 °C then stop the acquisition (acquisition + finalize acquisition + save data).
4. Turn off the vacuum pump.
5. Stop the gas analyzer, press the stop buttons.
6. Leave the nitrogen bottle opened for purging purposes, wait until the display shows the purging is complete and close the nitrogen bottle.
7. Turn off the power supply.
8. Turn off the computer.
9. Turn off the water.

B.5 Safety issues

1. In manual mode check if all devices are working properly.
2. In case of failing the ignition indicated by high intensive of smoke with no flame, then increase the fan velocity to provide more air to start the combustion.
3. Check always the water pump if the water flow rate value is constant between 400-600 L/h (\approx 500 L/h).
4. Continuously check if the temperature of water in the boiler (see in water temperature section) does not exceed 70 °C; if so then click the force manual, turn off the pellets motor, and let the ventilator (30–35 Hz) and water pump running until water temperature falls below 40 °C, then shut down the system (follow section turn off procedure).
5. Make sure the cooler is working.
6. Wear goggles all the time.

C. TGA data

C.1 Data for different heating rate

Table C.1. Ignition, peak and burnout temperatures and maximum combustion rates at different heating rates for the particles < 0.063 mm.

Parameter	Heating rate (°C/min)			
	5	10	20	51
Moisture release Temp. (°C)	183	87	244	234
Initial decomposition Temp. (°C)	252	239	231	211
Ignition Temp. (°C)	270	280	295	304
1 st peak Temp. (°C)	319	328	347	365
2 nd peak Temp. (°C)	443	451	449	462
Burnout Temp. (°C)	458	456	481	529
Burnout time (min.)	87	44	23	11
Max. comb. rate (%/min.) at 1 st peak	-6.40	-13.34	-22.64	-53.23
Max. comb. rate (%/min.) at 2 nd peak	-2.12	-27.06	-30.07	-26.57
Max. heat release (W/g) at DSC	9.63	151.26	198.45	296.99
Temp. at max. heat release (°C) at DSC	327	456	465	488
Remaining mass (%)	1.69	2.27	5.61	0.1
Heat released (μ J)	97.5	378	362	543

Table C.2. Ignition, peak and burnout temperatures and maximum combustion rates at different heating rates for the particles 0.125-0.25 mm.

Parameter	Heating rate (°C/min)					
	5	10	20	51	101	243
Moisture release Temp. (°C)	176	205	257	271	279	290
Initial decomposition Temp. (°C)	260	250	239	233	206	204
Ignition Temp. (°C)	280	290	300	314	329	330
1 st peak Temp. (°C)	321	332	350	371	386	401
2 nd peak Temp. (°C)	456	472	484	503	516	553
Burnout Temp. (°C)	473	492	523	559	600	688
Burnout time (min.)	90	47	25	11	6	4
Max. comb. rate (%/min.) at 1 st peak	-6.30	-12.07	-23.07	-53.09	-103.1	-213.45
Max. comb. rate (%/min.) at 2 nd peak	-2.09	-4.01	-7.38	-14.43	-22.75	-25.10
Max. heat release (W/g) at DSC	11.28	53.63	83.87	247.21	380.65	772.39
Temp. at max. heat release (°C) at DSC	333	476	495	528	540	658
Remaining mass (%)	0.16	3.84	1.55	4.84	5.12	2.79
Heat released (μ J)	118	230	235	418	640	2618

Table C.3. Ignition, peak and burnout temperatures and maximum combustion rates at different heating rates for the particles >1 mm.

Parameter	Heating rate (°C/min)			
	5	10	20	51
Moisture release Temp. (°C)	100	94	261	272
Initial decomposition Temp. (°C)	261	251	244	232
Ignition Temp. (°C)	283	290	301	318
1 st peak Temp. (°C)	321	330	350	369
2 nd peak Temp. (°C)	458	466	478	442
Burnout Temp. (°C)	475	483	523	533
Burnout time (min.)	91	47	25	11
Max. comb. rate (%/min.) at 1 st peak	-6.38	-12.87	-23.88	-60.21
Max. comb. rate (%/min.) at 2 nd peak	-2.45	-17.05	-20.42	-23.63
Max. heat release (W/g) at DSC	10.34	91.79	150.39	240.11
Temp. at max. heat release (°C) at DSC	461	473	480	522
Remaining mass (%)	0.57	0.93	0.75	0.49
Heat released (μJ)	53.2	449	367	499

Table C.4. Mass loss per stage of conversion at different heating rates and particle sizes.

Particle size (mm)	HR (°C/min)	Loss in 1 st stage (wt.%)	Loss in 2 nd stage (wt.%)	Loss in 3 rd stage (wt.%)	Total loss (wt.%)	Ash content (wt.%)	Unaccounted (wt.%)
< 0.063	5	4.65	51.94	27.48	84.07	0.6	15.33
	10	8.73	50.28	31.36	90.37		9.03
	20	10.08	47.65	29.46	87.19		12.21
	51	10.26	52.20	30.90	93.16		6.04
0.125 – 0.25	5	5.5	49.09	31.20	85.79		13.61
	10	7.71	47.71	30.89	86.31		13.09
	20	9.38	49.17	33.59	92.14		7.26
	51	9.18	50.25	30.28	89.71		9.69
	101	10.35	52.61	26.53	89.49		9.91
> 1	243	7.23	66.57	18.46	92.26		7.14
	5	6.13	47.53	31.48	85.14		14.26
	10	8.05	48.13	31.47	87.65		11.75
	20	8.80	51.10	34.72	94.62	4.78	
	51	11.01	51.50	31.50	94.01	5.39	

Table C.5. Effect of heating rates on combustion parameters of the pine wood particles.

Particle size (mm)	HR (°C/min)	T_{id} (°C)	T_I (°C)	T_{max} (°C)	R_{max} (10^2 /min)	T_b (°C)	t_b (min)	$D \times 10^4$	$S \times 10^{10}$
< 0.063	5	252	270	319	6.4	458	87	0.22	6.26
	10	239	280	451	27.06	456	44	2.33	59.01
	20	231	295	449	30.07	481	23	10.23	102.18
0.125 – 0.25	51	211	304	365	53.23	529	11	127	368.51
	5	260	280	321	6.3	473	90	0.21	5.73
	10	250	288	332	12.07	492	47	1.44	19.39
	20	239	300	350	23.07	523	25	9.69	65.74
	51	233	314	371	53.09	559	11	126	307.48
	101	206	329	386	103.1	600	6	644	952.70
> 1	243	204	330	401	213.45	688	4	5336	3389.15
	5	261	283	321	6.38	475	91	0.20	5.72
	10	251	290	466	17.05	483	47	1.35	29.36
	20	244	301	350	23.88	523	25	10	70.79
	51	232	318	369	60.21	533	11	123	426.88

C.2 Data for different air flow rate

Table C.6. Ignition, peak and burnout temperatures and maximum combustion rates at different air flow rates for the particles < 0.063 mm.

Parameter	Air flow rate (mL/min)			
	10	50	100	150
Moisture release Temp. (°C)	226	110	87	231
Initial decomposition Temp. (°C)	242	242	239	242
Ignition Temp. (°C)	282	283	280	282
1 st peak Temp. (°C)	332	331	328	332
2 nd peak Temp. (°C)	460	461	451	460
Burnout Temp. (°C)	476	474	456	473
Burnout time (min.)	45	46	44	45
Max. comb. rate (%/min.) at 1 st peak	-12.58	-13.39	-13.34	-12.63
Max. comb. rate (%/min.) at 2 nd peak	-5.13	-5.89	-27.06	-5.79
Max. heat release (W/g) at DSC	47.31	51.49	151.26	46.09
Temp. at max. heat release (°C) at DSC	463	463	456	461
Remaining mass (%)	3.37	3.32	2.27	4.34
Heat released (μ J)	210	225	378	175

Table C.7. Ignition, peak and burnout temperatures and maximum combustion rates at different air flow rates for the particles 0.125 – 0.25 mm.

Parameter	Air flow rate (mL/min)			
	10	50	100	150
Moisture release Temp. (°C)	235	237	205	263
Initial decomposition Temp. (°C)	250	248	250	250
Ignition Temp. (°C)	293	290	290	291
1 st peak Temp. (°C)	334	334	332	334
2 nd peak Temp. (°C)	474	471	472	476
Burnout Temp. (°C)	499	498	492	497
Burnout time (min.)	47	47	47	47
Max. comb. rate (%/min.) at 1 st peak	-12.30	-13.73	-12.07	-12.27
Max. comb. rate (%/min.) at 2 nd peak	-3.95	-4.39	-4.01	-4.15
Max. heat release (W/g) at DSC	34.14	42.24	53.63	36.7
Temp. at max. heat release (°C) at DSC	478	479	476	480
Remaining mass (%)	0.60	6.92	3.84	4.32
Heat released (μ J)	177	232	230	179

Table C.8. Ignition, peak and burnout temperatures and maximum combustion rates at different air flow rates for the particles > 1 mm.

Parameter	Air flow rate (mL/min)			
	10	50	100	150
Moisture release Temp. (°C)	105	220	94	242
Initial decomposition Temp. (°C)	251	251	251	251
Ignition Temp. (°C)	292	290	290	290
1 st peak Temp. (°C)	334	335	330	334
2 nd peak Temp. (°C)	456	476	466	475
Burnout Temp. (°C)	498	495	483	485
Burnout time (min.)	49	47	47	47
Max. comb. rate (%/min.) at 1 st peak	-12.61	-12.02	-12.87	-11.86
Max. comb. rate (%/min.) at 2 nd peak	-21.46	-5.63	-17.05	-16.49
Max. heat release (W/g) at DSC	91.86	57.06	91.79	93.96
Temp. at max. heat release (°C) at DSC	461	479	473	478
Remaining mass (%)	2.14	3.98	0.93	5.58
Heat released (μ J)	216	247	449	162,905

Table C.9. Mass loss per stage of conversion at different air flow rates and particle sizes.

Particle size (mm)	Air flow rate (mL/min)	Loss in 1 st stage (wt.%)	Loss in 2 nd stage (wt.%)	Loss in 3 rd stage (wt.%)	Total loss (wt.%)	Ash content (wt.%)	Unaccounted (wt.%)
< 0.063	10	7.76	50.39	29.28	87.43	0.6	11.97
	50	8.60	52.60	30.78	91.98		7.42
	100	8.73	50.28	31.36	90.37		9.03
	150	7.85	50.33	28.87	87.08		12.35
0.125 – 0.25	10	9.16	48.17	33.17	90.50		8.9
	50	8.97	53.40	35.86	98.23		1.17
	100	7.71	47.71	30.89	86.31		13.09
	150	8.39	48.50	32.96	86.85		12.55
> 1	10	8.35	48.64	33.97	90.96		8.44
	50	7.74	50.15	36.56	94.45		4.95
	100	8.05	48.13	31.47	87.65		11.75
	150	7.62	46.25	31.76	85.63		13.77

Table C.10. Effect of air flow rates on combustion parameters of the pine wood particles.

Particle size (mm)	Air flow rate (mL/min)	T_{td} (°C)	T_I (°C)	T_{max} (°C)	R_{max} (10^2 /min)	T_b (°C)	t_b (min)	$D \times 10^4$	$S \times 10^{10}$
< 0.063	10	242	282	332	12.58	476	45	1.61	22.45
	50	242	283	331	13.39	474	46	1.55	25.44
	100	239	280	451	27.06	456	44	2.33	59.01
	150	242	282	332	12.63	473	45	1.57	22.85
0.125 – 0.25	10	250	293	334	12.3	499	47	1.47	19.71
	50	248	290	334	13.73	498	47	1.64	24.22
	100	250	292	332	12.07	492	47	1.44	19.12
	150	250	291	334	12.27	497	47	1.57	19.77
> 1	10	251	292	456	21.46	498	49	1.74	34.95
	50	251	290	335	12.02	495	47	1.44	20.96
	100	251	290	466	17.05	483	47	1.35	29.36
	150	251	290	475	16.49	485	47	1.28	27.52

C.3 Kinetic analysis data for different heating rate

Table C.11. Estimated kinetic parameters for the combustion of pine wood particles at different heating rates (particles smaller than 0.063 mm).

β (°C/min)	E (kJ/mol)	A (min ⁻¹)	T (°C)	R^2
2nd stage				
5	124.12	8.42E+11	252 - 370	0.9373
10	118.96	2.72E+11	239 - 370	0.9566
20	99.90	2.85E+09	231 - 390	0.9937
51	93.55	5.52E+08	211 - 410	0.9749
3rd stage				
5	190.02	1.81E+15	370 - 458	0.9175
10	186.52	7.95E+14	370 - 456	0.8959
20	229.02	6.05E+17	390 - 481	0.9549
51	186.91	1.30E+14	410 - 529	0.9596
Global combustion				
5	64.36	8.32E+05	252 - 458	0.8234
10	68.30	1.71E+06	239 - 456	0.8534
20	66.06	8.23E+05	231 - 481	0.9444
51	66.19	6.18E+05	211 - 529	0.9453

Table C.12. Estimated kinetic parameters for the combustion of pine wood particles at different heating rates (particles between 0.125 and 0.25 mm).

β (°C/min)	E (kJ/mol)	A (min ⁻¹)	T (°C)	R^2
2nd stage				
5	136.64	9.63E+12	260 - 370	0.9408
10	125.27	6.88E+11	250 - 380	0.9544
20	116.03	6.95E+10	239 - 390	0.966
51	108.42	8.46E+09	233 - 415	0.9733
101	96.75	6.05E+08	206 - 430	0.9899
243	79.52	1.07E+07	204 - 510	0.9969
3rd stage				
5	162.37	8.75E+12	370 - 473	0.9149
10	159.40	2.96E+12	380 - 492	0.9246
20	145.35	1.33E+11	390 - 523	0.9361
51	147.41	8.03E+10	415 - 559	0.9351
101	130.80	3.67E+09	430 - 600	0.9373
243	141.41	2.32E+09	510 - 688	0.9374
Global combustion				
5	62.78	4.77E+05	260 - 473	0.8072
10	63.68	4.71E+05	250 - 492	0.8413
20	64.06	3.73E+05	239 - 523	0.881
51	65.29	3.48E+05	233 - 559	0.9038
101	64.57	2.76E+05	206 - 600	0.94
243	52.40	2.00E+04	204 - 688	0.9251

Table C.13. Estimated kinetic parameters for the combustion of pine wood particles at different heating rates (particles larger than 1 mm).

β (°C/min)	E (kJ/mol)	A (min ⁻¹)	T (°C)	R^2
2nd stage				
5	136.06	8.09E+12	261 - 372	0.9388
10	127.06	9.83E+11	251 - 380	0.9577
20	119.22	1.17E+11	244 - 395	0.968
51	112.29	1.97E+10	232 - 410	0.976
3rd stage				
5	164.24	1.06E+13	372 - 475	0.9139
10	172.42	3.24E+13	380 - 483	0.9252
20	165.87	4.23E+12	395 - 523	0.9515
51	162.88	1.73E+12	410 - 533	0.9321
Global combustion				
5	62.05	3.92E+05	261 - 475	0.7981
10	66.24	8.11E+05	251 - 483	0.8454
20	66.71	6.08E+05	244 - 523	0.8877
51	71.42	1.33E+06	232 - 533	0.9152

C.4 Kinetic analysis data for different air flow rate

Table C.14. Estimated kinetic parameters for the combustion of pine wood particles at different air flow rates (particles smaller than 0.063 mm).

\dot{Q}_a (mL/min)	E (kJ/mol)	A (min ⁻¹)	T (°C)	R^2
2nd stage				
10	115.64	1.04E+11	242 - 380	0.9544
50	115.99	1.13E+11	242 - 380	0.9546
100	118.96	2.72E+11	239 - 370	0.9566
150	116.06	1.15E+11	242 - 380	0.9541
3rd stage				
10	187.99	6.46E+14	380 - 476	0.9271
50	191.19	1.16E+15	380 - 474	0.9263
100	186.52	7.95E+14	370 - 456	0.8959
150	192.98	1.61E+15	380 - 473	0.9257
Global combustion				
10	66.19	9.45E+05	242 - 476	0.8651
50	66.50	1.02E+06	242 - 474	0.8635
100	68.30	1.71E+06	239 - 456	0.8534
150	66.62	1.05E+06	242 - 473	0.8621

Table C.15. Estimated kinetic parameters for the combustion of pine wood particles at different air flow rates (particles between 0.125 and 0.25 mm).

\dot{Q}_a (mL/min)	E (kJ/mol)	A (min ⁻¹)	T (°C)	R^2
2nd stage				
10	125.89	7.38E+11	250 - 380	0.9571
50	125.22	6.52E+11	248 - 380	0.9579
100	125.27	6.88E+11	250 - 380	0.9544
150	125.87	7.38E+11	250 - 380	0.9574
3rd stage				
10	153.17	9.03E+11	380 - 499	0.9243
50	153.05	8.82E+11	380 - 498	0.9227
100	159.40	2.96E+12	380 - 492	0.9246
150	154.02	1.04E+12	380 - 497	0.9232
Global combustion				
10	63.40	4.15E+05	250 - 499	0.8472
50	63.46	4.23E+05	248 - 498	0.8469
100	63.68	4.71E+05	250 - 492	0.8413
150	63.42	4.17E+05	250 - 497	0.8459

Table C.16. Estimated kinetic parameters for the combustion of pine wood particles at different air flow rates (particles larger than 1 mm).

\dot{Q}_a (mL/min)	E (kJ/mol)	A (min ⁻¹)	T (°C)	R^2
2nd stage				
10	127.42	9.90E+11	251 - 380	0.9588
50	127.35	9.51E+11	251 - 380	0.9563
100	127.06	9.83E+11	251 - 380	0.9577
150	126.66	8.77E+11	251 - 380	0.9588
3rd stage				
10	161.62	4.10E+12	380 - 498	0.9375
50	157.59	1.86E+12	380 - 495	0.922
100	172.42	3.24E+13	380 - 483	0.9252
150	169.30	1.64E+13	380 - 485	0.9173
Global combustion				
10	64.90	5.57E+05	251 - 498	0.8559
50	64.47	4.84E+05	251 - 495	0.846
100	66.24	8.11E+05	251 - 483	0.8454
150	65.32	6.33E+05	251 - 485	0.8426

D. Preliminary set up for mass loss of wood pellets

This section reports a set of preliminary starts carried out to validate the methodology.

D.1 Mass loss

In order to assess the feasibility to measure the mass loss and the devolatilization rate of the various components that make up the biomass, a preliminary set of experiments was developed in an existing oven. The results were of no practical significance to the purpose of this thesis but gave a reliable indication of the procedure.

The tests were performed at a set of temperature within the operating range of the oven, below 250 °C, as detailed in Table D.1. In addition, for each temperature, the time was set at the values detailed in Table D.1.

Table D.1. Time and temperature for the preliminary test.

Temperature (°C)	Time (s)			
144	120	300	600	1,800
191				
225				

In addition, a thermocouple was inserted longitudinally into a single thermocouple in order to record the temperature variation during the experiments.

For the samples at 225 °C, the elemental analysis (Carbon, Nitrogen, and Hydrogen) was performed at 10 minute and 5 hours. The experimental and modelling result with exponential equation and, the mass loss difference between the experimental and modelling are presented in Figure D.1 and Table D.2 respectively. The mass losses during the thermal treatment at different temperatures in Figure D.1 shows that the mass losses increased as the period of the heating time is increased up to ± 6 minutes at constant temperature. This condition is observed for all the temperatures tested and the highest temperature observed released the highest mass losses. The mass losses increase from 2-10% is due to the moisture content reducing and the initiation of volatile release. As mentioned in Arshanitsa *et al.* (2016) in the temperature range of 150-160 °C the moisture content from pellets is removed without any other volatiles' formation. The correlation coefficient (R^2) in Figure D.1 is > 0.75 ; the mass loss difference for experimental and modelling in Table D.2 is not significantly different, then the natural logarithm equation is appropriate to apply for this experiment.

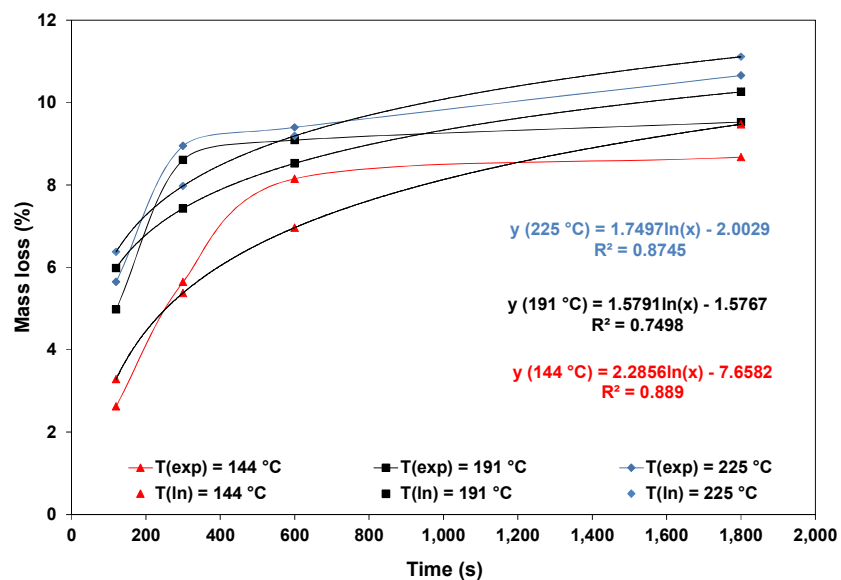


Figure D.1. Mass loss of wood pellets for experimental and modelling at temperature: 144, 191 and 225 °C.

Table D.2. Mass loss difference between experimental and modelling.

Time (s)	dm _{loss} (%).		
	T = 144 °C	T = 191 °C	T = 225 °C
120	-25.09	-20.26	-12.88
300	4.74	13.69	10.85
600	14.58	6.19	2.21
1,800	-9.18	-7.70	-4.24

D.2 Elemental analysis

In the elemental analysis, two different times (10 min and 5 hours) and one constant temperature (225 °C) for heating the pellets were applied. Besides evaluation of the chemical composition including Nitrogen, Carbon, and Hydrogen, and mass losses were also considered. The mass losses data are presented in Table D.3 and the elemental analysis data are presented in Table D.4. Table D.3 shows the mass losses during the heating up of the wood pellets for 10 minutes and 5 hours at 225 °C. The mass losses during 10 minutes of study are 9.45% which is indicated as the removal of the moisture content and some volatiles matter, as the water content of pellets was 6.9%.

Table D.3. Mass loss at T = 225 °C.

Time	Mass loss (%)
10 min	9.45
5 hours	20.48

The nitrogen content in wood pellets for 10 min is 0.10% which is smaller than 5 hours of heating, 0.18%. Even though the Carbon and Hydrogen content for 10 minutes is higher than 5 hours, 54.50% and 50.10% for Carbon and 6.87 and 6.07% for Hydrogen respectively. These results indicated that the heating up of wood pellets at constant temperature and different time will produce less Nitrogen and more Carbon and Hydrogen for a short period of time. The elemental analysis of pine and beech wood under torrefied conditions at increasing temperature indicate the increase of the Carbon content while decreasing the Hydrogen and the Oxygen contents (Melkior *et al.*, 2017).

Table D.4. Elemental analysis at T = 225 °C.

Parameter	Initial concentration	t = 10 min	t = 5 hours
Carbon (%)	50.8	54.50	50.10
Hydrogen (%)	5.39	6.87	6.07
Nitrogen (%)	1.55	0.10	0.18

D.3 Transient behavior of pellets

The mass loss of wood pellet was conducted in a small scale reactor, and the pellet was introduced into a small cup. Before introducing the sample the small cup was preheated to obtain the thermal equilibrium by applying the equation from the transient model (Eq. D.1) (Cengel, 2002), and with two different cups material (Carbon and stainless steel), then the result is presented in Figure D.2.

$$\frac{T(t) - T_{\infty}}{T_i - T_{\infty}} = e^{-\frac{hA_s}{\rho C_p V} t} \quad (\text{D.1})$$

where $T(t)$ is the temperature of a body at time t (s), T_{∞} is the ambient temperature (K), T_i is initial temperature, h is the convection heat transfer coefficient ($\text{W}/\text{m}^2\cdot\text{K}$), V is volume (m^3), C_p is a specific heat ($\text{kJ}/\text{kg}\cdot\text{K}$) and A_s is surface area (m^2).

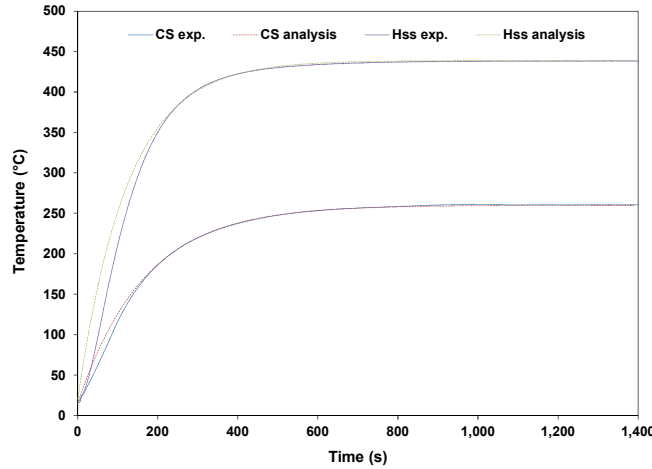


Figure D.2. Temperature profile for CS and HSS cup.

To observe the temperature profile in the center ($r = 0$) of the pellet, the simple model for 1D transient conduction in a cylinder was applied (Eq. D.2) (Cengel, 2002).

$$\theta_{0,cyl} = \frac{T_0 - T_\infty}{T_i - T_\infty} = A_1 e^{-\lambda_1^2 \tau} \quad (D.2)$$

where A_1 and λ_1 is constants and are functions of the Bi number and the zeroth-order Bessel function of the first kind, J_0 . τ is dimensionless time and $\theta_{0,cyl}$ the dimensionless temperature.

Figure D.3 presents the experimental study of the temperature profile in the center and on the surface of the wood pellet at different heating temperatures in a reactor with a temperature range of up to 250 °C. The temperature profiles at the surface and in the center of the wood pellet agree with the analytical study conducted by Gómez *et al.* (2015). The large temperature gradient between the surface and the center of the wood pellet is due to the low thermal conductivity and diffusivity of the biomass materials (Salema and Afzal, 2015). Kumar *et al.* (2008) modelled the temperature profile at 683 K on wood cylinder and revealed that the surface temperature attains the bulk temperature after a significant length of time, which suggests that the external heat transfer resistance cannot be neglected for this analysis. It was also shown that the distance between the two, the temperature always lies between the center and the surface temperature. Meanwhile, the peak temperature shown by the inner points is the largest for the center point, which corresponds to the temperature at 225 °C in Figure D.3.

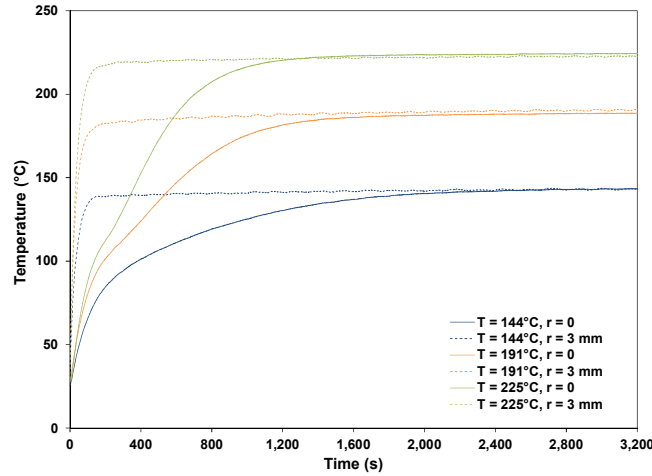


Figure D.3. Temperature profile on the center ($r = 0$) and surface ($r = 3$ mm) of wood pellets (experiment).

The result of the simulated temperature profile of a wood cylinder of 0.010 m radius conducted by Kumar *et al.* (2008) shows that when a particle is introduced into the reactor, the surface gets heated up fast and its temperature rises depending on the convective heat transfer coefficient and radiative effect. Besides, the center shows a temperature lag due to additional diffusive heat transfer resistance inside the particle. The highest temperature on the outside diameter of wood pellets results in fastest temperature equilibrium compared to the center temperature profile.

Figure D.4 presents the temperature profile in the center for both experimental data and the model predictions. The prediction and experimental analysis on the center of the pellets was also conducted by Kumar *et al.* (2008) at a bulk temperature of 643 K. For the model prediction in this study, the heat transfer coefficient applied was $10 \text{ W/m}^2\cdot\text{K}$. The temperature in the center corresponds to the result obtained by Kumar *et al.* (2008) and Paulauskas *et al.* (2015). Paulauskas *et al.* (2015) revealed that the heating temperature and chemical processes inside the wood pellet influenced the center temperature profile and as the temperature increases the profile changes become more intensive.

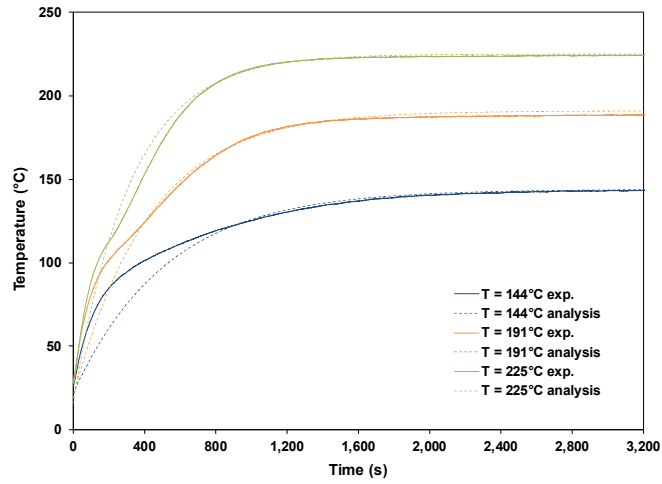


Figure D.4. Temperature profile at in the center of the pellet ($r = 0$).

E. Experimental data

The experimental data and figures obtained are presented in the following.

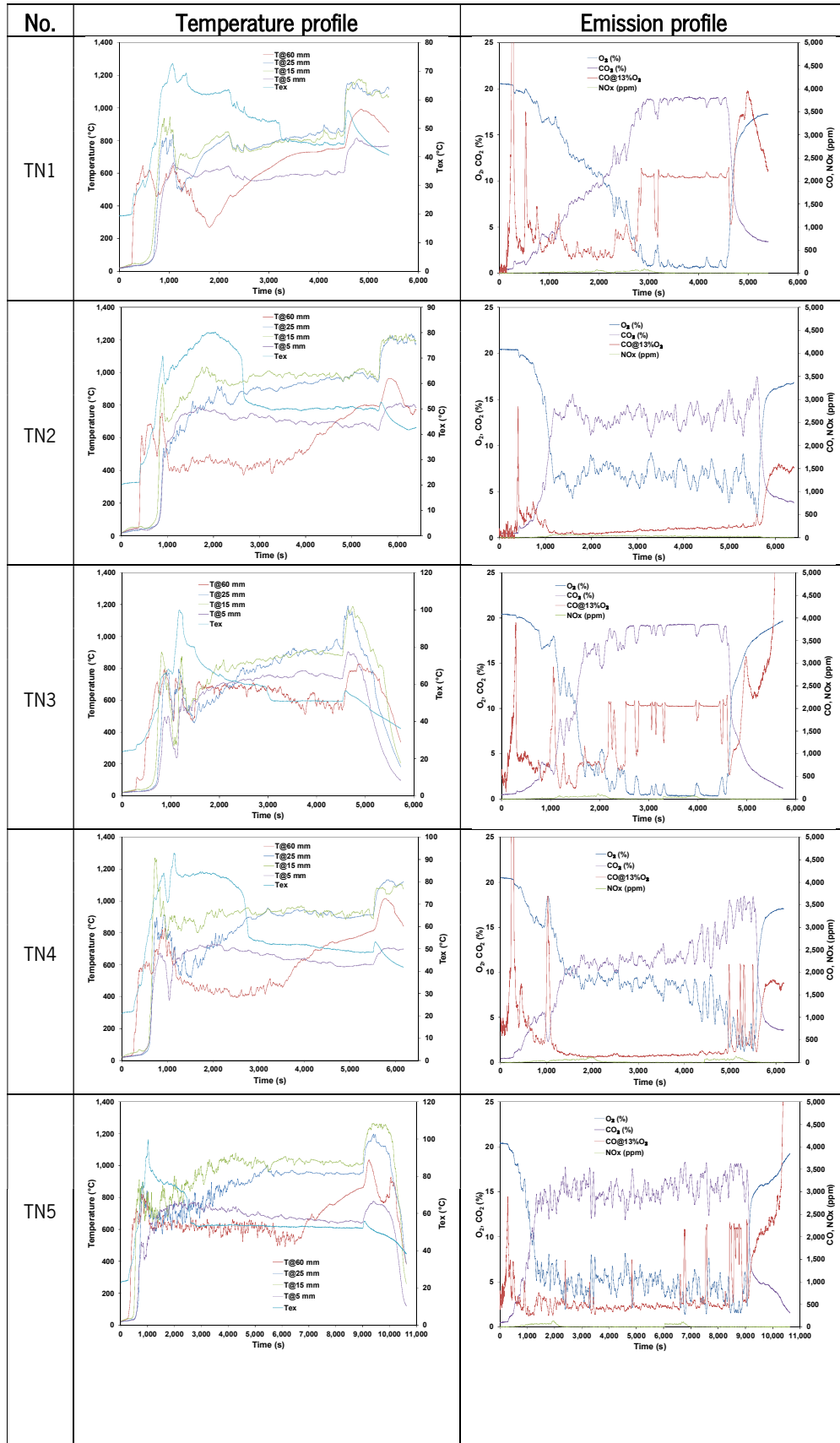
Table E.1. The experimental data.

No.	A		B		C		D		Emissions						Efficiency				Fuel bed temperature (°C)			
	Power (kW)	Excess air (%)	Grate area (mm ²)	Split ratio	O ₂ (%)	CO (ppm)			NOx (ppm)	CO ₂ (%)	η (%)	5 mm	15 mm	25 mm	60 mm	η (%)	5 mm	15 mm	25 mm	60 mm		
						Before	After	Total														
TN1	10	50	90 x 75	20/80	5.83	395	1,830	1,562	36.12	18.13	63.92	582	791	811	678							
TN2	10	50	115 x 75	30/70	6.69	149	217	209	31	13.42	74.96	700	983	933	572							
TN3	10	50	115 x 96	37/63	2.79	1,042	1,985	1,786	47.3	2.11	71.07	744	864	838	633							
TN4	10	70	90 x 75	30/70	8.34	143	334	262	64.3	13	72.63	627	931	916	624							
TN5	10	70	115 x 75	37/63	4.88	452	847	603	67.06	12.66	77.67	687	1,009	907	648							
TN6	10	70	115 x 96	20/80	8.25	157	470	286	58.67	13.08	69.25	691	855	853	514							
TN7	10	110	90 x 75	37/63	10.82	474	561	514	62	11.5	83.02	542	877	925	612							
TN8	10	110	115 x 75	20/80	10.87	209	282	268	49.44	10.4	81.16	630	961	983	765							
TN9	10	110	115 x 96	30/70	10.77	370	415	391	25.78	9.48	83.85	656	929	849	546							
TN10	13	50	90 x 75	37/63	6.75	110	149	146	54.94	13.58	87.08	626	1,039	1,012	741							
TN11	13	50	115 x 75	20/80	6.37	126	787	625	74.04	15.59	74.03	700	929	907	647							
TN12	13	50	115 x 96	30/70	6.5	128	176	166	37.69	14.38	86.01	699	951	957	631							
TN13	13	70	90 x 75	20/80	8.33	109	262	252	73.3	14.39	91.57	676	985	968	848							
TN14	13	70	115 x 75	30/70	8.32	228	490	412	37.12	11.78	88.85	651	1,006	986	753							
TN15	13	70	115 x 96	37/63	8.29	262	427	390	70	12.93	91.77	627	913	866	542							
TN16	13	110	90 x 75	30/70	10.5	134	218	205	32.46	10.11	87.26	619	1,054	1,041	831							

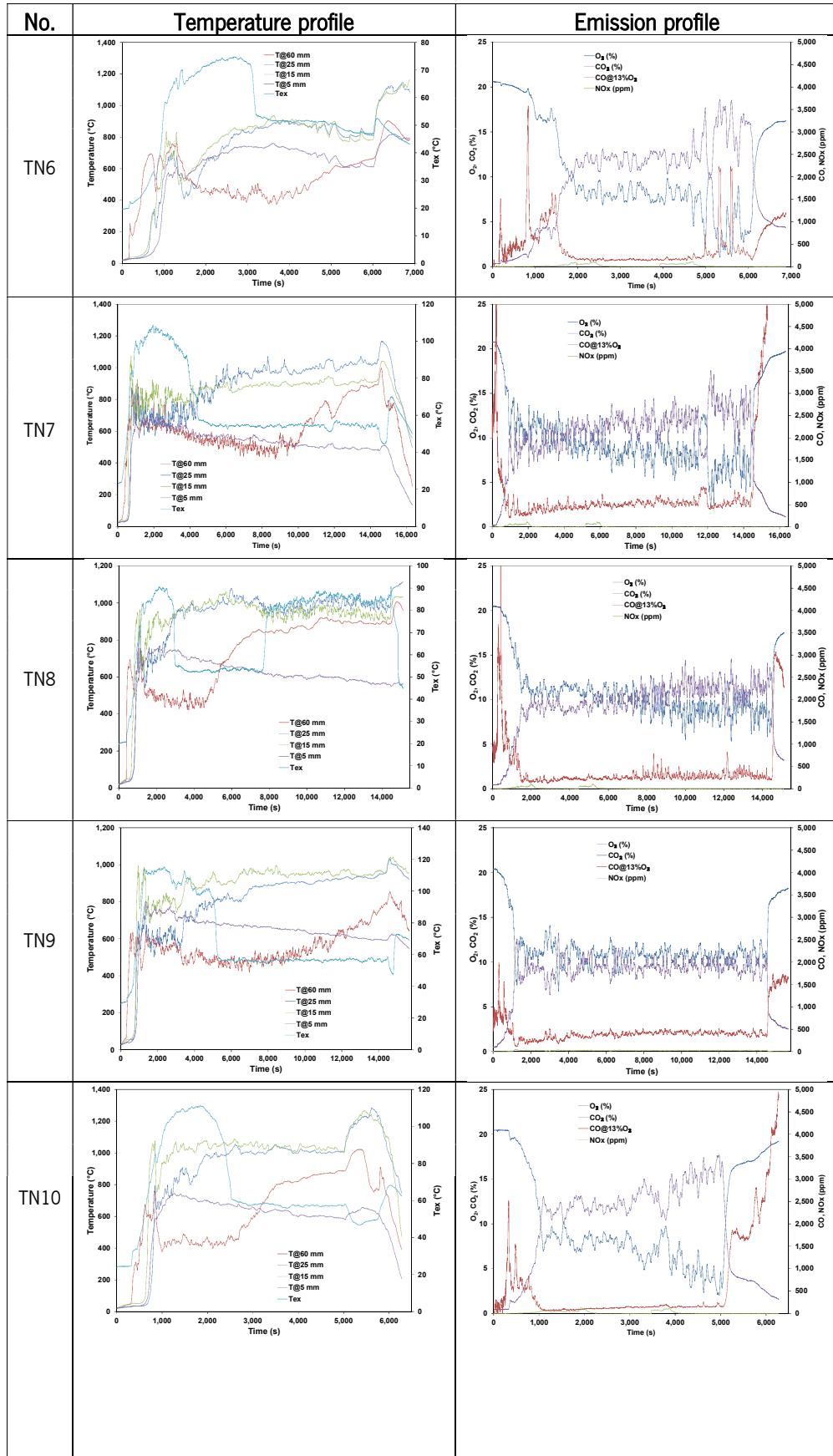
Annex E. Experimental data

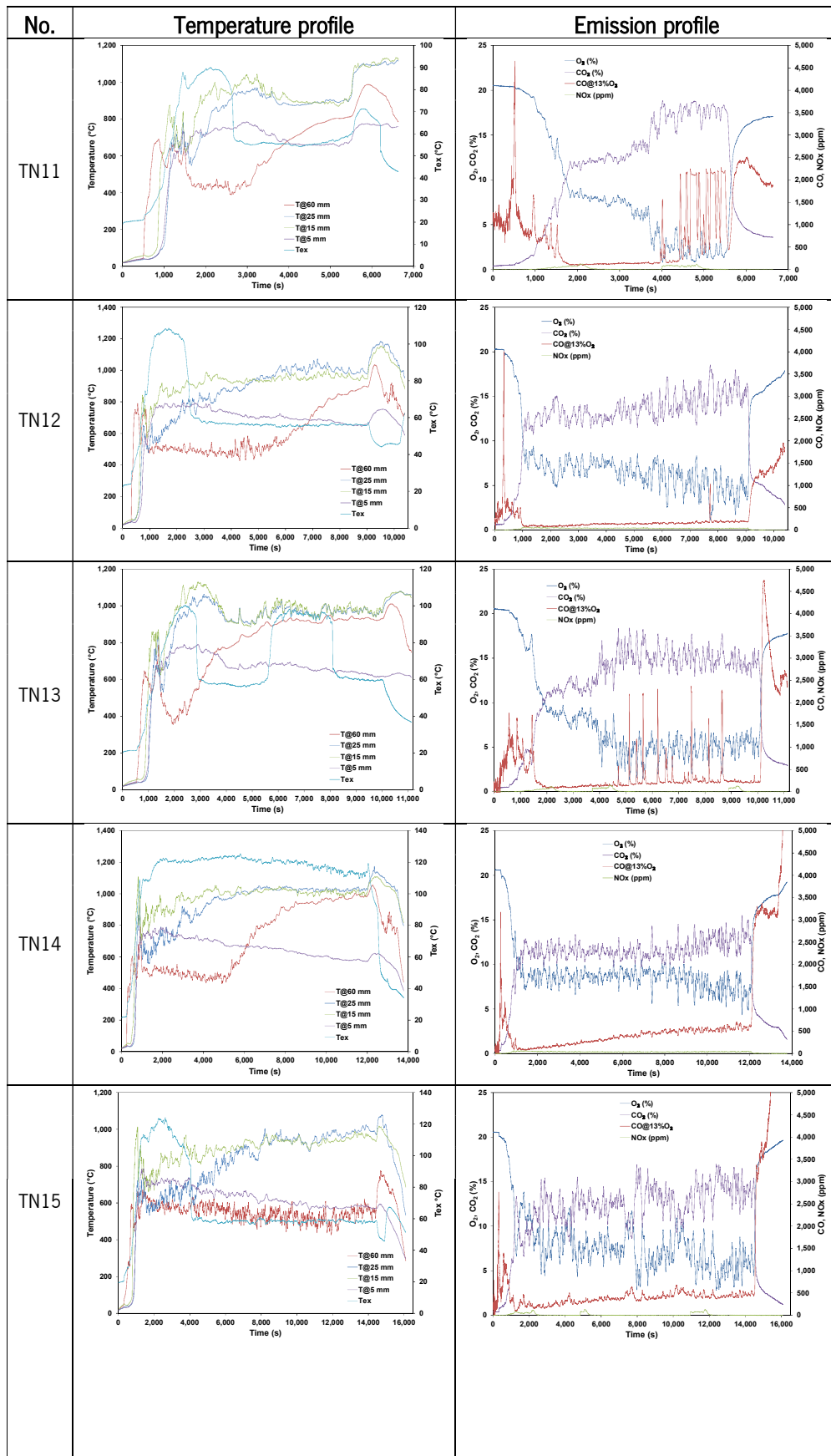
TN17	13	110	115 x 75	37/63	10.84	314	213	243	29.2	9.71	87.36	556	1,076	1,049	820
TN18	13	110	115 x 96	20/80	10.03	234	395	330	63.34	11.44	85.61	710	1,032	987	630
TN19	16	50	90 x 75	30/70	6.57	213	246	239	79.31	13.32	83.18	668	1,007	1,043	783
TN20	16	50	115 x 75	37/63	6.39	190	212	204	69.92	14.66	91.32	640	984	995	576
TN21	16	50	115 x 96	20/80	6.53	219	350	298	80.9	13.9	87.02	695	1,086	1,016	788
TN22	16	70	90 x 75	37/63	8.30	356	413	409	74.1	13.1	87.19	576	1,023	1,078	719
TN23	16	70	115 x 75	20/80	8.25	111	242	220	72.91	11.69	86.65	699	1,068	1,064	867
TN24	16	70	115 x 96	30/70	8.44	267	325	302	38.8	12.28	90.2	681	1,003	972	606
TN25	16	110	90 x 75	20/80	10.77	227	341	323	62.33	8.4	80.99	689	1,089	1,083	947
TN26	16	110	115 x 75	30/70	10.83	282	492	422	31.85	9.6	86.7	649	1,092	1,060	692
TN27	16	110	115 x 96	37/63	10.93	447	544	495	32.61	9.33	84.79	577	825	626	606

Figure E.1. Experimental results.

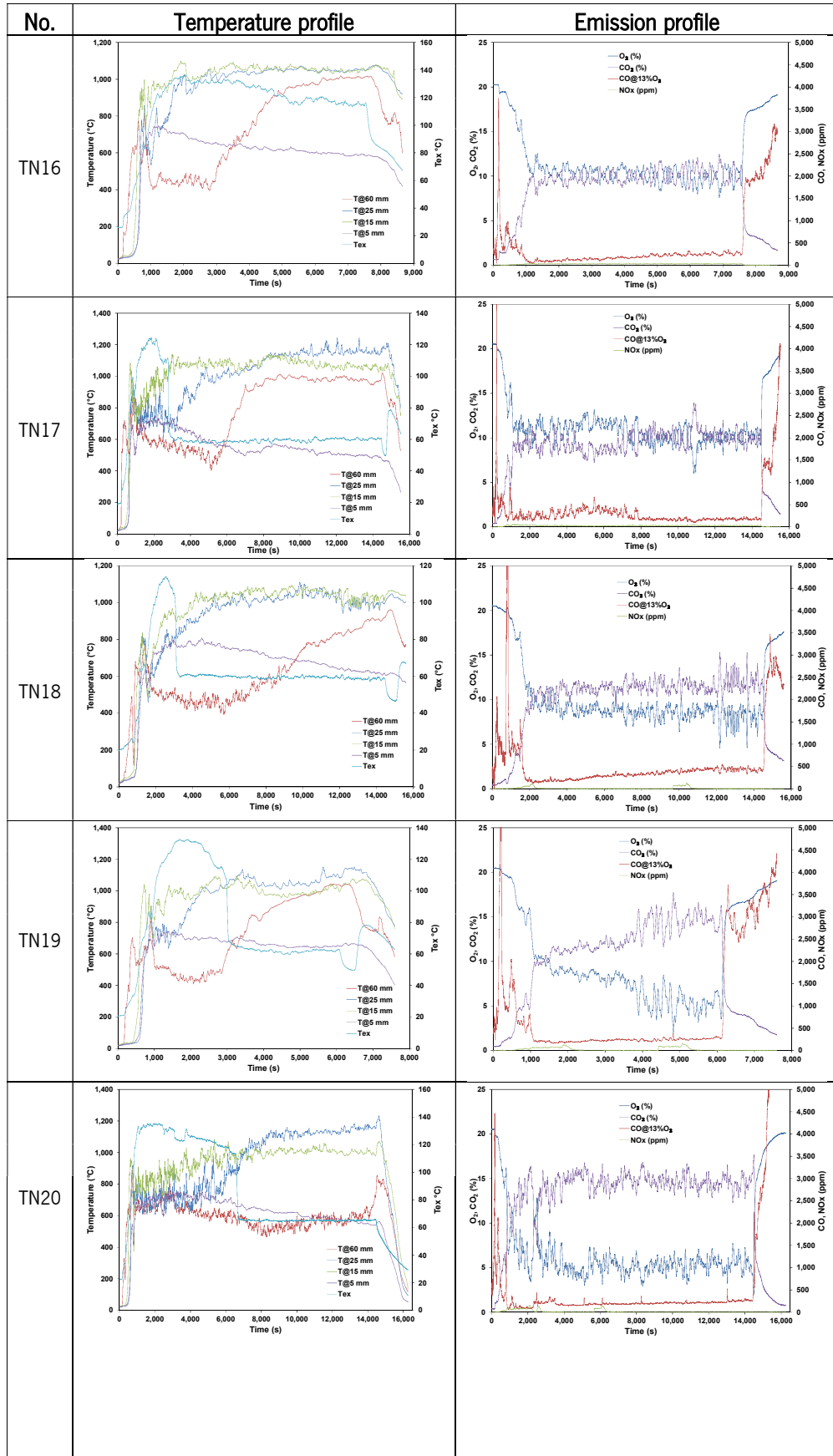


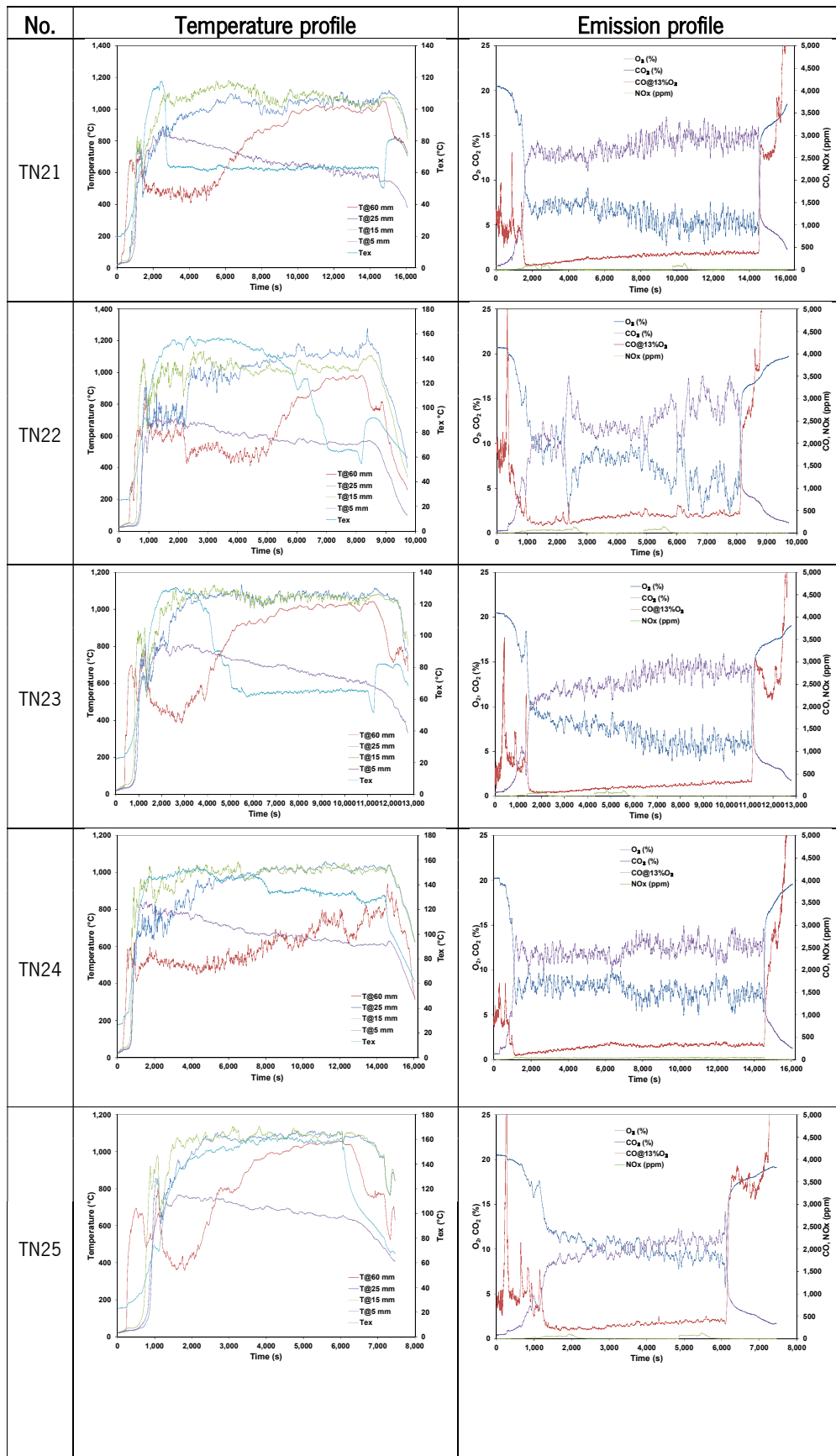
Annex E. Experimental data





Annex E. Experimental data





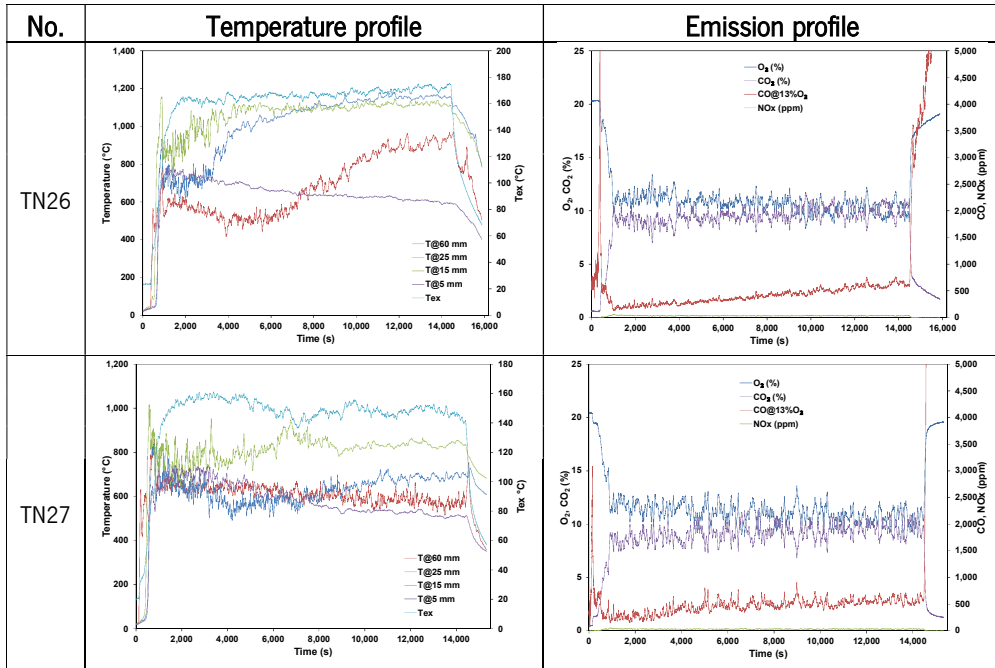

















Figure E.2. The ashes agglomeration data.






No.	P (kW)	EA (%)	GA (mm ²)	SR	d (mm)	Figure	Time (s)	Observation
TN1	10	50	90 x 75	20/80	7		4,500	The large ash agglomeration is 7 mm, and the residue are composed of some ashes and char.
TN2	10	50	115 x 75	30/70	3		5,500	The large ash agglomeration is 3 mm, and the residue are composed of some ashes and char.
TN3	10	50	115 x 96	37/63	10		4,600	The large ash agglomeration is 10 mm, and the residue are composed of some ashes and with almost no char.
TN4	10	70	90 x 75	30/70	6		5,500	The large ash agglomeration is 6 mm, and the residue are composed of some ashes and char.
TN5	10	70	115 x 75	37/63	17		9,000	The large ash agglomeration is 17 mm, and the residue are composed of some ashes and with almost no char.






Annex E. Experimental data

No.	P (kW)	EA (%)	GA (mm ²)	SR	d (mm)	Figure	Time (s)	Observation
TN6	10	70	115 x 96	20/80	3		6,000	The large ash agglomeration is 3 mm, and the residue are composed of some ashes and char.
TN7	10	110	90 x 75	37/63	17		14,400	The large ash agglomeration is 17 mm, and the residue are composed of some ashes and few char.
TN8	10	110	115 x 75	20/80	4		14,400	The large ash agglomeration is 4 mm, and the residue are composed of some ashes and char.
TN9	10	110	115 x 96	30/70	47		14,400	The large ash agglomeration is 47 mm, and the residue are composed of some ashes and char.
TN10	13	50	90 x 75	37/63	7		5,000	The large ash agglomeration is 7 mm, and the residue are composed of some ashes and with almost no char.



No.	P (kW)	EA (%)	GA (mm ²)	SR	d (mm)	Figure	Time (s)	Observation
TN11	13	50	115 x 75	20/80	10		5,600	The large ash agglomeration is 10 mm, and the residue are composed of some ashes and few char.
TN12	13	50	115 x 96	30/70	6		14,400	The large ash agglomeration is 6 mm, and the residue are composed of some ashes and few char.
TN13	13	70	90 x 75	20/80	7		10,000	The large ash agglomeration is 7 mm, and the residue are composed of some ashes and few char.
TN14	13	70	115 x 75	30/70	23		12,000	The large ash agglomeration is 23 mm, and the residue are composed of some ashes and char.
TN15	13	70	115 x 96	37/63	28		14,400	The large ash agglomeration is 28 mm, and the residue are composed of some ashes and with almost no char.

Annex E. Experimental data

No.	P (kW)	EA (%)	GA (mm ²)	SR	d (mm)	Figure	Time (s)	Observation
TN16	13	110	90 x 75	30/70	28		7,500	The large ash agglomeration is 28 mm, and the residue are composed of some ashes and few char.
TN17	13	110	115 x 75	37/63	20		14,400	The large ash agglomeration is 20 mm, and the residue are composed of some ashes and few char.
TN18	13	110	115 x 96	20/80	12		14,400	The large ash agglomeration is 12 mm, and the residue are composed of some ashes and few char.
TN19	16	50	90 x 75	30/70	12		6,000	The large ash agglomeration is 12 mm, and the residue are composed of some ashes and few char.
TN20	16	50	115 x 75	37/63	32		14,400	The large ash agglomeration is 32 mm, and the residue are composed of some ashes and few char.

No.	P (kW)	EA (%)	GA (mm ²)	SR	d (mm)	Figure	Time (s)	Observation
TN21	16	50	115 x 96	20/80	20		14,400	The large ash agglomeration is 20 mm, and the residue are composed of some ashes and with almost no char.
TN22	16	70	90 x 75	37/63	25		8,000	The large ash agglomeration is 25 mm, and the residue are composed of some ashes and with almost no char.
TN23	16	70	115 x 75	20/80	24		11,000	The large ash agglomeration is 24 mm, and the residue are composed of some ashes and with almost no char.
TN24	16	70	115 x 96	30/70	17		14,400	The large ash agglomeration is 17 mm, and the residue are composed of some ashes and few char.
TN25	16	110	90 x 75	20/80	10		6,000	The large ash agglomeration is 10 mm, and the residue are composed of some ashes and few char.

Annex E. Experimental data

No.	P (kW)	EA (%)	GA (mm ²)	SR	d (mm)	Figure	Time (s)	Observation
TN26	16	110	115 x 75	30/70	59		14,400	The large ash agglomeration is 59 mm, and the residue are composed of some ashes and with almost no char.
TN27	16	110	115 x 96	37/63	10		14,400	The large ash agglomeration is 10 mm, and the residue are composed of some ashes and with almost no char.